EXPERIMENTAL STUDY OF EVOLUTION OF TURBULENCE LEVEL IN STABLY STRATIFIED SHEAR FLOWS

By

P. M. V. SUBBARAO

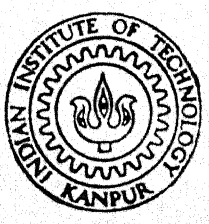

DEPARTMENT OF MECHANICAL ENGINEERING

INDIAN INSTITUTE OF TECHNOLOGY KANPUR

JANUARY, 1991

EXPERIMENTAL STUDY OF EVOLUTION OF TURBULENCE LEVEL IN STABLY STRATIFIED SHEAR FLOWS

A Thesis submitted
in Partial Fulfillment of the Requirements
for the Degree of

MASTER OF TECHNOLOGY

by

P. M. V. SUBBARAO

to the
Department of Mechanical Engineering
INDIAN INSTITUTE OF TECHNOLOGY, KANPUR
JANUARY 1991

ME - 1991 - M - SUB - EXP

CERTIFICATE

It is certified that the work contained in the thesis entitled ***EXPERIMENTAL STUDY OF EVOLUTION OF TURBULENCE LEVEL IN STABLY STRATIFIED SHEAR FLOWS***, by **P.M.V.SUBBARAO**, has been carried out under my supervision and that this work has not been submitted elsewhere for a degree.

Dr. K. MURALIDHAR
DEPT. OF MECHANICAL ENGG.
I.I.T, KANPUR.

January, 1991.

ACKNOWLEDGEMENTS

I express my deep sense of gratitude to my guide Dr. K Muralidhar for the untirir guidance and commendable encouragement.

I express my profound satisfaction and heartfelt thanks to Mr. Shambu Sharm without whose cooperation and help the fabrication of Test Cell would have been impossibilty.

Finally I thank all my friends who helped me very much during and before tl thesis work.

(P M V Subbarao)

CONTENTS

LIST OF FIGURES

LIST OF TABLES

LIST OF SYMBOLS

A	Area
C_p	Specific Heat of Air at constant Pressure
C_v	Specific Heat of Air at constant Volume
E	Output of Hot Wire
E_c	Output of Hot Wire for varying Overheat Resistance
f	Friction Factor
g	Acceleration due to Gravity
G_r	Grashoff Number
h	Convective Heat Transfer Coefficient
M	Mesh Spacing
M_a	Mach Number
N_u	Nusselt Number
k_f	Thermal Conductivity of Fluid
k_w	Thermal Conductivity of Hot Wire
P	Electrical Input to Hot Wire Sensor
q'	Convective Heat Loss
R_e	Reynolds Number
RHC	Operating Overheat Resistance
RHV	Variable Overheat Resistance
R_i	Richardson Number
R_0	Resistance of Wire at 0°C
S_h	Shear Parameter
T_b	Temperature of the Fluid at the bottom of the Wake
T_f	Ambient Fluid Temperature
THC	Operating Temperature of Wire
TR	Reference Fluid Temperature
T_t	Temperature of the Fluid at the top of the Wake
U	Free Stream Velocity
u'	X–Component of Velocity Fluctuation
v'	Y–Component of Velocity Fluctuation

$\overline{u}$	X–Component of Mean Velocity
$\overline{v}$	Y–Component of Mean Velocity
α	Temperature Coefficient of Resistance
α_i	Eigen Values
ν	Kinematic Viscosity
ρ	Density of Air
λ	Taylor's Micro Scale

ABSTRACT

The growth and decay patterns of free stream turbulence subjected to nearly uniform shear and density stratification are experimentally studied. The flow parameters are chosen so as to model portions of the earth's atmosphere. A new test cell has been fabricated to carry out the study. This test cell uses turbulence behind a mesh as well as the far wake of a cylinder. The conditions under which percentage turbulence grows or decays with distance are obtained from experiments. Shear is introduced in the test cell both by the wall boundary–layers as well as by a specially constructed variable–length honeycomb. Density stratification is produced by differentially heating layers of air using electrical wire heaters. Only stable stratification, i.e., the hot – above cold – below configuration is studied in the present work.

Velocity, velocity fluctuations and local temperature level are measured using a 2–wire hot wire anemometer. Each wire measures velocity and temperature respectively. A hot wore calibration procedure to include non–isothermal effects via the use of a variable overheat ratio is developed in this work. Turbulence statistics are computed numerically by first acquiring the anemometer signal in digital form through a GPIB interface located on storage scope.

Results show that in isothermal flow, mild shear irrespective of its sign leads to a growth in mesh – generated turbulence level. In non–isothermal flow, stable stratification does damp fluctuations and a decaying pattern is visible. When the cylinder is used as a turbulence generator, an initial period of decay is observed in all cases, followed by growth or decay pattern depending on the applied external factor as shear or stratification. The combined effect of these two factors is seen to alter the base flow and temperature profiles themselves and a systematic trend has not been observed.

INTRODUCTION

The earth's atmosphere is an interesting field for researchers who work in the areas of fluid mechanics and aerodynamics. It is so because the atmosphere is a flow with multiple features. In fluid mechanics it is classified as Stratified Turbulent Shear Flow. Interest in this field arises from both its complexity and important engineering applications. Some of the applications are given below.

1.1.1. AIRCRAFT APPLICATIONS

The turbulence level and turbulence spectrum of the atmosphere depend on the mean velocity and temperature gradients existing in it. The time dependent drag acting on an aircraft depends on the turbulence spectrum of the atmosphere. Another important point is that the natural frequency of an aircraft should not coincide with frequencies existing in turbulence spectrum since this can lead to damaging vibrations and consequent instability.

1.1.2. WEATHER FORECASTING

The phenomenon of turbulence influences cloud formation and possible changes in the weather. The level of circulation in the atmosphere is also affected by the turbulence spectrum of eddy scales. High levels of circulations called cyclones must be forecast accurately to prevent crop and life damage.

1.1.3. DISPERSION OF POLLUTANTS

Turbulence increases transport of mass, momentum and energy much beyond the diffusion limit. The dispersion of a pollutant depends on the eddy sizes occurring in atmospheric flows. This in turn determines the rate at which a pollutant can be discharged into atmosphere in order that safe conditions in the surrounding environment is maintained.

1.2. Need for Theoretical Predictive Methods

As mentioned earlier fluid flow in the atmosphere classifies as stratified turbulent shear flow. The velocity and temperature gradients vary from one place to the other place and one altitude to another altitude. The temperature gradients decide the density gradients and hence the level of stratification. A configuration in which the density of an upper layer is less than that of lower layer is called as stable. Similarly, the configuration in which the density of an upper layer is more than that of lower layer is called as unstable. The stability of the flow and values of turbulent parameters depend on the temperature and velocity gradients existing in the atmosphere. It is not possible to measure the turbulent parameters everywhere in the atmosphere. To calculate these turbulent parameters of the atmosphere a theoretical formula is essential.

Such a formula will involve the appropriate dimensionless parameters of the problem. Broadly speaking, the shear parameter is the Reynolds number and the stratification parameter is called as the Richardson number. The specific forms of these parameters depend on the state of flow in the atmosphere. The length scale can be identified with the largest eddy size and hence with the size of the turbulence generator in a laboratory experiment. In this work, we study the growth patterns of turbulence and mechanisms which lead to this growth in a test cell in which velocity and temperature profiles prevail simultaneously. Hence we define the dimensionless parameters as,

$$\text{Reynolds Number, } R_e = \frac{U\ d}{\nu} \tag{1.1}$$

$$\text{Richardson Number, } R_i = (g/\rho)\ (\frac{\partial \rho}{\partial y})\ /\ (\frac{\partial u}{\partial y})^2 \tag{1.2}$$

Here d is the diameter of the cylinder used to produce turbulence. u is the average velocity in the test cell. The Reynolds number is constant over the entire length of the test cell; however R_i changes from one location to another. We define the Richardson number based on inflow conditions as,

$$R_i = \frac{g\ \Delta T L}{T_{ave} \cdot (\Delta u)^2} \tag{1.3}$$

where, L = size of the region over which velocity and temperature gradients exist,
$\Delta T = T_{max} - T_{min}$, $\Delta U = U_{max} - U_{min}$ and $T_{ave} = (T_{max} + T_{min})/2$

It is of interest to understand growth patterns of turbulence as a function of R_e and R_i.

1.3. Difficulties in Deriving Theoretical Formulae

Turbulence at this time of writing is a phenomenological process. This is because the derivation of theoretical expressions for any turbulent flow requires considerable input from experiments. Even for simple flow situations such as flow over flat plate and flow through pipes, extensive experiments are required to determine pressure drop and heat transfer rates. The popular $k - \epsilon$ model of turbulence also requires several constants whose values can be determined only from experimental data. The values of these parameters may show variation among different class of problems.

Jones and Launder (1972) have used the $k - \epsilon$ model of turbulence to predict laminarization in favorable pressure gradient flows. They proposed a set of empirical constants for this model. Singhal and Spalding (1981) have used the same model for prediction of two–dimensional boundary–layers. The values of the model constants used by them are different. Further, the constants also depend on whether the flow is at high Reynolds number or a low Reynolds number at which transitional effects are significant. In atmospheric flows, no comprehensive model is available for including turbulence in the analysis.

1.4. Review of Theoretical and Experimental Work

The first serious studies of flow instability and turbulence date from the late nineteenth century with the pioneering contributions by Reynolds and Rayleigh (1867). Reynolds famous investigations of pipe flow clearly established that there are two fundamentally different modes of flow, laminar and sinuous. He has demonstrated that an important non–dimensional parameter that determines the kind of flow exists and is known as Reynolds number (Eq. 1.1.).

Reynolds also determined the value of the critical value of R_e beyond which the flow becomes turbulent in pipe flows.

Rayleigh investigated the stability of parallel inviscid flows. His famous theorem, known as Rayleigh's Inflexion Point Theorem states the following.

A necessary condition for instability is that the basic velocity profile should have an inflexion point. More recent stability results include Miles Theorem (Drazin and Reid, 1984) and the experimental results of Van Atta et al (1988). Miles theorem states that Richardson number $R_i > 1/4$ in stably stratified flow guarantees laminarization of flow. Van Atta states that the shear parameter, $(x/u)\ \partial u/\partial y < 4$ isolates the turbulent fluctuations from the mean shear and prevents their growth.

The post–stability of analysis of fluid flows has not followed an established pattern. For example, Boussinesq (1877) and Prandtl (1925) have treated the turbulent flow as modified laminar by introducing additional fictitious turbulent stresses over and above the molecular shear stress. A second example is the statistical theory of turbulence directed at the treatment of homogeneous and isotropic turbulent flows with many ideas borrowed from the kinetic theory of gasses. It was Taylor (1923 , 1935) who first introduced new notions into the study of the statistical theory of turbulence. These are further developed by Von Karman (1937), Kolmograff (1941), Heisenberg (1938) and others (Pai 1957). The most important notions are the correlation function and the spectral function. The mathematical foundation to the theory of the correlation function and the spectral function has been studied extensively by Kampe de Feriet (1951), Batchelor (1953).

Substitution of correlation functions in continuity and Navier–Stokes equations for turbulent flow and further simplification for isotropic turbulence yields the two–point correlation equation. The integration of correlation equation for isotropic turbulence gives a famous second–order correlation equation known as Karman–Howarth equation. This can be stated as

$$\frac{\partial}{\partial t}\left(\overline{v'^2}\, f\right) = 2\overline{v'^2}\left(\frac{\partial}{\partial r} + \frac{u}{r}\right)\left(\frac{\partial f}{\partial r} - \frac{\overline{\left(v'^2\right)}}{r}\, h\right)$$

where,

$$f = \frac{\overline{v'_1\, v''_2}}{\overline{v'^2_1}} \quad \text{and} \quad h = \frac{\overline{v'^2_3\, v''_1}}{\left(\overline{v'^2_1}\right)^{3/2}}$$

Stewart (1951) has verified the above equations through hot–wire anemometry measurements.

The equation for the change of v' with time was obtained by setting r=0 in Von Karman – Howarth equation and by using Taylor's expressions for the micro scale of turbulence.

On the basis of dimensional arguments Taylor proposed following relation for grid generated turbulence from the above equation.

$$\frac{\lambda}{M} = A\sqrt{V/M\sqrt{(\overline{v'^2})}} \qquad (1.4)$$

Where λ = Taylor's micro scale
M = Mesh spacing
A = a constant

Integration of equation 1.4. gives

$$V/\sqrt{\overline{v'^2}} = \frac{5}{M\ A^2\ x} + \text{constant}$$

The above equation is experimentally verified by Taylor and others (Bird et. al 1960).

From an experimental viewpoint the decay of initially isotropic turbulence in stratified flow also presents severe problems. For stratification effects to become important the Richardson number must be high, i.e. the length scales and density differences must be large compared to the velocity differences. In the atmosphere the large vertical length scale generally ensures that buoyancy effects play a major role, but in the laboratory, with its prescribed length scale, strong stable stratification can only be achieved using large density gradients and relatively small velocities. For this reason most stratified experiments have been done using salt–stratified water. Much of this work is reviewed by Itswiere, Helland & Van Atta (1986) and Hopfinger (1987). Recently, however, Lienhard and Van Atta (1990) have shown that large temperatures gradients may be achieved in air tunnels and that this flow has many advantages over stratified salt–water experiments.

Salt–stratified water experiments fall into two categories, transient, where the grid is pulled or dropped through the stationary fluid, and steady state, where the fluid moves in a channel and the turbulence characteristics do not change with time. The former experiments, notably by Dickey and Mellor (1980), who dragged a grid through the fluid, while yielding interesting data, particularly on the velocity decay rate, provided relatively little information on turbulent transport and spectral characteristics. Steady state, salt–stratified water flow in a closed loop channel is described by Stillinger et al. (1983a). These experiments revealed new information on spectra, mass transfer and the evolution of the velocity field. They showed that in an evolving flow turbulence becomes fossilized and internal waves appear. Their results are compared to the predictions of Gibson (1980) and good agreement is found. Lienhard (1988) notes that scalar dissipation is difficult to measure because of the small diffusivity of the salt. The experiments are not truly steady since the density profile degrades with time and sample times are further limited because of bubble formation on the hot film sensors. Thus spectral and variance data lacks accuracy because of the limited sampling duration.

Such considerations motivated the wind–tunnel work of Lienhard and Van Atta (1990) and Yoon & Warhaft (1990). The results of above two show qualitative similarity in the evaluation of the variances and fluxes and other single–point quantities. However there are also some significant differences. Lienhard and Van Atta observed rapid decay and laminarization at smaller downstream distance than Yoon and Warhaft, because they were able to maintain large temperature gradients for a longer distance parallel to the main flow.

1.5. Need for Further Research and Scope of the Present Work

Study of the turbulent properties of gird generated turbulence under the action of stable stratification is one recent work carried out to understand the atmosphere. Study of atmospheric turbulence requires more information than this. Stratified shear flows whose Richardson number is close to that of the atmosphere will model the problem closely. Spectral and variance data measured in stratified shear flow with specific values of Richardson number will be useful in this regard. Further, certain engineering applications such as heat exchangers and air conditioning equipment require information on rate of growth and decay of free stream turbulence fluctuations since these determine the bulk velocity, temperature, heat transfer rates and pressure drops.

With the above considerations in view, we have constructed a test cell which can produce both stably and unstably stratified shear flow. We have used a special method of calibration for the hot–wire anemometer to measure mean and fluctuating velocities in a non–isothermal flow field. We have measured the mean velocity profiles and turbulence intensities beyond stratified uniform flow which uses a horizontal cylinder as a turbulence generator. We have also studied the evolution of grid generated turbulence. Finally stratified shear flows with Richardson numbers that match the atmosphere have been studied.

Grid generated turbulence tends to be nearly isotropic while the cylinder produces turbulence with a considerable degree of anisotropy. Hence these two cases may be taken to represent extreme limits realized in an application.

To obtain typical values of parameters required in the design of the test cell, the structure of the earth's atmosphere is required. This is described below.

1.6. Physics of the Earth's Atmosphere

The earth's atmosphere extends outward from the surface of the planet many thousands of kilometers where, in the rarefied world of interplanetary space, it merges with the outer most fringes of the solar atmosphere. At the bottom of this atmospheric ocean a shallow layer, 700–900m in depth exists, whose behavior is principally governed by the characteristics of its frictional coupling with the underlying surface. This layer is known as "Friction Layer". The atmosphere above this layer is known as Free Atmosphere.

The atmosphere is divided into different layers depending on the temperature profiles prevailing in it. Fig. 1.1. shows the temperature distribution and the nomenclature associated with it.

Although the earth's atmosphere is many thousand of kilometers deep, we shall focus our attention on the lowest 50 kilometers —— comprising the friction layer, troposphere, tropopause and stratosphere.

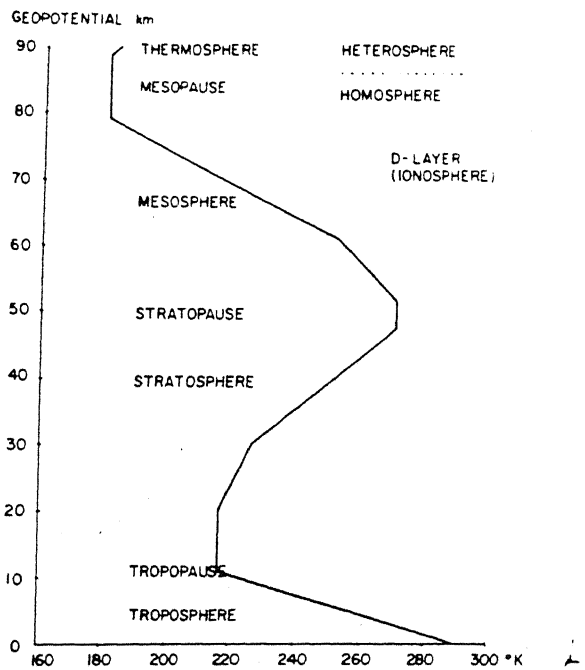

FIG. 1.1 NOMENCLATURE OF STANDARD ATMOSPHERE

1.6.1. FRICTION LAYER

The physics of the friction layer is both interesting and important chiefly because of the large variations occurring in them, both with respect to space and time. This is largely due to the fact that at the ground surface, radiant energy form the sun is absorbed and communicated to the soil as heat and to the atmosphere as heat and evaporated moisture. This, along with boundary–layers formed by the wind at the ground surface gives rise to a great variety of phenomena. There exists a strong variation of flow and temperature conditions with exposure to sun and with the height above the surface. This shallow layer contains information on atmospheric behavior since a major part of all available driving energy of fluid flow must transit this air–surface interface. The mechanism of heat, moisture and momentum transport across this inter face must be understood before the sophisticated atmospheric modeling experiments are performed.

Deacon (1969) has gathered extensive data on the friction layer. Figures 1.2 and 1.3 show variation of temperature and wind speed with height over an open grass plain. These observations for a clear noon in summer were made Great Plains Expedition in Nebraska (Lettu and Davidson, 1957).

In these figure the surface gains energy from radiation at the rate of 135 mw/cm^2. 55% of this radiation is transferred back to air.

1.6.1.1. Temperature Profile

The heat transferred through the surface layer necessitates a large temperature gradient. This is the more so because near the earth's surface, the free play of turbulent convection currents is hampered by the presence of the solid boundary. The ground surface temperature of around 43 °C is about 10 °C warmer than the air at height of 1m. In strong contrast to this gradient of 10°C in the first meter, there is only 2 °C in the next 100m. With lighter winds and smoother surfaces, the temperature gradients in close proximity to the surface become even more extreme and desert surfaces with high sun can be 25–30 °C warmer than the air at heights of 1 or 2m.

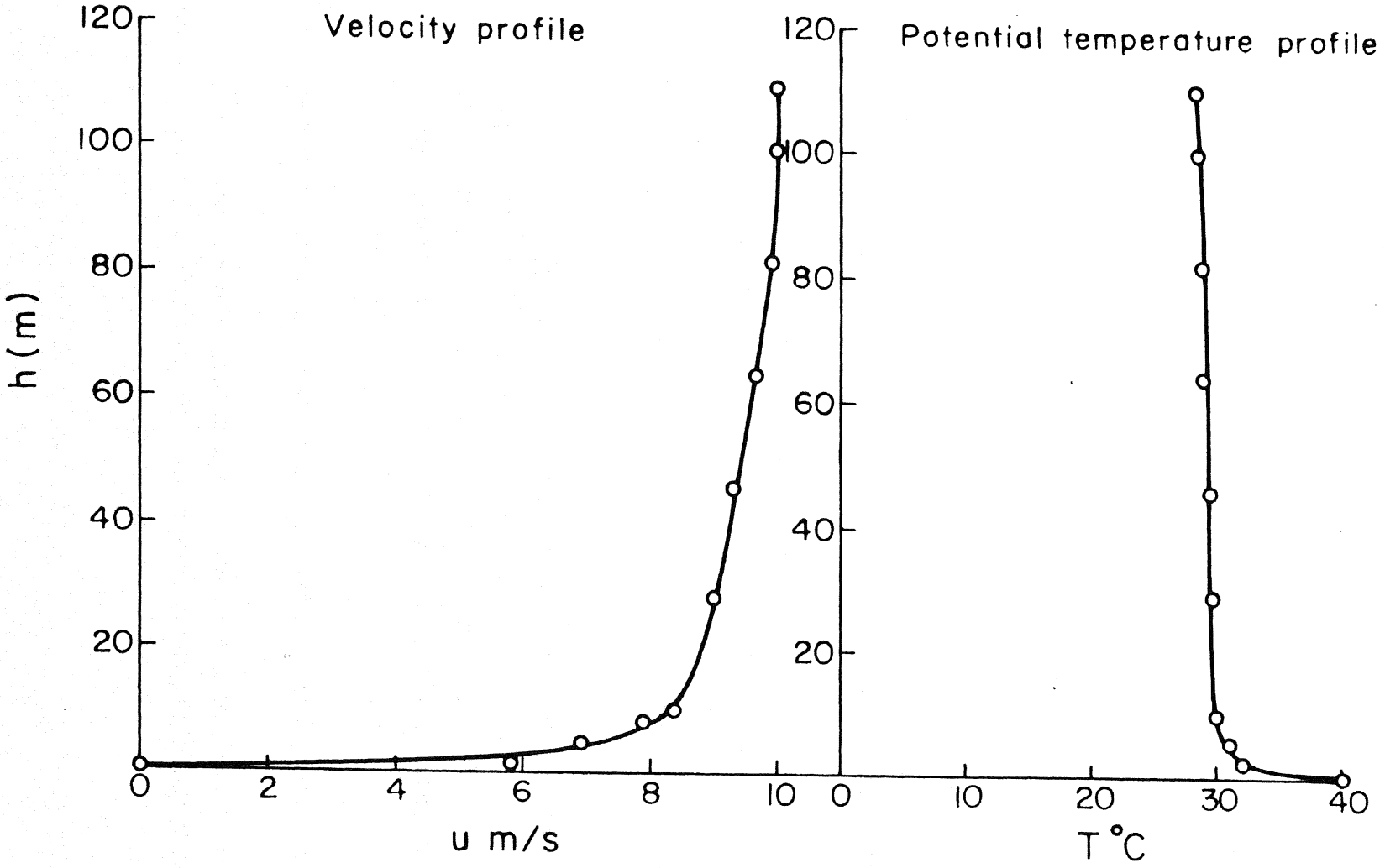

FIG. 1.2 & 1.3 FRICTION LAYER OF EARTH'S ATMOSPHERE

1.6.1.2. Wind Speed Profile

The profile of wind speed in Fig. 1.3. shows a similar gradient into the lower layers. The retardation of wind by surface friction under these conditions is only clearly evident in the lowest 100m. At a height of 5m the wind is reduced by about 25%, at 0.5m by 50% and so the half–meter layer adjacent to the ground has as great a difference in wind speed across it as the next 100m above.

1.6.1.3. Turbulent Nature of Friction Layer

If the sun's heat absorbed at the ground surface were propagated up through the air in the same way as it travels downward into soil, i.e., by purely molecular conduction then, as the thermal diffusivity for air is 0.2 cm"/sec, the diurnal temperature wave would vanish at barely 4m above the surface. Further, at a height of 2m the maximum temperature should occur at midnight (Deacon, 1969). Measurements show that the diurnal variation of air temperature usually extends well above 1,000m. Hence a more effective process than molecular diffusion alone must operate in the atmosphere. This is turbulent diffusion associated with the chaotic swirling motions that may readily be seen in watching the dispersal of smoke from a chimney.

A factor strongly influencing turbulent transfer is the vertical temperature gradient. The effect of the temperature gradient can be explained through the non–dimensional quantity, Richardson number. The Richardson number, Ri, expresses the ratio of buoyancy to shear effects in terms of the vertical gradients instead of fluxes and is defined earlier in this chapter (equation 1.2).

In terms of Richardson number three main states can be distinguished.

1) R_i positive; stable stratification: Turbulence causes heat to be transferred downward, volumes of air displaced vertically experience buoyancy forces in opposition to the displacement with the consequence that turbulence is diminished.

2) R_i zero; neutral or adiabatic conditions: heat transferred by turbulent eddies is zero: heat transfer is by pure molecular diffusion.

3) R_i negative; unstable stratification: air displaced vertically experiences buoyancy forces that assist its movement. Hence the potential energy of the unstable density stratification goes towards producing increased turbulence.

Fig. 1.4. shows the variation of Richardson number for cases discussed in Fig. 1.2. and 1.3. Fig. 1.5. shows the effect of temperature gradient on wind velocity profiles. Fig. 1.6. shows the variation of Richardson number with height for different stability conditions.

1.6.2. TROPOSPHERE

The atmospheric layers above the friction layer and below 10km are known as Troposphere. The temperature and wind speed profiles for summer and winter are shown in figures 1.7, 1.8. Figures 1.9. and 1.10. shows the variation of Richardson number with height for summer and winter seasons.

The troposphere contains most of the atmosphere's water vapor and virtually all cloudforms and hydrometeors. Wind system with most kinetic energy are observed near the tropopause (10–30km). The value of Richardson number prevailing in tropopause is responsible for the extent of cloud formation.

1.6.3. STRATOSPHERE

The region between 30km and 50km is known as the stratosphere. Figures 1.11., 1.12., 1.13 and 1.14 show profiles of temperature wind speed and Richardson number.

The stratosphere contains the largest concentrations of atmospheric Ozone. Owing to strong absorption of ultra–violet radiation, these ozone–rich regimes represent major stratospheric heat sources.

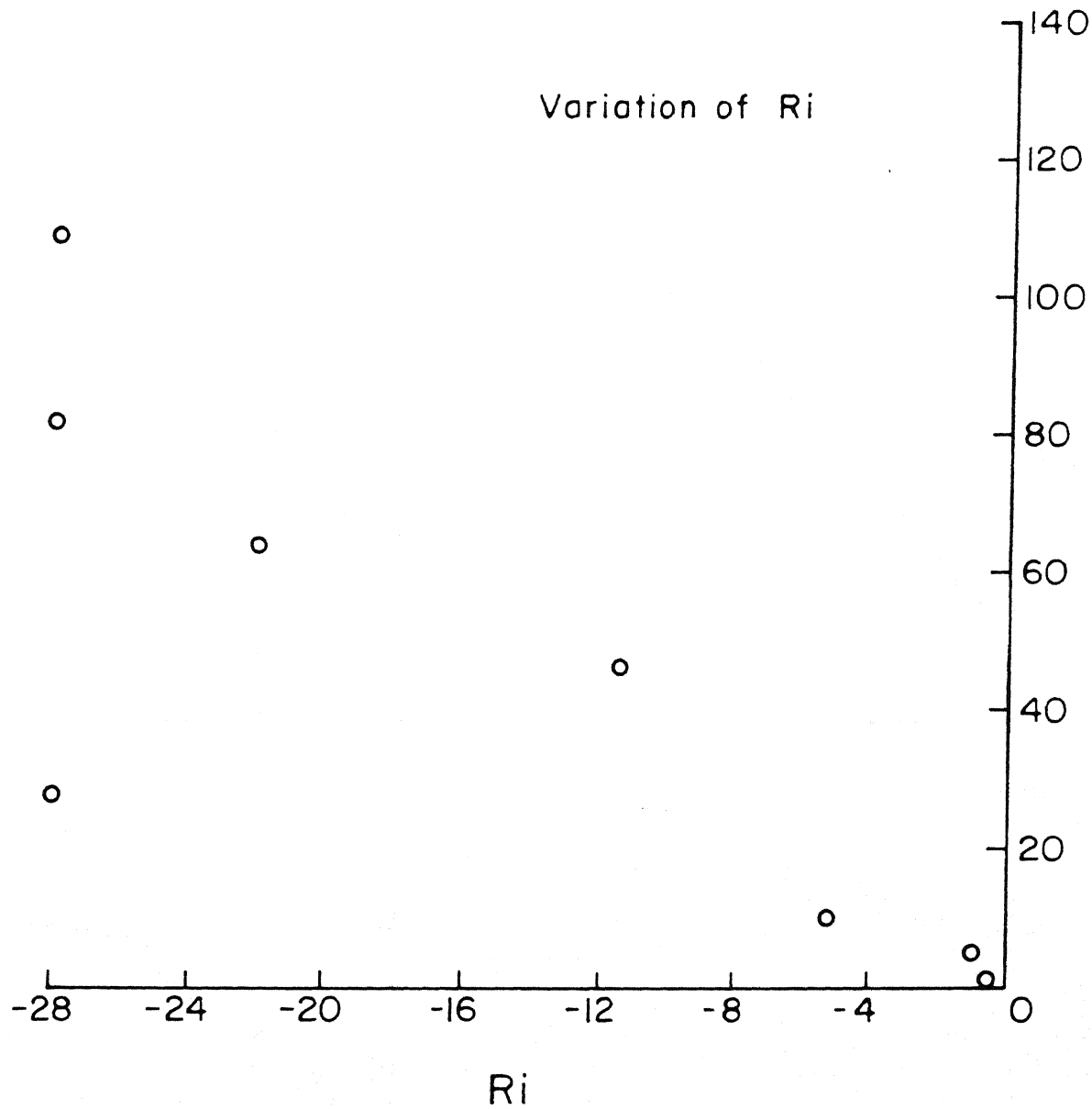

Fig. 1.4 Friction layer of earth's atmosphere

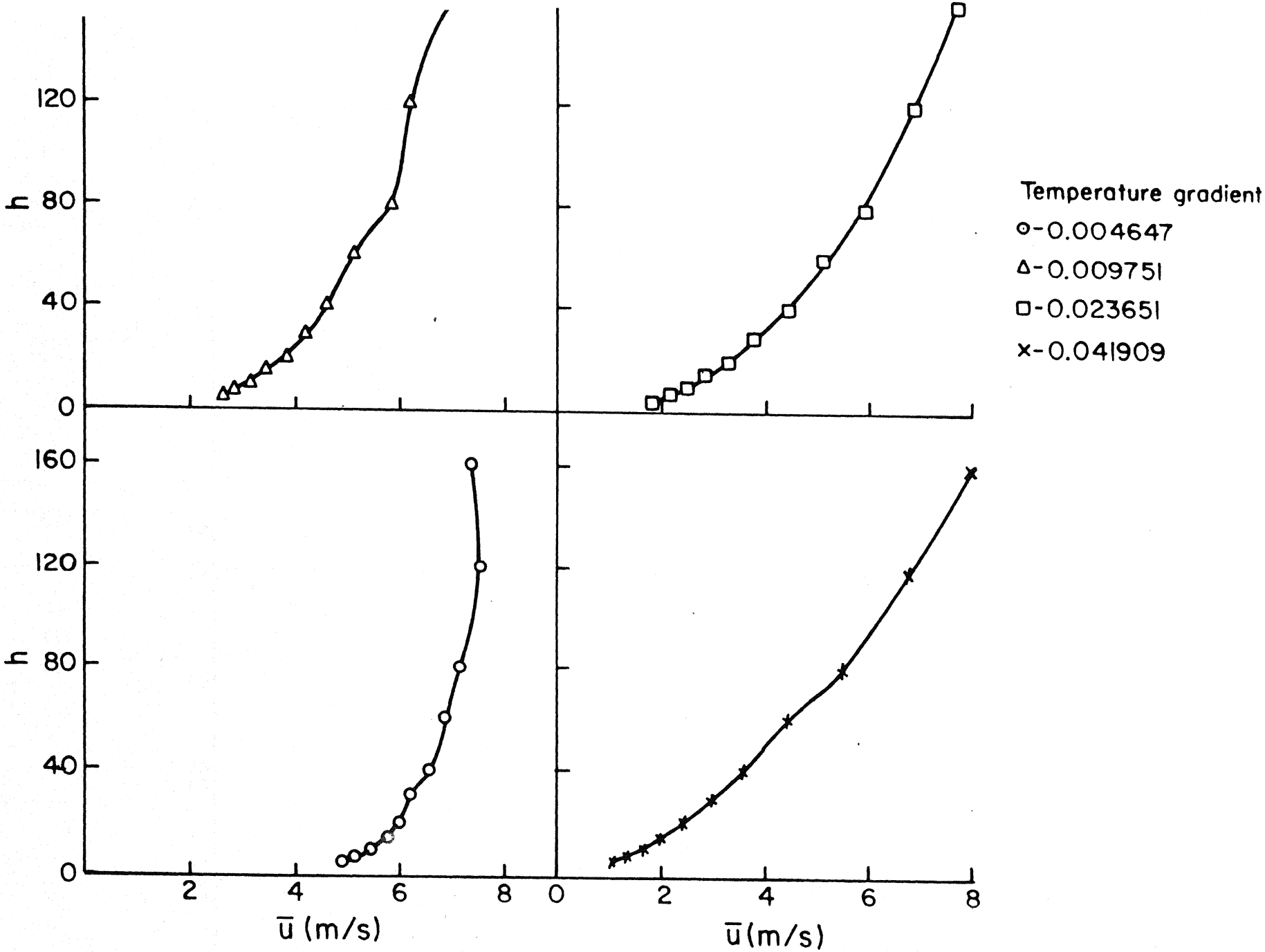
h
120
80
40
0
160
120
80
40
0
2
4
6
8
0
2
4
6
8
ū (m/s)
ū (m/s)
Temperature gradient
⊙-0.004647
Δ-0.009751
□-0.023651
×-0.041909

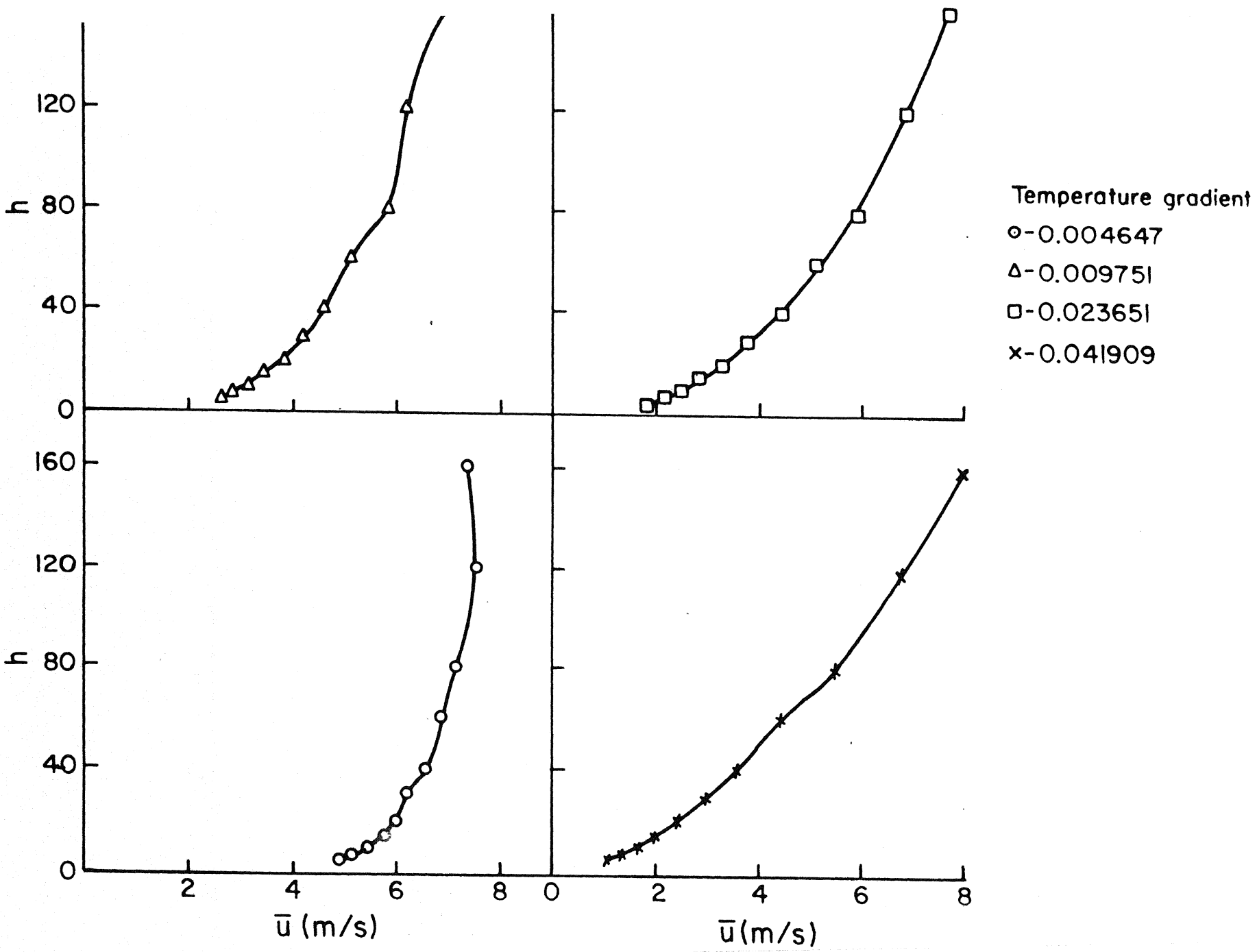
h
120
80
40
0
160
120
80
40
0
2
4
6
8
0
2
4
6
8
ū (m/s)
ū (m/s)
Temperature gradient
⊙-0.004647
Δ-0.009751
□-0.023651
×-0.041909

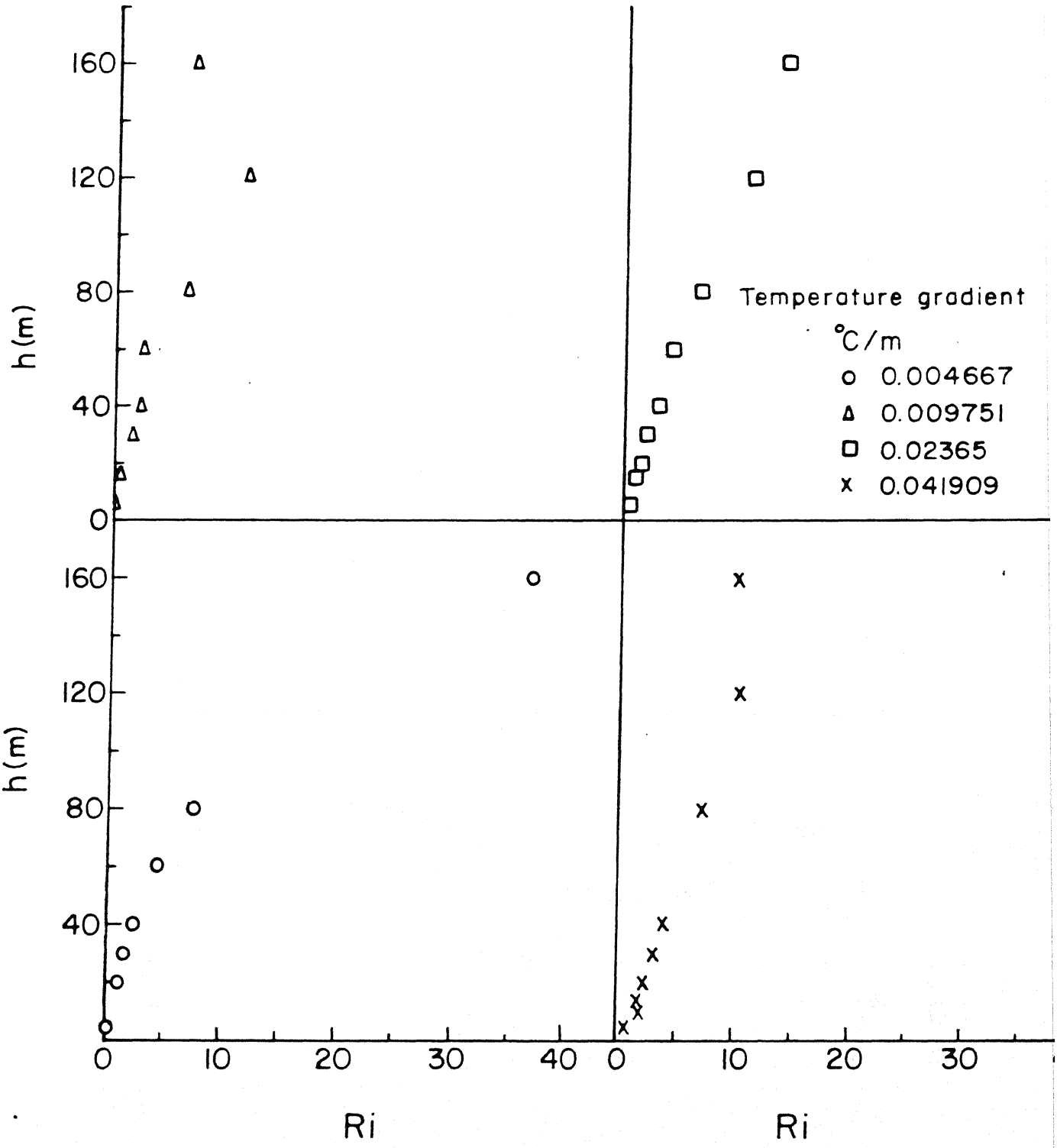

Fig 1.6 Effect of temperature gradient on Ri

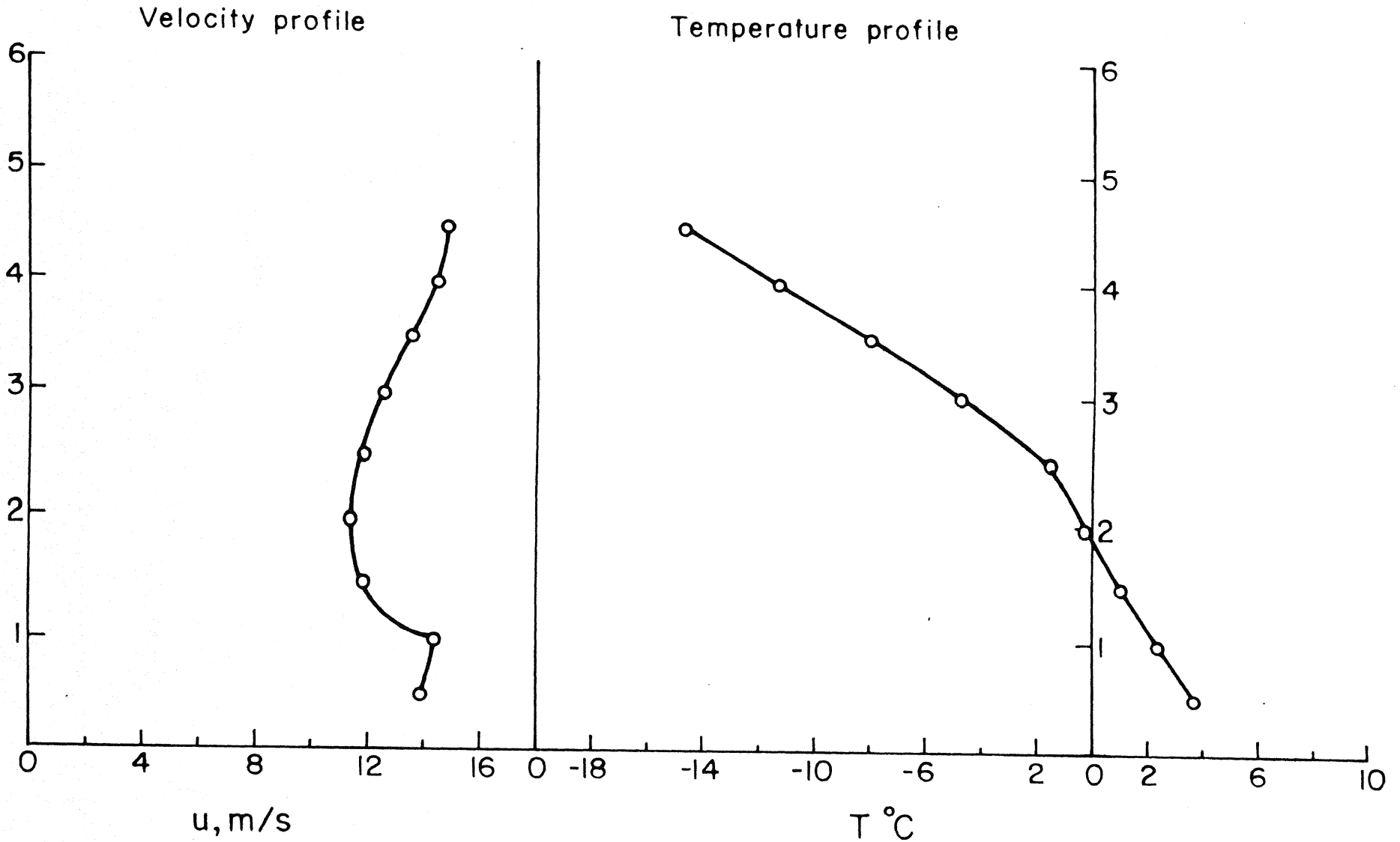
Velocity profile
Temperature profile
6
5
4
3
2
1
0
4
8
12
16
u, m/s
0
-18
-14
-10
-6
2
0
2
6
10
T °C

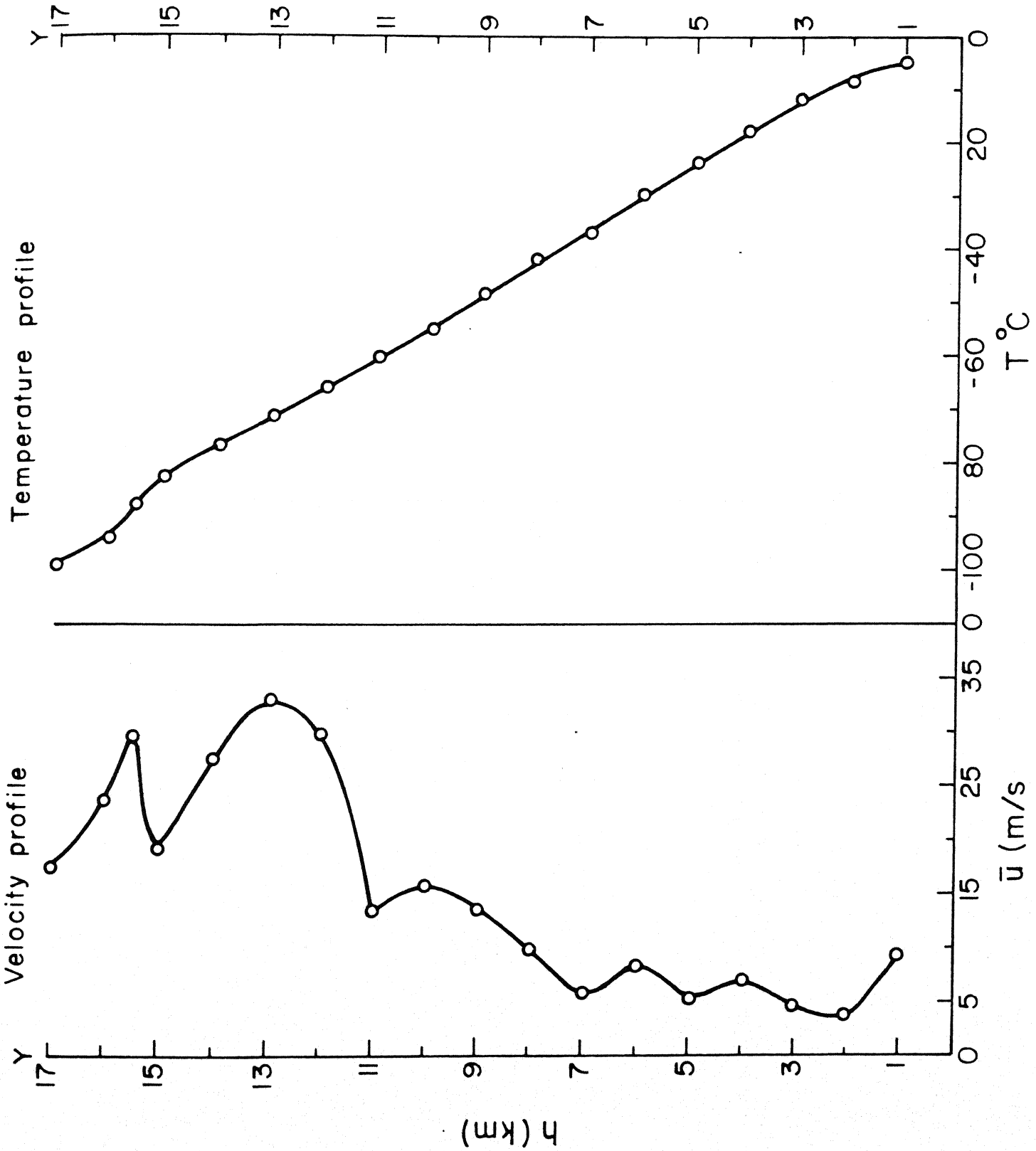

FIG 1.8 TROPOSPHERE (Winter)

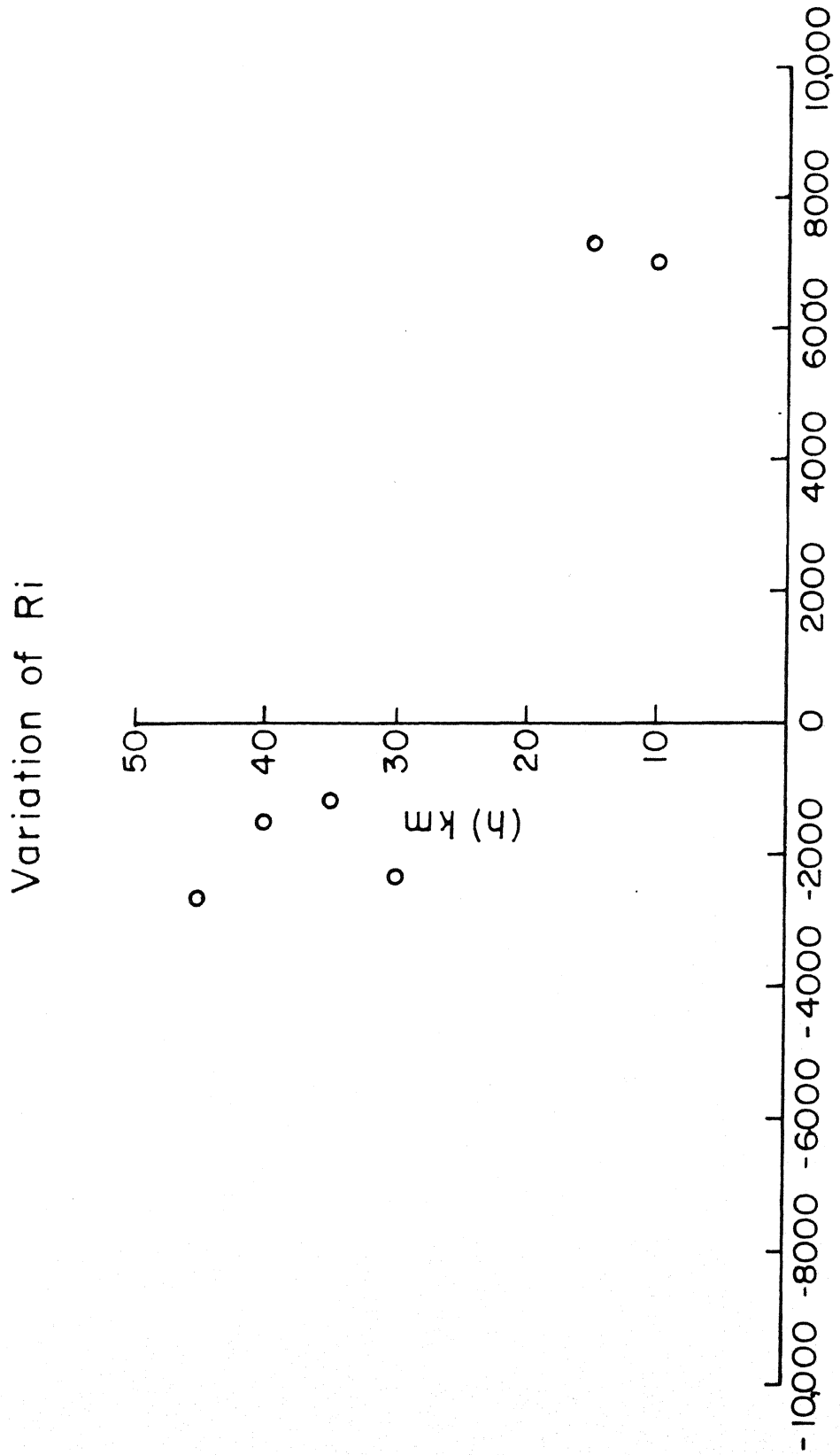

FIG. 1.9 TROPOSPHERE (Summer)

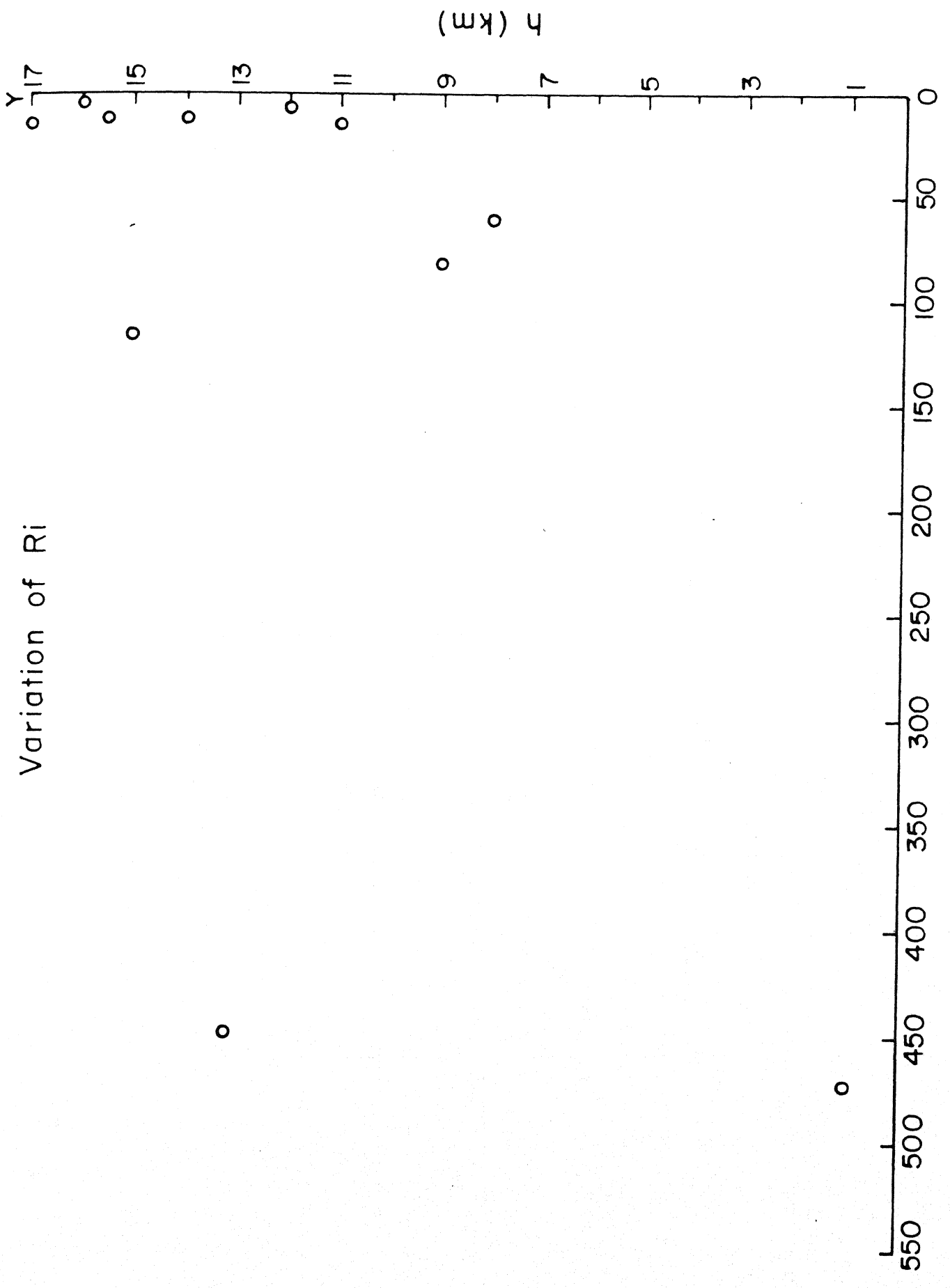

FIG.1.10 TROPOSPHERE (Winter)

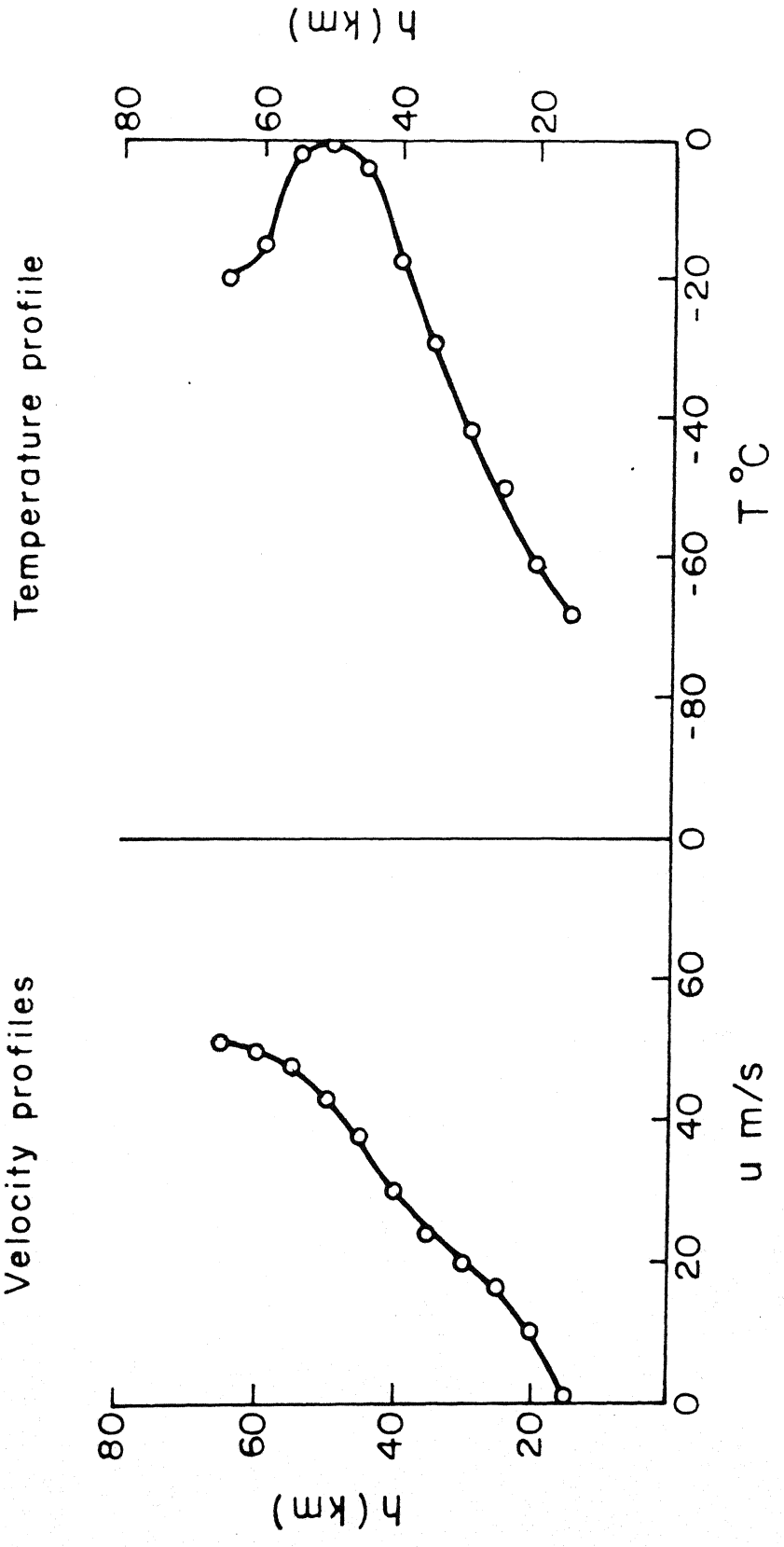

Fig. 1.11. STRATOSPHERE (SUMMER)

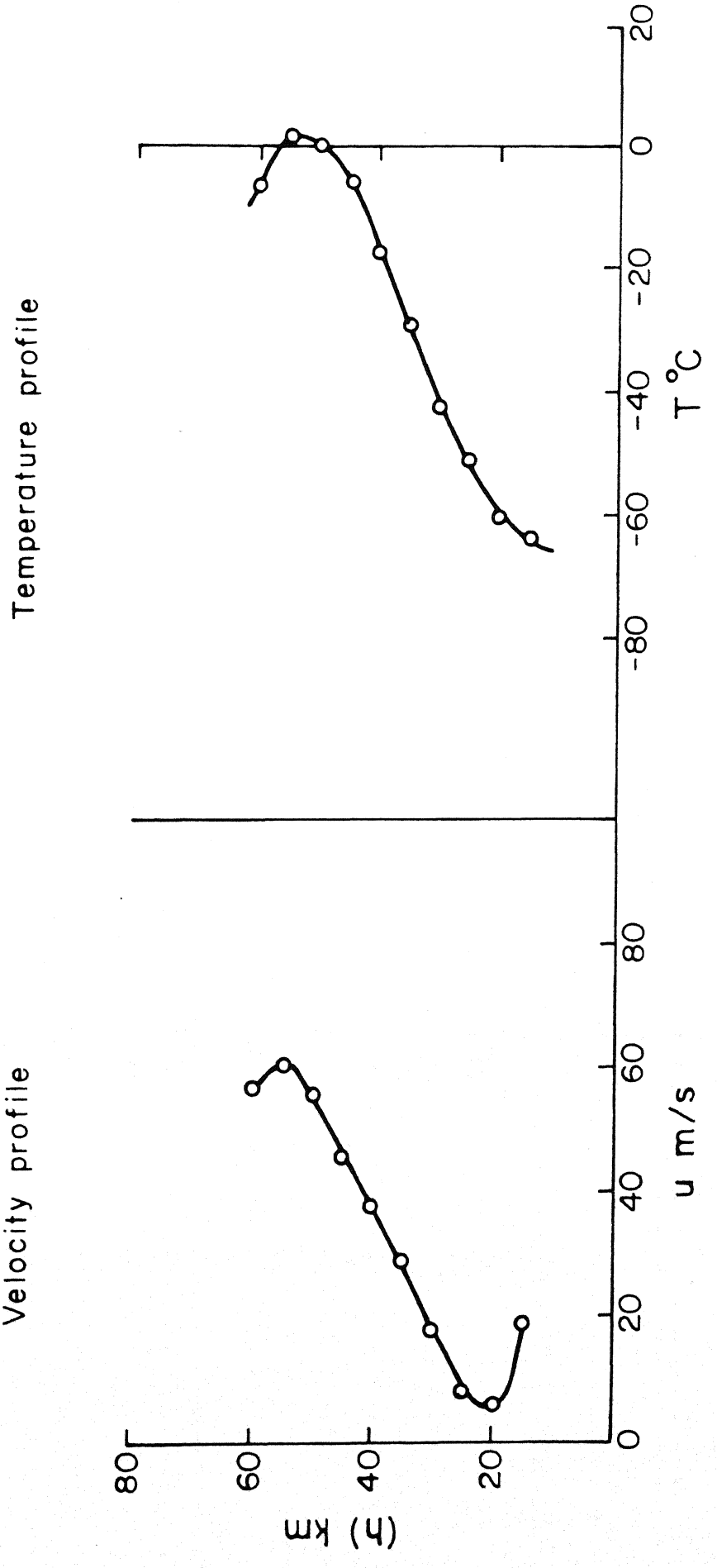

FIG. I.12 STRATOSPHERE (Winter)

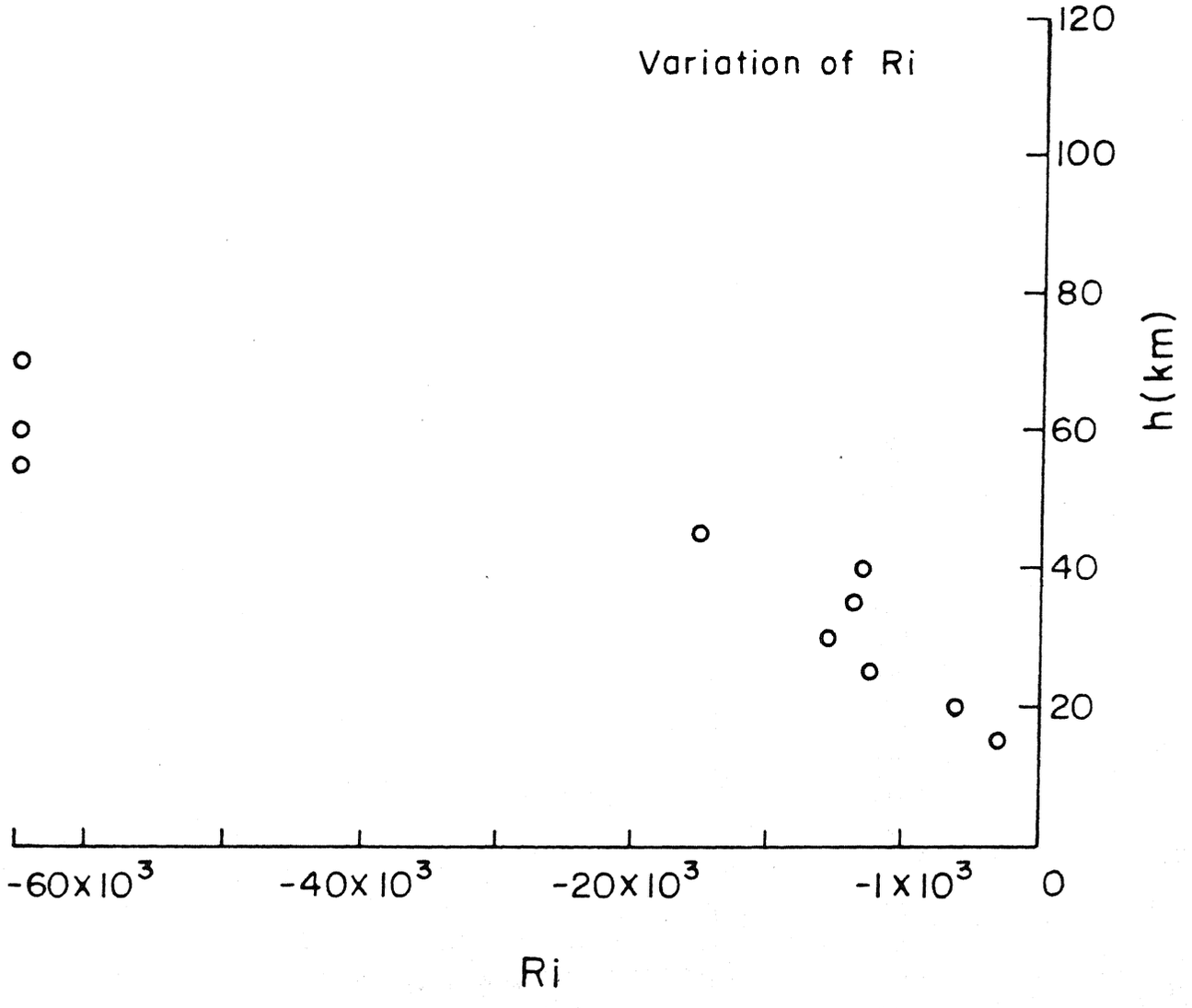

Fig. 1.13. STRATOSPHERE (SUMMER)

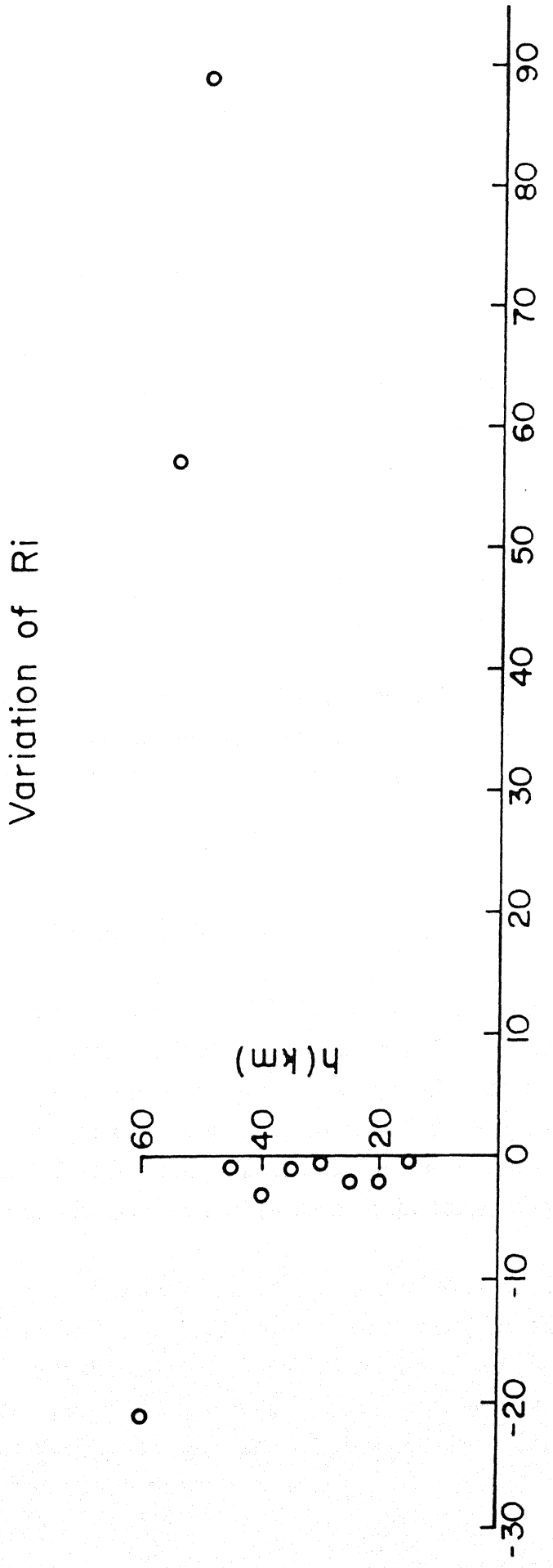

FIG. I.14 STRATOSPHERE (Winter)

DESIGN AND CONSTRUCTION OF TEST CELL

A test cell has been constructed in this study to simulate air streams under controlled laboratory conditions. The test cell resembles a wind tunnel except that its geometric scales are considerably smaller in proportion. The use of a wind tunnel gives an idea of fluid flow past a stationary object and evolution of certain flow patterns. The purpose of design of any wind tunnel is to achieve the required conditions for model and flow testing with minimum power consumption and at the smallest possible cost.

Wind tunnels are of two types. Subsonic and supersonic. The present experiment is concerned with subsonic flow. If incompressible flow is to be studied, the range of velocities for the subsonic wind tunnel is limited to a Mach number of 1/3.

Subsonic wind tunnels are classified as (i) open circuit, where air is not guided to return back to the tunnel, and (ii) closed circuit, where air from the exhaust is returned to the intake. Our test cell is of the open circuit type in which non–isothermal conditions prevail.

2.1. Design Considerations

In Chapter 1 we presented the velocity and temperature profiles prevailing in atmosphere at different altitudes. Producing a flow, whose velocity and temperature gradients equal those of atmosphere at a particular location, is difficult, because, the magnitude of these gradients is small. Any stratified flow generated in a test cell can model atmospheric flow if its Richardson number is equal to that prevailing in the atmosphere. In the present work, this has been used as the basis for design of the test cell.

The values of Richardson numbers prevailing in the friction layer and troposphere are relatively small when compared with those occurring in stratosphere. A large positive value of Richardson number denotes high stability of the flow and the flow can undergo transition and subsequent laminarization. Alternatively, a large negative value of Ri denotes high instability and growth of turbulence. But the values near zero will show characteristics appropriate for isothermal flow.

Generation of large Richardson number flows is difficult because they require mild velocity and large temperature gradients. Recall that the definition of Ri is,

$$\mathrm{Ri} = \frac{g}{\rho}\left(\frac{\partial \rho}{\partial y}\right) / \left(\frac{\partial u}{\partial y}\right)^2$$

In the present work we produce flows with relatively high value of Ri when compared to previous research work. We have designed a test cell to produce relatively mild velocity gradients. Two different theoretical solutions have been used in this study to estimate the velocity gradients.

2.1.1. FLOW DEVELOPMENT IN A PARALLEL–PLATE CHANNEL

Sparrow and Lin (1964) describe a method of analysis for developing laminar flow in the entrance regions of tubes and channels. They apply this analysis to tubes and parallel–plate channels and derive relations for velocity distribution. This relation for flow development in parallel–plate channel is used as an initial guess. The mathematical analysis of Sparrow and Lin (1964) is summarized below.

Navier stokes equations are linearized for following flow situation.

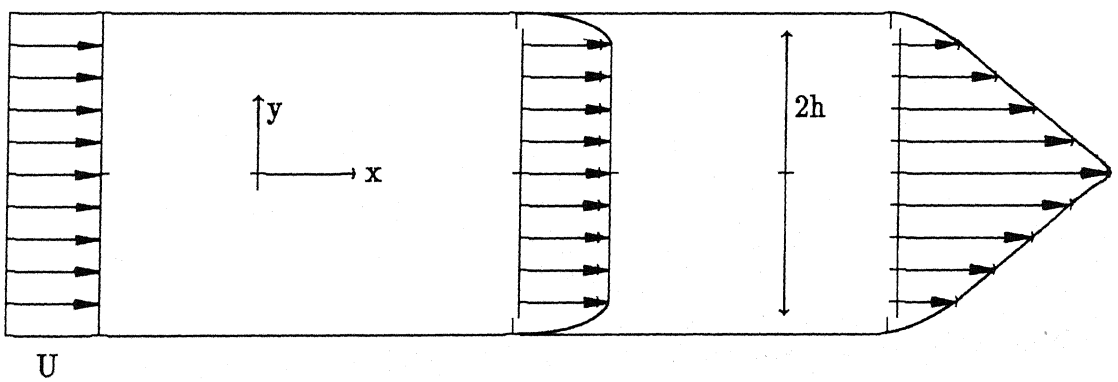

Let U be the magnitude of inflow velocity and h, the half–channel width. The Reynolds number is defined as Re = Uh/v.

$$u \cdot \frac{\partial u}{\partial x} + v \cdot \frac{\partial u}{\partial y} = -\frac{\partial p}{\partial x} + \frac{1}{\mathrm{Re}}\left(\frac{\partial^2 u}{\partial x^2} + \frac{\partial^2 u}{\partial y^2}\right) \qquad (2.1)$$

$$u \cdot \frac{\partial v}{\partial x} + v \cdot \frac{\partial v}{\partial y} = -\frac{\partial p}{\partial y} + \frac{1}{R_e}\left(\frac{\partial^2 v}{\partial x^2} + \frac{\partial^2 v}{\partial y^2}\right) \tag{2.2}$$

$$\frac{\partial u}{\partial x} + \frac{\partial v}{\partial y} = 0 \tag{2.3}$$

Where u and v are x and y components of velocity. Noting that the flow develops in boundary layers, and the rate of change of u in x direction is small, we can make following assumptions:

$$v << u \text{ and hence } \frac{\partial p}{\partial y} \cong 0,$$

$$\frac{\partial^2 u}{\partial x^2} << \frac{\partial^2 u}{\partial y^2}.$$

The reduced Navier–Stokes equations are,

$$u \cdot \frac{\partial u}{\partial x} + v \cdot \frac{\partial u}{\partial y} = -\frac{\partial p}{\partial x} + 1/R_e \cdot \frac{\partial^2 u}{\partial y^2} \tag{2.4}$$

$$\frac{\partial u}{\partial x} + \frac{\partial v}{\partial y} = 0$$

Non–linear inertial terms are linearized through approximation as,

$$u \cdot \frac{\partial u}{\partial x} + v \cdot \frac{\partial u}{\partial y} = \epsilon(x) \frac{\partial u}{\partial x} \tag{2.5}$$

defining a new co–ordinate x* known as stretched co–ordinate

$$\epsilon \, dx^* \longrightarrow dx$$

the left side of equation (2.4) becomes

$$\frac{\partial u}{\partial x^*} = -\frac{\partial p}{\partial x^*} + \frac{1}{R_e} \frac{\partial^2 u}{\partial y^2} \tag{2.6}$$

The equations are integrated to give a relation for velocity development in parallel–plate channel. This relation is,

$$\frac{u}{U} = 1.5\,(1-\eta^2) + \sum_{i=1}^{\infty} \frac{2}{\alpha_i^2}\left(\frac{\cos(\alpha_i \eta)}{\cos \alpha_i} - 1\right) e^{-(\alpha_i^2 X^*_i)} \tag{2.7}$$

where $\eta = y/h$, $X = \frac{x/h}{Uh/y}$, $X^* = \frac{x^*/h}{Uh/y}$

α_i, $i = 1 \rightarrow \infty$ are the eigen values and are roots of $\tan\alpha_i - \alpha_i = 0$.

The first 25 values of α_i are listed in Sparrow and Lin (1964). We wrote a program to calculate velocity profiles. The results are listed below.

X*	X	variation in u/U	variation in y/h
0.02	0.01	1.1819–1.1356	0.2–0.6
0.03	0.0175	1.2298–1.1846	0 – 0.5
0.05	0.035	1.3087–1.2468	0 – 0.5

The value of h used in this work is h = 4.8 cm.

We have $X = \frac{x/h}{Uh/\nu} \cdot \frac{\nu x}{Uh^2}$

ν at room temperature = 15.84×10^{-6} m^2/sec

Let U = 3 m/sec

$\Rightarrow$ Length of the channel, $x = \frac{Uh^2X}{\nu} = 4.35m$

It is possible to generate a ΔT of $10^\circ C$ in the Laboratory. So,

$\frac{\partial T}{\partial y} = \frac{\Delta T}{2h} = \frac{10}{2x4.8}$ °C/cm

$\frac{\partial u}{\partial y} = 0.01930 \frac{m/sec}{cm}$

Tm = 30

from the definition of Richardson number, $R_i = 9.76$

Hence the value of x=4.35m gives very small gradients (whose magnitude $|\frac{\partial u}{\partial y}|$ is less than $0.01930 \frac{m/sec}{cm}$). Owing to laboratory constraints this length is limited to 4m.

The above analysis is valid for two dimensional laminar flow through a channel. However, the flow prevailing in the laboratory test cell is 3–dimensional turbulent flow. Hence it is anticipated that these gradients will occur earlier than this length of 4m. Therefore, the above analysis gives the maximum length required to produce the mild velocity gradients.

2.1.2. TWO DIMENSIONAL CIRCULAR WAKE

Schlichting (1960) has given the analytical solution for flow in a two dimensional wake behind a circular cylinder. This solution is given below.

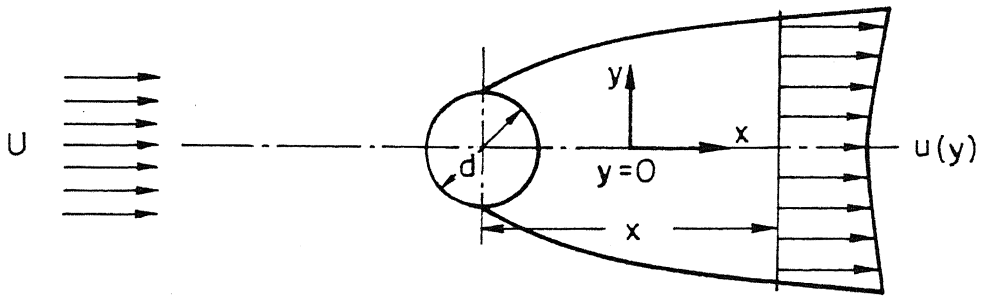

Let ,

velocity defect ul = U − umin.

width of the wake $b = 3.18\ B\sqrt{(x\ C\ d)}$,

where C and B are constants

C = 0.8

B = 0.18

x = down stream distance from cylinder center.

d = diameter of the cylinder

U = free stream velocity

umin = velocity of the fluid at distance x on the cylinder axis.

Then,

$$ul = U\left[\frac{3.18}{18\ B}\left[\frac{x}{C\ d}\right]^{-1/2}\left[1-\left[\frac{y}{b}\right]^{3/2}\right]^{2}\right]$$

valid for $\frac{x}{C\ d} > 50.$

The velocity gradient of the wake at given value of x is given by

$$\frac{\partial u}{\partial y} = \frac{ul\ (at\ y \equiv 0)}{b/2}$$

$$ul\ (at\ y \equiv 0) = \frac{U\ 3.18}{3.24}\ K^{-1/2}$$

where $K = \frac{x}{C\ d}$

and $b = 0.56921\ C\ d\ K^{1/2}$

$$\frac{\partial u}{\partial y} = 6.692 \frac{U}{C\ K\ d}$$

The average temperature gradient in the test cell is

$$\frac{\partial T}{\partial y} = \frac{T_t - T_b}{b}$$

where T_t = temperature of the fluid at the top of wake
T_b = temperature of the fluid at the bottom of wake

The potential temperature gradient is related to the average temperature gradient by,

$$\frac{\partial T_p}{\partial y} = \frac{\partial T}{\partial y} + ALR$$
$$\cong \frac{\partial T}{\partial y}$$

where ALR, Adiabatic Lapse Rate = $0.0098^{\circ}C/m$

It is possible to generate $\Delta T \cong 10^{\circ}C$ in the laboratory. From the definition of Richardson number given earlier, we obtain the following.

Let, $T_m = 35C$ and $\Delta T = 10^{\circ}C$. h, the half channel width of the test cell is 4.8 cm, as stated earlier.

$$R_i = 0.11 \frac{C\ K^{3/2} d}{U^2}, \text{ for the wake of a cylinder}$$

In terms of x,

$$R_i = 0.11 \frac{x^{3/2}}{|C\ d|^{1/2}\ U^2}$$

given C = 0.8,

$$R_i = 0.123 \frac{x^{3/2}}{d^{1/2}\ U^2}$$

For, d = 0.01 m and U = 3 m/sec,

$$R_i = 0.0137 \frac{x^{3/2}}{d^{1/2}}$$

At x = 3.5 m, the wake width is 9.5 cm, the size of the test cell. The theoretical value of R_i is prevailing in the core of the test cell at x = 3.5 m is 0.897. Hence, with the cylinder as the turbulence generator, we have $0 < x < 3.5\ m \Rightarrow 0 < R_i < 0.897$.

We summarize the salient features of the test cell below.

* Length of the wind tunnel = 4.0m
* cross section of wind tunnel = 9.6cm X 5.0cm

2.2. Description of Our Test Cell

According to the classification of wind tunnels our test cell is classified as Open Circuit, Subsonic and Non–isothermal. Fig. 2.1 and Fig. 2.2 show the over all view of the test cell.

The major parts of the test cell are,

Entrance Cone containing honey comb and filter
Differential Heating Window
Flow perturbation section including placement of objects
Measurement section
Diverging Adapter
Centrifugal Blower
Traversing Mechanism.

HONEY COMB :

In paper of Loehrke and Nagib (1976) honey combs are represented as operators to suppress the level of free stream turbulence that comes as input flow to the honey comb. The transverse component of velocity is suppressed and this component is absent in the flow reaching the exit of the honey comb cell. They observe the growth of shear instability and subsequent randomization of eddies leading to the turbulence generation at the lips of adjacent honeycomb cells. However this high frequency vigorous turbulence decays rapidly with distance resulting in a net suppression of free stream turbulence by honeycombs. The shorter length honeycomb has the advantage of small pressure drop and less turbulence generation by shear layer instability.

The honeycomb used in this study has overall dimensions of 260mm X 160mm X 55mm. Plastic circular straws are used as cells. The diameter of each cell is 3.5mm. Fig 2.3 shows the sketch of honey comb.

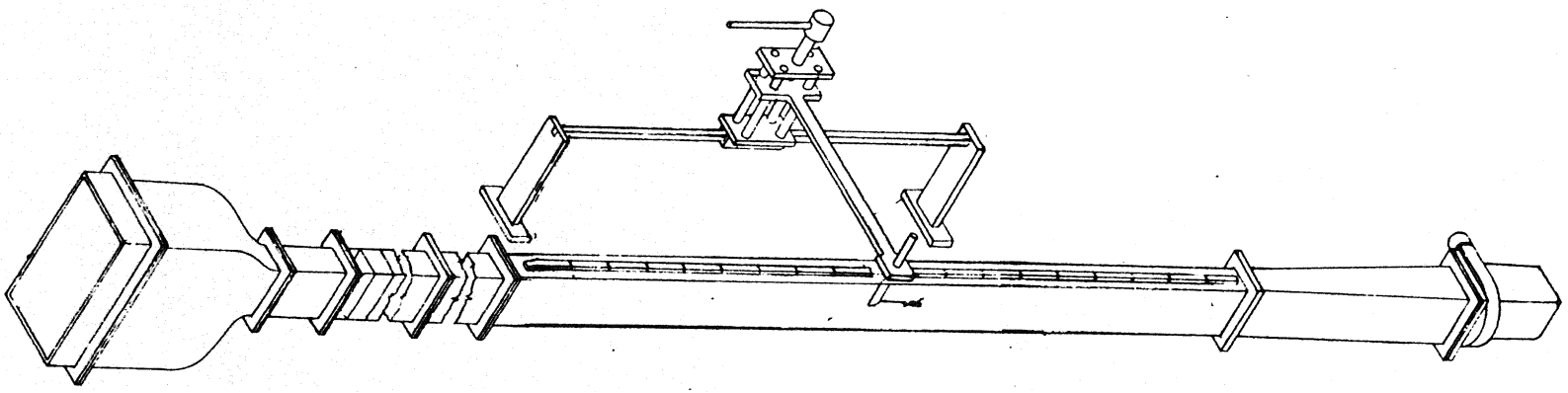

Fig. 2.1. TEST CELL

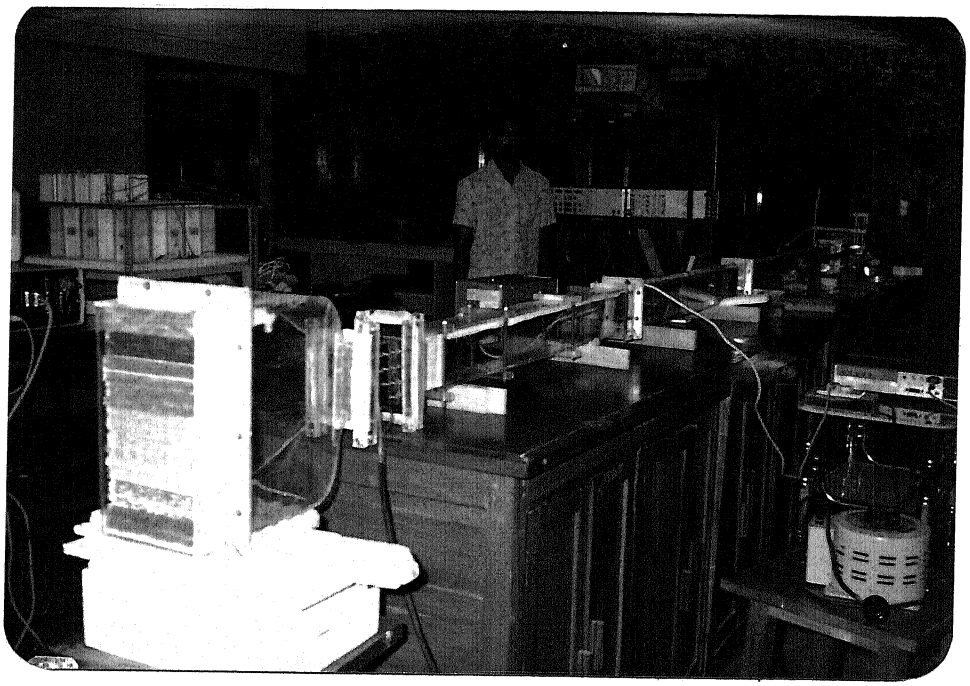

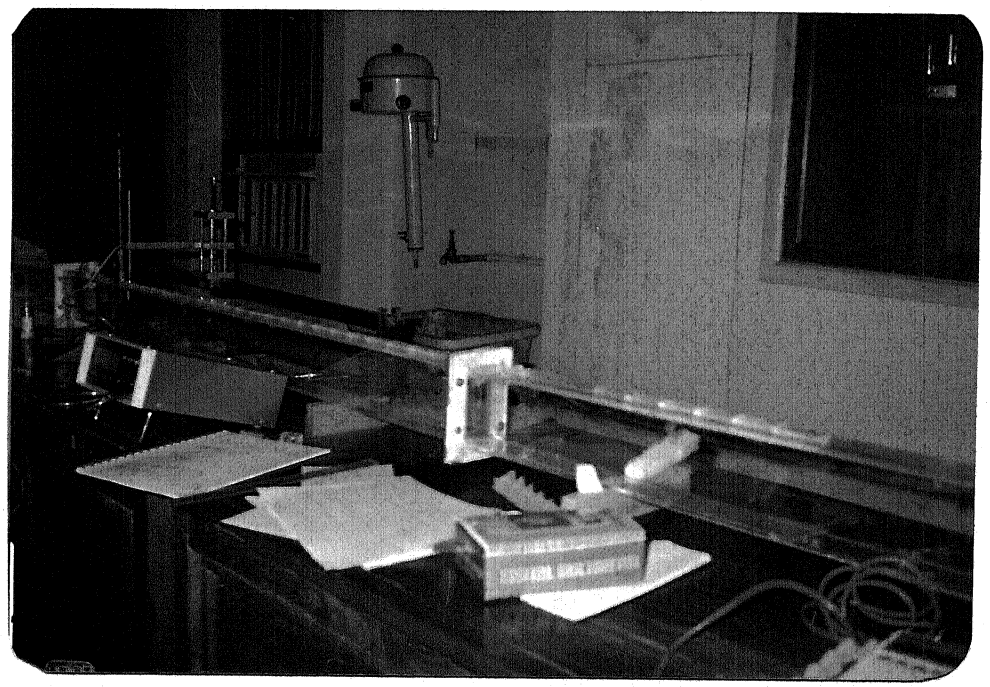

Test Cell

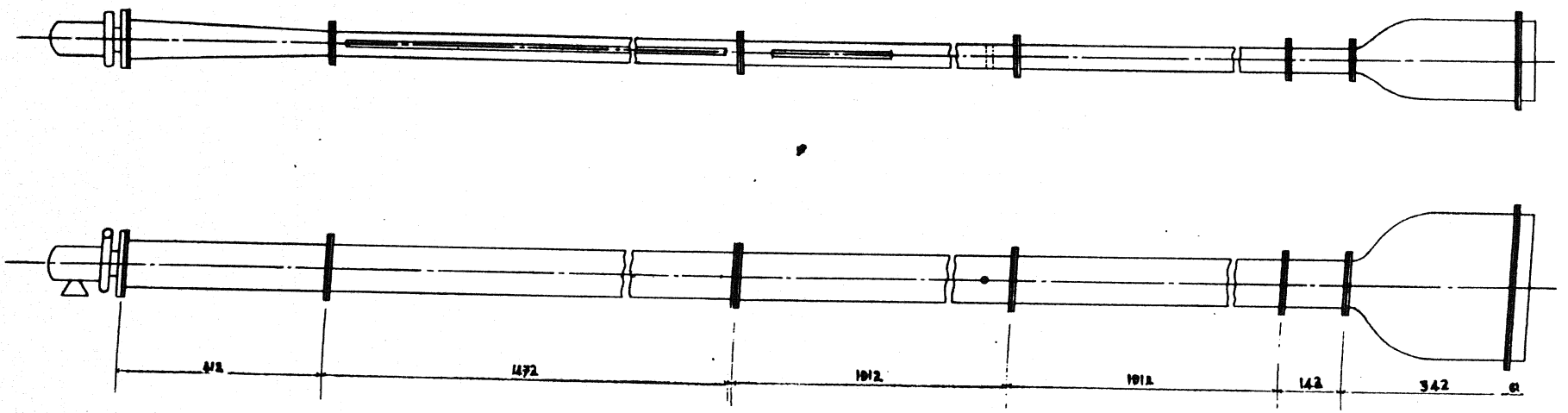

Fig. 2.2. TEST CELL

ALL DIMENSIONS ARE IN MM

SCALE: 1:3

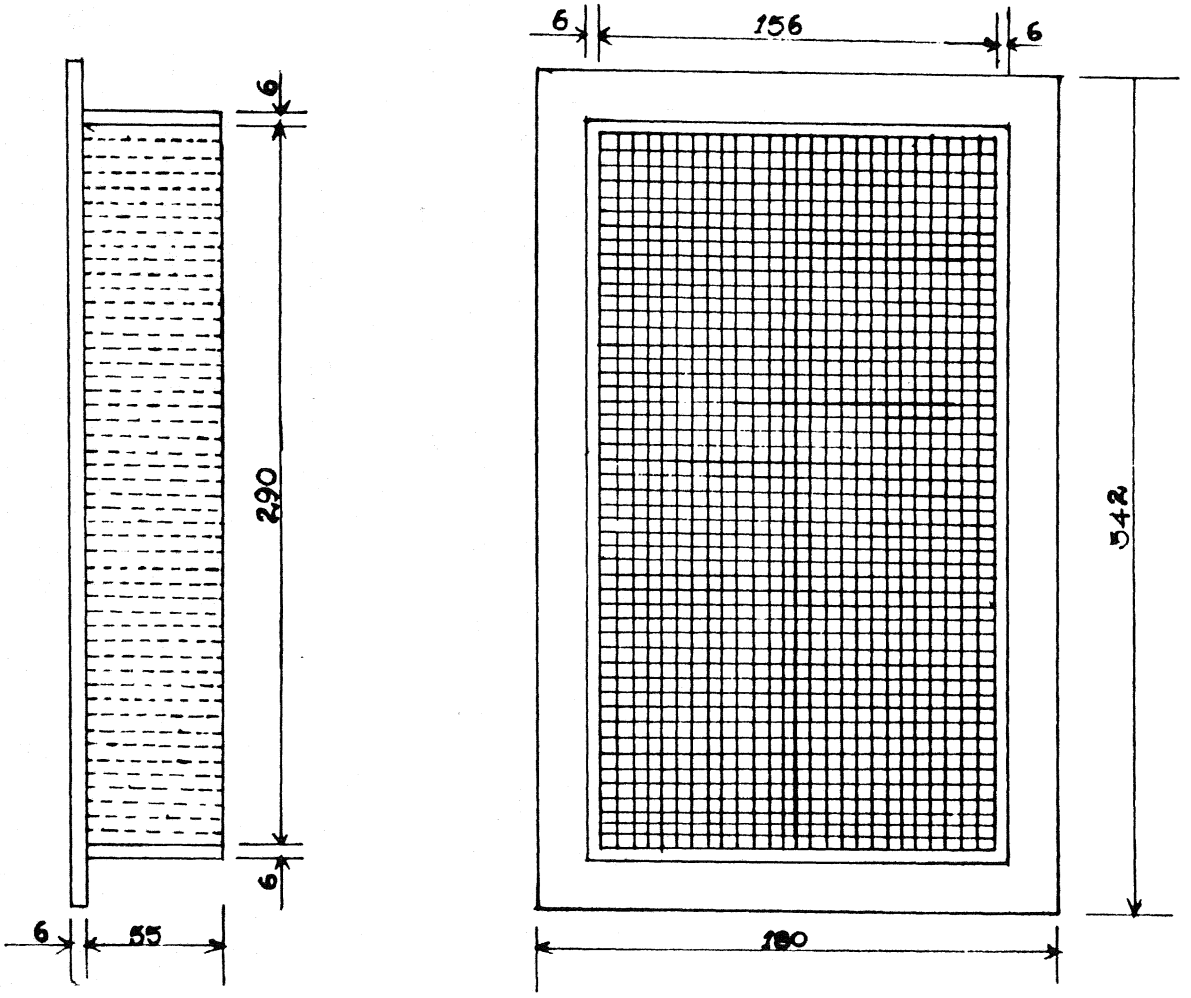

FIG. 2.8 HONEY COMB

FILTER :

The level, structure and decay of turbulence can be modified by altering the shear layers and their instabilities. This is possible if a fine mesh screen is placed at close proximity downstream of the honeycomb. From the point of optimum performance, the combination of honeycomb and fine mesh screen placed downstream of honeycomb is suitable for turbulence suppression. A sequence of a honeycomb, a mesh close to it and one farther away can be used in combination to produce adjustable turbulence levels in a test cell. We have used a fine mesh of specification 100 as a filter.

ENTRANCE CONE :

The entrance cone can be divided into two parts, Settling chamber and Contraction cone. Fig. 2.4 shows the two parts.

The flow from filter enters the settling chamber and becomes stable before entering into the contraction cone. The small eddies formed by screen and honeycomb die gradually.

Contraction cone: Flow from settling chamber enters into gradually converging cone which decreases the free stream turbulence and increases the velocity. Dryden (1940) constructed a wind with contraction cone at National Bureau of Standards, Wshington D.C. Schaubaner and Skranstad (1940) designed a contraction for wind tunnel and found satisfactory results. They suggested a value of contraction ratio of 6 to 8. Their experiments produced a flow with a turbulence level of 0.02%. Fig. 2.4. shows the details of contraction cone.

$$\text{Contraction ratio} = \frac{A_1}{A_2}$$

Where

A_1 = area of the contraction cone at the entrance.

A_2 = area of the contraction cone at the exit.

In the present work

A_1 = 291mm X 156mm

A_2 = 96mm X 50mm

Hence, contraction ratio = 9.4575.

ALL DIMENSIONS ARE IN MM

SCALE : 1:5

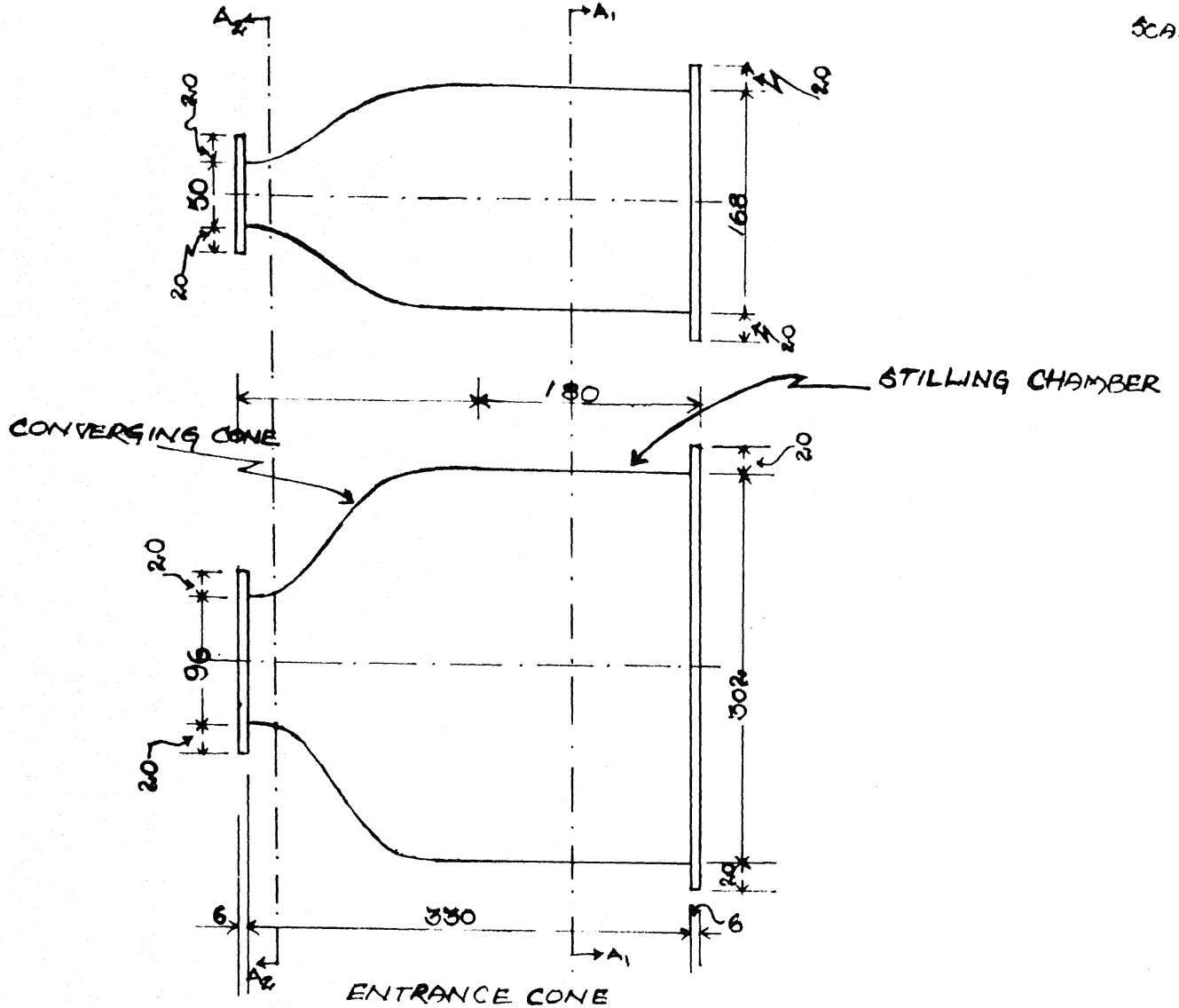

FIG. 2. 4

DIFFERENTIAL HEATING WINDOW :

Figure 2.5. shows the sketch of the differential heating window. It is placed in the tunnel to produce thermally stratified flows. The arrangement of heating wires is shown in Fig. 2.5. The number of wires decrease from the top to the bottom of the window. All the heater wires are connected in series and so the same current flows through all the wires. Thus the temperature of fluid varies in the vertical direction, being more at the top and less at the bottom.

The dimensions of Window are,

Cross section = 96mm X 50mm.

Length = 120mm.

Specifications of the wire :

Resistance of wire = 1.5 ohms. (R)

Max. allowable current = 5A. (i)

Determination of number of Wires :

Max. power dissipated per wire $= i^2 R$

$= 5^2 \, 1.5 = 37.5$ watts.

The total height of the window is divided into four boxes.

Height of each box = 24mm

Cross sectional area of each box = 24mm X 50mm

$= 1200mm^2 = 0.0012m^2$

Max. allowable velocity = 5m/sec.

Ambient air temperature = 25 C

Convective heat transfer coefficient = 75 $w/m^2 \, ^\circ C$

Max. temperature allowed = 50 $^\circ C$

Let number of wires = n

Total power dissipated = n·37.5 watts.

Assuming no losses

heat dissipated = change in internal energy of air

Mass flow rate of air = density · area of C.S. · velocity

$= 1.137 \cdot 0.0012 \cdot 5$

$= 0.006822$ Kg/sec.

Change in internal energy of air $= m' \cdot Cp \cdot \Delta T$

$= 0.006822 \cdot 1007 \cdot 25$

$= 174.75$ watts.

FIG 2. 5 DIFFERENTIAL HEATING WINDOW

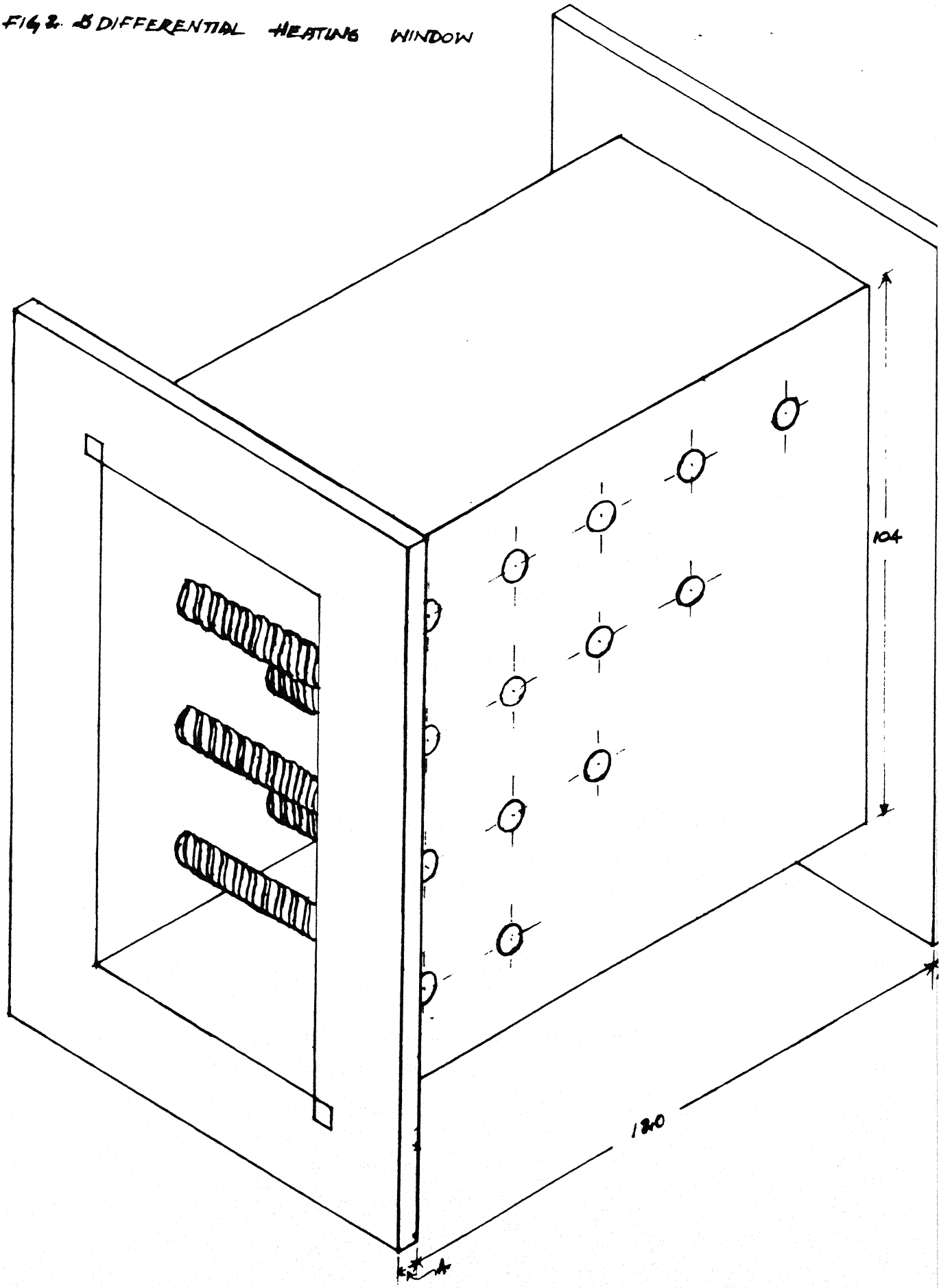

$$n \cdot 37.5 = 174.75$$
$$n = 4.66$$

Hence, we require 5 heater wires for a maximum temperature rise of 50°C.

Considering the above calculations as a guide line, a total of 14 pieces of heating wire are used and arranged as shown in Fig. 2.5. The performance of heater for various velocities is shown in Table 2.1.

FLOW PERTURBATION SECTION :

The first one meter length of the test cell beyond the heating window is named as flow perturbation section. Fig. 2.6. shows various parts of this section. It has a detachable top plate. This provision is made in this section to insert flow modifying honeycombs. A small honey comb of size 96mm X 50mm X 50mm is inserted at the entrance of the this section to suppress the turbulence generated by heater wires.

A honeycomb of varying length is placed at the exit of the section to produce shear flows. The dimensions and shape of this shear honeycomb are given in Fig. 2.7.

SHAPED HONEYCOMB :

Kotansky (1966) proposed the use of shaped honeycombs to produce shear flow. Lee and Ahamed (1988) experimentally verified the use of shaped honeycombs. They proposed the following formula to calculate the shape of the honeycomb.

$$L(y) = \frac{D}{4\,f}\left| \frac{K}{1/2\ \rho\ U(y)^2} - 1 - \frac{v^2(0,y)}{U(y)^2} \right|$$

where,

K = constant (its value depends on wind tunnel)
D = Width of the tunnel
f = friction factor ($0.0073 < f < 0.0082$)
ρ = density of air
v(0,y) = lateral velocity component
U(y) = required velocity profile

ALL DIMENSIONS ARE IN MM

SCALE : 1:5

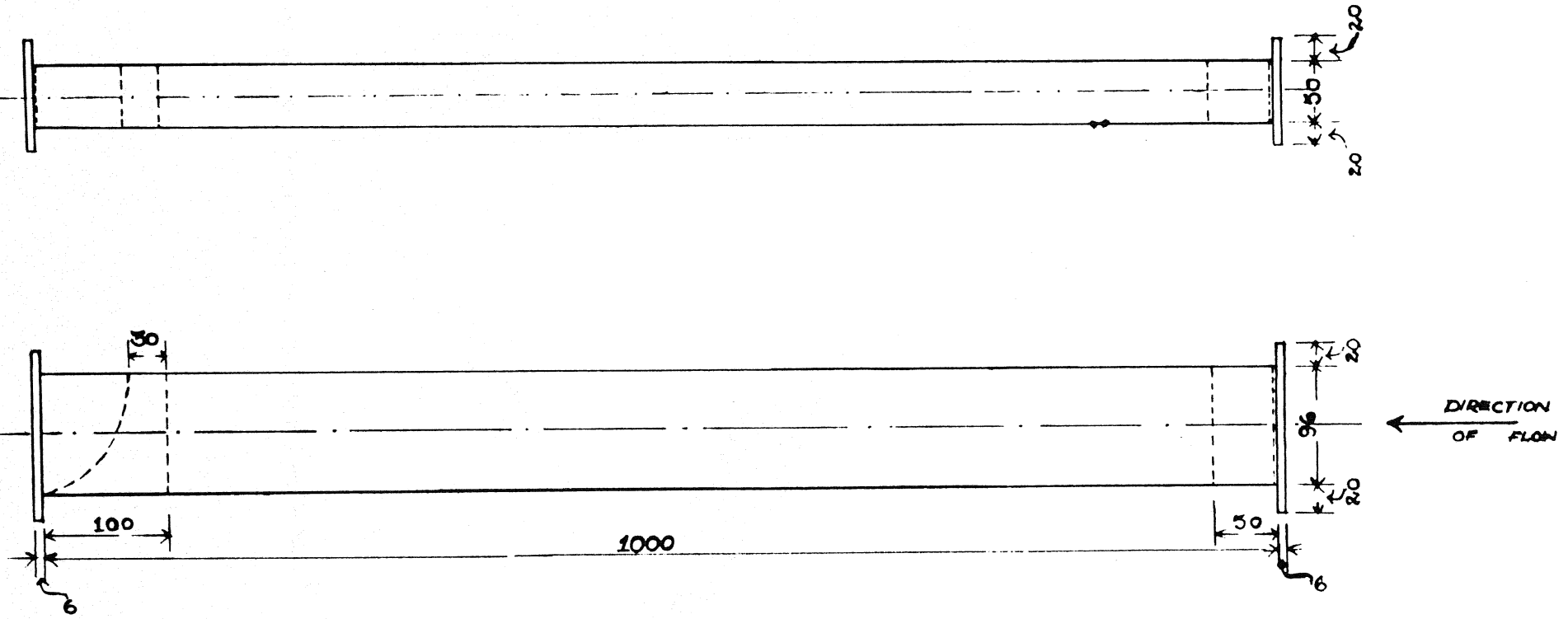

FIG. 2.6 FLOW PERTURBATION SECTION

ALL DIMENSIONS ARE IN MM

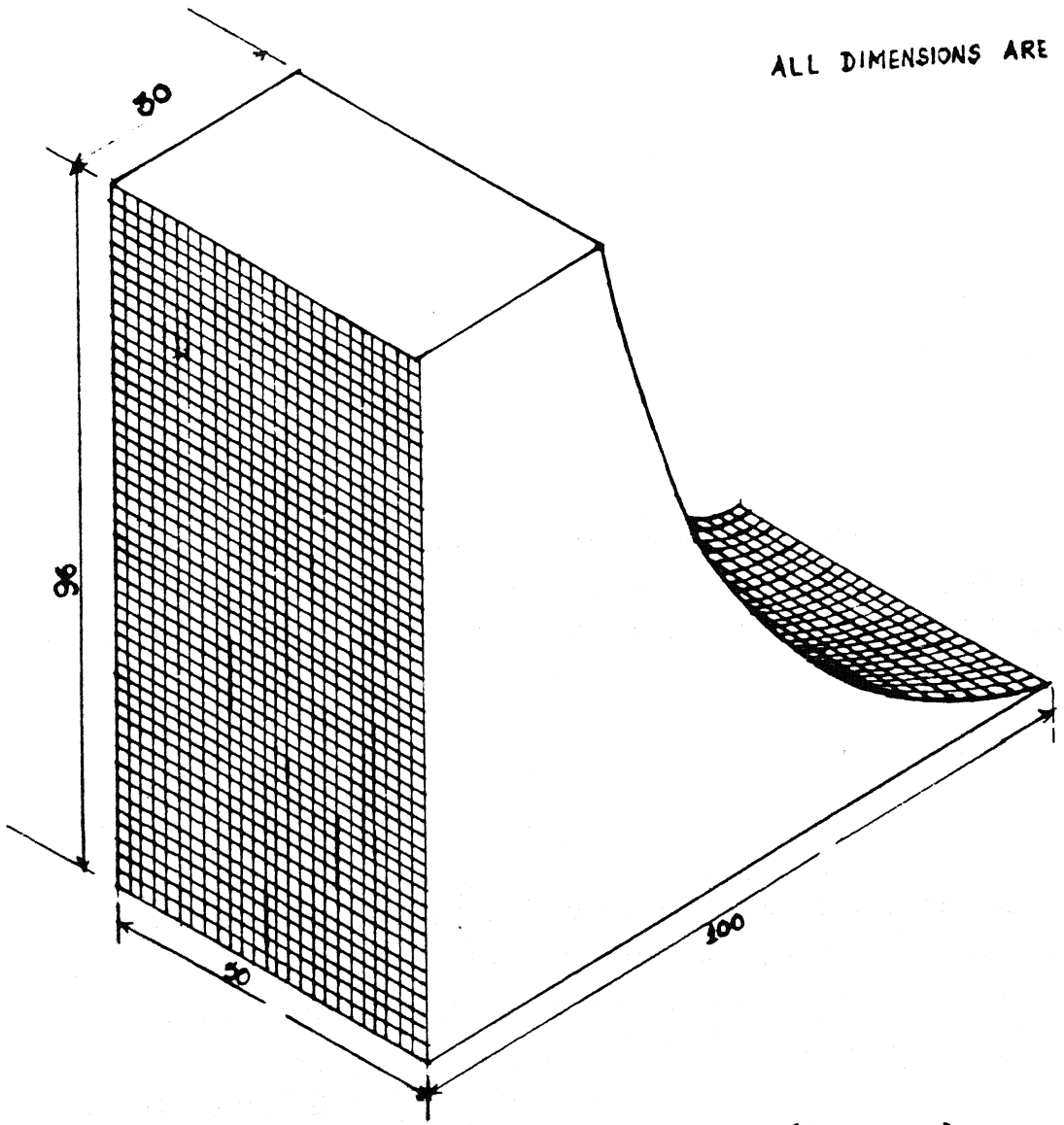

FIG. 2. PROFILED HONEY COMB (PARABOLIC)

The value if v(0,y) is very small compared with U(y), and the value of v^2/U^2 can be neglected. Therefore the length profile of the honeycomb is inversely proportional to square of velocity profile. For linear velocity profile, the length profile of the honeycomb will be proportional to square of the distance. We prepared two parabolic shaped honey combs to produce linear shear flows. The specifications of these two are given below.

Profile $L(y) = K\, y^2 + C$

K1= 0.076, C1 = 3.0

K2= 0.054, C2 = 5.0 (y and L(y) are in cms.)

OBJECT PLACEMENT SECTION :

The second part of the wind tunnel is intended for object placement. Fig. 2.8. shows this section and the object location. The orientation of the object (eg., cylinder) is such that the wake behind it experiences shear in the transverse direction. The flow is uniform parallel to the object axis.

A perspex cylinder of dia 10mm is used as flow obstacle. The total distance between the object axis and the first measuring station is 27cm. This gives an initial x/d ratio of 27, and for the cylinder. This distance is large enough to destroy formation of organized structures in the flow, but perhaps, not large enough for turbulence to have reached dynamic equilibrium.

MEASUREMENT SECTION :

This is an important part of the wind tunnel since measurements are made here. Fig. 2.9. shows a drawing of this section. A narrow slot of 10mm width is made on the top of this channel to insert and traverse the hot wire probe.

DIVERGING ADAPTER :

It is prepared to join the wind tunnel with the blower opening. Since the dimensions of the blower opening are slightly greater than the channel dimensions, we fabricated a diverging section with small angle of divergence. The divergence angle of the diffuser is 2.14 degrees. It is provided with a plate which has a hole of contour identical to the blower opening.

ALL DIMENSIONS ARE IN MM

SCALE : 1:5

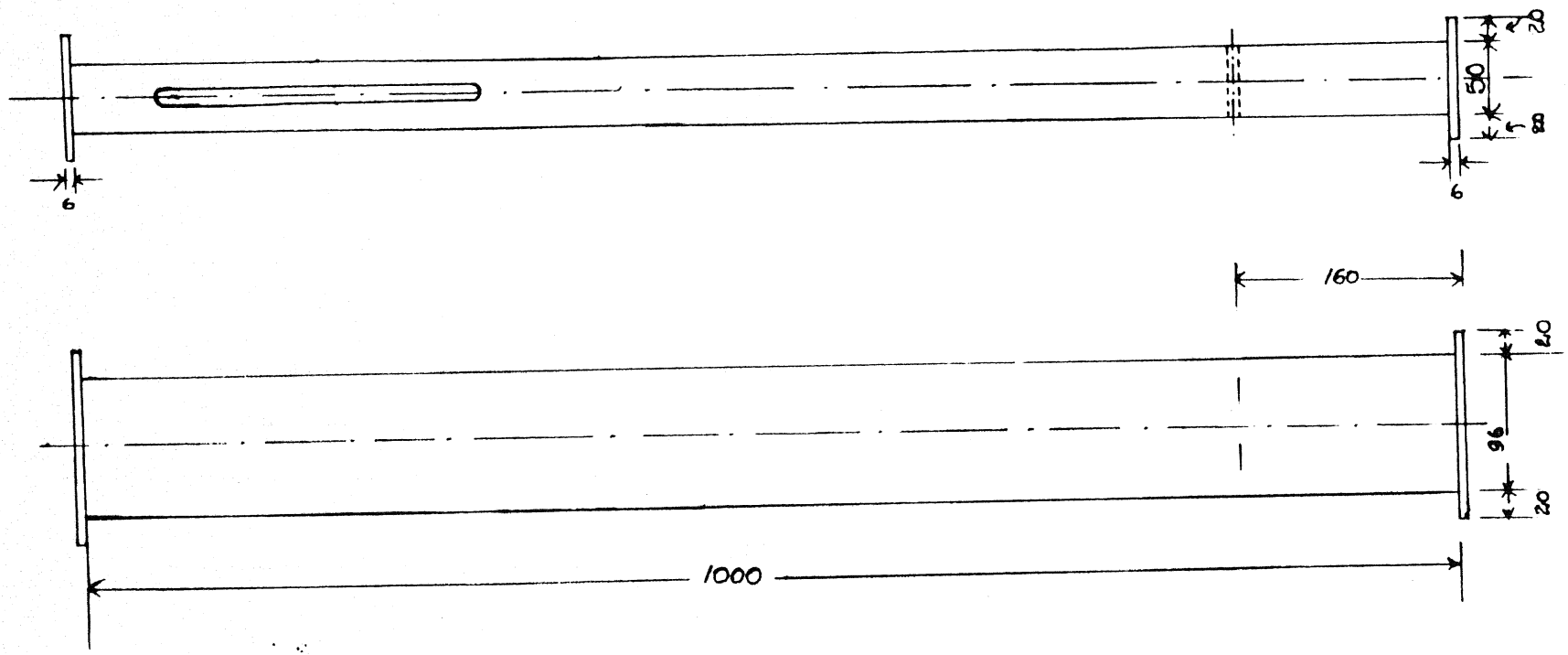

FIG. 2 & 3 OBJECT PLACEMENT SECTION

ALL DIMENSIONS ARE IN

SCALE : 1:6

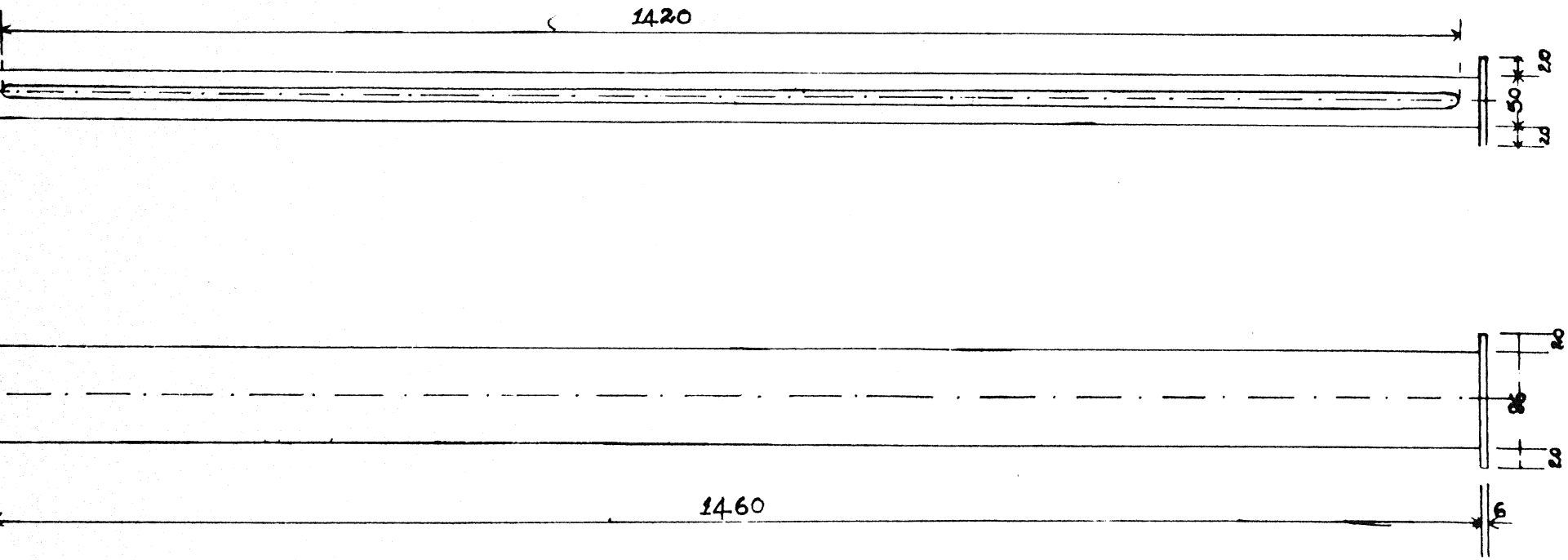

FIG. 2 MEASUREMENT SECTION

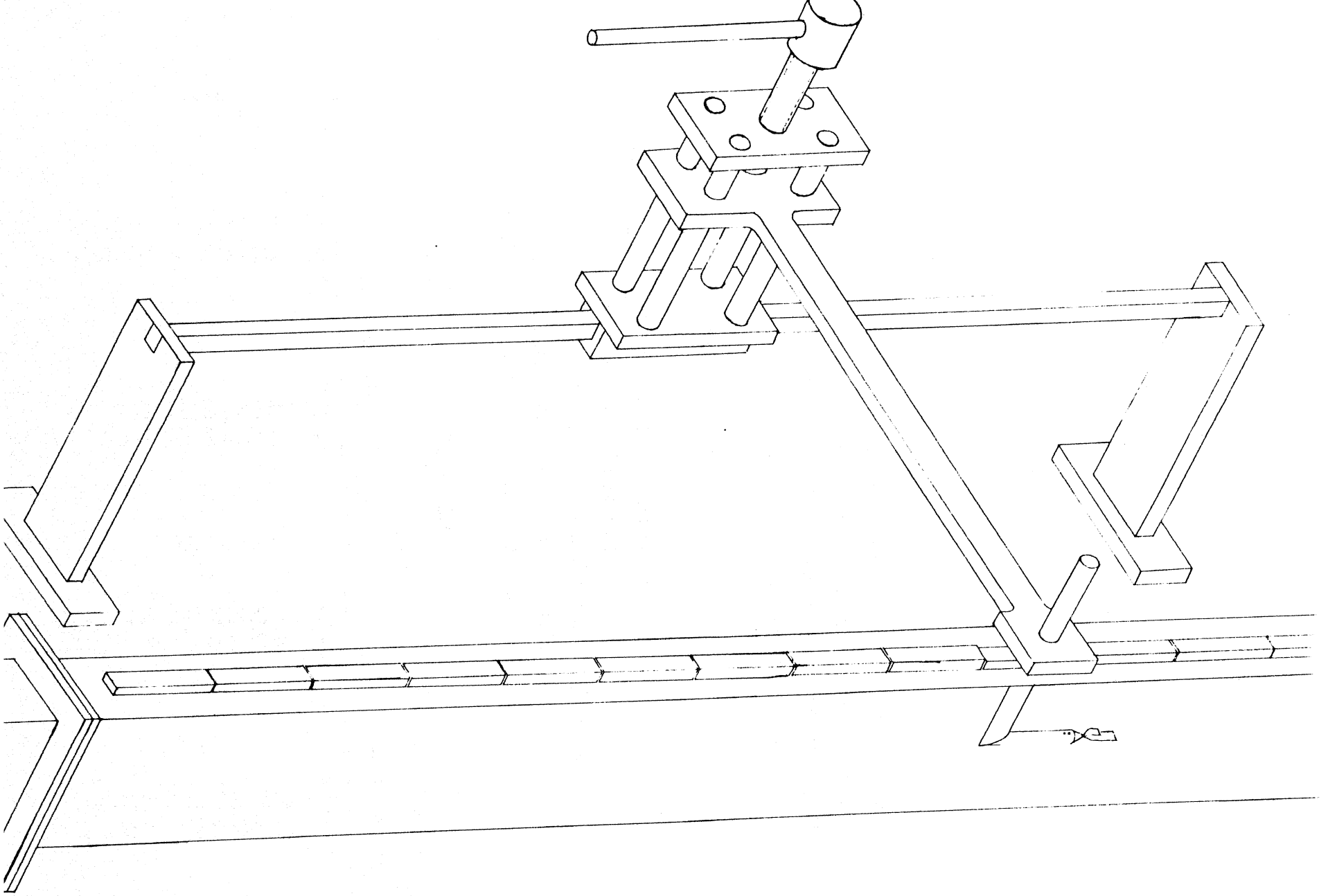

FIG. 2.10 TRAVERSING MECHANISM.

CENTRIFUGAL BLOWER :

A 400 watts blower to sustain air velocity over the range of 1 to 10 m/sec in the entire region of the test cell is used. The specifications of the blower are given below.

Outlet	: radial
Voltage rating	: 240V
Current rating	: 5A

TRAVERSING MECHANISM:

Fig. 2.10. shows the traversing mechanism to move the hot wire probe inside the tunnel. A single slider on a square horizontal rod carries the probe without overturning. With the slider, the probe can be moved parallel and across the test cell with respect to the mean flow direction. A screw pair is used for vertical movement of the probe.

TESTING OF THE TEST CELL PERFORMANCE :

Following observations show the performance of the test cell.

Uniformity of mean flow (Table 2.2.).

Fully developed state and Growth of % turbulence (Table 2.3.).

Temperature profile and extent of mixing (Table 2.4.).

Stability of blower and test cell (Table 2.5.).

TABLE 2.1.

y(cm)	BVS 70V (°C)		BVS 80V (°C)	
	HVS 30V	HVS 40V	HVS 40V	HVS 50V
2.0	27.48	34.56	31.45	36.30
2.5	27.16	33.94	30.95	35.87
3.0	26.97	33.46	30.15	35.28
3.5	26.80	30.49	27.72	34.44
4.0	26.53	29.27	26.03	33.92
4.5	26.04	29.11	25.55	33.30
5.0	25.56	27.72	25.47	31.90
5.5	25.05	26.20	25.01	29.62
6.0	24.43	24.63	23.25	29.05
6.5	23.56	22.93	21.48	26.67
7.0	22.93	22.34	20.75	24.71

TABLE 2.2.

y(cm)	Hot Wire Output (V)
2.0	1.2500
3.0	1.2638
4.0	1.2721
5.0	1.2724
6.0	1.2735

TABLE 2.3.

x(cm)	Hot Wire Output (V)	RMS fluctuation(V)
140	1.2605	0.0042
160	1.2635	0.0050
180	1.2753	0.0040
200	1.2783	0.0040
220	1.2792	0.0060
240	1.2806	0.0070
260	1.2810	0.0070

TABLE 2.4.

y(cm)	T °C			
	x=110 cm	130 cm	150 cm	170 cm
2.0	31.45	31.25	28.30	28.07
3.0	30.15	28.95	28.95	28.65
4.0	26.03	25.45	28.54	28.46
5.0	25.47	25.65	25.72	26.76
6.0	23.25	22.35	24.10	24.53
7.0	20.75	21.20	21.93	22.89

TABLE 2.5.

Input to blower(v)	D.C. Output of Manometer (V)	
	10–9–1990	12–9–1990
50.2 – 50.4	0.40	0.45
60.1 – 60.4	0.95	1.00
70.1 – 70.4	1.80	1.80
80.3 – 80.7	2.40	2.50
89.9 – 90.5	3.60	3.40
99.8 – 100.1	4.40	4.40

HOT WIRE ANEMOMETRY AND CALIBRATION

Almost all experimental research involved in aerodynamics and turbulence is performed by measuring the components of the mean velocity and velocity fluctuation. The hot–wire anemometer is suitable for this purpose. A single wire can measure one component of velocity, two wires can measure two components of velocity or temperature and one component of velocity. In the present work, a two wire probe has been used to measure one component of velocity and the local temperature. A shortcoming of a hot–wire is that it is insensitive to the direction of flow. Hence, it can not detect a separated flow region unless special treatment is used.

Basically a hot wire functions as a thermal transducer. The hot wire is a fine tungsten wire of 5μm diameter. Tungsten combines high sensitivity of resistance to temperature with electrical stability and is an ideal choice as a wire material. The tungsten wire is placed between two tapered prongs fixed in a ceramic tube and terminating in two gold plated connector pins. The length of the wire is 4mm. This gives the l/D ratio of the wire as 800.

The wire is generally placed in the wind tunnel perpendicular to the flow direction where the velocity is to be measured. The wire becomes hot when as current passes through it. Tungsten has a specific temperature co–efficient of resistance. When a hot wire is held in a flow field, heat generated by Joule heating is dissipated mainly by forced convection. The heat loss by convection is dependent on parameters like velocity, temperature and the pressure of the medium where thermal energy is dissipated. The amount of heat loss by radiation and conduction along the prong is usually small. The effect of heat dissipation is manifested as temperature drop of the wire. The resistance of the wire changes with a change in its temperature. This change is sensed by a feed back circuit which passes additional current till the wire temperature is restored. Since the wire temperature is maintained constant independent of the flow velocity, the hot–wire – feed back circuit combination is referred to as a constant temperature anemometer (CTA). This temperature is usually much higher than the room temperature typically 100–200 ^{o}C. Higher temperatures make the wire fragile.

The following specification of the two–wire probe gives as idea of the effect of resistance. Model numbers referred to in this thesis refer to the hot wire instrument made by DANTEC, Denmark.

Resistance of hot–wire 1 at 20oC = 9.3854 Ω

Resistance of hot–wire 2 at 20oC = 9.4625 Ω

$\alpha_{20} = 0.36$ %

Maximum wire temperature $T_{sensor} < 300$oC

$R = R_{total} + \alpha_{20} \cdot R_{20} (T_{sensor} - T_0)$

One of the two wires of the probe constitutes the fourth arm of wheatstone bridge. The remaining parts of the bridge are located in the anemometer itself. The ratio of the operating resistance R (which along with the temperature is kept constant by the CTA) to its cold resistance R20 is called as the overheat ratio. The hot wire sensitivity to velocity increases with increasing overheat ratio.

The hot wire anemometer is operated in a constant current mode when temperature is to be measured. In this mode of operation, a small constant current flows through the wire. The change of temperature will have the tendency to alter the wire resistance. This change in resistance is a measure of the local fluid temperature. The ratio of the voltage drop corresponding to the resistance to the constant current is a measure of the local temperature.

As shown in Fig. 3.1. the constant temperature anemometer (CTA) consists of a Wheatstone bridge and a servo–amplifier. The temperature of the probe will cause a change of voltage at the servo–amplifier inputs. The output voltage of the servo–amplifier is applied to the bridge. So that the original temperature of the hot wire is maintained by varying the bridge's operating voltage. The higher the gain of the servo system, the more rapidly the amplifier responds and lower will be the error voltage of the horizontal bridge diagonal to compensate for a temperature change in the sensor. The DANTEC model 56C17CTA is used in the present work as a bridge. The main unit 56C01CTA delivers the servo–voltage as the output of the instrument and this is a measure of flow velocity. The feed back circuit of the plays an important role in improving the frequency response of the hot wire from about 100 Hz to 10 KHz.

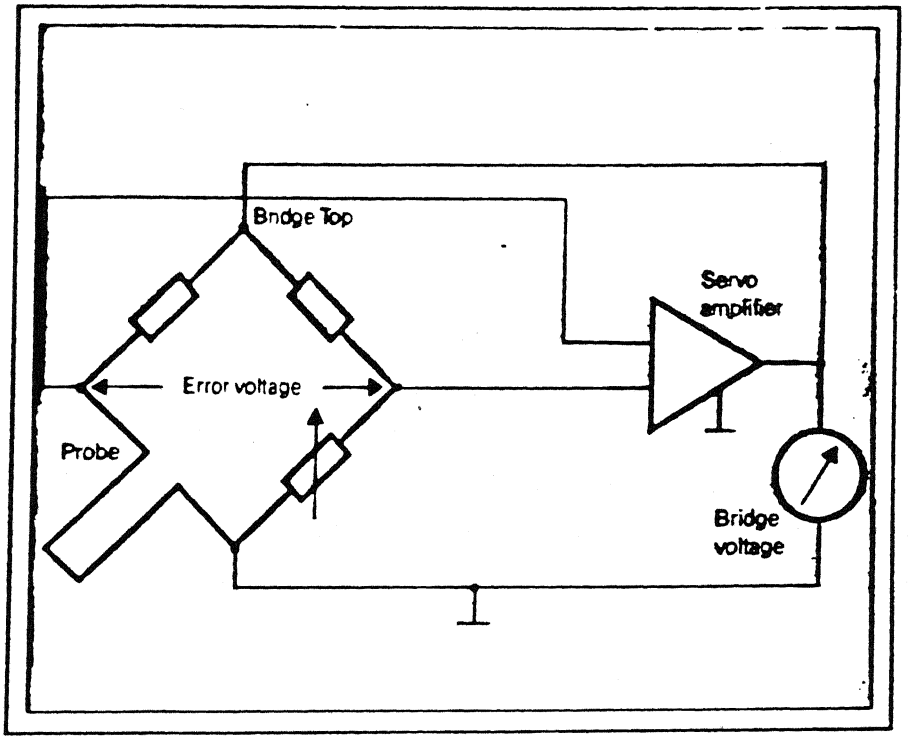

FIG 3.1 SIMPLIFIED DIAGRAM OF CONSTANT - TEMPERATURE ANEMOMETER SYSTEM

Though there is a one–to–one relation between velocity and servo–voltage, this relation is not linear. It can however, be linearized through an algebraic transformation. This is accomplished on a 'linearizer' (model no. 56N21) module that is located next to the bridge unit on the instrument. This is followed by a signal processor unit (model no. 56N20).

A mean value unit 56N22 is a 4 digit voltmeter and is used to measure the DC component of output voltages from the other units in the system. An analog processing unit (model no. 56N23) is also available to get sum or difference of the output signals of two channels.

The 56C01CTA (constant temperature anemometer) contains a function switch with 3 modes for operation viz., TEMP, STD.BY & FLOW. In TEMP position, the resistance of the connected probe can be measured as a current is supplied to it. In 'STD.BY' position no current flows through the bridge. In the 'FLOW' setting , the CTA starts operating with the function of the servo–amplifier. A setting named 'BRIDGE ADJ' enables the adjustment of the bridge balance for measurement of probe resistance and setting of the desired overheat.

3.1. Convective Principles Governing the Operation of Hot Wire

The operation of a hot wire can be explained as a phenomena of heat transfer from fine wires. The analysis is given in given below.

With the assumption of the uniform radial temperature distribution within a fine wire, the thermal equilibrium of the wire in a fluid gives following heat balance relation:

$$P = H + K$$

where

P = electrical power input to sensor= i^2 RH

RH = resistance of the wire Ω/m

H = convective heat transfer to fluid

$= A\ h\ (T_w - T_f)$

here, A = area of wire per unit length

h = convective heat transfer coefficient

T_w = temperature of the wire

T_f = temperature of the fluid

K = change in internal energy of the wire

$$= m\,C\,\frac{dT_w}{dt}$$

here, m = mass of the wire per unit length

C = specific heat of the wire material

The governing differential equation can be written as

$$V \cdot C\,\frac{dT_w}{dt} + A \cdot h\,(T_w - T_f) - i^2\,R = 0 \qquad (3.1)$$

The quantity of primary interest here is the convective heat transfer h; the rate change of internal energy is made zero by operating the wire in CTA mode. For the hot

$$H = Nu\ 2\pi\ K_f\ l\ (T_w - T_f)$$

Where, Nu = hd/K_f = Nusselt number

d = sensor diameter

K_f = thermal conductivity of fluid

2l = length of sensitive area of hot wire

The problem is to find a representative expression for the Nusselt number in ter of the fluid and sensor parameters.

A general expression for Nu would be

$$Nu = f(R_e, Pr, a_1, Gr, Ma, \gamma, aT, 2l/d, K_f/K_w)$$

Where R_e = Vd/ν = Reynolds number

V = free–stream velocity

ν = kinematic viscosity

Pr = $\mu\ C_p/k$ = Prandlt number

C_p = specific heat of fluid at constant pressure

a_1 = angle between free–stream flow direction and normal to cylinder

Gr = Grashof number

Ma = Mach number

γ = C_p/C_v

C_v = specific heat at constant volume

aT $= (T_w - T_f)/T_f$ = temperature loading overheat ratio $- 1$

K_w = thermal conductivity of hot wire material

Fortunately, most applications permit a significant reduction in the number parameters that must be included. The reasons are stated below:

i) forced convection parallel to the wire is small.

ii) Pr depends only of fluid properties, and buoyancy effects can be neglect for $Gr^* < Re^2$. For velocities of fluid greater than 5.2 cm/s., buoyan effects can be neglected.

iii) for low density and low velocities Mach number (=0), C_p and C_v can assumed to be constant.

With these assumptions Collis and Willims (1959) suggested most accura formula which accounts the change in properties of the fluid.The expression can be stated a

$$Nu = (A + B \cdot R_e^n) \{1 + aT/2\}$$

Where, $A = 0.24$, $B = 0.56$, $n = 0.45$ for $0.02 < R_e < 44$

$A = 0$, $B = 0.48$, $n = 0.51$ for $44 < R_e < 140$.

Koch and Gartshore (1970) suggested slightly different formula with a differe value of a.

$$Nu\ (T_m/T_f)^a = A + B \cdot R_e^n$$

where, $T_m = (T_w + T_f)/2$, $A = 0.24$, $B = 0.56$, $a = 0.67$

It is finally understood that the values of these constants depend on the l/d ra of the wire and material of the wire. The values given above correspond to $l/d > 250$. T above referred formulas are particularly developed for non–isothermal flows and can be us only when the local fluid temperature is measured.

In our present work we used two different relations – one for the study of t isothermal fluid flow and another for study of non–isothermal fluid flow. For isothern calibration (Sikdhar, 1989) a mathematical curve fitting technique which uses the sa transfer function as employed by the 'linearizer' module has been used. For non–isothern calibration a relation which considers overheat ratio of the wire as a variable has been us A calibration procedure suggested by Hollasch and Gebart (1972) has been used. T calibration procedures are discussed in the following sections.

3.2. Calibration of Constant Temperature Hot Wire in Isotherma Fluid

In the calibration method adopted in our experiment, a mathematical curve fittin technique which uses the same transfer function as employed by the 'linearizer' module ha been used. The voltage response from a CTA is not a linear function of velocity of fluid pa the probe. The linearization of CTA signal becomes necessary to linearize the non–linea output signal from the constant temperature anemometer 56C01CTA before this transmitted to other units or to an external unit.

The incoming signal voltage varies from a minimum to maximum. The linearizir circuit accomplishes the mathematical operation,

$$y = 10^{A + Bx + Ey} + Cx + D \qquad (3.2)$$

for a given voltage x. Here A, B, C, D, E are constants. Normally the constants a selected to give y = 10 m/sec for x = 10 Volt. y is the linearizer output of velocity m/sec. The normalized voltage, x is defined

$$x = \left[\frac{V - V_0}{V_{max} - V_0} \right] \cdot 10 \text{ Volts}$$

where, V_0 is the Voltage corresponding to the minimum velocity.

To obtain an output velocity, y of 10 m/sec for x = 10 Volts, y is normalized as,

$$y = 10 \cdot \frac{U}{U_{max}}$$

The constants A, B, C, D and E can be calculated by means of a least square er approach. For any calibration point (x_i,y_i) the above equation (3.2) will produce an er ϕ_i, given by

$$\phi_i = y_i - [10^{A+Bx_i+Ey_i} + Cx_i + D]$$

The least square approach requires $\Sigma_i \phi_i^2$ to be minimum i.e.,

$$\phi = \Sigma_i \phi_i^2 = \Sigma \{ y_i - [10^{A+Bx_i+Ey_i} + Cx_i + D] \}^2$$

and $\frac{\partial \phi}{\partial A} = \frac{\partial \phi}{\partial B} = \frac{\partial \phi}{\partial C} = \frac{\partial \phi}{\partial D} = \frac{\partial \phi}{\partial E} = 0.$

Let I be any of the parameters A, B , C, D or E, then

$$\frac{\partial \phi}{\partial I} = 2 \Sigma_i \phi_i \frac{\partial \phi_i}{\partial I} = 0$$

Hence A, B, C, D and E can be calculated. This is shown in the computer program *CONST.FOR* (Sikdar, 1988).

Values of A, B, C, D and E calculated for the data in Table 3.1. and Table 3.2. are A = –1.2603720, B = 0.1513271, C = 0.5294150, D = 3.2 and E = –0.0068722

3.3. Calibration of Constant–Temperature Hot Wire Anemometer using Method of Variable over Heat Resistance

Calibration of hot wire in constant–temperature fluids may be carried out by many techniques. However, the anemometer output varies with the ambient temperature even when the local velocity is kept constant. Therefore, to measure a fluctuating velocity field in a non–isothermal fluid or thermally stratified fluid, calibration at various temperatures must be considered.

A constant–temperature anemometer maintains an invariable (but adjustable) overheat resistance and produces a voltage signal proportional to a fractional root of velocity of an iso–thermal fluid. In non–isothermal flows, an effect of varying temperature on a hot wire anemometer signal is comparable to the effect of varying velocity. However, an independent measure of varying the temperature is necessary in order to construe the hot wire output. A separate temperature measurement, when used with a wire calibrated for various fluid temperatures at fixed overheat resistance, will yield the velocity. This approach is developed here.

It is true that calibrating hot wire over adequately large ranges of ambient fluid temperature is experimentally cumbersome and difficult, especially when the expected fluid temperatures differ greatly from the ambient fluid temperature. Large temperature differences induce appreciable natural convection effects in the test fluid. This causes an inaccurate determination of the zero velocity voltage. In addition, if the flows to be measured have velocities of the same order as any natural convection currents in the calibration cell, the anemometer output during calibration will be in error.

The present dissertation introduces a technique of calibrating constant–temperature anemometer probes, accounting for varying ambient fluid

temperatures by varying the overheat resistances at a single reference fluid temperature. Varying overheat resistance is experimentally convenient since modern anemometers usually incorporate decade resistances which expedite setting various overheat resistances.

The central idea behind the proposed technique is as follows.

An increase in the ambient fluid temperature (TA) decreases the temperature difference between the wire at (THC) and the ambient fluid. Heat loss rate from the wire may be represented by,

$$q' = h(U,TA)\ (THC-TA)$$

where h is indicated as a function of velocity and the local fluid temperature. However, a change in overheat resistance from RHC to RHV will also reduce the difference between the wire and ambient fluid. If h is a weak function of temperature, the anemometer output characteristics observed when ambient temperature is varied may be approximated as varying the overheat resistance.

3.4. Thermal Analysis

The heat loss from a hot wire probe by convection process, neglecting conduction loss to the probe support, is

$$q' = h\ A\ (THC-T_f) = E^2/RHC$$

where h = convective heat transfer coefficient
A = Surface area of the wire
THC = operating temperature of the wire
T_f = ambient fluid temperature.

Or,

$$E^2 = RHC\ (THC-T_f)\ h\ A \tag{3.4}$$

Over a wide temperature range the probe resistance may be assumed to be a linear function of temperature as

$$RHC = R_0\ (1 + \alpha\ THC) \tag{3.5}$$

$$THC = \frac{RHC\ -\ R_0}{R_0} \tag{3.6}$$

where R_0 is the resistance of the wire at zero degree centigrade

Substitution of (3.6) in (3.4) gives

$$E^2 = RHC \{ \frac{RHC - R_0}{\alpha R_0} - T_f \} h A \qquad (3.7)$$

Consider a small change (RHV–RHC) in RHC, such that anemometer output voltage, when operated with a variable overheat resistance matches the output voltage that would read when operated at fixed overheat resistance RHC and ambient temperature equal to the reference temperature TR, we have

$$\frac{E c^2}{RHV} = (THV-TR)\, h(TR,U)\, A \qquad (3.8)$$

where h(TR,U) is the film coefficient of heat transfer which is a function of velocity and reference ambient fluid temperature. A is the area of wire, (THV–TR) temperature difference between the hot wire and reference ambient fluid temperature. The output voltage with variable fluid temperature must be equal to the output voltage with variable overheat resistance.

$$RHV(THV-TR)\, h(TR,U)\, A = RHC\,(THC - T_f)\, h(T_f,U)\, A \qquad (3.9)$$

but,
$$THV = \frac{RHV - R_0}{\alpha R_0}$$
$$THC = \frac{RHC - R_0}{\alpha R_0}$$

Equation (3.9) can be written as

$$RHV\{\frac{RHV - R_0}{\alpha R_0} - TR\}\, h(TR,U) = RHC\{\frac{RHC - R_0}{\alpha R_0} - T_f\}\, h(T_f,U) \qquad (3.10)$$

$$RHV\{RHV-R_0-TR\ \alpha R_0\}\, h(TR,U) = RHC\{RHC-R_0-T_f\ \alpha R_0\}\, h(T_f,U) \qquad (3.11)$$

Assume h(TR,U)=h(T_f,U), which is equivalent to assuming that fluid property variations are negligible in determining h.

Then,

$$RHV\{RHV-(R_0+TR\ \alpha R_0)\} = RHC\{RHC-(R_0+T_f\ \alpha R_0)\} \qquad (3.12)$$

$$RHV^2 - RHV(R_0+TR\ \alpha R_0) - RHC(RHC-R_0-T_f\ \alpha R_0) = 0 \qquad (3.13)$$

Let
$$B = R0+TR\ \alpha R_0$$
$$C = RHC\{RHC - R_0 - T_f\ \alpha R_0\}$$

$$RHV^2 - B\cdot RHV - C = 0 \qquad (3.14)$$

$$RHV = \frac{B}{2} + \frac{\sqrt{B^2 + 4\cdot C}}{2} \qquad (3.15)$$

Hence, calibration performed at overheat resistance RHC with fluid temperature Tf would produce nearly identical output voltages to a calibration performed at an overheat resistance of RHV and a constant fluid temperature TR.

Equation (12) gives the value of new overheat resistance that required to simulate the variable temperature of ambient fluid. However, a small difference in output may be expected due to fluid property variations. The error is caused because h(TR,U) will in general different from h(Tf,U).

A correlation term to account for fluid property variation can be calculated using the data which is in principle, already available from calibration. Expanding h(Tf,U) in Taylors series about TR, equation (4) yields;

$$E^2 = \text{RHC}\{\frac{\text{RHC} - R_0}{\alpha R_0} - T_f\}\, A \left[h(TR,U) + \frac{dh(TR,U)}{dT}\bigg|_U (T_f - TR) + \frac{d^2h(TR,U)}{dT^2}\bigg|_U \frac{(T_f - TR)^2}{2!} + \ldots\right] \quad (3.16)$$

$$E^2 = \text{RHC}\{\frac{\text{RHC} - R_0}{\alpha R_0} - T_f\}\, A\, h(TR,U) \text{RHC}\{\frac{\text{RHC} - R_0}{\alpha R_0} - T_f\}\, A \left[\frac{dh(TR,U)}{dT}\bigg|_U (T_f - TR) + \frac{d^2h(TR,U)}{dT^2}\bigg|_U \frac{(T_f - TR)^2}{2!} + \ldots\right] \quad (3.17)$$

from equations (3.12) and (3.15)

$$\text{RHC}\{\frac{\text{RHC} - R_0}{\alpha R_0} - T_f\} = \text{RHV}\{\frac{\text{RHV} - R_0}{\alpha R_0} - TR\} \quad (3.18)$$

substitution of (3.18) in (3.17) gives

$$E^2 = \text{RHV}\{\frac{\text{RHV} - R_0}{\alpha\ R_0} - \text{TR}\}\ A\ h(\text{TR,U})$$

$$\text{RHC}\{\frac{\text{RHC} - R_0}{\alpha\ R_0} - T_f\}\ A \left[\frac{dh(\text{TR,U})}{dT}\bigg|_U (T_f - \text{TR}) \right.$$

$$\left. + \frac{d^2h(\text{TR,U})}{dT^2}\bigg|_U \frac{(T_f - \text{TR})^2}{2!} + ... \right] \qquad (3.19)$$

from equation (3.8), the equation (3.19) can be written as

$$E^2 = Ec^2 + \text{RHC}\{\frac{\text{RHC} - R_0}{\alpha\ R_0} - T_f\}\ A \left[\frac{dh(\text{TR,U})}{dT}\bigg|_U (T_f - \text{TR}) \right.$$

$$\left. + \frac{d^2h(\text{TR,U})}{dT^2}\bigg|_U \frac{(T_f - \text{TR})^2}{2!} + ... \right] \qquad (3.20)$$

⇒Square output of anemometer with variable fluid temperature
= square output of anemometer with variable overheat resistance.

Consider equation (3.8)

$$Ec^2 = \text{RHV}\{\frac{\text{RHV} - R_0}{\alpha\ R_0} - \text{TR}\}\ A\ h(\text{TR,U})$$

$$\Rightarrow \quad h(\text{TR,U}) = \frac{Ec^2}{\text{RHV}\{\frac{\text{RHV} - R_0}{\alpha\ R_0} - \text{TR}\}\ A} \qquad (3.21)$$

$$\frac{dh(\text{TR,U})}{dT}\bigg|_U = \frac{1}{\text{RHV}\{\frac{\text{RHV} - R_0}{\alpha\ R_0} - \text{TR}\}\ A} \qquad (3.22)$$

substituting (3.22) in (3.18) we get

$$E^2 = Ec^2 + \left[\frac{\text{RHC}\{\frac{\text{RHV} - R_0}{\alpha\ R_0} - \text{TR}\}A}{\text{RHV}\{\frac{\text{RHV} - R_0}{\alpha\ R_0} - \text{TR}\}A} \right] \frac{dEc^2(\text{RHV,U})}{dT}\bigg|_U (T_f - \text{TR}) \qquad (3.23)$$

from equation (3.5)

$$RHV = R_0 (1+ \alpha T_f)$$

$$\frac{dRHV}{dT} = \alpha R_0$$

$$\frac{dEc^2(TR,U)}{dT} = \frac{dEc^2}{dRHV}\Big|_U \cdot \frac{dRHV}{dT}$$

$$= \frac{dEc^2(RHV,U)}{dRHV}\Big|_U (\alpha R_0) \qquad (3.24)$$

substitution of equation (3.24) in (3.23) gives

$$E^2 = Ec^2 + \left[\frac{RHC(RHC-R_0-T_f \ \alpha \ R_0)}{RHV(RHV\_R_0-TR \ \alpha \ R_0)}\right] \frac{dEc^2}{dR} \alpha R_0 (T_f-TR)$$

$$+ \text{higher order terms} \qquad (3.25)$$

square of output of hot wire for varying fluid temperature

= square of output of hot wire for varying overheat resistance

$$+ \left[\frac{RHC(RHC-R_0-T_f \ \alpha \ R_0)}{RHV(RHV\_R_0-TR \ \alpha \ R_0)}\right] \frac{dEc^2}{dR} \alpha R_0 (T_f-TR)$$

+ higher order terms (3.26)

Above analysis proves that calibration of hot wire in varying temperature fluid can be simulated as calibration of hot wire for varying overheat resistance in constant temperature fluid. Hollasch and Gebhart (1972) presented an experimental study to test the first order analysis given above for correcting for variable property effects.

3.5. Correlation of Mathematical Relation

Collis and Williams (1959) suggested a simple expression of the form:

$$(Nu)\,(T_m/T_f)^a = A + B\,(Re)^n \qquad (3.27)$$

where, $Tm = \frac{T_w + T_f}{2}$, $a = -0.17$, $A = 0.24$, $B = 0.56$ for $0.02 < 44$ and $n = 0.45$

Koch and Gartshore (1972) determined the values of constants most accurately by considering the effect of variation of fluid properties. They used following relations to calculate fluid properties.

Dynamic viscosity of air = 1.87×10^{-5} [1.0 + 1.26×10^{-3}(T_m–38)] Kg/m sec.

Thermal conductivity of air = 0.0267[1.0 + 0.00159(Tm–38) W/m °C

valid for 38 < Tm < 45 °C

$$Nu = \frac{3.413\ E_w^2\ \alpha}{r(\frac{R_h}{R_r} - 1)\ k\pi}$$

$$\text{and } E_w = \frac{1.08\ E_b\ r\ l}{100.6 + r\ l}$$

where, E_b = bridge voltage

l = length of the wire

r = resistance of the wire per unit length

a = 0.67, n = 0.45, A = 0.72, B = 0.80.

Alternatively, they defined another relation which uses the concept of overheat ratio and gave an expression as

$$(Nu)\ (R-1)^b = A + B\ (Re)^n$$

where b = 0.16

R = $\frac{R_h}{R_r}$

R_h = mean resistance of the wire

R_r = Resistance of the wire at reference fluid temperature

A = 0.64, B = 0.57, n = 0.45.

The experimental results obtained with different types of hot wire probes and anemometers have demonstrated the lack of a general relationship between the Nusselt and Reynolds numbers of hot wire probes. The observed discrepancies are mainly caused by:

1) Mode of operation of anemometer: constant current or constant temperature.
2) Conductive loss to prongs. This is significant for probes with small aspect ratio (l/d < 200).
3) Reference temperature TR for the flow property evaluation.
4) Probe Geometry: The wire aspect ratio l/d and the support orientation influence the relationship between the Nusselt number and Reynolds number.

Due to above reasons one should calibrate the probe to be used before the actual measurement.

In our work we used a relation of the form:

$$Ec^2 (R-C)^b = A + B\,U^n \qquad (3.28)$$

Where Ec = out put of hot wire equivalent to variable overheat resistance.

$R = \frac{RHV}{R_0}$

C = constant

If we use equation (3.28) as a global relation we should use some regression analysis to determine the values of constants. But many authors have expressed that it is difficult to get a global relation which will produce same results as observations. In our work we use equation (3.28) as a local relation and we determine the local values of constants using regression analysis stated below.

3.6. Method of Localized Calibration

* Select different hot wire output values: Ei, i= 1 ....n.
* Select Different values of overheat resistances RHVj, j=1..m.
* Set the overheat resistance of wire equals to Rj.
* For the above over heat resistance Rj go through following steps:
  a) Adjust the air flow Ui,j in the calibration cell such that the output of the hot wire matches one value of Ei.
  b) Measure the value of air velocity with pitot tube.
  c) Repeat steps a & b for all values of Ei.
* Repeat steps a,b & c for all values of Rj.
* Record and arrange all values of Ei, Rj & Ui,j as show in fig.*.
* The following figure shows the formation of grids using calibration data.

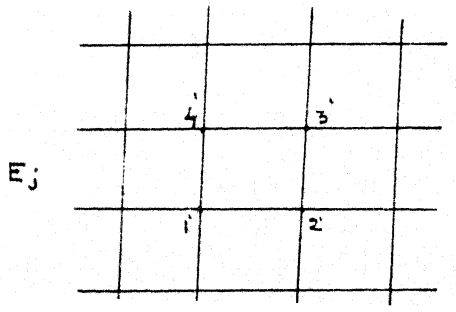

* Calculate the values of local constants of localized correlation using linear regression analysis.

3.7. Least Squares Analysis to Calculate Local Constants

Correlation assumed:

$$Ec^2\,(R-C)^b = A + B\,U^n$$

where $n = 0.45$

ALGORITHM LOCAL.CALIB:

The above figure shows the grid, grid points and numbering of grid points.

Eci, i=1...4: output of hot wire.

Overheat ratio, $Ri = \frac{RHVi}{R_0}$, i=1...4

Overheat resistance, RHVi, i=1...4

Velocity of air, Ui, i=1...4

calculate the error function, F using

$$F = \sum_{i=1}^{4} (Eci^2\,(Ri-C)^b - A - B\,U^n)^2 = \sum_{i=1}^{4} Gi^2$$

To obtain A,B,C and b, we set

$$\frac{dF}{dA} = \frac{dF}{dB} = \frac{dF}{dC} = \frac{dF}{db} = 0.$$

Hence we get the system of equations,

$$\Sigma\, Gi = 0 \qquad \text{(i)}$$

$$\Sigma\, Ui^n\, Gi = 0 \qquad \text{(ii)}$$

$$\Sigma\, Gi\, Eci^2\,(Ri-C)^b = 0 \qquad \text{(iii)}$$

$$\Sigma\, Eci^2\,(Ri-C)^b \ln(Ri-C)\, Gi = 0 \qquad \text{(iv)}$$

Solving equations i and ii for A and B we get,

$$B = \frac{\Sigma\, Ei^2\,(Ri-C)^b\, Ui^n - 0.25\,\Sigma\, Ui^n\,\Sigma\, Eci^2\,(Ri-C)^b}{\Sigma\, Ui^n - 0.25\,\Sigma\, Ui^n\,\Sigma\, Ui^n}$$

$$A = 0.25\,\Sigma\,(Eci^2\,(Ri-C)^b - B\,Ui^n)$$

b is the root of,

$$\Sigma\, Eci^2\, (Ri-C)^b \ln(Ri-C)\, Gi = \Sigma\, Hi = 0$$

Hence b is computed iteratively, at the P th iteration as,

$$b^{(P+1)} = b^{(P)} - \left[\frac{\Sigma\ Hi}{\Sigma\ \frac{dHi}{db}} \right]^P$$

where

$$\frac{dHi}{db} = \frac{Hi(b+db)\ -\ Hi(b)}{db},\ db \cong 0.01$$

C is the root of ,

$$\Sigma\, Gi\, Eci^2\, (Ri-C)^b = \Sigma\, Fci = 0$$

Hence C is calculated iteratively at Q th iteration as,

$$C^{(Q+1)} = C^Q\ - \left[\frac{\Sigma\ Fci}{\Sigma\ \frac{dFci}{dC}} \right]^Q$$

here

$$\frac{dFci}{dC} = \frac{Fci(C+dC)\ -\ Fci(C)}{dC},\ dC \cong 0.01$$

A global iteration scheme computes A,B,b and C. A program *NCAL.F* (Appendix A) is used to calculate all values of A,B,b and C using above algorithm. For the probe used in this work, the calibration data is given in Table 3.3. Values of constants for each cell are given in Table 3.4.

Table 3.1.

Anemometer Output (V)	measured Velocity (m/s)
1.3726	1.60
1.4150	2.12
1.4447	2.46
1.4671	2.89
1.4859	3.28
1.5023	3.47
1.5174	3.73
1.5307	3.97
1.5435	4.26
1.5530	4.48
1.5667	4.78

Table 3.2.

Anemometer Output (V)	smoothed Velocity (m/s)
1.3726	1.606619
1.4150	2.083472
1.4447	2.531413
1.4671	2.892586
1.4859	3.303946
1.5023	3.482922
1.5174	3.750103
1.5307	3.998721
1.5435	4.255418
1.5530	4.460836
1.5667	4.786359

TABLE 3.3

Ri (Ohms)	Ei (V)	Velocity (m/s)	Temp corrected Velocity (m/sec)
11.4000	1.1938	3.2800	3.3456
11.4000	1.2045	3.4300	3.4986
11.4000	1.2134	3.6300	3.7026
11.4000	1.2248	4.0200	4.1004
11.4000	1.2335	4.2100	4.2942
11.4000	1.2423	4.4400	4.5288
11.4000	1.2525	4.6700	4.7634
11.4000	1.2635	5.0900	5.1918
11.4000	1.2728	5.3900	5.4978
11.4000	1.2834	5.7400	5.8548
11.5000	1.1938	2.5800	2.6316
11.5000	1.2045	2.8000	2.8560
11.5000	1.2134	3.0300	3.0906
11.5000	1.2248	3.3100	3.3762
11.5000	1.2335	3.5000	3.5700
11.5000	1.2423	3.7500	3.8250
11.5000	1.2525	3.9300	4.0086
11.5000	1.2635	4.2000	4.2840
11.5000	1.2728	4.4900	4.5798
11.5000	1.2834	4.6900	4.7838
11.5000	1.2934	5.0400	5.1408
11.5000	1.3033	5.3200	5.4264
11.5000	1.3118	5.6300	5.7426
11.5000	1.3233	6.0300	6.1506
11.6000	1.2423	3.1400	3.2028
11.6000	1.2525	3.3900	3.4578
11.6000	1.2635	3.5000	3.5700
11.6000	1.2728	3.7000	3.7740
11.6000	1.2834	3.9100	3.9882
11.6000	1.2934	4.2600	4.3452
11.6000	1.3033	4.5500	4.6410
11.6000	1.3118	4.7800	4.8756
11.6000	1.3233	5.1800	5.2836
11.6000	1.3315	5.4300	5.5386
11.6000	1.3434	5.7400	5.8548
11.8000	1.2834	3.3000	3.3660
11.8000	1.2934	3.4900	3.5598
11.8000	1.3033	3.7300	3.8046
11.8000	1.3118	3.9500	4.0290
11.8000	1.3233	4.2600	4.3452
11.8000	1.3315	4.5900	4.6818
11.8000	1.3434	4.9200	5.0184
11.8000	1.3535	5.2000	5.3040
11.8000	1.3654	5.5500	5.6610
11.8000	1.3754	5.9300	6.0486
11.9000	1.3033	3.1600	3.2232
11.9000	1.3118	3.3800	3.4476
11.9000	1.3233	3.6400	3.7128
11.9000	1.3315	3.8500	3.9270
11.9000	1.3434	4.1300	4.2126
11.9000	1.3535	4.4300	4.5186
11.9000	1.3654	4.7600	4.8552

11.9000	1.3754	5.0000	5.1000
11.9000	1.3834	5.1900	5.2938
11.9000	1.3934	5.5000	5.6100
11.9000	1.4032	5.7900	5.9058
11.9000	1.3315	3.2400	3.3048
11.9000	1.3434	3.3400	3.4068
11.9000	1.3535	3.6400	3.7128
11.9000	1.3654	3.9900	4.0698
11.9000	1.3754	4.2500	4.3350
11.9000	1.3834	4.4300	4.5186
11.9000	1.3934	4.6800	4.7736
11.9000	1.4032	5.0100	5.1102
11.9000	1.4116	5.2300	5.3346
11.9000	1.4236	5.6000	5.7120
11.9000	1.4334	5.8800	5.9976
12.0000	1.3535	3.2200	3.2844
12.0000	1.3654	3.4700	3.5394
12.0000	1.3754	3.6500	3.7230
12.0000	1.3834	3.8300	3.9066
12.0000	1.3934	4.0500	4.1310
12.0000	1.4032	4.2600	4.3452
12.0000	1.4116	4.4900	4.5798
12.0000	1.4236	4.7800	4.8756
12.0000	1.4334	5.0300	5.1306
12.0000	1.4421	5.1900	5.2938
12.0000	1.4514	5.5300	5.6406
12.0000	1.4647	5.9000	6.0180
12.1000	1.3834	3.2900	3.3558
12.1000	1.3934	3.4800	3.5496
12.1000	1.4032	3.7100	3.7842
12.1000	1.4116	3.9100	3.9882
12.1000	1.4236	4.1800	4.2636
12.1000	1.4334	4.4100	4.4982
12.1000	1.4421	4.6000	4.6920
12.1000	1.4514	4.8500	4.9470
12.1000	1.4647	5.2000	5.3040
12.1000	1.4733	5.5000	5.6100
12.1000	1.4854	5.8700	5.9874
12.2000	1.4032	3.1400	3.2028
12.2000	1.4116	3.4300	3.4986
12.2000	1.4236	3.5900	3.6618
12.2000	1.4334	3.8000	3.8760
12.2000	1.4421	3.9200	3.9984
12.2000	1.4514	4.2000	4.2840
12.2000	1.4647	4.4600	4.5492
12.2000	1.4733	4.7200	4.8144
12.2000	1.4854	5.0300	5.1306
12.2000	1.4971	5.3300	5.4366
12.2000	1.5067	5.5800	5.6916
12.2000	1.5153	5.8800	5.9976
12.3000	1.4334	3.3600	3.4272
12.3000	1.4421	3.4800	3.5496
12.3000	1.4514	3.6700	3.7434
12.3000	1.4647	3.9200	3.9984
12.3000	1.4733	4.2100	4.2942

12.4000	1.5464	5.3600	5.4672
12.4000	1.5542	5.5800	5.6916
12.4000	1.5644	5.8000	5.9160
12.4000	1.5749	6.0200	6.1404
12.4000	1.5868	6.3700	6.4974
12.5000	1.4733	3.3000	3.3660
12.5000	1.4854	3.5000	3.5700
12.5000	1.4971	3.7300	3.8046
12.5000	1.5067	3.9500	4.0290
12.5000	1.5153	4.1000	4.1820
12.5000	1.5236	4.3200	4.4064
12.5000	1.5324	4.5600	4.6512
12.5000	1.5464	4.7600	4.8552
12.5000	1.5542	4.9500	5.0490
12.5000	1.5644	5.2300	5.3346
12.5000	1.5749	5.4600	5.5692
12.5000	1.5868	5.8100	5.9262

TABLE 3.4
VALUES OF CONSTANTS Aij,ANij,Bij,bij AND Cij

1.0299	.449999	.246285	-.50651	.272298
1.2987	.449999	9.54807E-02	-.86351	.272145
1.2195	.449999	.150676	-1.3637	.272146
1.1976	.449999	.171287	-1.59	.272161
1.1438	.449999	.207194	-1.8133	.272163
1.0912	.449999	.241807	-2.0648	.272154
1.0882	.449999	.250007	-2.3094	.272157
1.0835	.449999	.257259	-2.4748	.272159
1.0729	.449999	.267825	-2.6755	.272152
1.0729	.449999	.267825	-2.6755	.272152
1.177	.449999	.212551	-.16038	.28339
1.177	.449999	.212551	-.16038	.28339
1.177	.449999	.212551	-.16038	.28339
1.177	.449999	.212551	-.16038	.28339
1.177	.449999	.212551	-.16038	.28339
1.177	.449999	.212551	-.16038	.28339
1.4465	.449999	7.44377E-02	-.57541	.28319
1.4163	.449999	.102371	-.90831	.283257
1.3722	.449999	.135995	-1.215	.283253
1.3007	.449999	.181641	-1.5322	.283273
1.2253	.449999	.225677	-1.793	.283273
1.1916	.449999	.247543	-1.964	.283277
1.1345	.449999	.279235	-2.2116	.283271
1.1345	.449999	.279235	-2.2116	.283271
.684271	.449999	.534806	-.67011	.300386
.684271	.449999	.534806	-.67011	.300386
.684271	.449999	.534806	-.67011	.300386
.684271	.449999	.534806	-.67011	.300386
.684271	.449999	.534806	-.67011	.300386
1.347	.449999	.180015	-.80686	.299845
1.3195	.449999	.201895	-.89932	.299854
1.2718	.449999	.233115	-1.0456	.29984
1.2329	.449999	.257618	-1.1035	.299858
1.1148	.449999	.319265	-1.2278	.299836
1.1148	.449999	.319265	-1.2278	.299836
1.6082	.449999	5.68850E-02	-7.50143E-02	.316296
1.6082	.449999	5.68850E-02	-7.50143E-02	.316296
1.6082	.449999	5.68850E-02	-7.50143E-02	.316296
1.5518	.449999	.100092	-.671	.316549
1.5124	.449999	.131473	-.9564	.31661
1.4423	.449999	.177018	-1.3757	.316592
1.3767	.449999	.218994	-1.647	.316606
1.2775	.449999	.274758	-1.9607	.316603
1.2639	.449999	.287416	-2.1482	.316606
1.2639	.449999	.287416	-2.1482	.316606
1.6977	.449999	5.05739E-02	1.34167E-02	.327715
1.6977	.449999	5.05739E-02	1.34167E-02	.327715
1.6977	.449999	5.05739E-02	1.34167E-02	.327715
1.6977	.449999	5.05739E-02	1.34167E-02	.327715
1.7198	.449999	5.31355E-02	8.89104E-03	.327715
1.7065	.449999	7.36540E-02	1.16795E-02	.327713
1.771	.449999	5.39624E-02	8.73304E-03	.32771

```
1.8321 .449999 3.48963E-02 5.76642E-03 .32771
1.8064 .449999 5.85739E-02 8.37319E-03 .327713
1.8209 .449999 6.32205E-02 7.74641E-03 .327708
1.8209 .449999 6.32205E-02 7.74641E-03 .327708
1.0261 .449999 .459315 -.47464 .327928
1.0261 .449999 .459315 -.47464 .327928
1.0261 .449999 .459315 -.47464 .327928
1.6063 .449999 .147126 -.85413 .327701
1.5647 .449999 .178896 -1.0706 .327724
1.4792 .449999 .232027 -1.3664 .327717
1.4498 .449999 .254815 -1.6072 .327722
1.4304 .449999 .270844 -1.7693 .327724
1.3565 .449999 .31334 -2.0464 .327715
1.3307 .449999 .331869 -2.2146 .327719
1.3307 .449999 .331869 -2.2146 .327719
1.147 .449999 .431778 -.49863 .33902
1.147 .449999 .431778 -.49863 .33902
1.147 .449999 .431778 -.49863 .33902
1.147 .449999 .431778 -.49863 .33902
1.6683 .449999 .154726 -.85938 .338818
1.5889 .449999 .206147 -1.1077 .338836
1.4651 .449999 .278986 -1.4941 .338824
1.39 .449999 .32469 -1.7147 .338833
1.3094 .449999 .370685 -1.8707 .338833
1.282 .449999 .388397 -1.978 .338838
1.2172 .449999 .42302 -2.2275 .338827
1.2172 .449999 .42302 -2.2275 .338827
1.2681 .449999 .399868 -.43351 .350149
1.2681 .449999 .399868 -.43351 .350149
1.2681 .449999 .399868 -.43351 .350149
1.6968 .449999 .170625 -.89211 .349909
1.6436 .449999 .211187 -1.1857 .34994
1.6157 .449999 .235212 -1.3662 .349943
1.5571 .449999 .273184 -1.5737 .349947
1.4481 .449999 .335815 -1.9212 .349932
1.4507 .449999 .340975 -2.0334 .349947
1.3956 .449999 .37202 -2.2549 .349938
1.3956 .449999 .37202 -2.2549 .349938
1.0322 .449999 .573819 -.49156 .361243
1.0322 .449999 .573819 -.49156 .361243
1.0322 .449999 .573819 -.49156 .361243
1.0322 .449999 .573819 -.49156 .361243
1.7483 .449999 .187134 -.84686 .36105
1.5977 .449999 .278798 -1.3272 .361036
1.5133 .449999 .330664 -1.4705 .361066
1.3663 .449999 .409907 -1.7509 .361054
1.3292 .449999 .434644 -1.9871 .361052
1.2698 .449999 .467106 -2.0105 .361061
1.2231 .449999 .490906 -2.0786 .361059
1.2231 .449999 .490906 -2.0786 .361059
.753425 .449999 .76428 -.55332 .372397
.753425 .449999 .76428 -.55332 .372397
.753425 .449999 .76428 -.55332 .372397
1.738 .449999 .226997 -.86811 .372173
1.6099 .449999 .304069 -1.2807 .372155
```

```
1.4832 .449999 .379803 -1.5909 .372162
1.4921 .449999 .381734 -1.7206 .372173
1.4617 .449999 .40123 -1.8454 .372171
1.4294 .449999 .419732 -1.8695 .372175
1.3962 .449999 .439444 -1.999 .372166
1.2827 .449999 .498975 -2.2492 .372159
1.2827 .449999 .498975 -2.2492 .372159
.838856 .449999 .749521 -3.1371 .383267
.838856 .449999 .749521 -3.1371 .383267
.838856 .449999 .749521 -3.1371 .383267
.81541 .449999 .761919 -3.073 .383271
.786891 .449999 .774661 -2.9539 .383275
.874903 .449999 .726453 -2.8959 .383273
1.0291 .449999 .645609 -2.8029 .383275
.927111 .449999 .695154 -2.7796 .383273
.83679 .449999 .741303 -2.8965 .383267
.971011 .449999 .678623 -2.8787 .383273
.892046 .449999 .715255 -2.8584 .383273
.720834 .449999 .794219 -2.8793 .383271
.755343 .449999 .776979 -2.6782 .38328
.755343 .449999 .776979 -2.6782 .38328
.838856 .449999 .749521 -3.1371 .383267
.81541 .449999 .761919 -3.073 .383271
.786891 .449999 .774661 -2.9539 .383275
.874903 .449999 .726453 -2.8959 .383273
1.0291 .449999 .645609 -2.8029 .383275
.927111 .449999 .695154 -2.7796 .383273
.83679 .449999 .741303 -2.8965 .383267
.971011 .449999 .678623 -2.8787 .383273
.892046 .449999 .715255 -2.8584 .383273
.720834 .449999 .794219 -2.8793 .383271
.755343 .449999 .776979 -2.6782 .38328
.755343 .449999 .776979 -2.6782 .38328
```

RESULT AND DISCUSSION

In Chapter 3 the methods of calibration of the hot–wire in isothermal and non–isothermal fluid flows have been discussed. The following procedure is used to obtain velocity, velocity fluctuations and temperature at a point in the test cell.

4.1. Measurement and Calculation Procedures for Isothermal Fluid Flow

A single wire probe calibrated as discussed in previous chapter is used to measure the velocity and to produce instantaneous signal corresponding of voltage signal of the wire. The velocity and turbulence level of the flow are then calculated as given below. Turbulence statistics such as autocorrelation and probability density function are obtained numerically from the computer–acquired digitized signal. Data acquisition is carried out on a storage–scope which has 2 MHz sampling speed and 8 bit digitizing accuracy. Data transfer to the computer, a PC–XT is in integer form.

Sample calculations.
RAW DATA.

Isothermal Shear Flow
Blower Variac Setting BVS = 70 V
Down Stream distance x = 150 cm
Ambient Fluid Temperature 21.5 C

LOCATION y(cm)	HOT–WIRE OUTPUT E(Volts)	RMS VOLTAGE e'(Volts)
2.0	1.4632	0.0150
2.5	1.4775	0.0140
3.0	1.4948	0.0090

LOCATION y(cm)	HOT–WIRE OUTPUT E(Volts)	RMS VOLTAGE e'(Volts)
2.0	1.4632	0.0150
2.5	1.4775	0.0140
3.0	1.4948	0.0090
3.5	1.4983	0.0045
4.0	1.4967	0.0035
4.5	1.4954	0.0040
5.0	1.4920	0.0060
5.5	1.4833	0.0075
6.0	1.4783	0.0090
6.5	1.4675	0.0090
7.0	1.4615	0.0080

Temperature Correction :

Temperature of the wire $T_w = 150^{\circ}C$

Ambient fluid temperature during calibration $T_c = 21.5^{\circ}C$

Correction factor $= \sqrt{\frac{T_w - T_f}{T_w - T_c}}$

Corrected voltage $X_i = E_i \cdot \text{Factor}$

For i=1, $X_1 = E_1 * 1 = 1.4632$

Normalization of Hot–wire Output :

$$XT_i = 10 \cdot (X_i - XO_1)/(XO_n - XO_1)$$

Where XO_n and XO_1 are first and last values of the smoothed calibration data.

$$XO_n = 1.5667 \text{ V}$$

$$XO_1 = 1.3726 \text{ V}$$

Hence, for i=1, $XT_1 = 4.6677$.

Similarly repeating the same procedure for all values of E_i, we get the normalized values of Ei. These values are tabulated below:

Normalized data.

XT1 = 4.6677

XT2 = 5.4044

XT3 = 6.2957

XT4 = 6.4760

XT5 = 6.3936

$$XT6 = 6.3266$$
$$XT7 = 6.1515$$
$$XT8 = 5.7032$$
$$XT9 = 5.4456$$
$$XT10 = 4.8892$$
$$XT11 = 4.5801$$

THE LINEARIZER EQUATION:

The equation

$$Y = 10^{(A+BX+EY)} + CX + D$$

relates normalized voltage to normalized velocity ($u/u_{x_{max}}$).
Here, A = –1.2603720, B = 0.1513271, C = 0.5294150, D = 3.2000000 and E = –0.0068722, are the curve fitting parameters.

CALCULATION OF VELOCITY (Newton–Raphson scheme) :

1. Calculate the value of $G = 10.0^{(A+B\cdot XT_i)}$.
2. Calculate the value of $F = (C\cdot XT_i+D)/G$.
3. Let YCO = 5.0
4. Find the value of $\Delta Y = \dfrac{10.0^{(E\cdot YCO)} - \dfrac{YCO}{G} + F}{E\cdot\ 10.0^{(E\cdot YCO)}\cdot ALOG(10.0-1.0/G)}$
5. YCO = YCO – ΔY

TEST FOR THE CONVERGENCE

6. Obtain the value of $Big = 100 \cdot ABS\left(\dfrac{\Delta Y}{G}\right)$
7. If Big is less than or equal to 0.01, go to step 8. Otherwise repeat steps 4 – 9.
8. Calculate the velocity of the fluid $ui = YO_n * \dfrac{YCO}{10}$
9. Thus u1 = 2.83611 m/s.

CALCULATION OF RMS VELOCITY FLUCTUATION

10. Calculate the gradient of curve at YCO and XT_i

$$dYX = \frac{B\cdot 10^{(A+B\cdot XT_i+E\cdot YCO)}.\ ALOG(10.0) + C}{1.0 - (E\cdot ALOG(10.0)\cdot(10.0^{(A+B\cdot XT_i+E\cdot YCO)}))}$$

11. $dYX = \frac{YO_n}{(XY_n - XO_1)} \cdot dYX.$
12. RMS value of velocity fluctuation ui' = dYX · ei'.
13. Turbulence level $= \frac{ui'}{ui} \cdot 100.$
14. Thus turbulence level of the first reading = 8.02%
15. Repeat the above steps to calculate the values of all the readings.

A program *REDUCE.F* is written to perform these steps and to obtain the flow properties. The table given below gives the calculated values of the flow presented earlier as Raw data.

Output of REDVC.FOR
Isothermal Shear Flow
Blower Variac Setting 70V
Downstream distance 150 cm.

Location (cm)	Output (V)	Velocity (m/s)	e' (V)	u' (m/s)	u' %
2.00000	1.46320	2.83611	.01500	.22768	8.02781
2.50000	1.47750	3.05726	.01400	.22088	7.22465
3.00000	1.49480	3.33802	.00900	.15055	4.51002
3.50000	1.49830	3.39696	.00450	.07630	2.24620
4.00000	1.49670	3.36992	.00350	.05897	1.75002
4.50000	1.49540	2.34807	.00400	.06706	2.00301
5.00000	1.49200	3.29143	.00600	.09932	3.01762
5.50000	1.48300	3.14959	.00750	.12049	3.82543
6.00000	1.47830	3.06990	.00900	.14233	4.63645
6.50000	1.46750	2.90172	.00900	.13809	4.75886
7.00000	1.46150	2.81036	.00800	.12093	4.30313

4.2. Measurement and Calculation Procedure for Non–Isothermal Fluid Flow

A two–wire probe is used to measure the properties of non–isothermal fluid flow. The wires are parallel to each other and 5 mm apart. One measures the velocity of the fluid in the constant temperature mode and the other measures the local fluid temperature as a resistance thermometer. All measurements are carried out after the flow attains an equilibrium thermal configuration. This usually requires a waiting period of 20 minutes for each experiment. The following is a list of the instruments used and their measurands.

Hot–wire1	Temperature	Programmable Digital Multimeter
Hot–wire2	Mean Velocity	Mean value unit
Hot–wire2	RMS velocity	RMS voltmeter.

Calculation of mean velocity and turbulence level in non–isothermal flow is given below.

Sample Calculations

RAW DATA

Non–isothermal Flow
Blower Variac Setting 80 V
Heater Variac Setting 50 V
Downstream distance 100 cm

Location y(cm)	Hot wire E(V)	RMS Voltage e'(V)	Fluid Temperature Tf K(C)
2.0	1.3602	0.0060	36.30
2.5	1.3691	0.0070	35.87
3.0	1.3756	0.0075	35.88
4.0	1.3991	0.0100	33.92
4.5	1.4136	0.0100	33.30
5.0	1.4267	0.0120	31.90
5.5	1.4480	0.0100	29.62
6.0	1.4629	0.0100	28.05
6.5	1.4737	0.0090	26.67
7.0	1.4808	0.0080	24.71

Method of Varying Overheat Resistance :

Reference overheat Resistance of wire (Rhc) = 12.50 Ohm.

Reference Fluid temperature CTr = 23.0

Resistance of wire at $0^{\circ}C$, RO = 9.4719 Ohm.

Temperature coefficient of resistance of hot wire

Material $\alpha = 0.36\%$

1. Calculate $b = RO + Tr \cdot \alpha \cdot RO$
2. Calculate $c = Rhc \cdot (Rhc - RO - \alpha \cdot RO \cdot Tfk)$
3. Equivalent overheat resistance of fluid temperature Tfk,

$$Rhvk = \frac{b}{2} + \frac{\sqrt{(b^2 + 4 \cdot C)}}{2}$$

Thus for i = 1, the equivalent overheat resistance of fluid temperature 36.3°C is 12.1049 Ohms. The following table shows the values of Rhvi.

Fluid temperature °C	Overhear resistance Ohm
36.3000	12.1049
35.8700	12.1180
35.2800	12.1360
34.4400	12.1615
33.9200	12.1772
33.3000	12.1960
31.9000	12.2381
29.6200	12.2381
28.0500	12.3525
26.6700	12.3931
24.7100	12.4504

Equation Governing the Hot Wire Operation in Non–isothermal Fluid Flow :

For small changes in the anemometer voltage Ec and R the overheat resistance Rhvk, we assume the following interpolation equation to hold.

$$Eck^2 \cdot \left(\frac{Rhvk}{RO} - Cij\right)^{bij} = Aij + Bij \cdot uk^n$$

where, n = 0.45

In the previous chapter we calculated the values of Aij, Bij, bij and Cij for all readings of calibration data. Let Uij, Ri and E1j be the calibration data. The following procedure shows the way of calculating the output of the hot–wire when the equivalent overheat resistance is computed.

4. Find two successive values of Ri,such that Ri < Rhvk < Ri+1.
5. Find two successive values of E1j, such that E1j < Ek < E1j+1.
6. Obtain the values of Aij, Bij, bij and Cij.
7. Calculate the gradient of E and Rhv from the relation

$$derij = \left.\frac{dE_1^2}{dR}\right|_{i,j} = \frac{-bij \cdot (Aij + Bij \cdot uij^n}{RO \cdot \left(\frac{R_i}{RO} - Cij\right)^{(bij+1)}}$$

8. Calculate the output of the wire for equivalent overheat resistance Ec as

$$Ecj^2 = Ej^2 - \frac{Rhc(Rhc-RO-\alpha \cdot RO \cdot Tfk)}{Rhvk(Rhvk-RO-\alpha \cdot RO \cdot Tr)} \cdot derij \cdot (\alpha \cdot RO \cdot (Tfk-Tr)).$$

The following table gives the values of derij and Ecj for all values of Tfk given earlier in the table of raw data.

Hot–wire output for varying fluid temperature (V)	der V2/Ohm	Hot–wire output for varying overheat resistance (V)
1.3602	.0613	1.3499
1.3691	.0612	1.3593
1.3756	.0611	1.3663
1.3869	.0942	1.3736
1.3991	.0950	1.3864
1.4136	.1996	1.3886
1.4267	.1127	1.4147
1.4480	.1297	1.4379
1.4629	.1314	1.4551
1.4737	.3129	1.4604
1.4808	.7704	1.4656

Calculation of Fluid Velocity :

9. Find two successive values of Ri, such that Ri < Rhvk < Ri+1.
10. Find two successive values of E1j, such that E1j < Eck < E1j+1.
11. Obtain the values of Aij, Bij, bij and Cij.
12. Calculate the velocity of the fluid uk as,

$$uk = \left[\frac{Eck^2 \left(\frac{Rhvk}{RO} - Cij \right)^{bij}}{Bij} - Aij \right]^{(1/45)}$$

13. Calculate duek as

$$duek = \frac{\left[\frac{Rhvk}{RO} - Cij \right]^{bij} \cdot 2 \cdot Eck}{Bij \cdot 0.45 \cdot uk^{-0.55}}$$

14. RMS value of fluctuation u' = ek'. duek.

15. Turbulence level $= \frac{u'}{u} \cdot 100$

The above steps are repeated to calculate the flow properties for all data collected in this work. The following table shows the flow quantities for the raw data referred above.

y–Location cm	Temp °C	Vel m/s	u' m/s	u' %
2.0000	36.3000	2.0999	.0646	6.4618
2.5000	35.8700	2.3066	.0727	7.2721
3.0000	35.2800	2.4635	.0760	7.5955
3.5000	34.4400	2.6285	.0790	7.9025
4.0000	33.9200	2.9599	.0944	9.4444
4.5000	33.3000	3.0037	.1033	10.3274
5.0000	31.9000	3.2150	.0778	7.7797
5.5000	19.6200	2.2670	.0486	4.8556
6.0000	18.0500	3.6220	.0427	4.2674
6.5000	16.6700	3.6807	.0377	3.7700
7.0000	24.7100	3.4480	.0299	2.9863

We have developed a program READ.F to calculate the flow properties in non–isothermal problems. The following sections present the results of the experimental study of turbulent flow in stratified shear flows. The x coordinate referred below has the following meaning:

Configuration	x (Measured from)
No cylinder	exit of contraction cone
With cylinder	center of the cylinder

Isothermal Parallel Flow :

This is a case of undisturbed flow through the test cell. No perturbing object or a shearing honeycomb is placed in the flow. The vertical distribution of velocity is mainly due to turbulent boundary–layers growing on the channel walls. Two different mean flow velocities are studied. Blower variac settings (BVS) of 70V and 80V are used. BVS of 70V produces a fully developed mean flow of 3.6 m/s and 80V produces a flow of 4.7 m/s. Fig. 4.1 shows the vertical distribution of velocity at three different downstream distances, X =

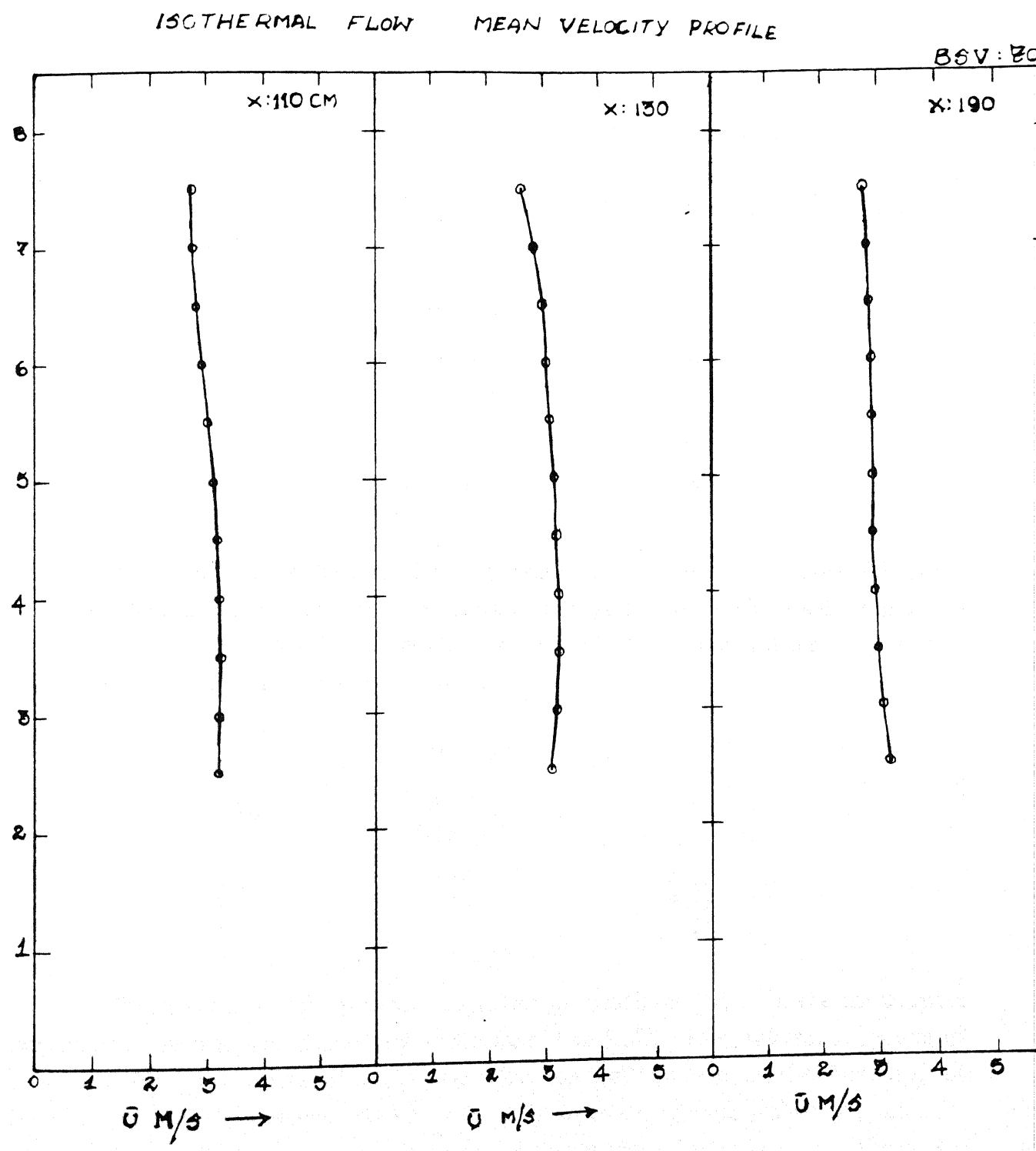

FIG. 4.1 ISOTHERMAL PARALLEL FLOW

100 cm, X = 130 cm and X = 190cm. Van Atta et al (1988) have analyzed growth of turbulence in shear flow through a dimensionless number defined as

$$Sh = \frac{u}{Um} \cdot \frac{du}{dy}$$

They observe growth of turbulence for Sh > 4 in all their studies. In this study du/dy is calculated as (umax − umin)/L, (umin > 0), for monotonically varying velocity profiles and L is the separation between these points. For symmetric profiles, only one half of the test cell is examined to form the derivative. The following list shows the variation of Sh in the downstream direction.

BVS = 70V

X(m)	du/dy (m/s/m)	Sh
1.1	10	3.3
1.3	10	4.19
1.9	10	6.33

Figure 4.2 shows the vertical distribution of turbulence level at three different X positions. The average turbulence level increases downstream from 2% to 4%. Figure 4.3 shows the vertical distribution of velocity for BVS = 80V at three different X positions. The variation of du/dy and Sh are given below.

BVS = 70V

X(m)	du/dy (m/s/m)	Sh
1.1	14	4.28
1.3	16	5.62
1.9	22	11.94

Figure 4.4 shows the vertical distribution of turbulence level. In the downstream direction the average turbulence level varies from 2 to 2.5%. The preferential growth of turbulence for large values of y (i.e. near the top wall) is due to the formation of boundary–layer in this region. A similar trend is expected for small values of y as well. This data has not been obtained due to limitations in the traversing mechanism. Figure 4.5 shows the development of mean flow and evolution of turbulence level for both BVS = 70 and 80V along the mid–plane of the channel.

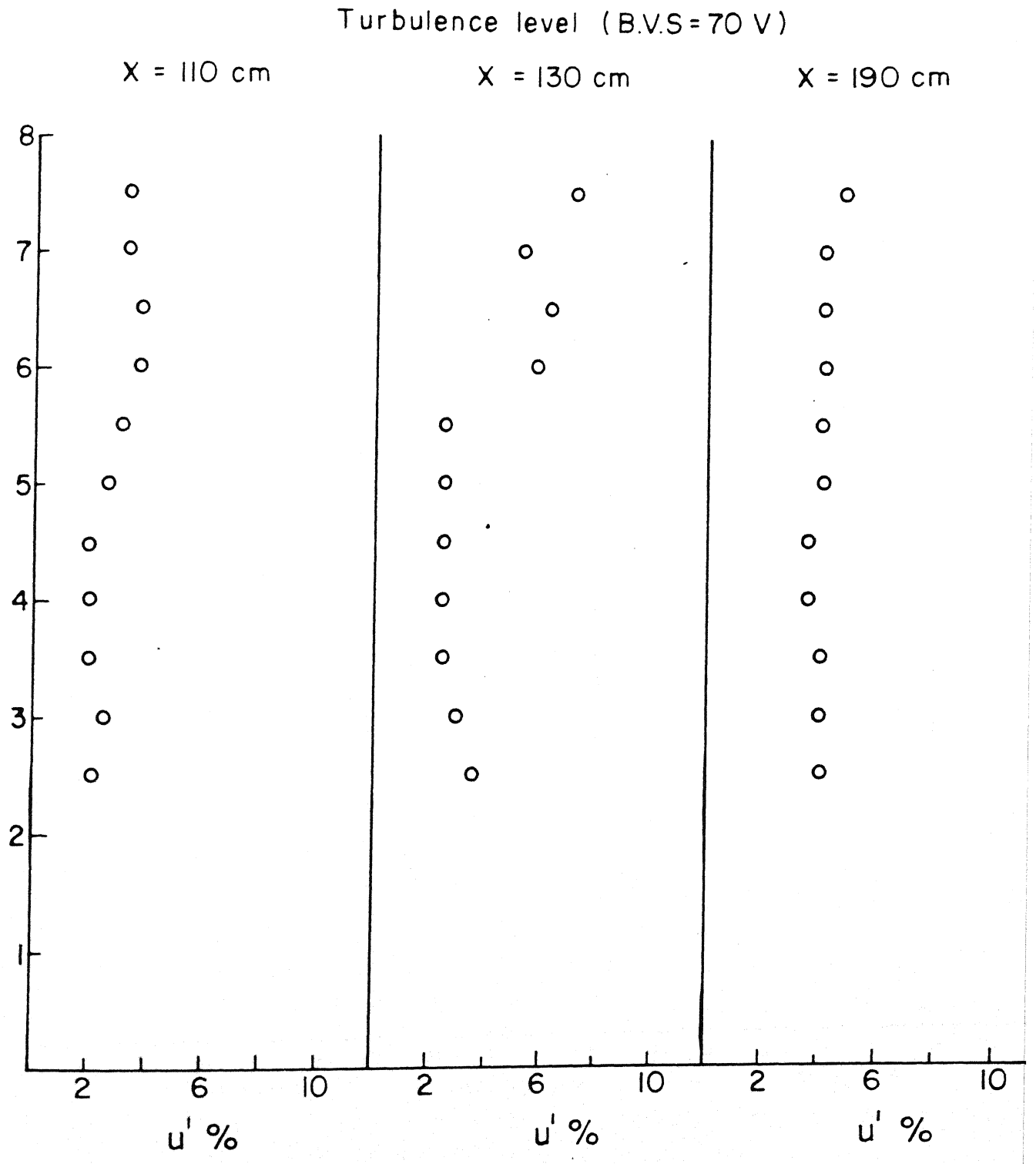

FIG. 4.2 ISOTHERMAL PARALLEL FLOW

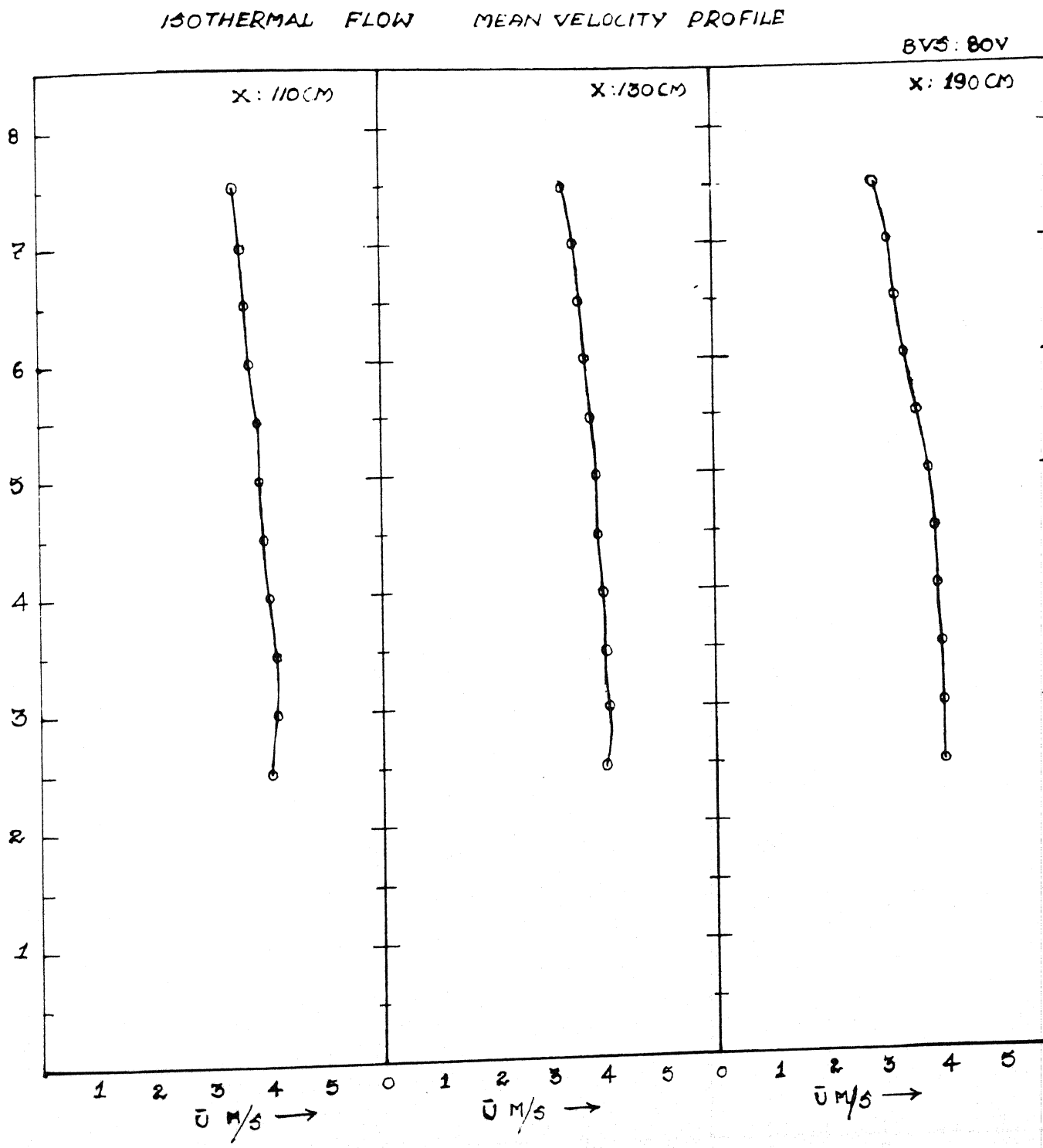

FIG. 4.3 ISOTHERMAL PARALLEL FLOW

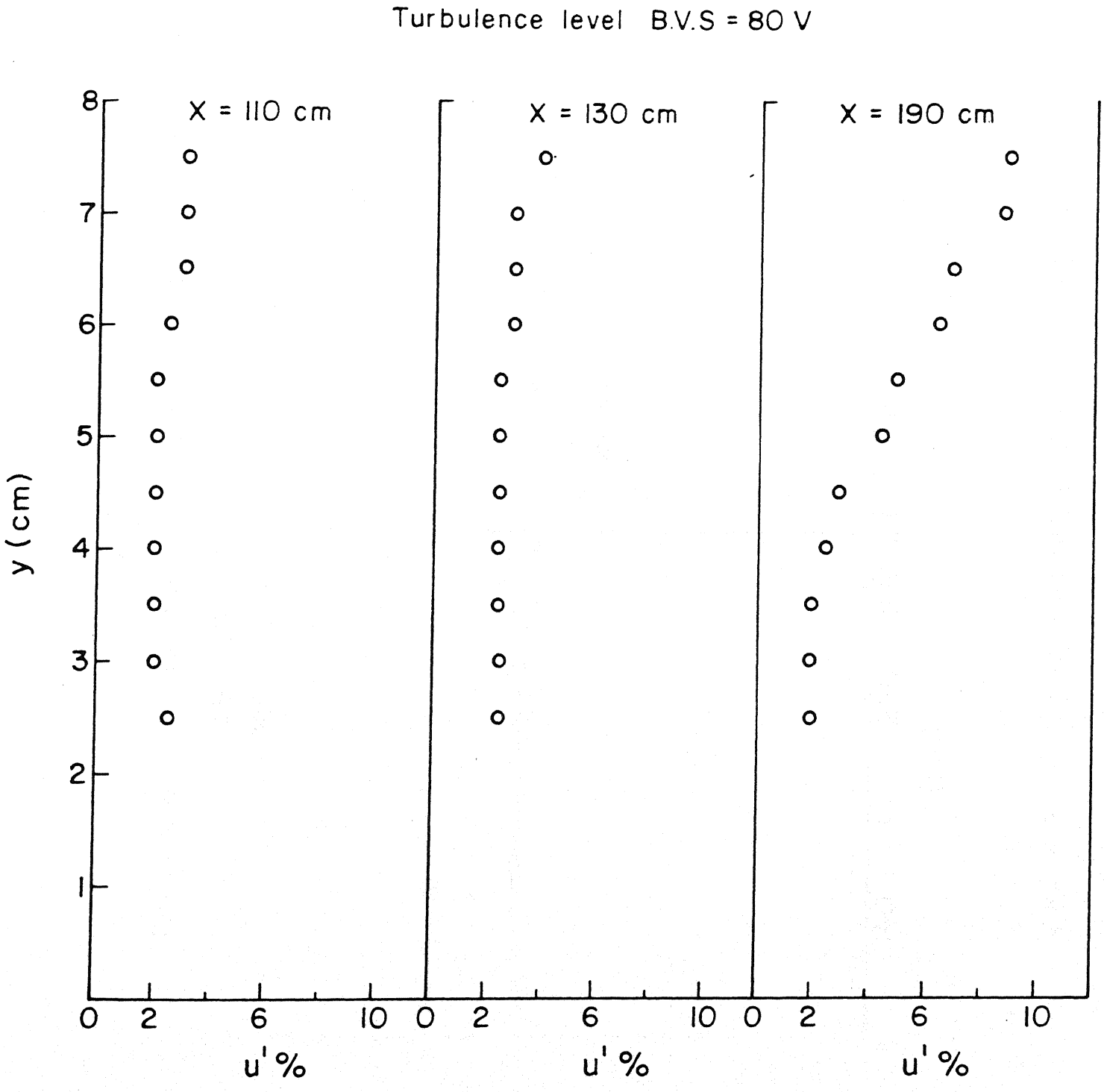

FIG. 4.4 ISOTHERMAL PARALLEL FLOW

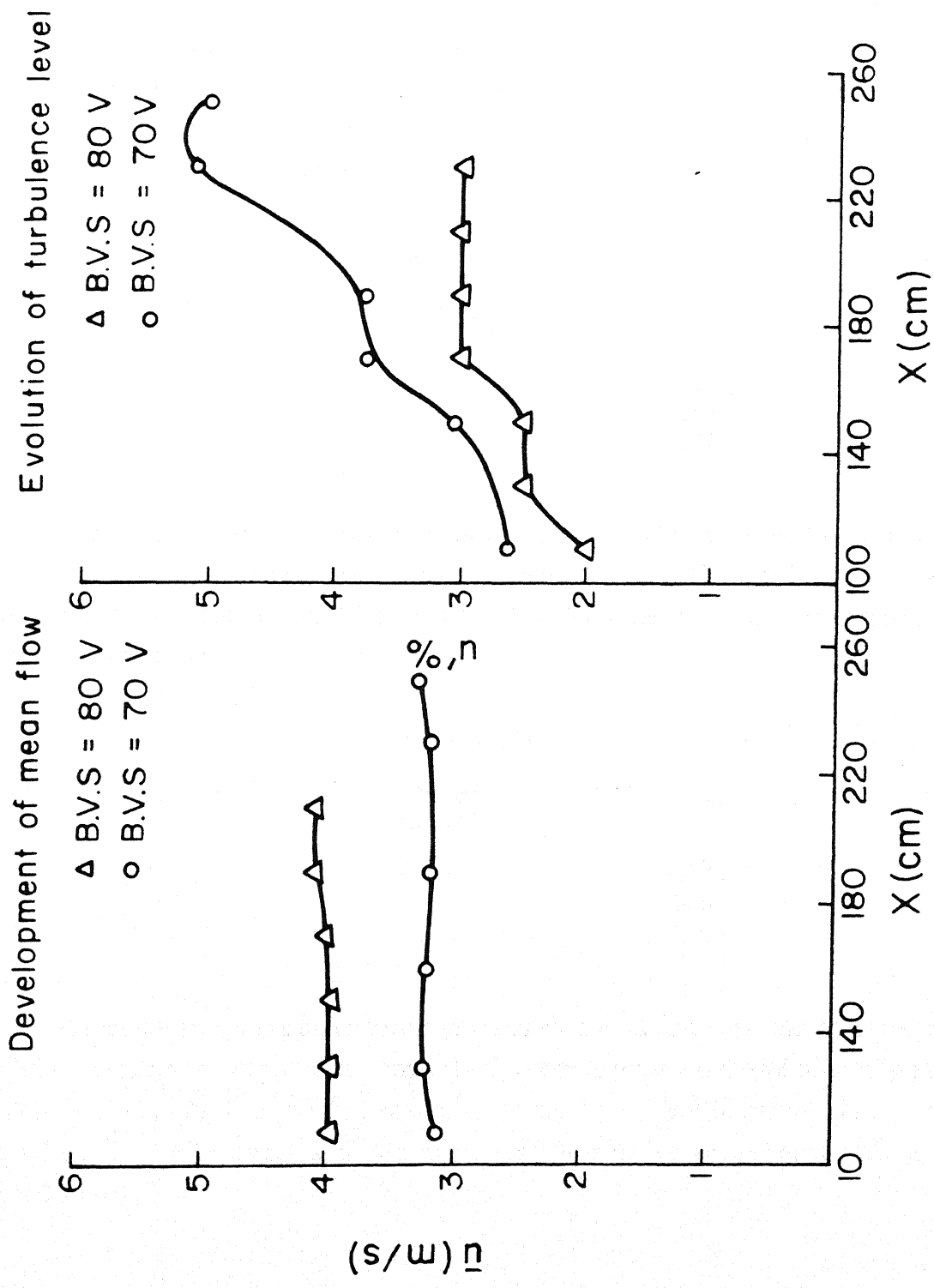

FIG. 4.5 ISOTHERMAL PARALLEL FLOW

Isothermal Parallel Flow over Cylinders :

A cylinder of 1 cm diameter is placed in the flow at the inflow plane (x = 0). This point is itself 73cm away from the exit plane of the converging cone. Two values BVS are again used to study the behavior of flow past the cylinder. The value of Red is calculated to discuss the behavior of the flow. Figure 4.6 shows the vertical distribution of velocity at three different downstream distances. The following table shows the values of du/dy and Red for the three different X positions.

BVS = 70V

X(m)	du/dy (m/s/m)	Red	Sh
1.1	4	1923	1.42
1.3	6	2051	2.40
1.9	16	2151	9.21

Figure 4.7 shows the distribution of turbulence level at three different X positions. The average value of turbulence level is seen to decrease from 4.5% to 2%. Figure 4.8 shows the vertical velocity profiles for BVS = 80V. The following list shows the variation flow parameters downstream.

BVS = 80V

X(m)	du/dy (m/s/m)	Red	Sh
1.1	4	2244	1.31
1.3	6	2308	2.17
1.9	14	2404	6.82

Figure 4.9 shows the distribution of turbulence level and it is seen to decrease from 4%–2% in downstream. Figure 4.10 shows the flow development and evolution of turbulence level along the mid–plane of the channel. There is a slow increase in mean velocity due to a decrease in the velocity defect and also due to the flow in the tunnel approaching a fully developed state.

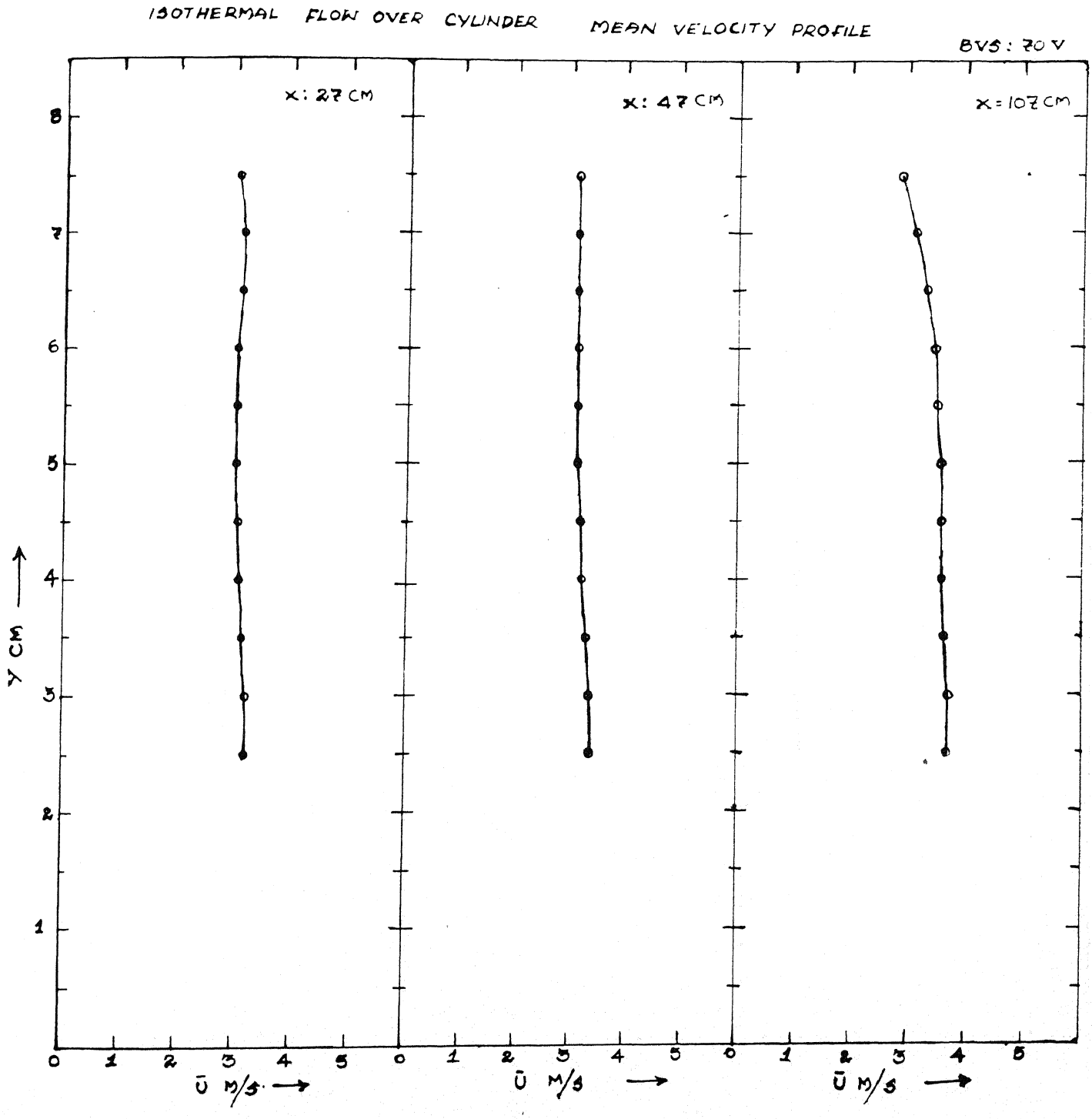

FIG. 4.6 ISOTHERMAL PARALLEL FLOW PAST A CYLINDER

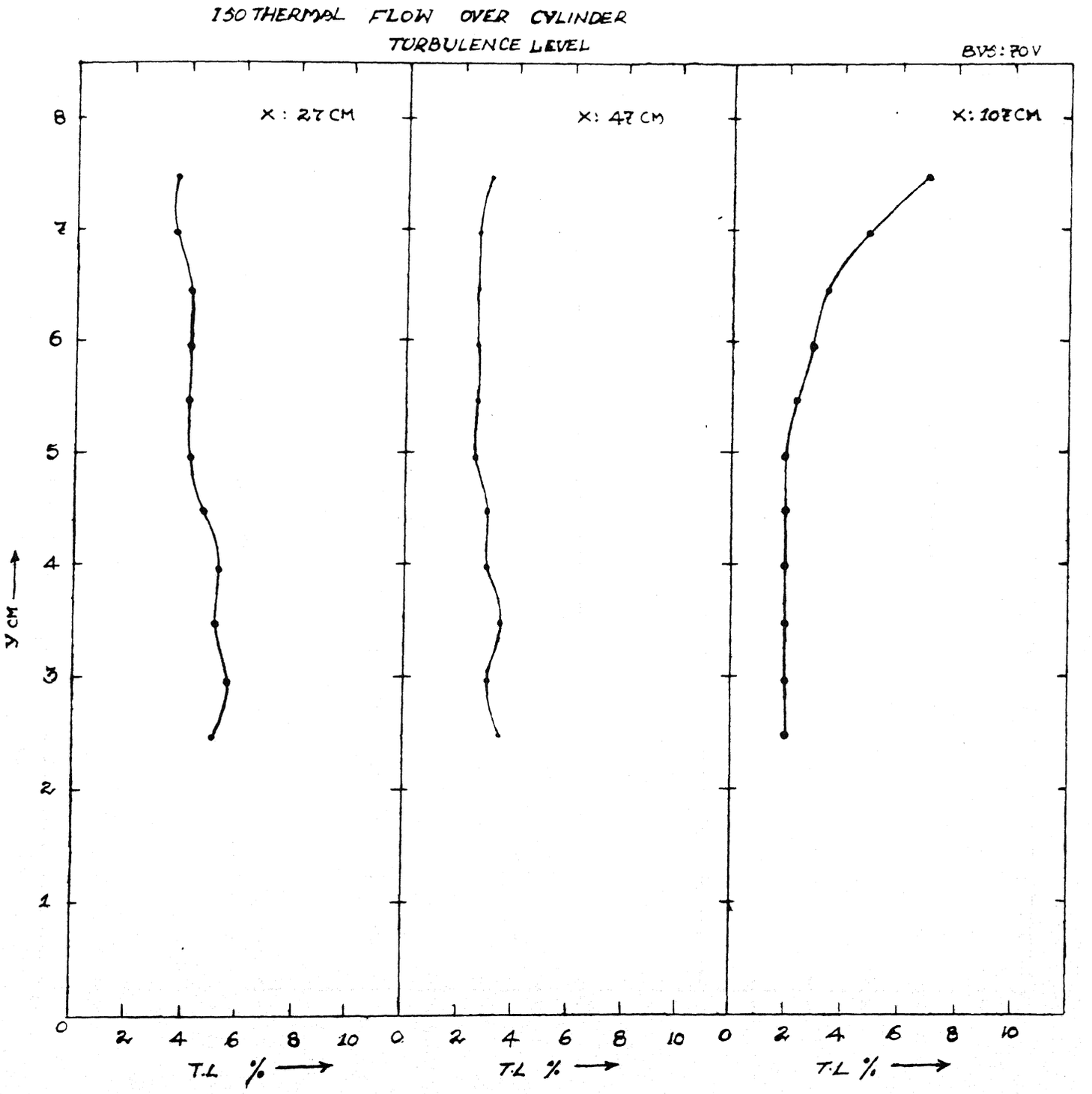

FIG. 4.7 ISOTHERMAL PARALLEL FLOW PAST A CYLINDER

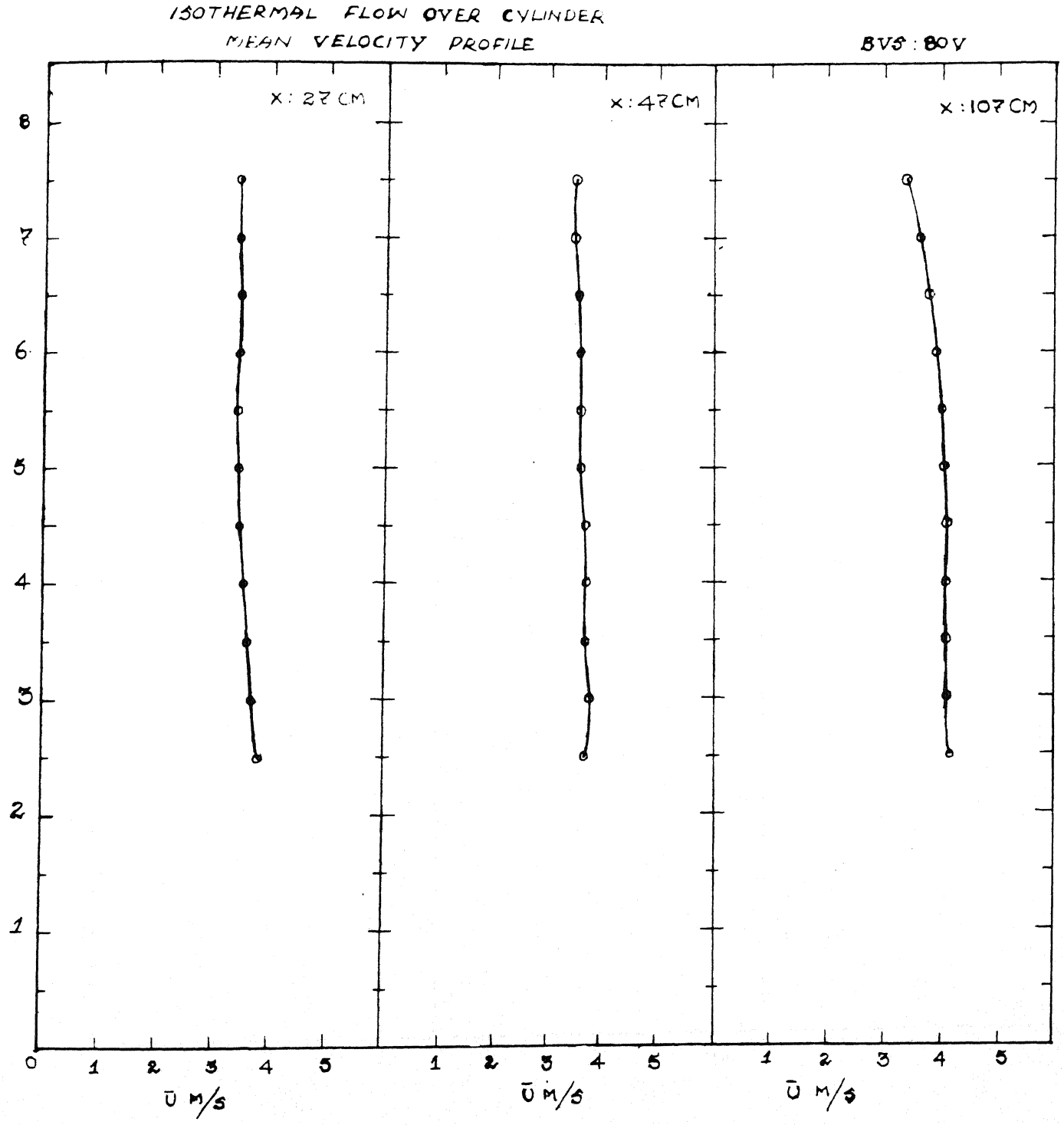

FIG. 4.8 ISOTHERMAL PARALLEL FLOW PAST A CYLINDER

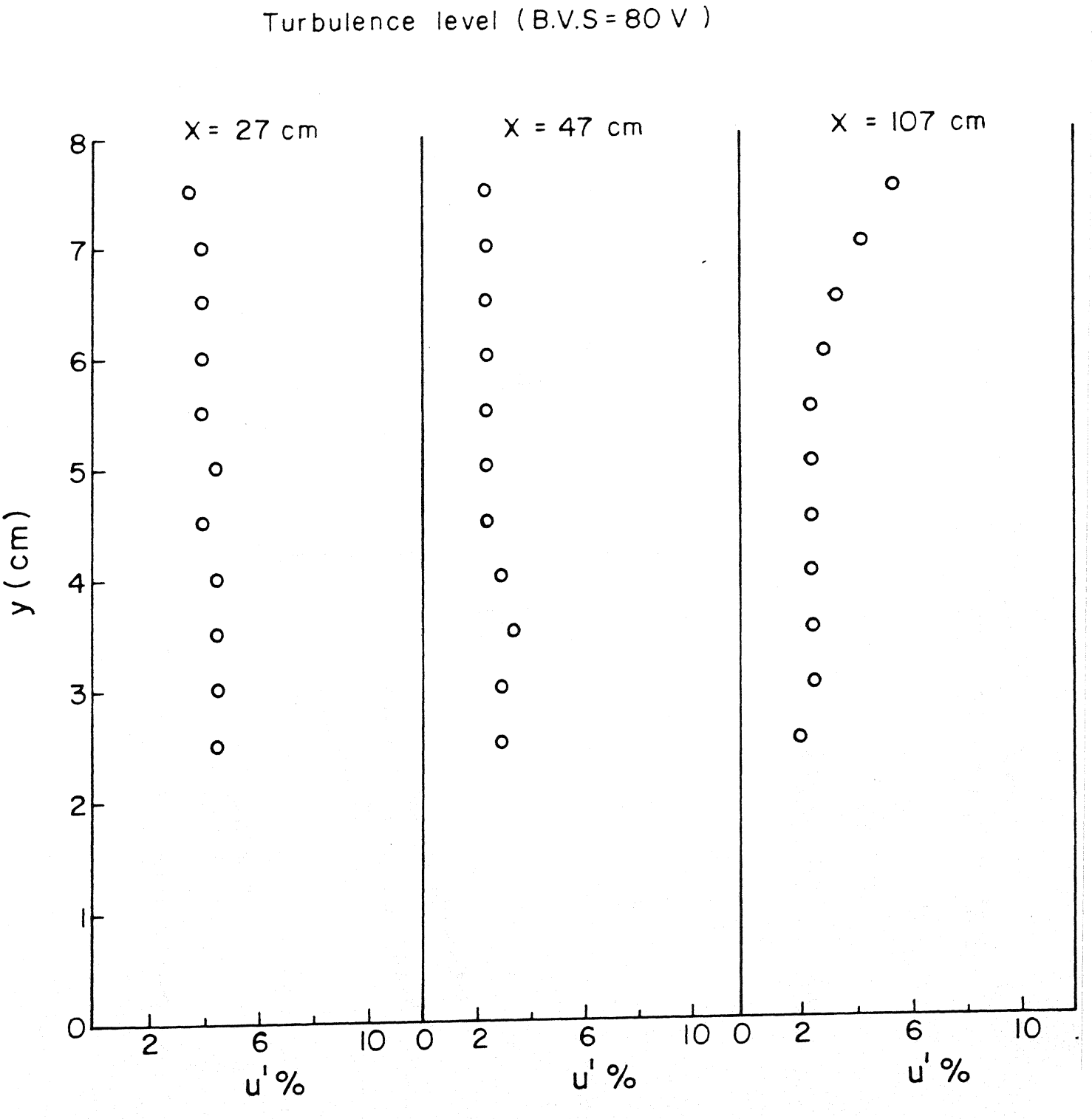

FIG. 4.9 ISOTHERMAL PARALLEL FLOW PAST A CYLINDER

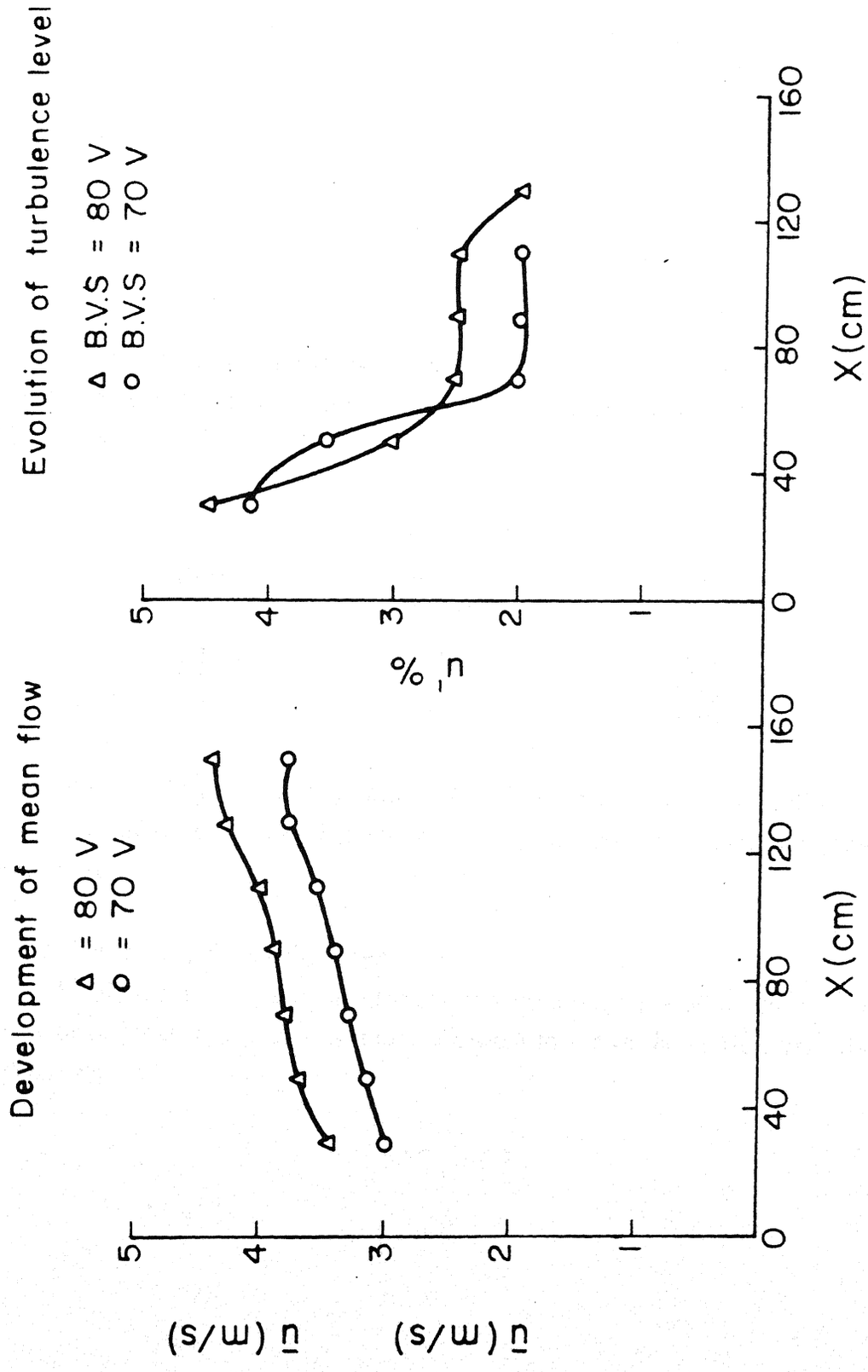

FIG. 4.10 ISOTHERMAL PARALLEL FLOW PAST A CYLINDER

Isothermal Shear Flow :

A parabolic shaped honeycomb is placed in the channel to produce shear flows. Figure 4.11 shows the vertical velocity profiles at two different X positions. The variation flow parameters is given in following table:

BVS = 70V

X(m)	du/dy (m/s/m)	Sh
1.1	18	6.6
1.5	20	8.125

Figure 4.12 shows the variation of turbulence level in the downstream direction. The average turbulence level increases in this direction. Figure 4.13 shows the velocity profiles for BVS = 80V.

BVS = 80V

X(m)	du/dy (m/s/m)	Sh
1.1	22	7.68
1.3	14	5.53
1.5	12.5	5.60

Figure 4.14 shows the variation turbulence level in the y–direction. Figure 4.15 shows the downstream flow development and change of turbulence level along the mid–plane of the channel.

Isothermal Shear Flow Past a Cylinder :

A cylinder and a parabolic–shaped honeycomb are placed in the test cell to study the behavior of shear flow past a cylinder. Figure 4.16 shows the vertical velocity profiles at three positions.

BVS = 70V

X(m)	du/dy (m/s/m)	Red	Sh
1.1	18	1891	6.71
1.2	14	1923	5.60
1.5	2	1923	1.00

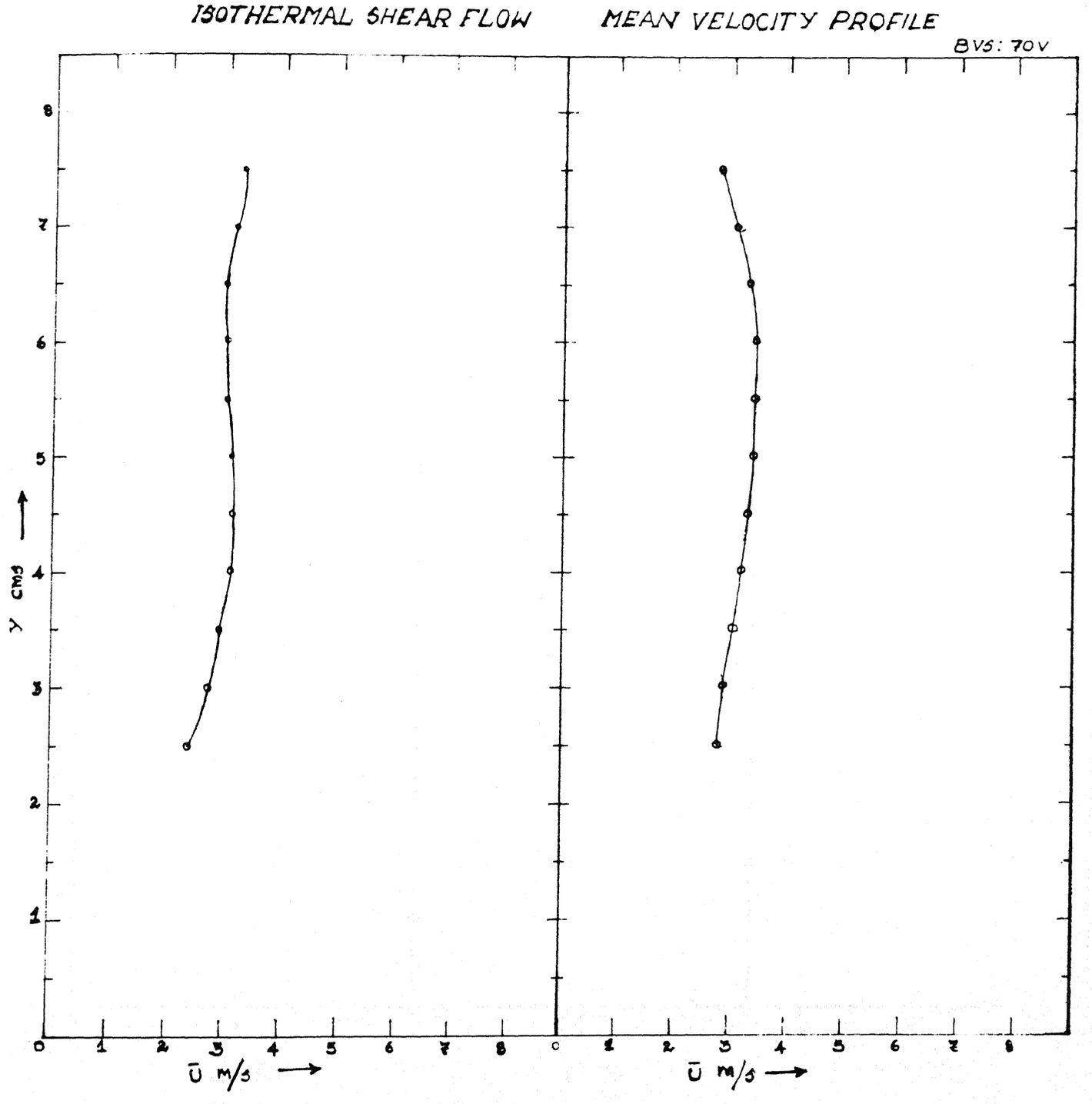

FIG. 4.11 ISOTHERMAL SHEAR FLOW

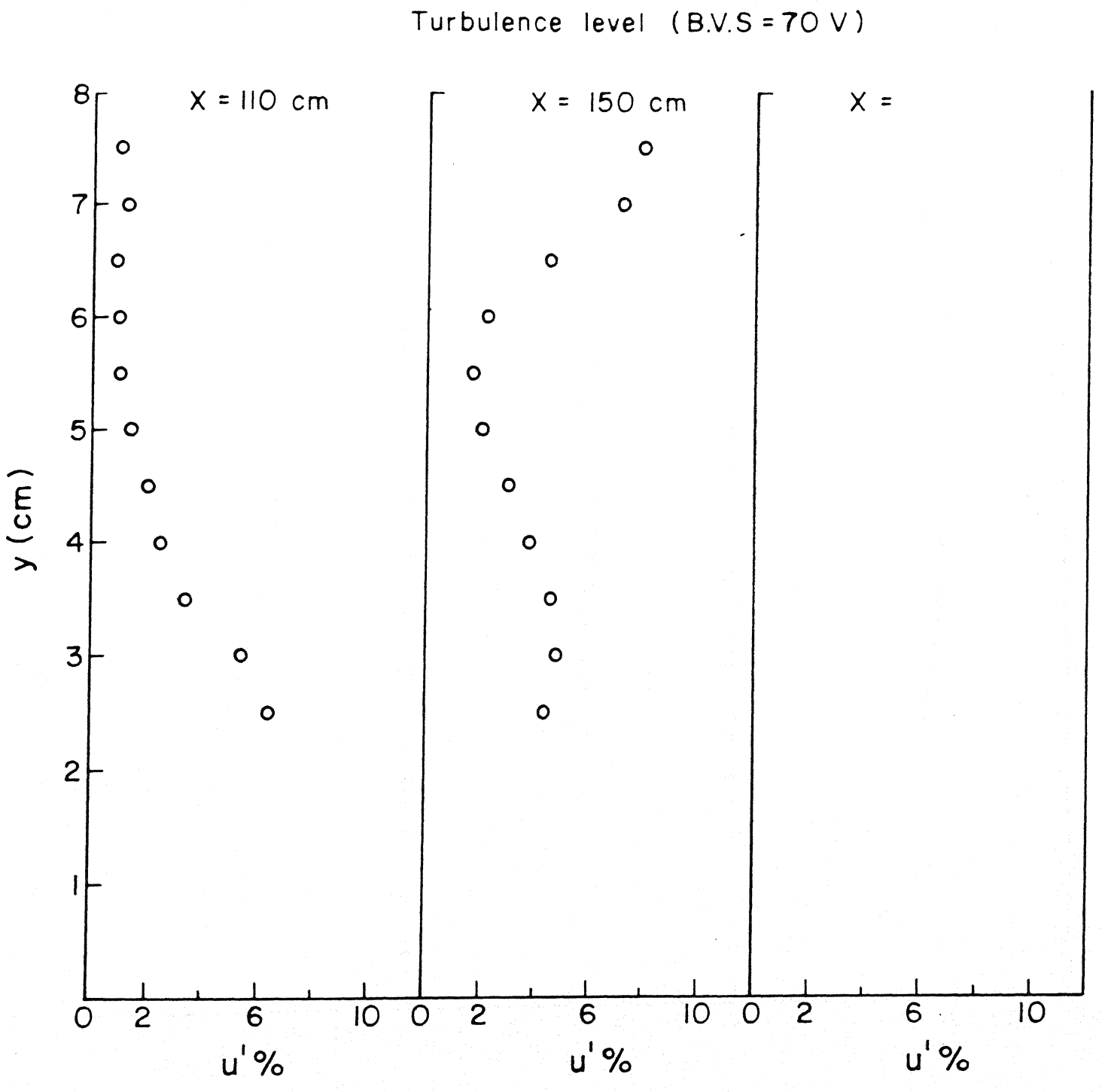

FIG. 4.12 ISOTHERMAL SHEAR FLOW

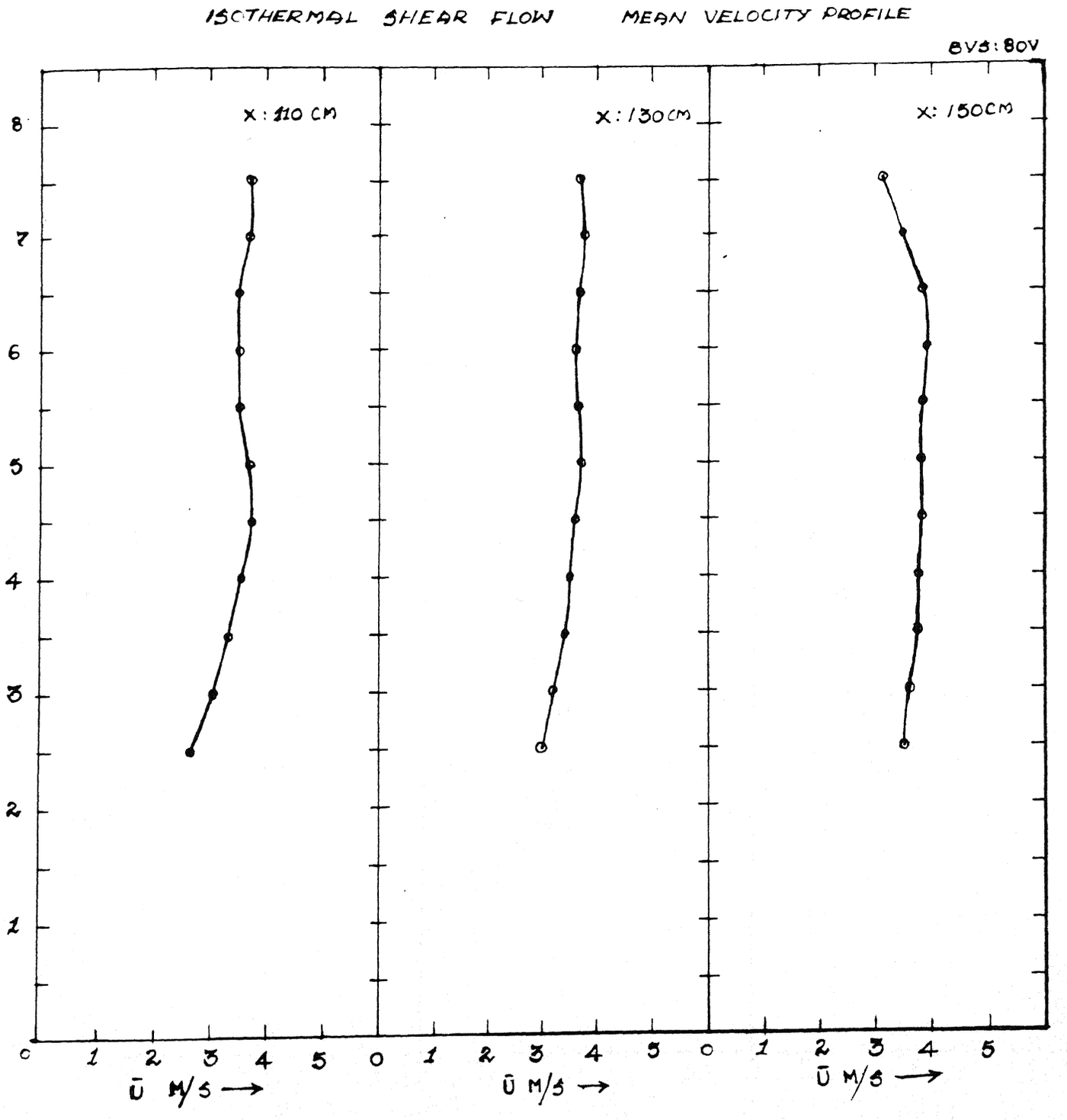

FIG. 4.13 ISOTHERMAL SHEAR FLOW

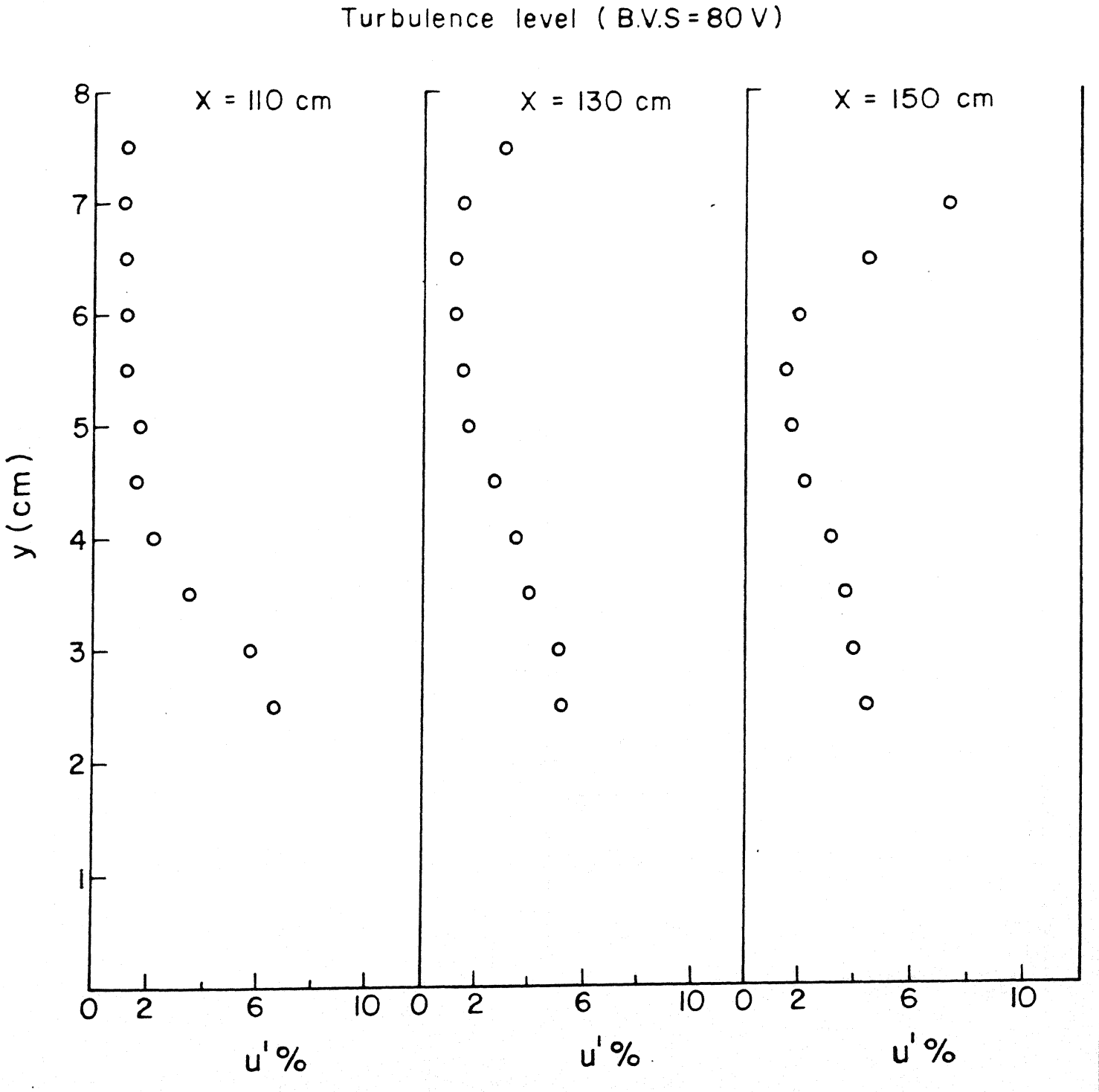

FIG. 4.14 ISOTHERMAL SHEAR FLOW

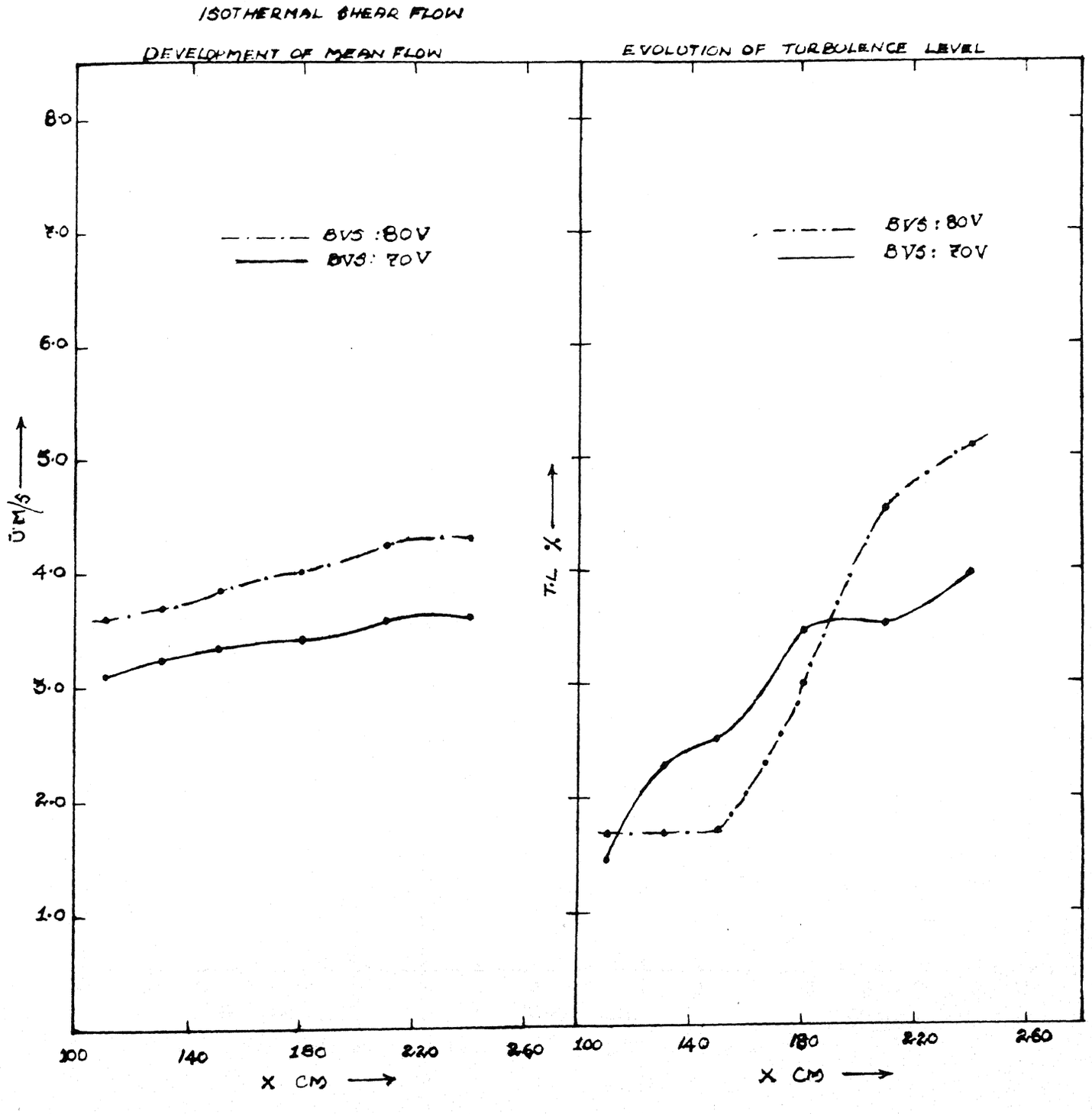

FIG. 4.15 ISOTHERMAL SHEAR FLOW

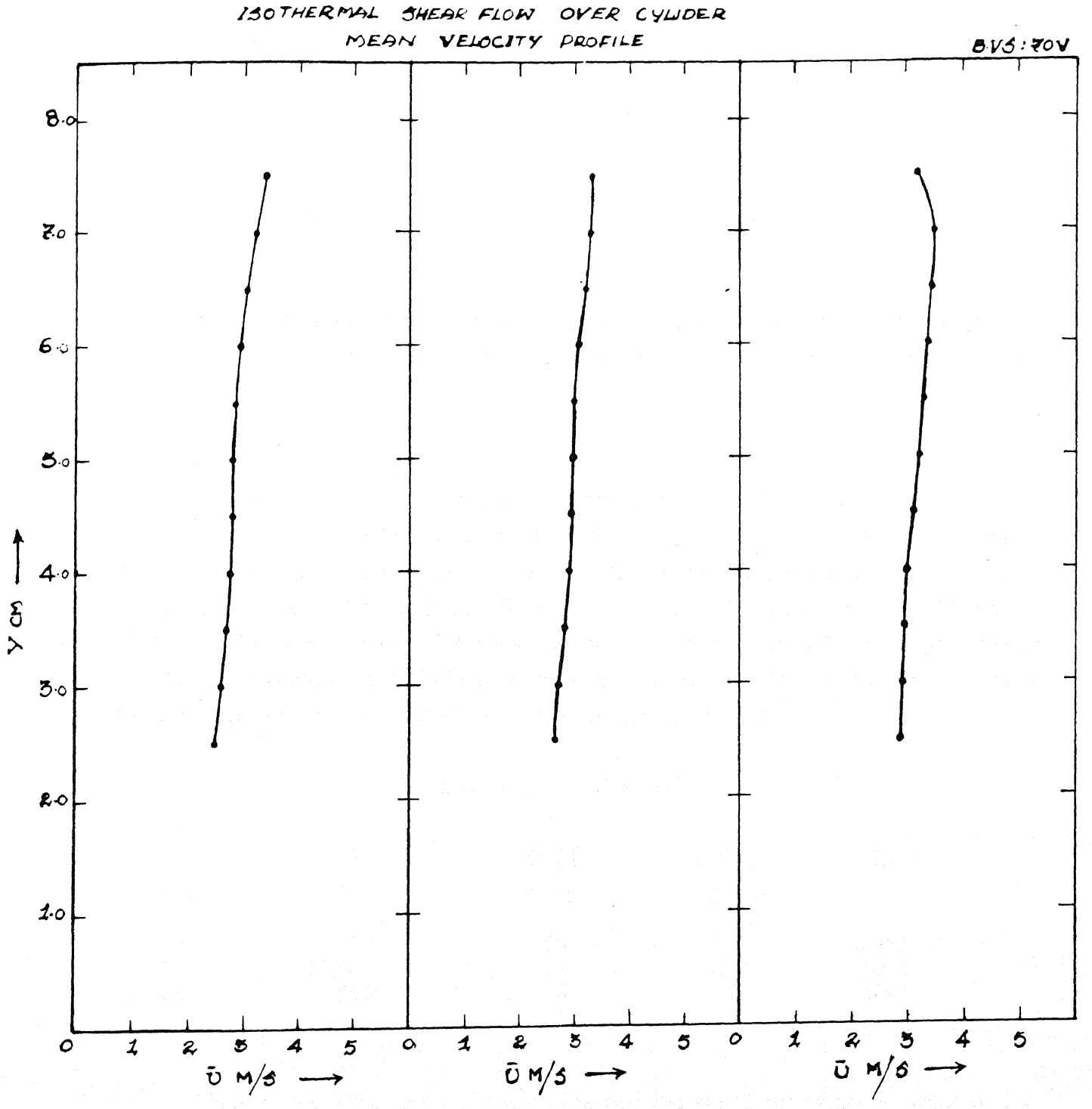

FIG. 4.16 ISOTHERMAL SHEAR FLOW PAST A CYLINDER

Figure 4.17 shows the variation of turbulence level along the y–direction.

BVS = 80V

X(m)	du/dy (m/s/m)	Red	Sh
1.1	14	2147	4.60
1.3	15.56	2147	6.13
1.5	15.56	2147	8.47

Figure 4.19 shows the vertical distribution of turbulence level at three different X locations. Figure 4.20 shows the variation of velocity and turbulence level along the axis of the test cell.

Non–isothermal Parallel Flow :

Air flow through the test cell is differentially heated so that it becomes stably stratified in density. In the first case, no obstacle is placed in the cell and homogeneous parallel flow is studied to understand the effect of heating. Figure 4.21 shows the vertical distribution of temperature at three different X positions. The heater variac (HVS) setting is 30V and BVS is 70V. Figure 4.22 shows the velocity distribution at 3 X positions. Figure 4.23 shows the variation of turbulence level in the y–direction. The table shows the values of the average flow variables including Ri, the Richardson number.

BVS = 70 V HVS = 30V

x (m)	Tm (°C)	dT/dy °C/m	du/dy (m/s/m)	Ri
1.1	25.3	88	12	0.237
1.3	25.1	92	8	0.562
1.9	25.2	48	14	0.0953

Figure 4.24, 4.25 and 4.26 shows the distribution of temperature, velocity and turbulence level respectively for the BVS = 70V HVS = 40V

BVS = 70 V HVS = 40V

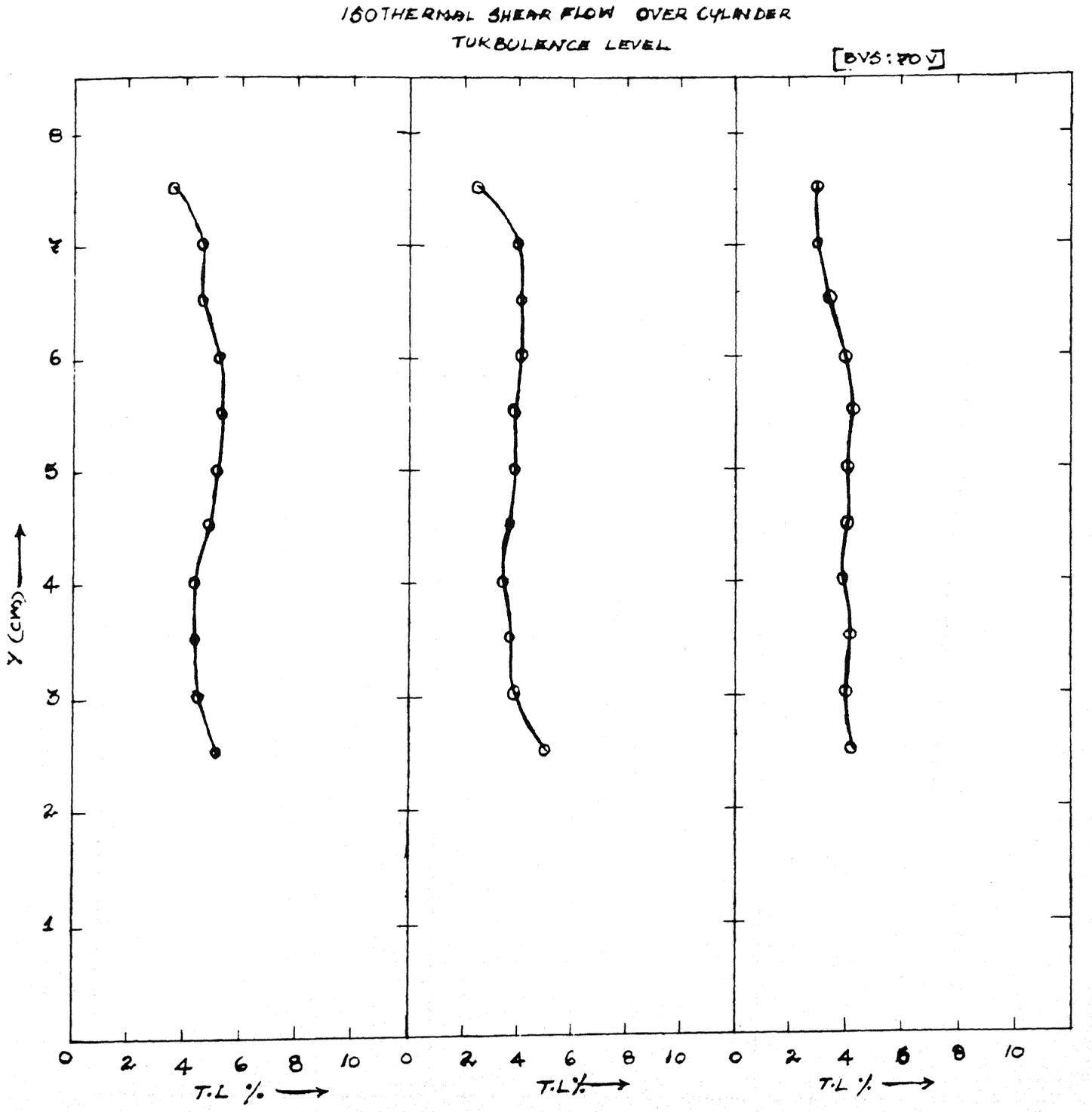

FIG. 4.17 ISOTHERMAL SHEAR FLOW PAST A CYLINDER

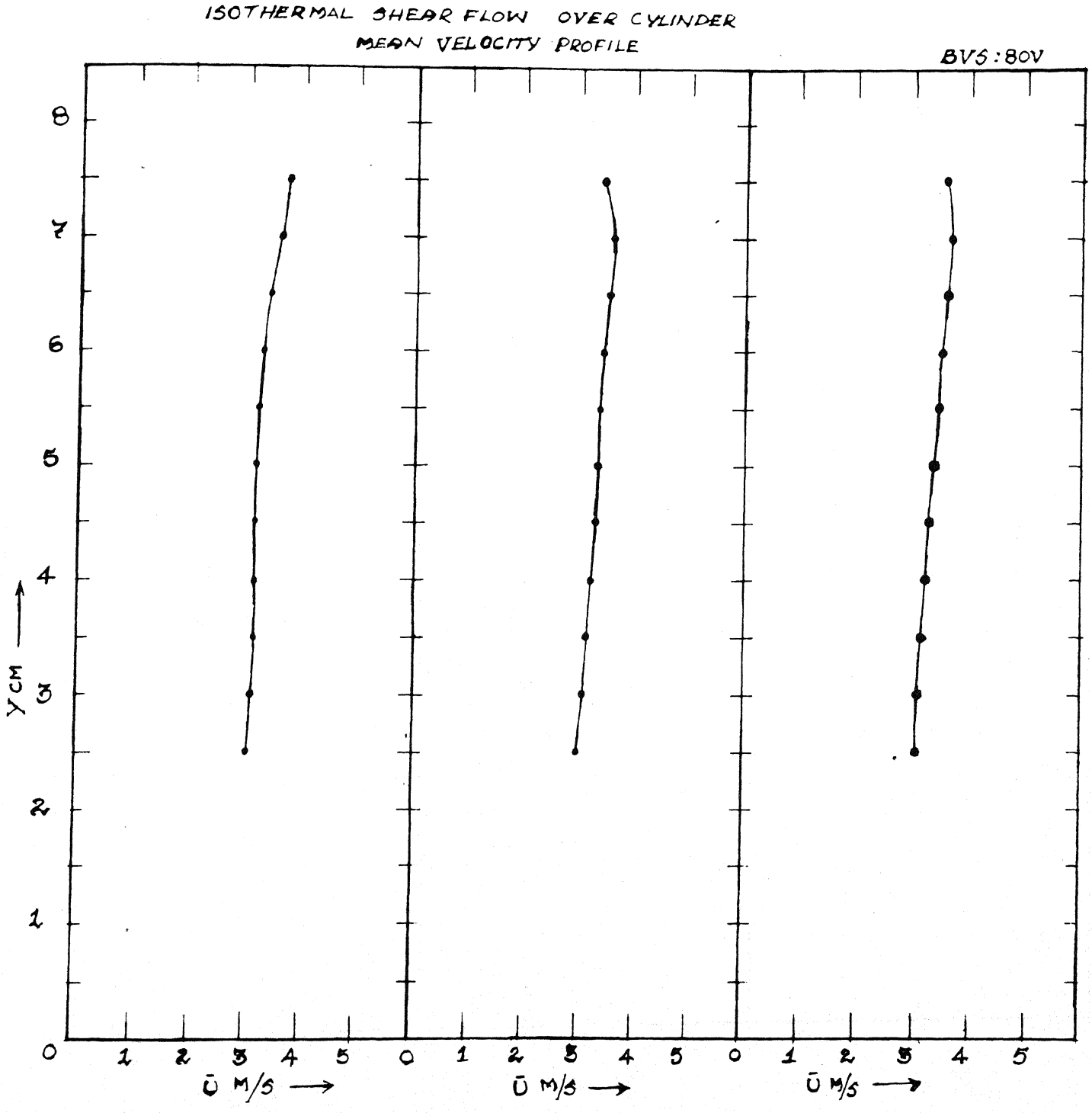

FIG. 4.18 ISOTHERMAL SHEAR FLOW PAST A CYLINDER

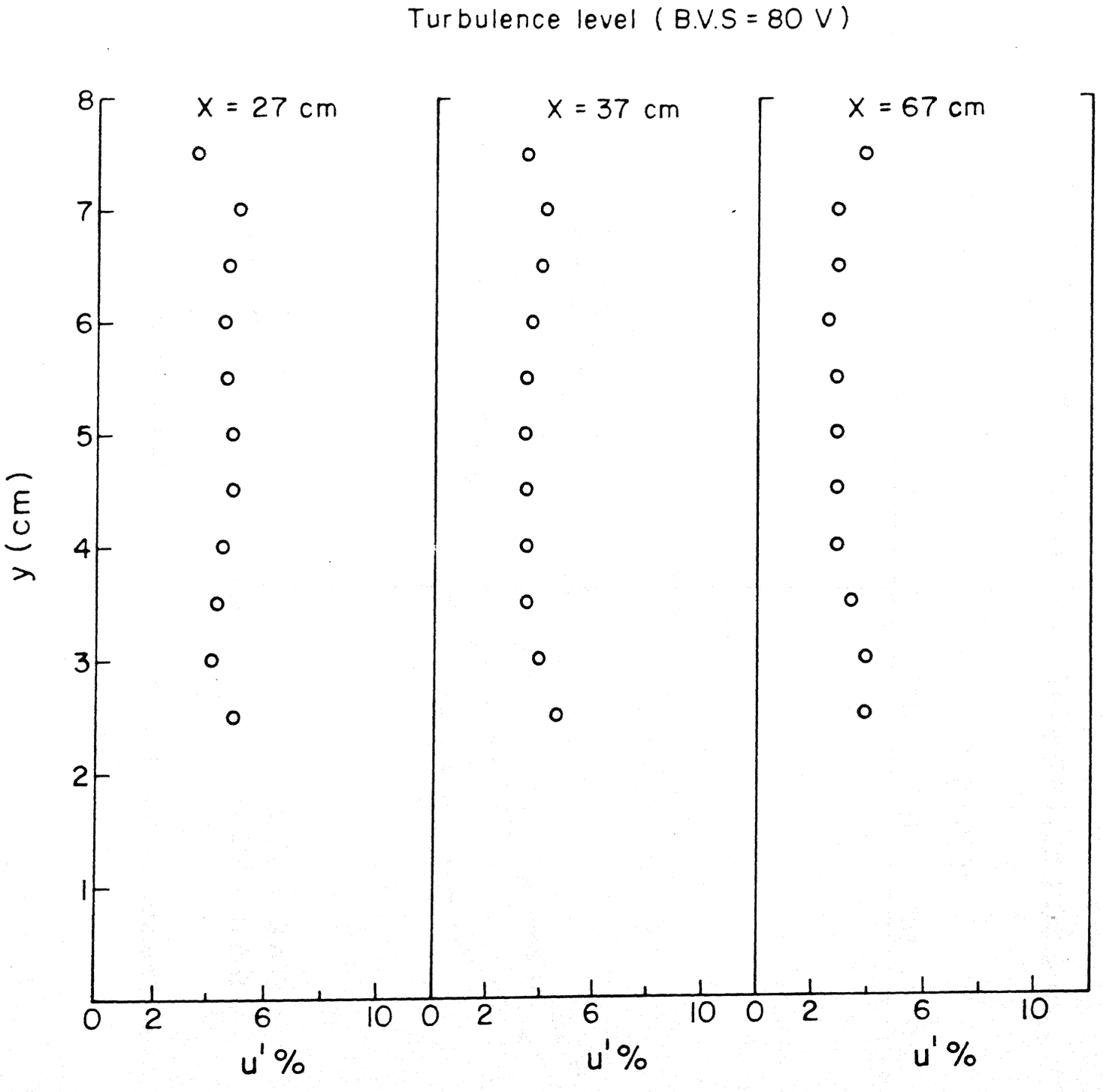

FIG. 4.19 ISOTHERMAL SHEAR FLOW PAST A CYLINDER

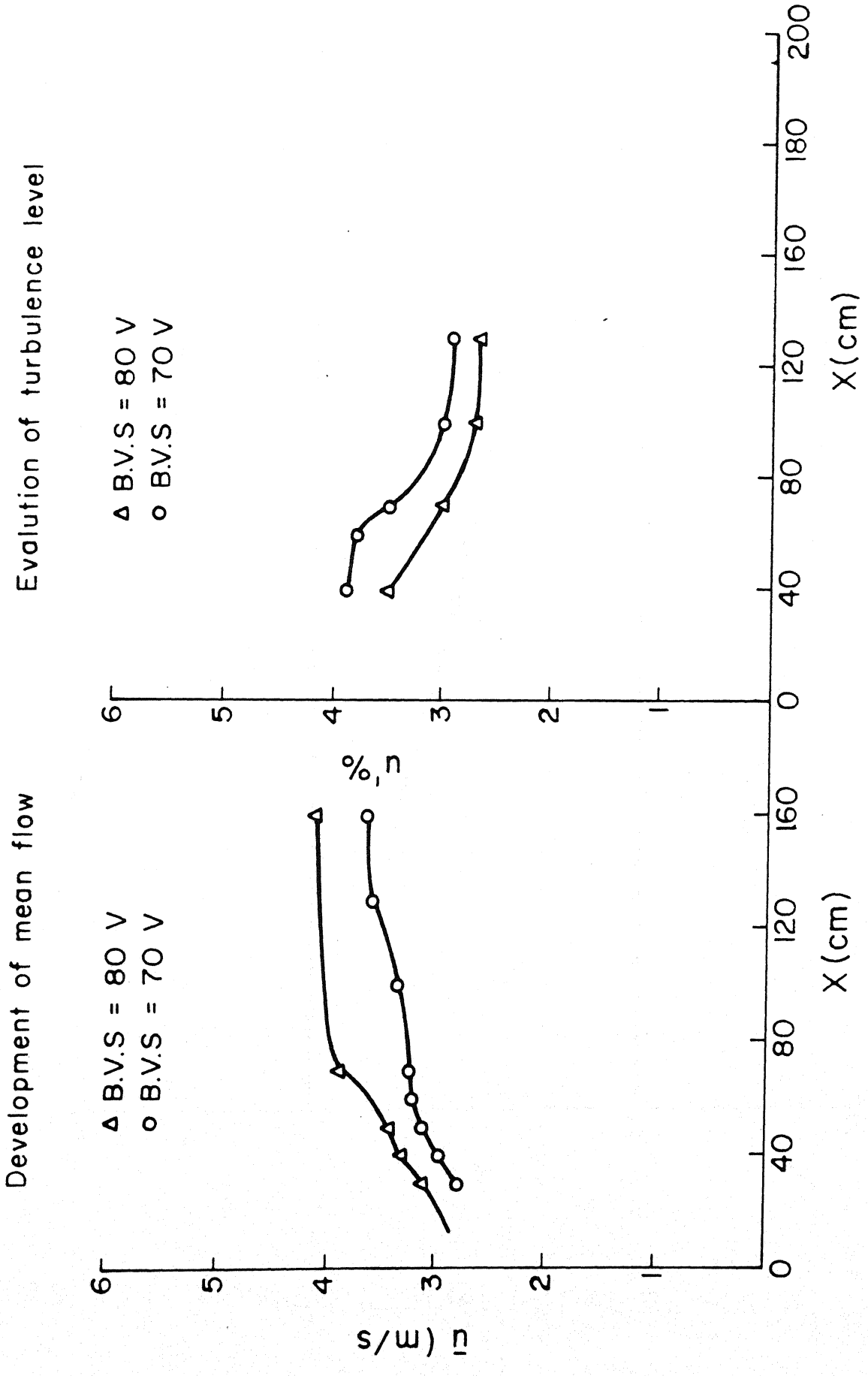

FIG. 4.20 ISOTHERMAL SHEAR FLOW PAST A CYLINDER

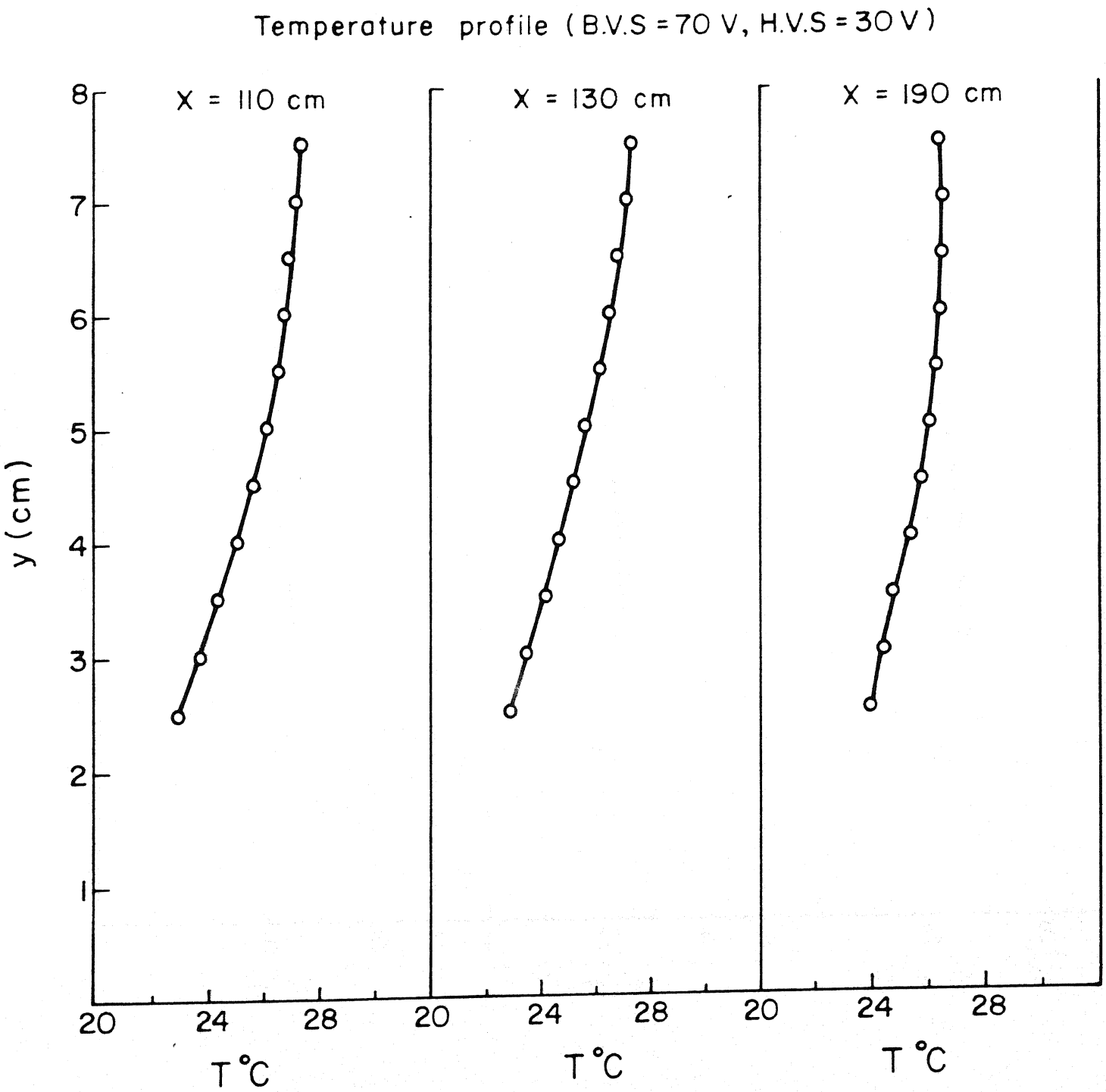

FIG. 4.21 NON-ISOTHERMAL PARALLEL FLOW

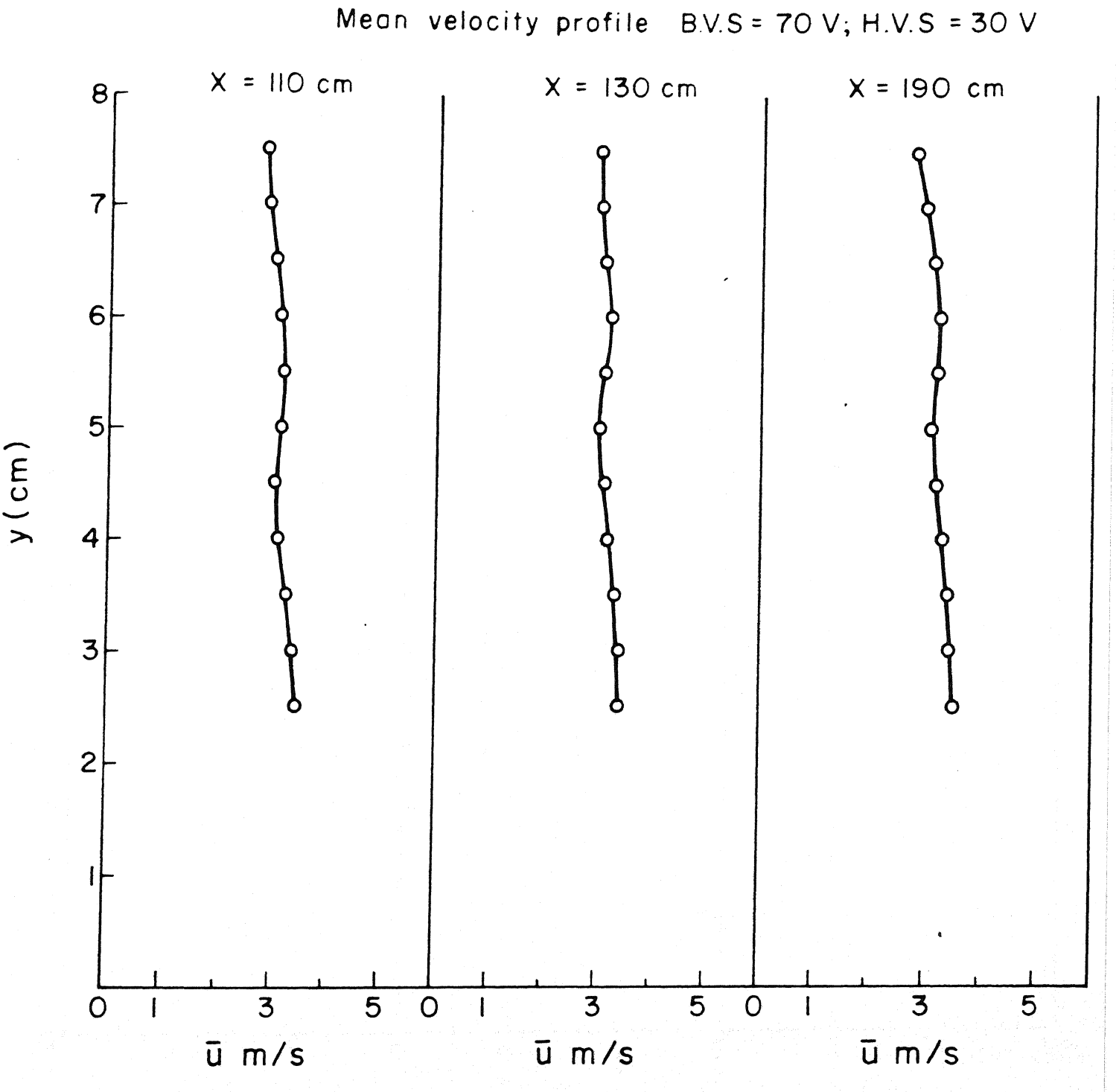

FIG. 4.22 NON-ISOTHERMAL PARALLEL FLOW

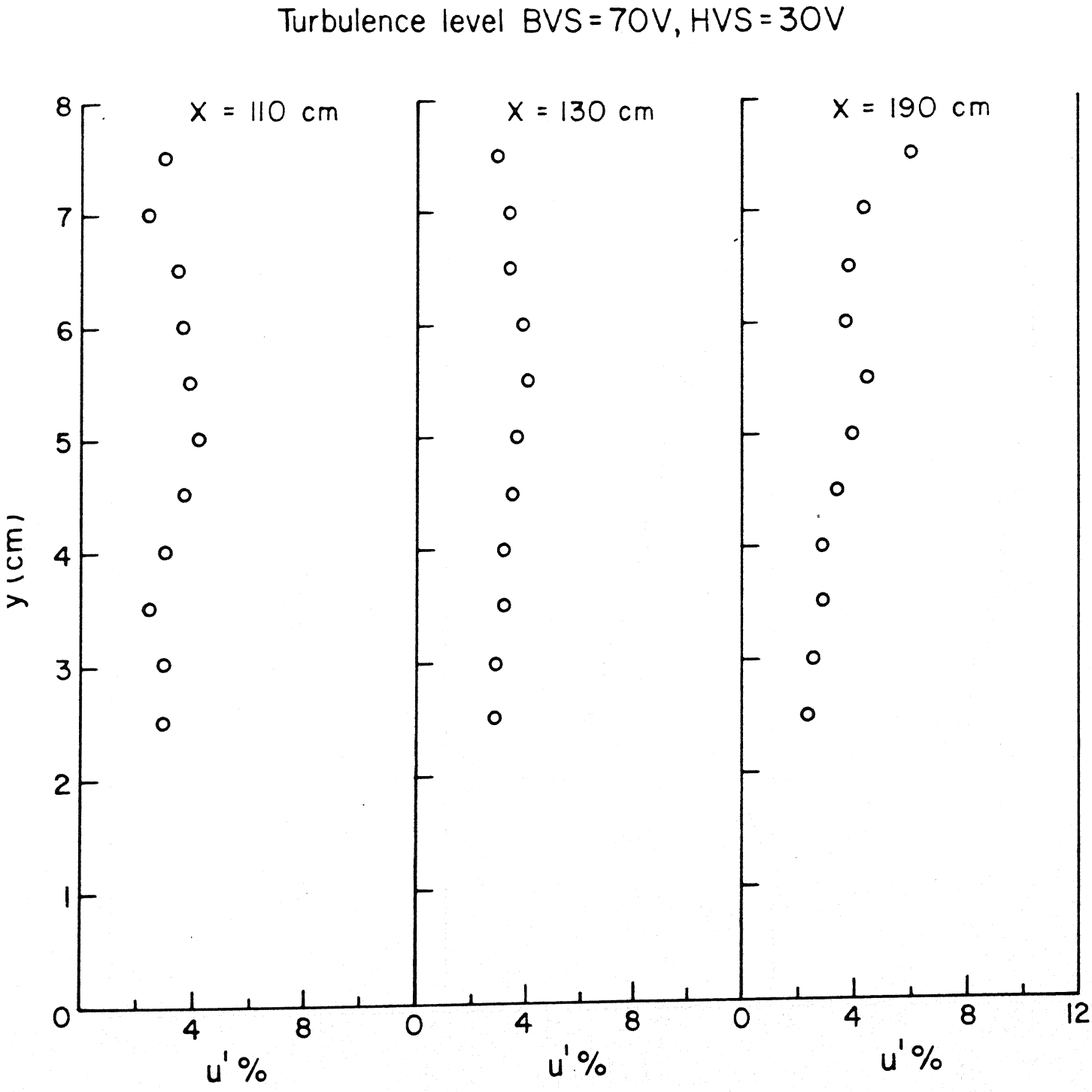

FIG. 4.23 NON-ISOTHERMAL PARALLEL FLOW

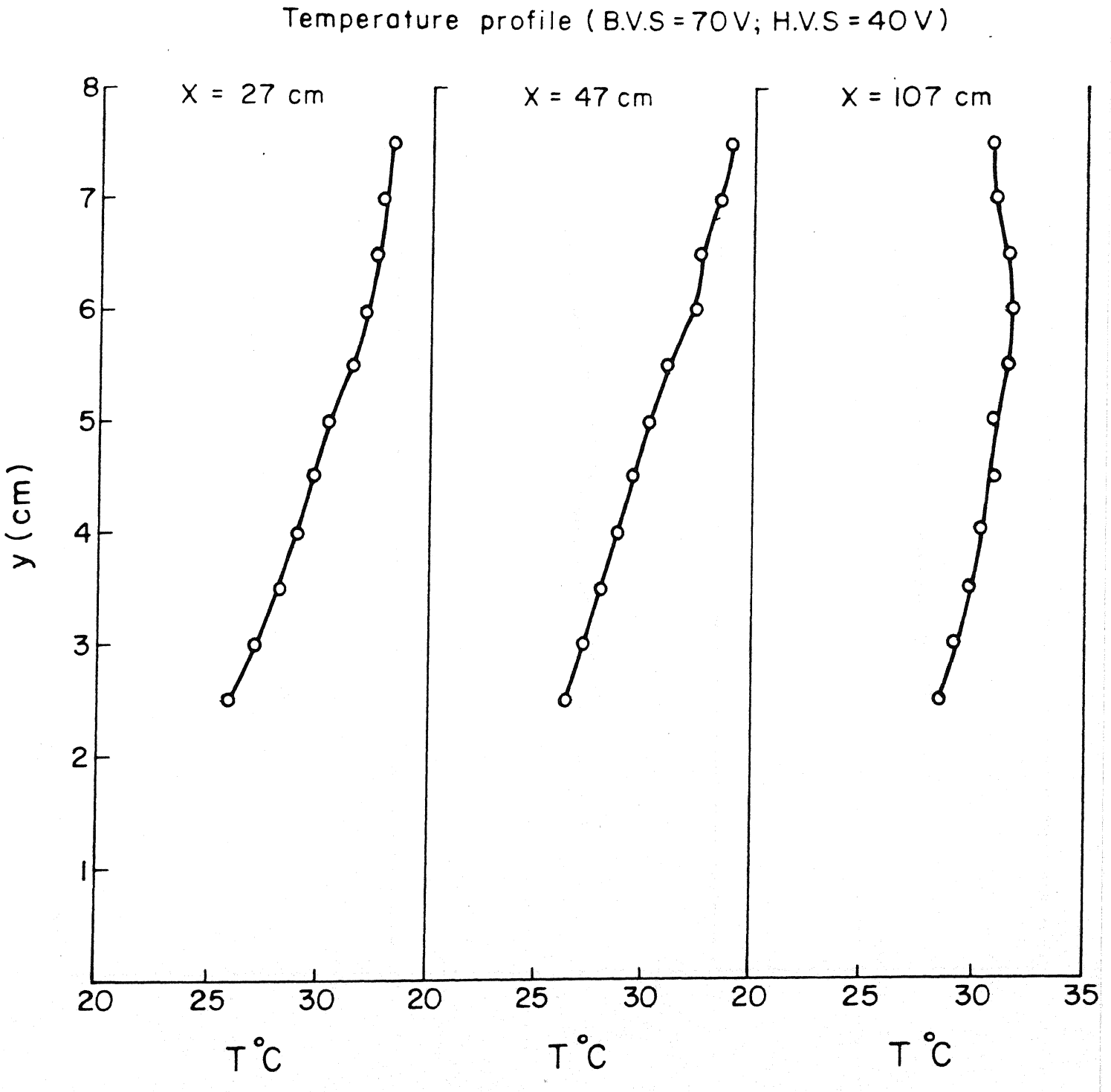

FIG. 4.24 NON-ISOTHERMAL PARALLEL FLOW

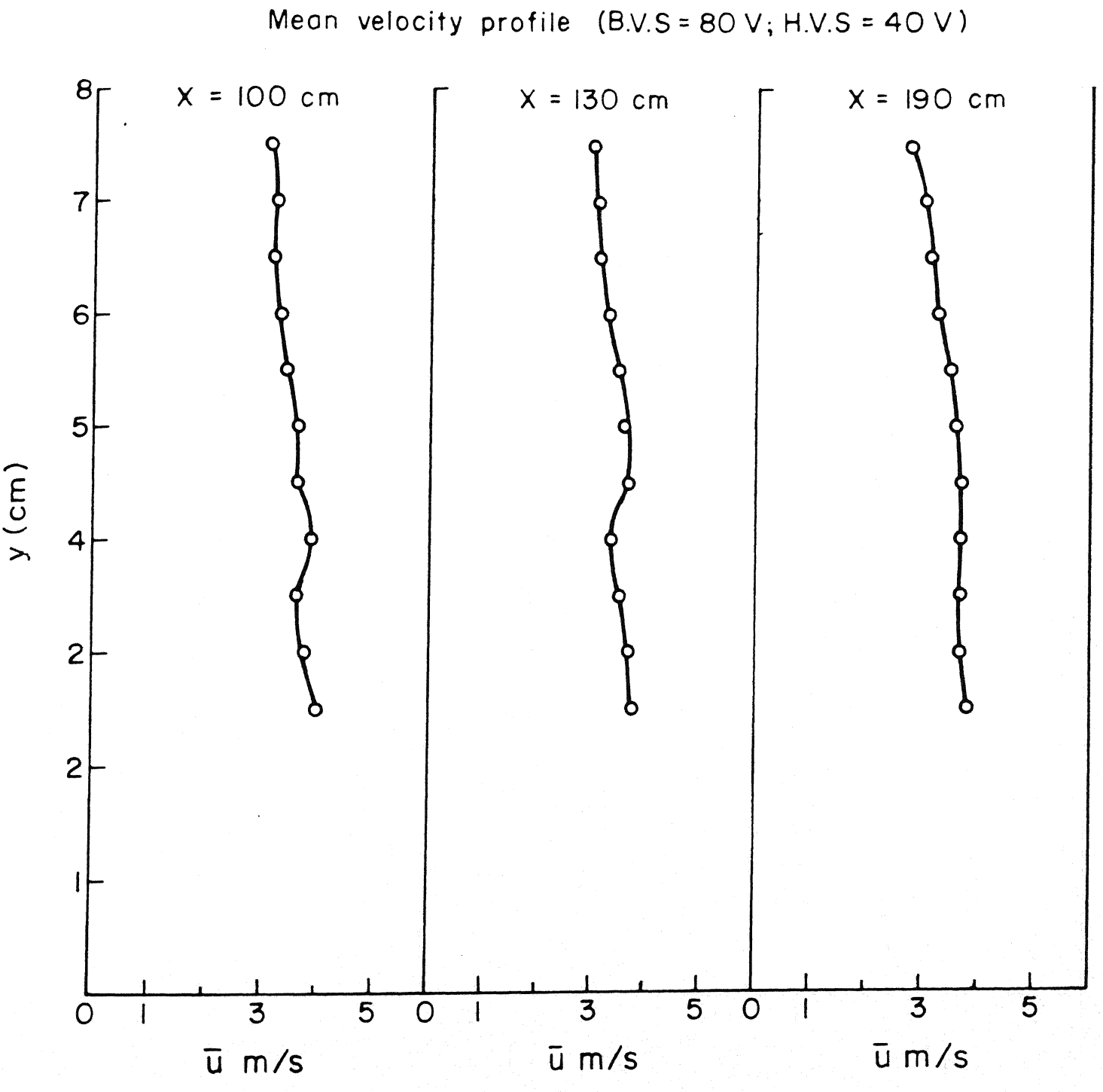

FIG. 4.25 NON-ISOTHERMAL PARALLEL FLOW

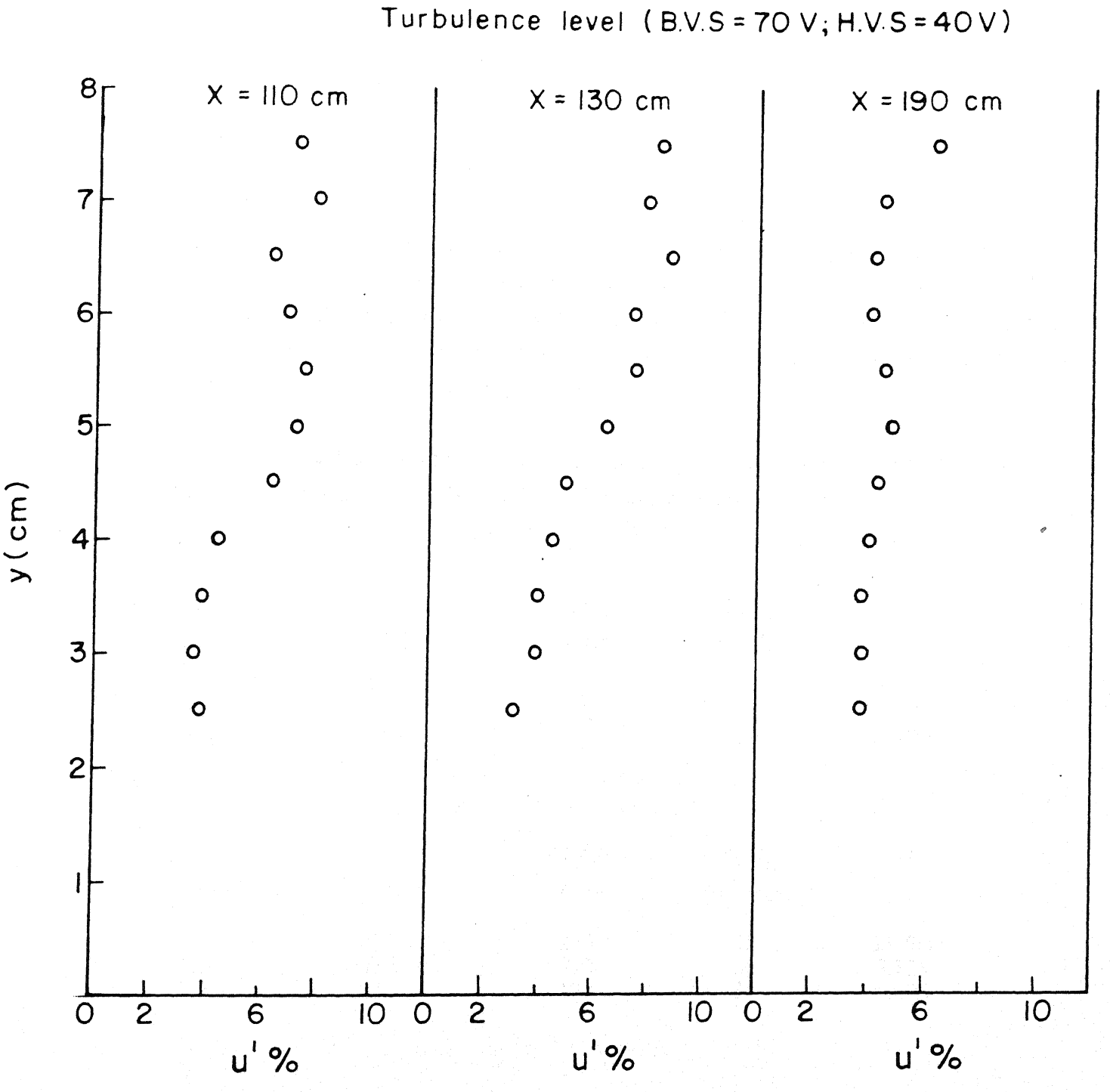

FIG. 4.26 NON-ISOTHERMAL PARALLEL FLOW

x (m)	Tm (°C)	dT/dy °C/m	du/dy (m/s/m)	Ri
1.1	27.5	140	26	0.0739
1.3	29.5	180	14	0.305
1.9	28.4	100	16	0.1370

As the fluid flow along the test cell the temperature of the air layers near the top wall decreases due to cooling effect at this wall. This causes a locally unstable stratification at X = 190 cm. The value of the Richardson number at this location is –0.152. This negative value is the responsible increased turbulence level in the portion near the top wall. Figure 4.27 shows the development of mean flow and decay of turbulence level in downstream for two different heating conditions.

Similarly Figures 4.28 – 4.34 shows the temperature, velocity and turbulence level for different combination of BVS and HVS. The average flow properties are listed below.

BVS = 80 V and HVS = 40 V

x (m)	Tm (°C)	dT/dy °C/m	du/dy (m/s/m)	Ri
1.1	26.6	128	18	0.149
1.3	26.6	132	16	0.191
1.9	28.3	56	20	0.0524

BVS = 80 V HVS = 50V

x (m)	Tm (°C)	dT/dy °C/m	du/dy (m/s/m)	Ri
1.1	30.4	240	32	0.0756
1.3	30.1	212	20	0.173
1.9	28.9	172	24	0.1013

Non–isothermal Flow Over a Cylinder :

A cylinder 10mm diameter is placed in plain heated flow to see the effect of stable stratification of the turbulence level generated by it. Figures 4.35 – 4.48 show the variation

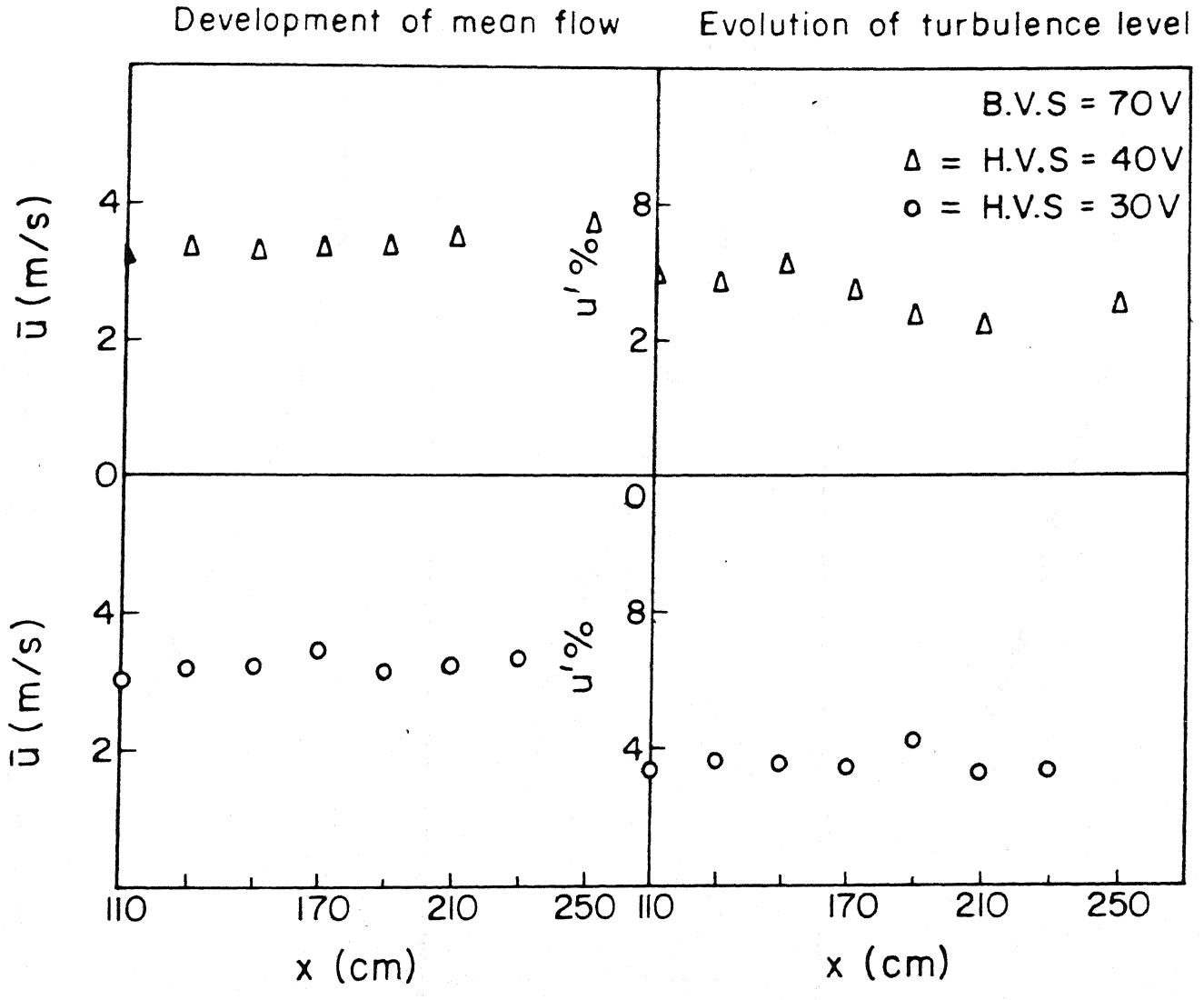

FIG. 4.27 NON-ISOTHERMAL PARALLEL FLOW

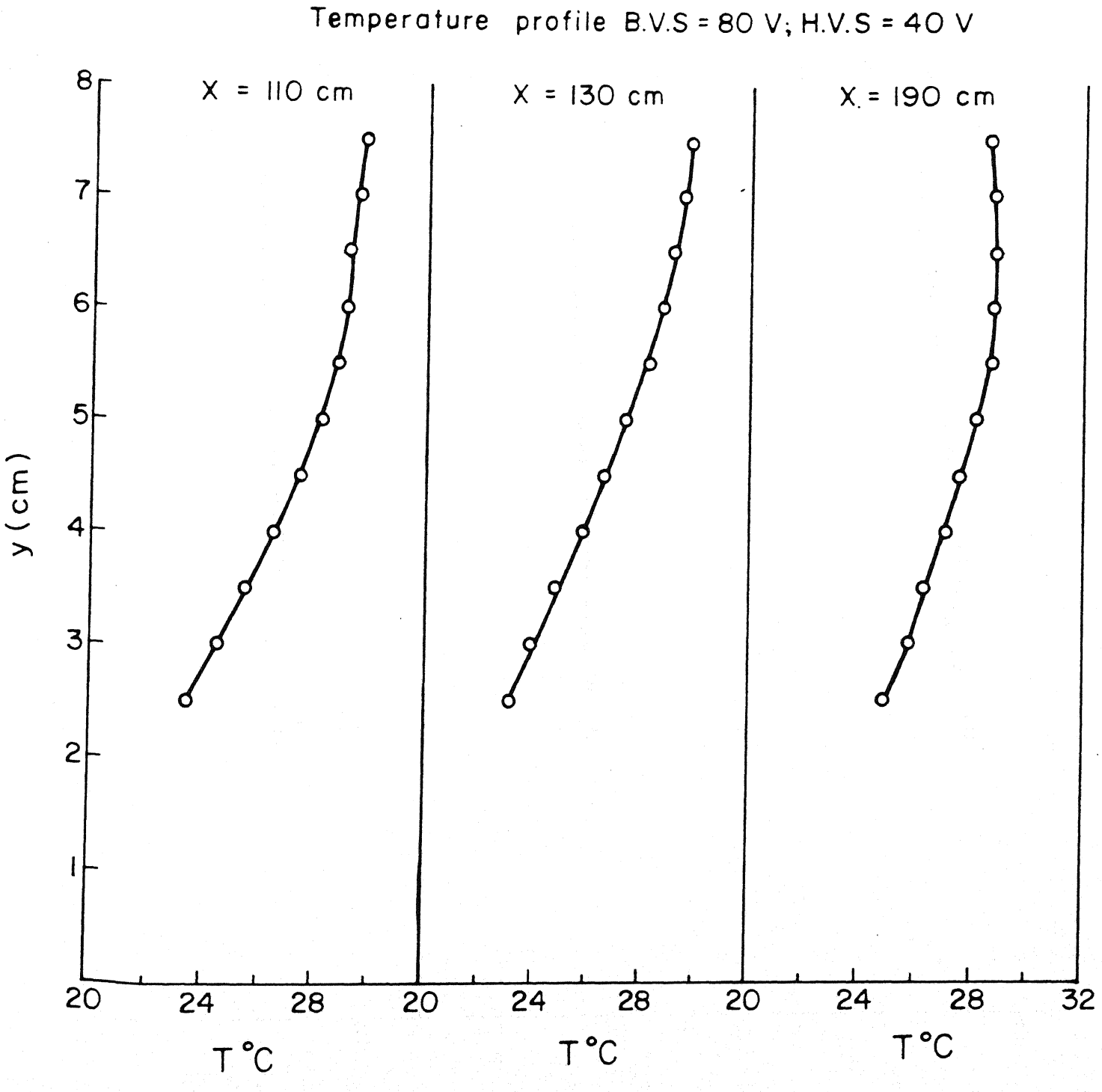

FIG. 4.28 NON-ISOTHERMAL PARALLEL FLOW

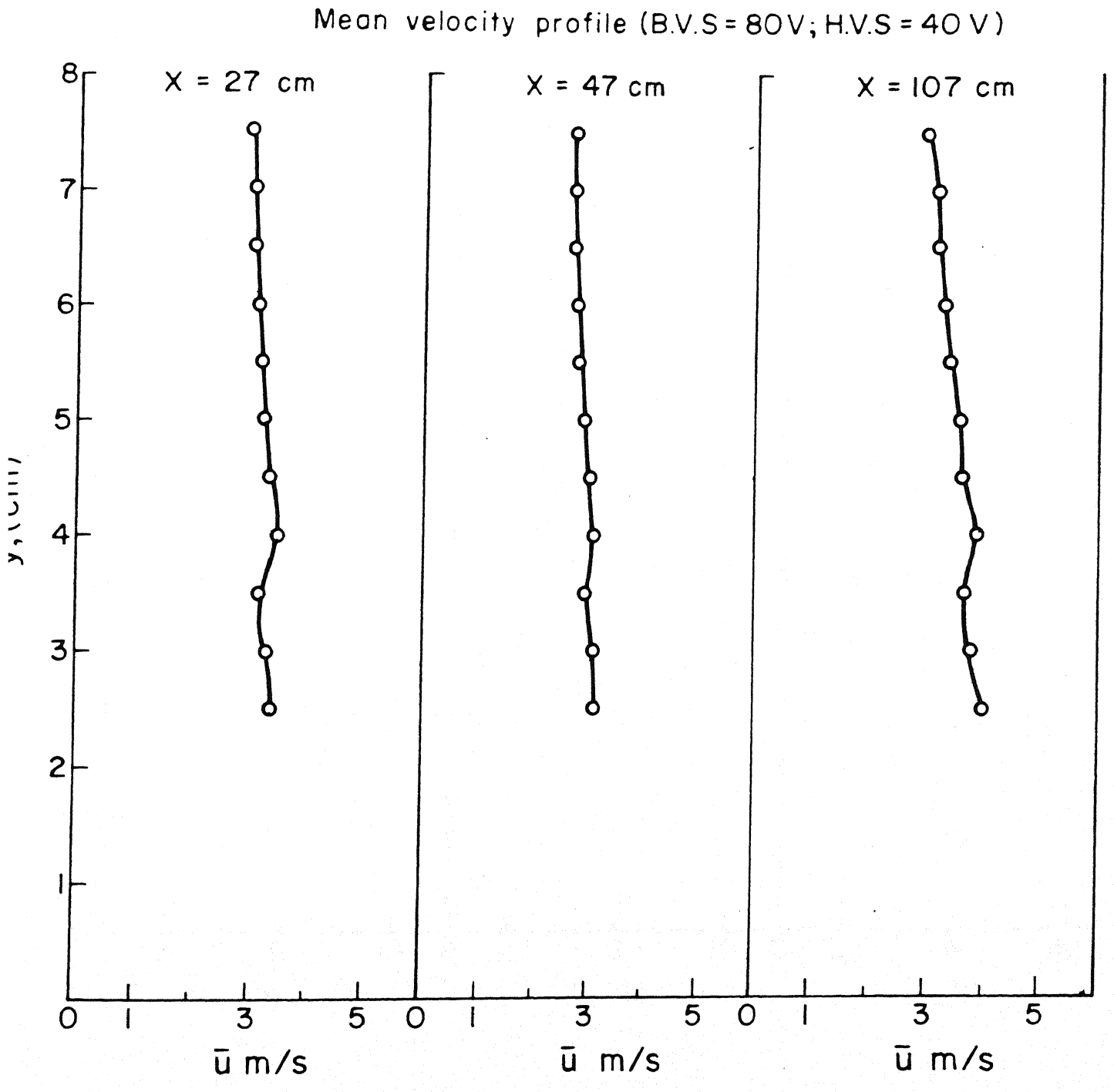

FIG. 4.29 NON-ISOTHERMAL PARALLEL FLOW

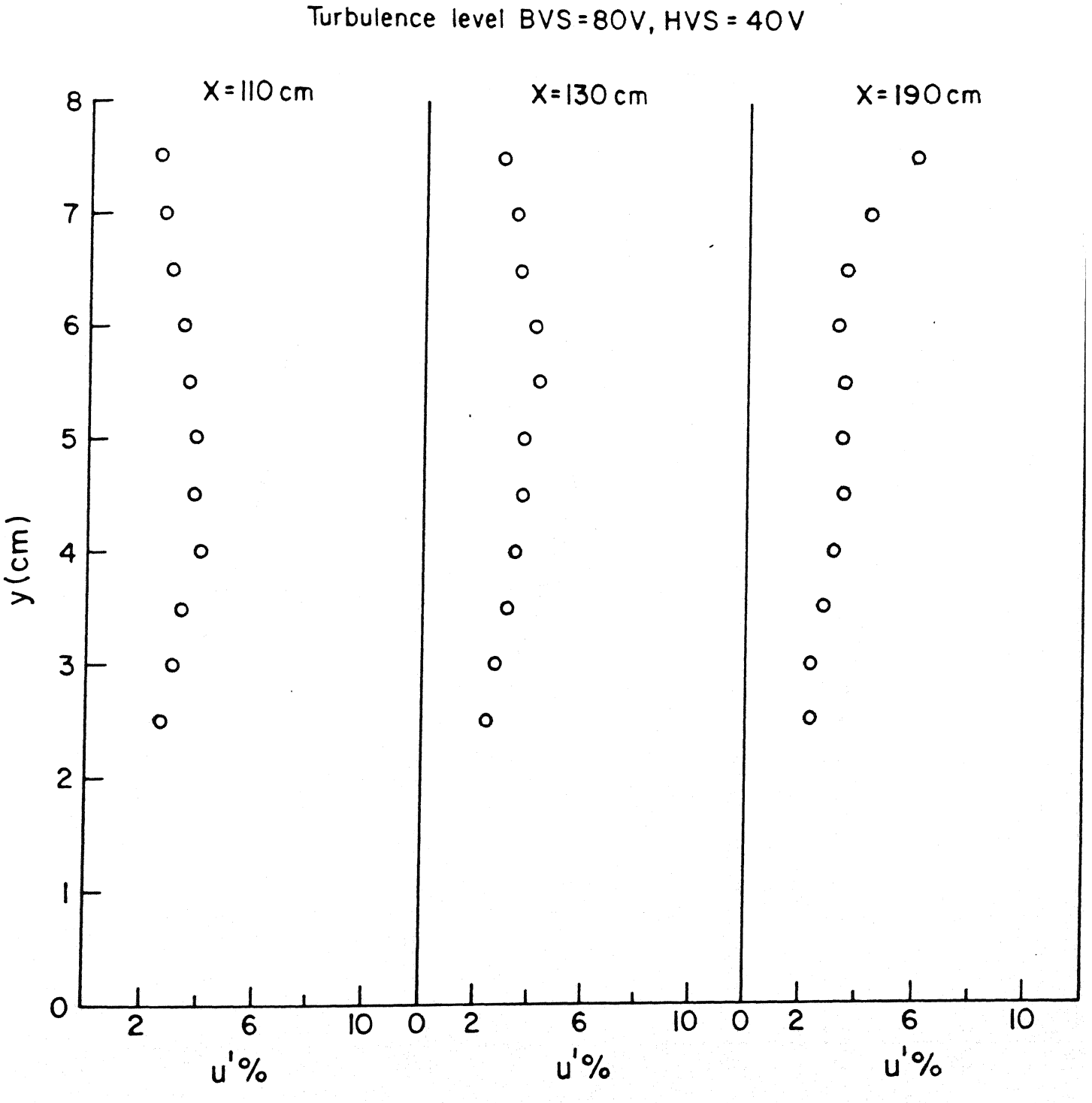

FIG. 4.30 NON-ISOTHERMAL PARALLEL FLOW

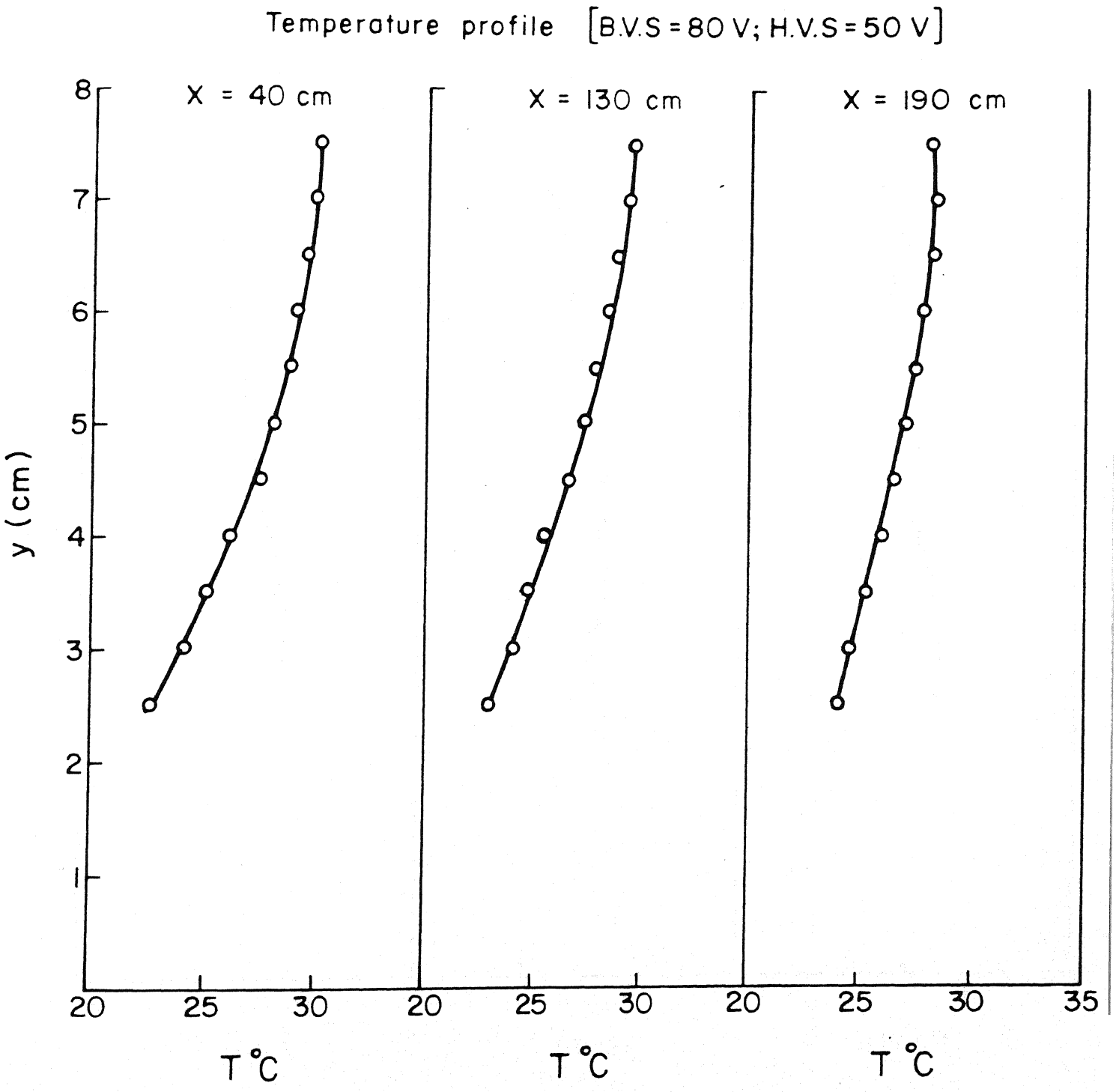

FIG. 4.31 NON-ISOTHERMAL PARALLEL FLOW

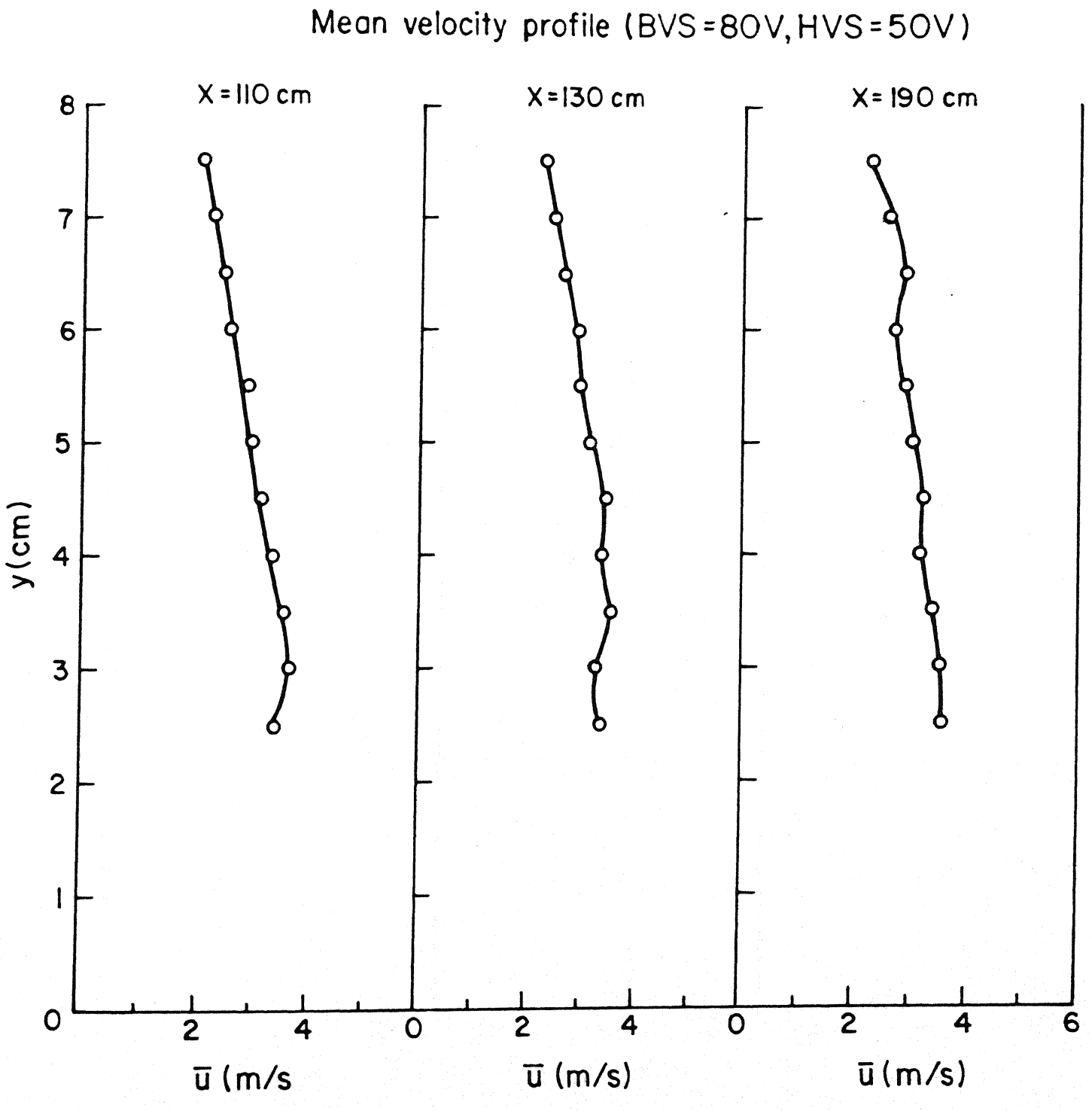

FIG. 4.32 NON-ISOTHERMAL PARALLEL FLOW

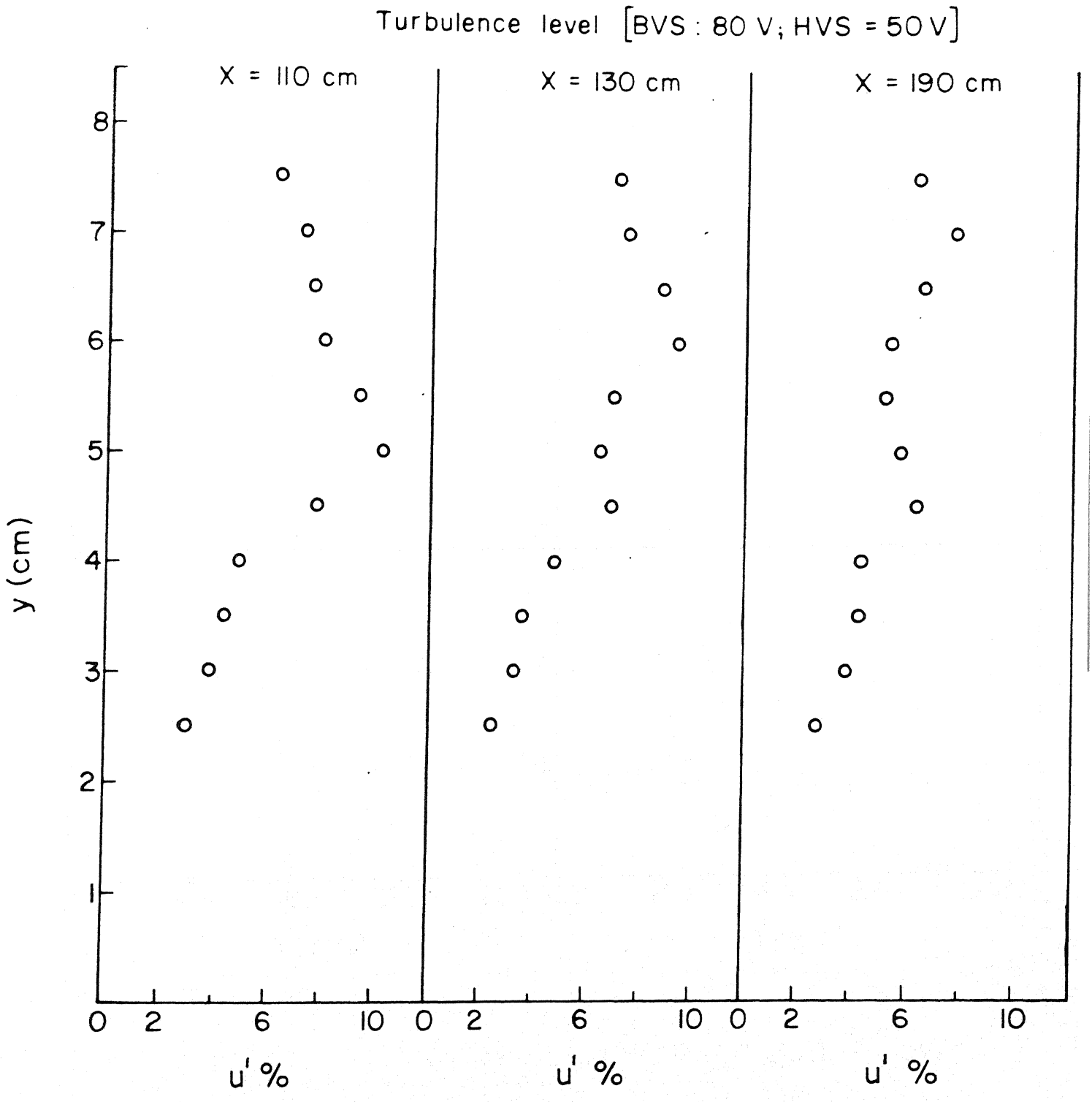

FIG. 4.33 NON-ISOTHERMAL PARALLEL FLOW

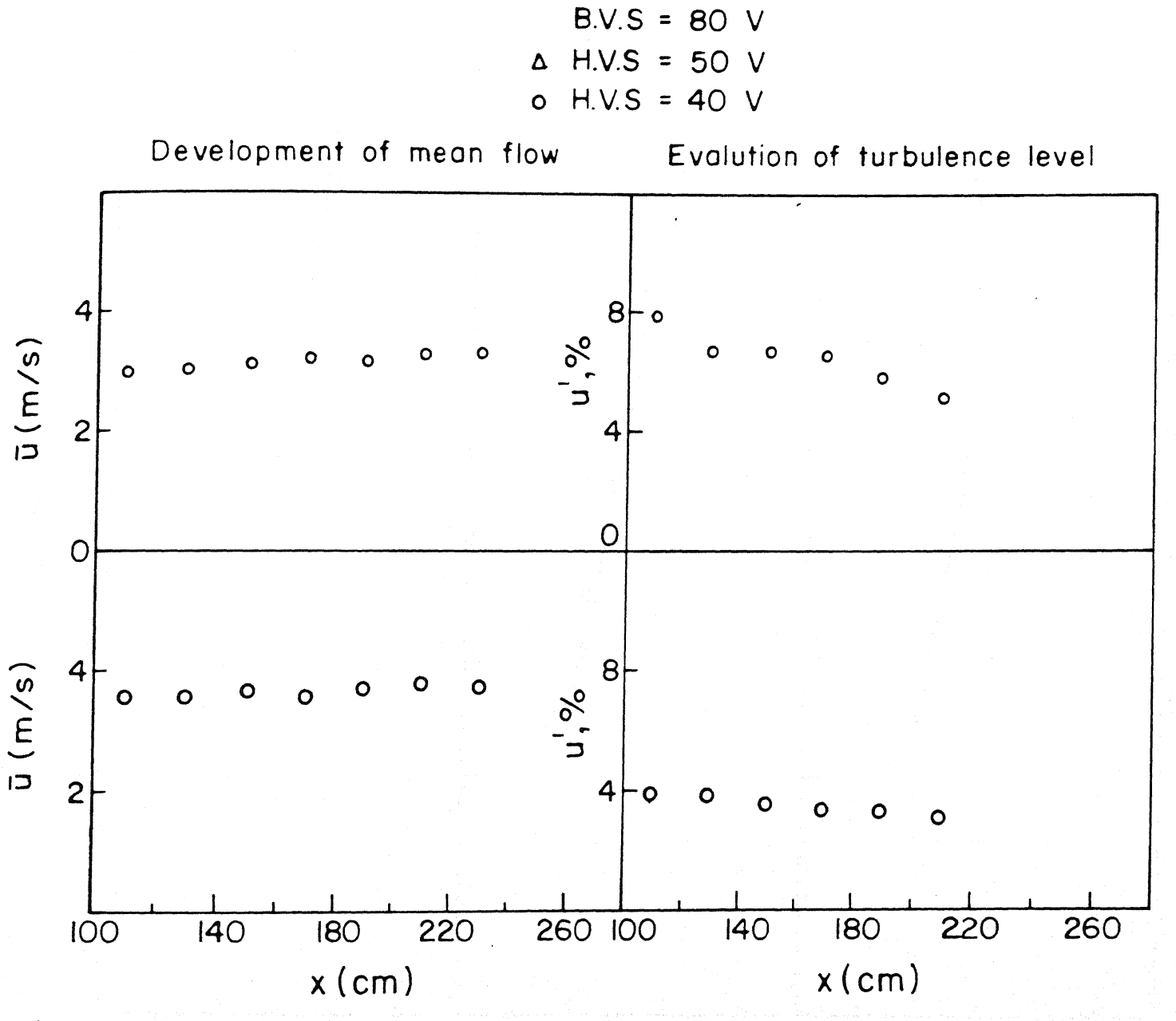

FIG. 4.34 NON-ISOTHERMAL PARALLEL FLOW

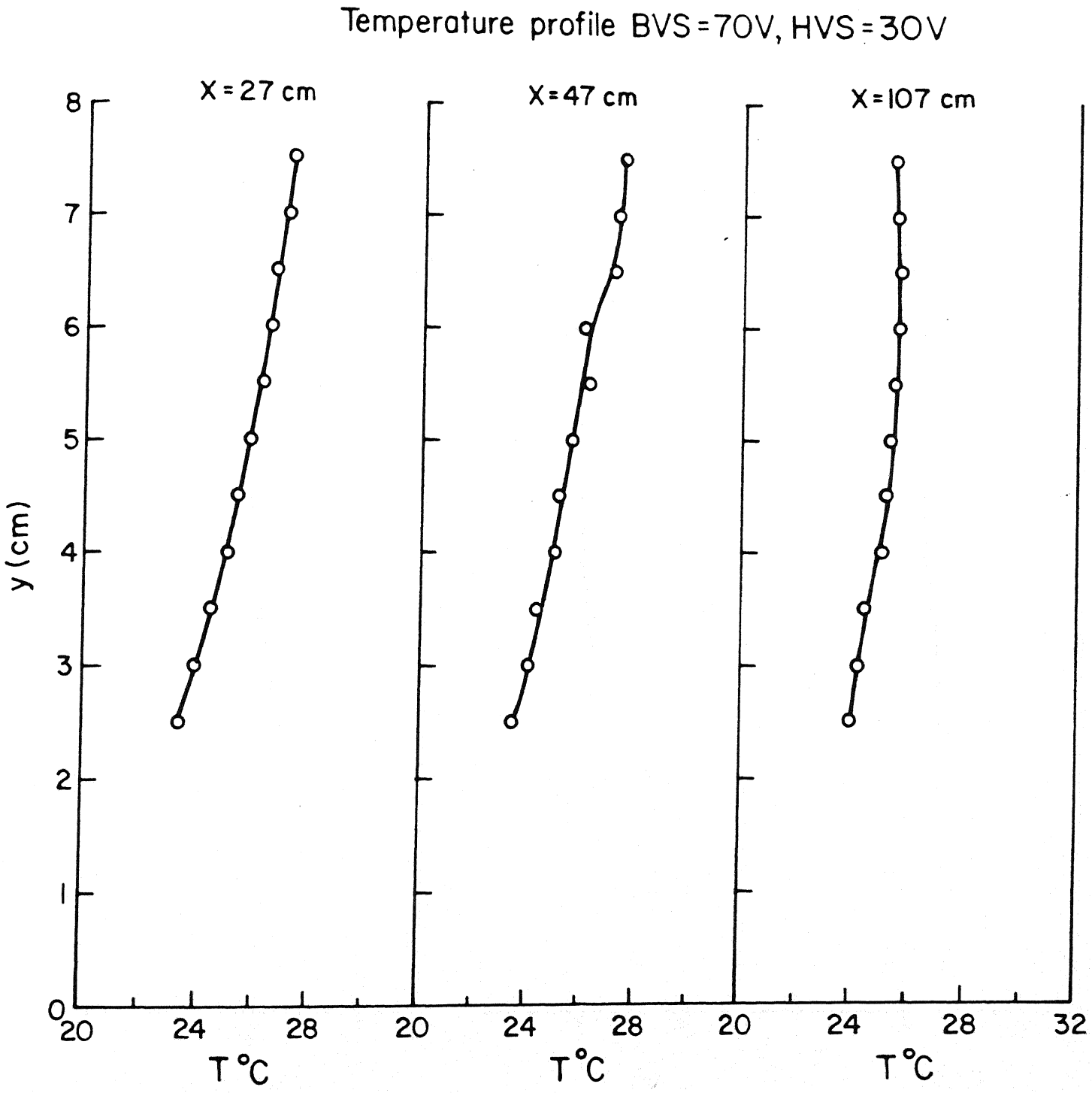

FIG. 4.35 NON-ISOTHERMAL PARALLEL FLOW PAST A CYLINDER

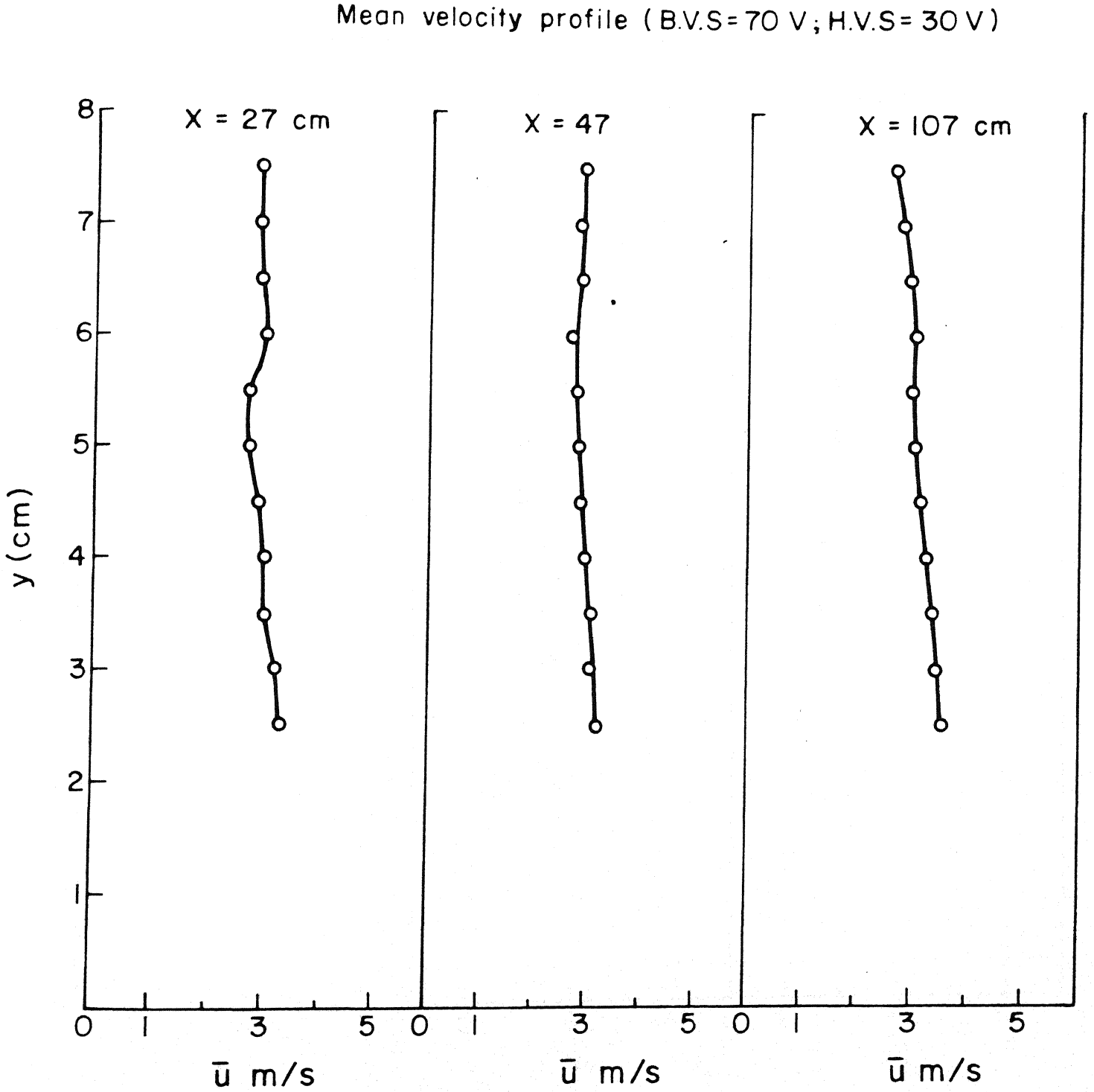

FIG. 4.36 NON-ISOTHERMAL PARALLEL FLOW PAST A CYLINDER

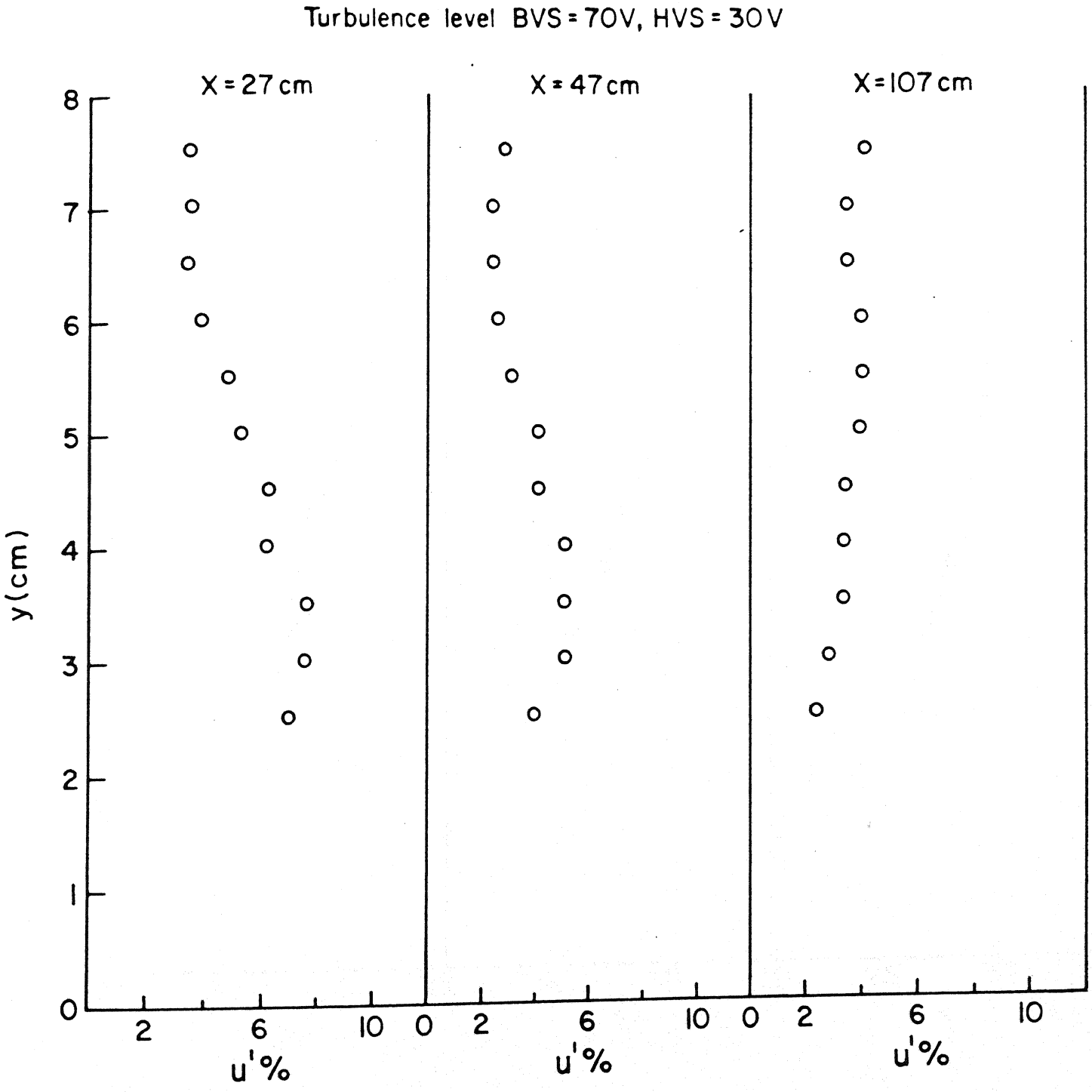

FIG. 4.37 NON-ISOTHERMAL PARALLEL FLOW PAST A CYLINDER

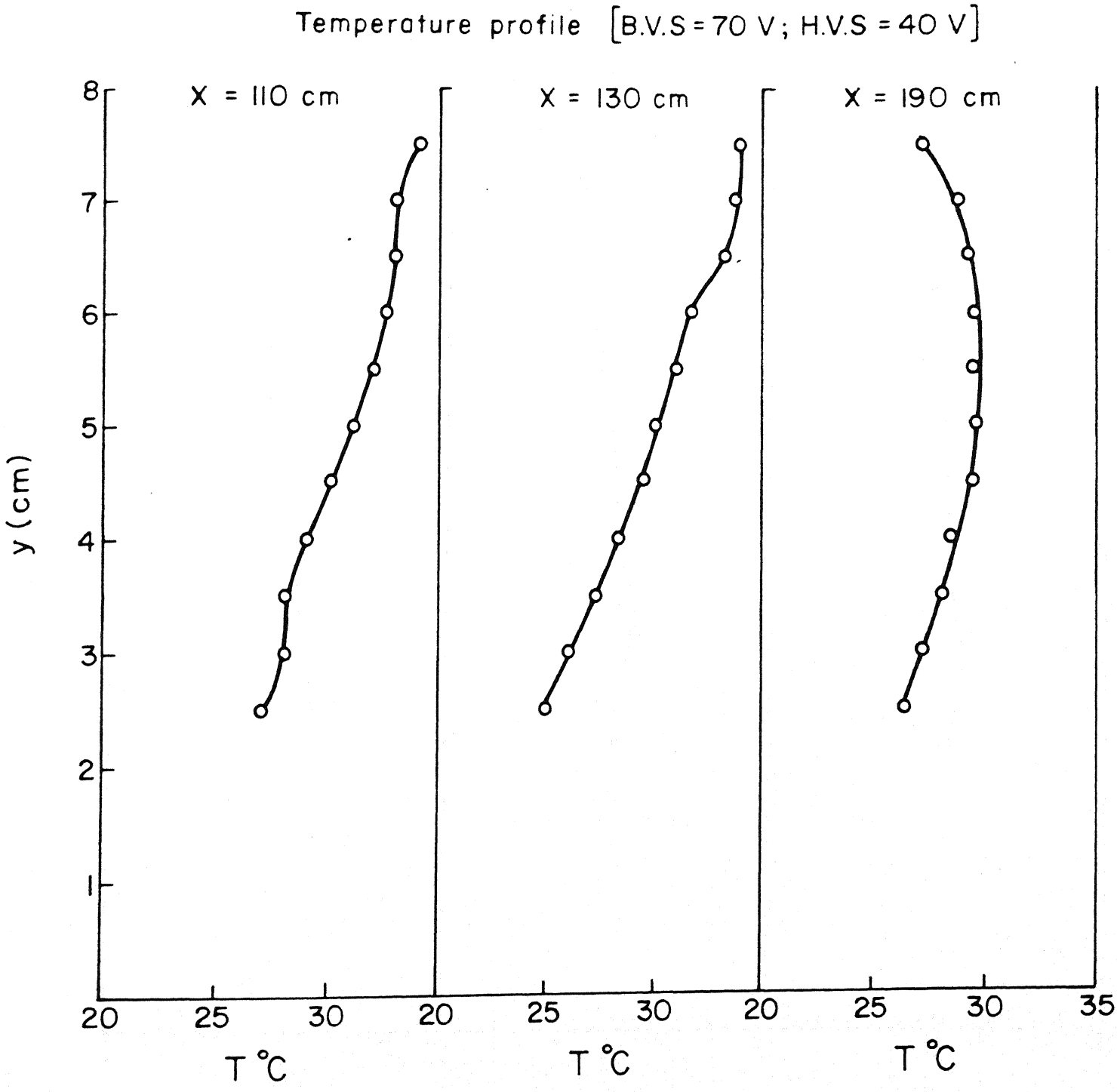

FIG. 4.38 NON-ISOTHERMAL PARALLEL FLOW PAST A CYLINDER

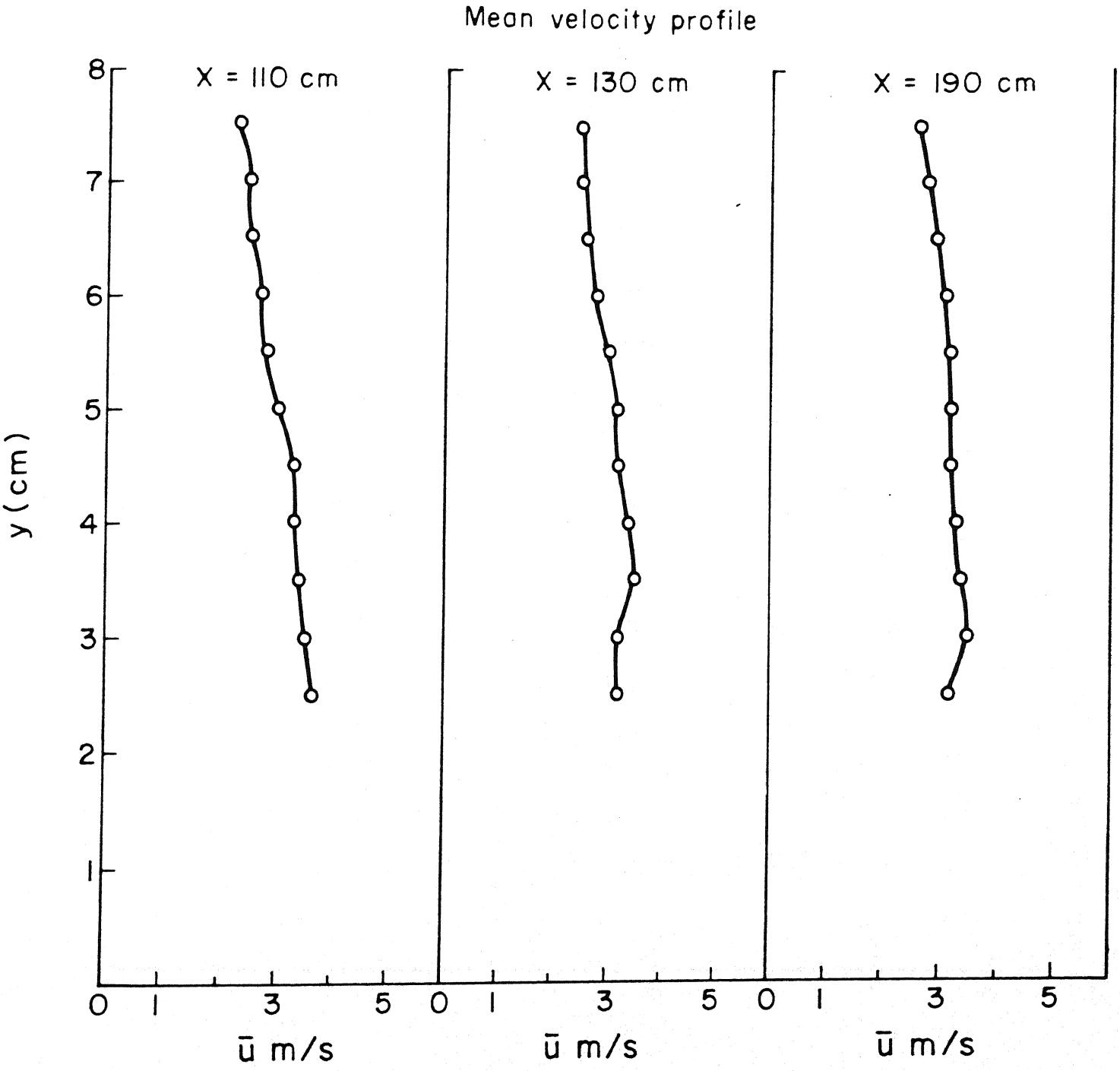

FIG. 4.39 NON-ISOTHERMAL PARALLEL FLOW PAST A CYLINDER

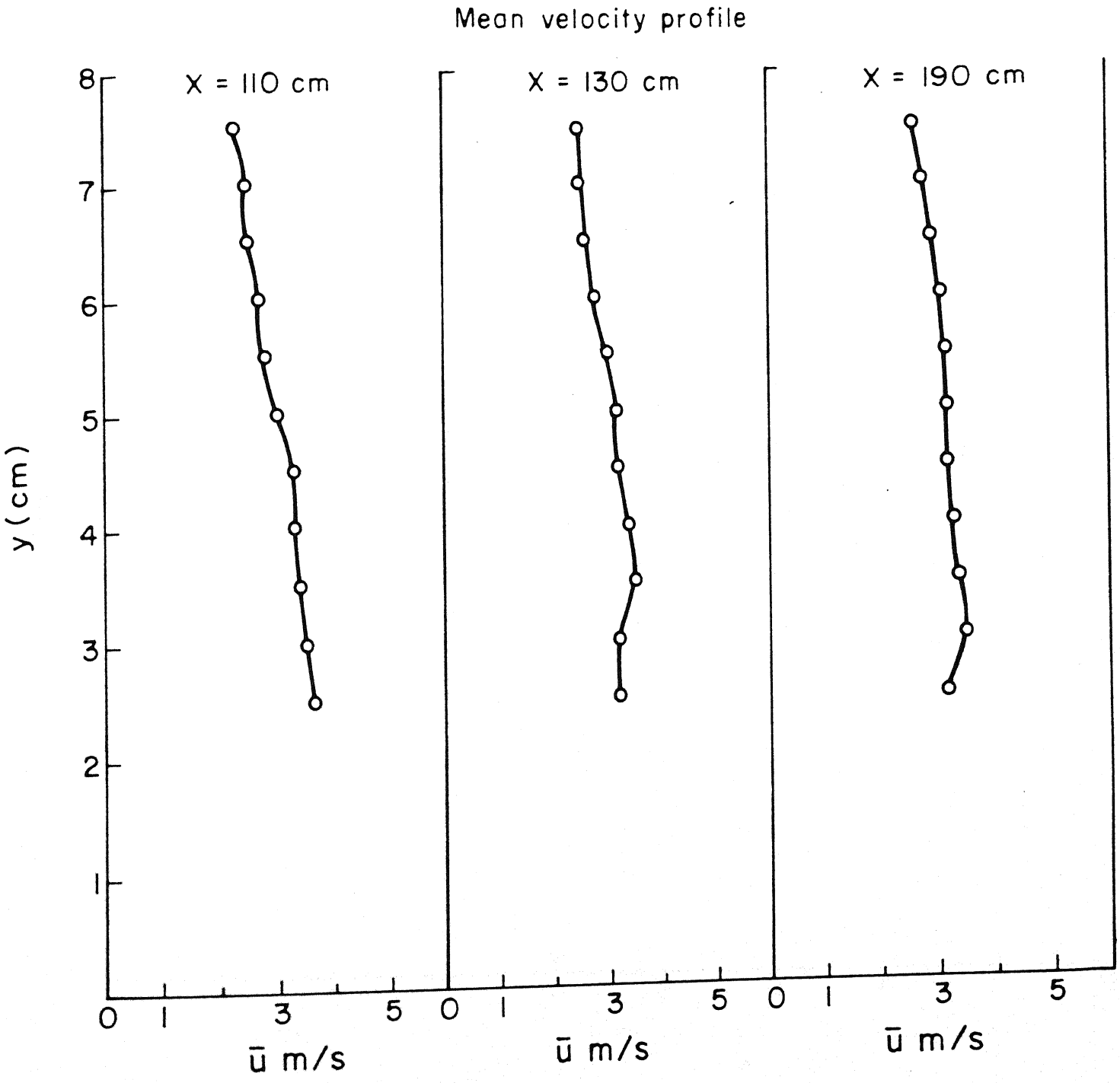

FIG. 4.39 NON-ISOTHERMAL PARALLEL FLOW PAST A CYLINDER

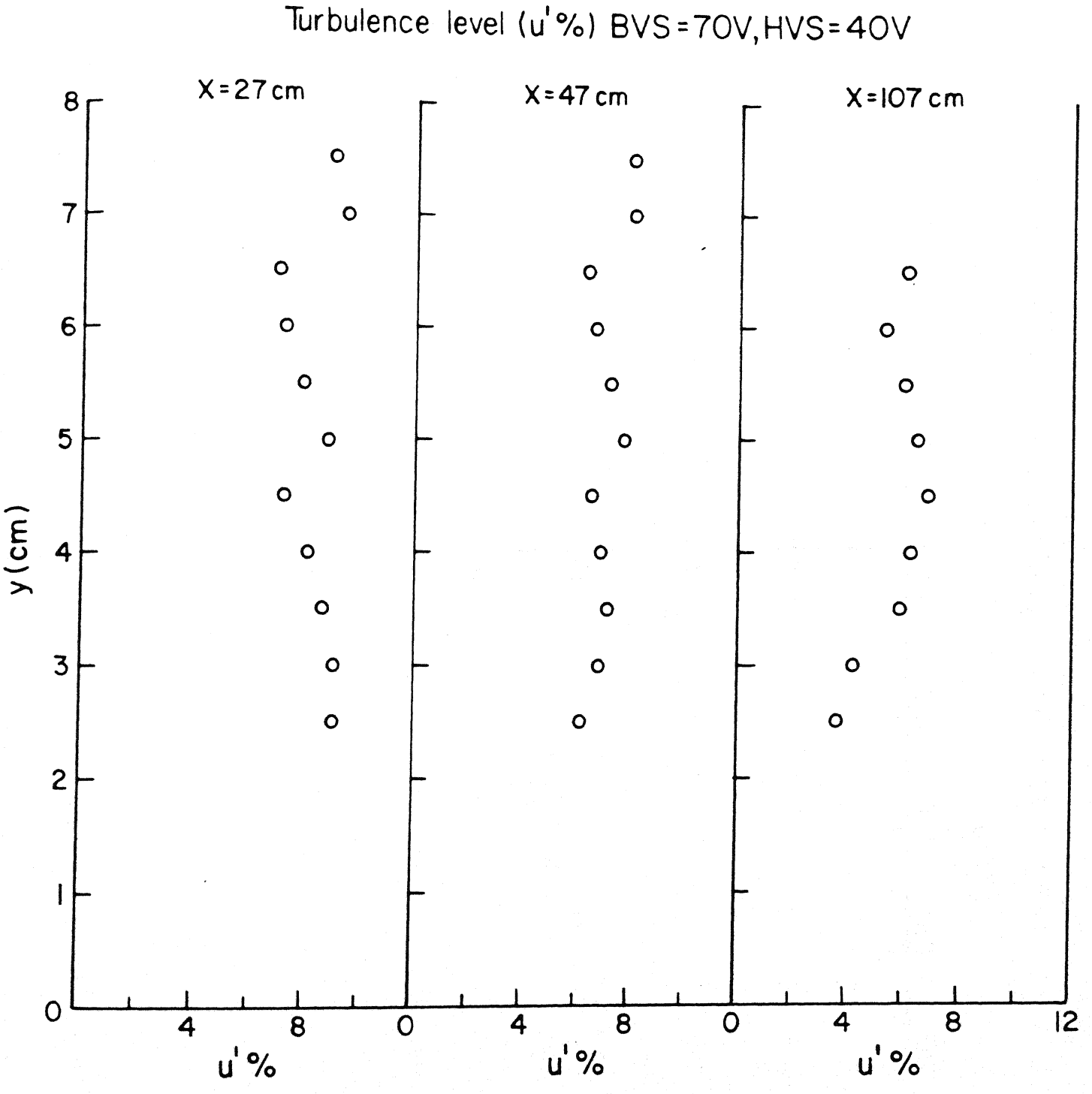

FIG. 4.40 NON-ISOTHERMAL PARALLEL FLOW PAST A CYLINDER

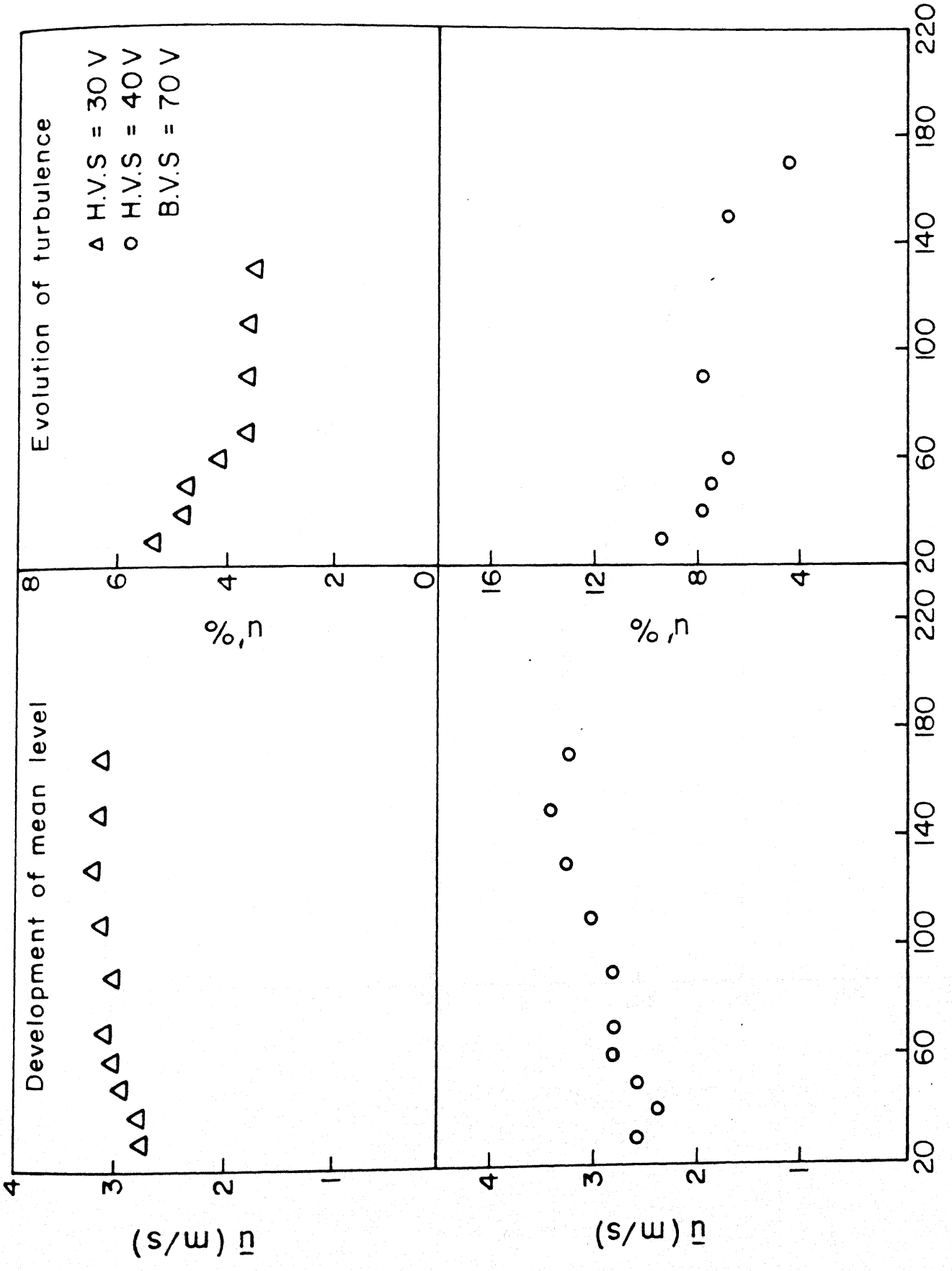

FIG. 4.41 NON-ISOTHERMAL PARALLEL FLOW PAST A CYLINDER

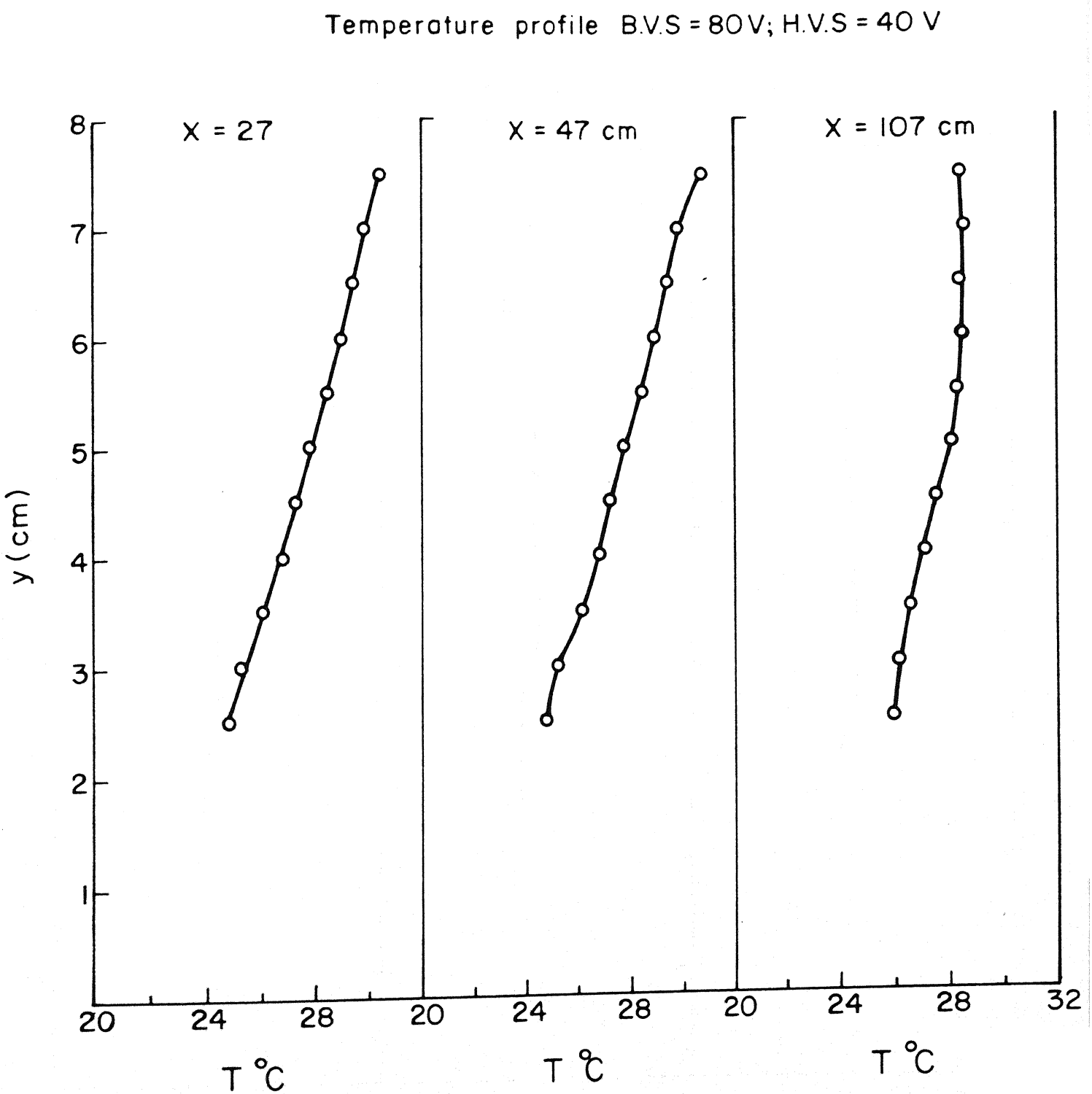

FIG. 4.42 NON-ISOTHERMAL PARALLEL FLOW PAST A CYLINDER

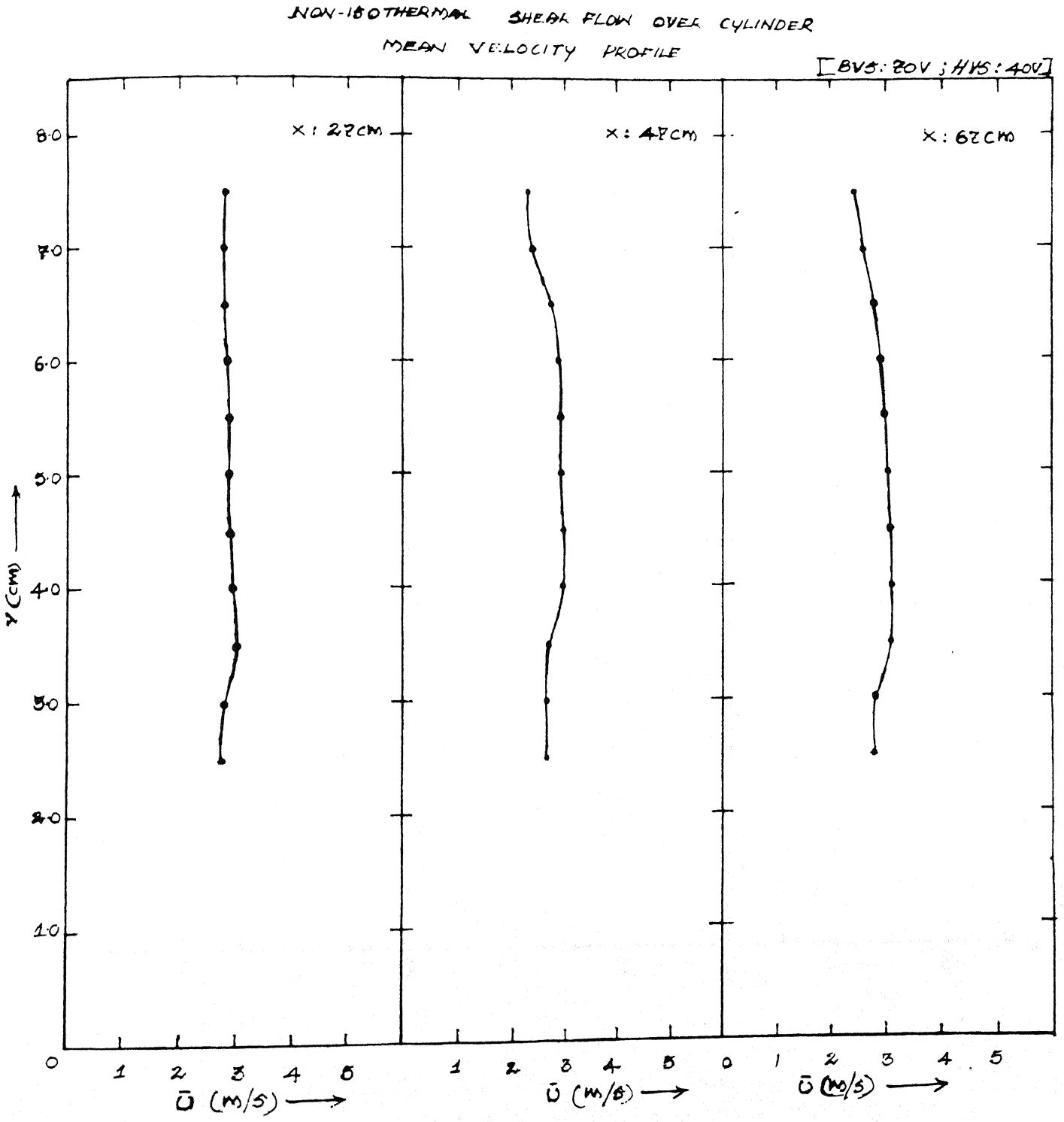

FIG. 4.43 NON-ISOTHERMAL PARALLEL FLOW PAST A CYLINDER

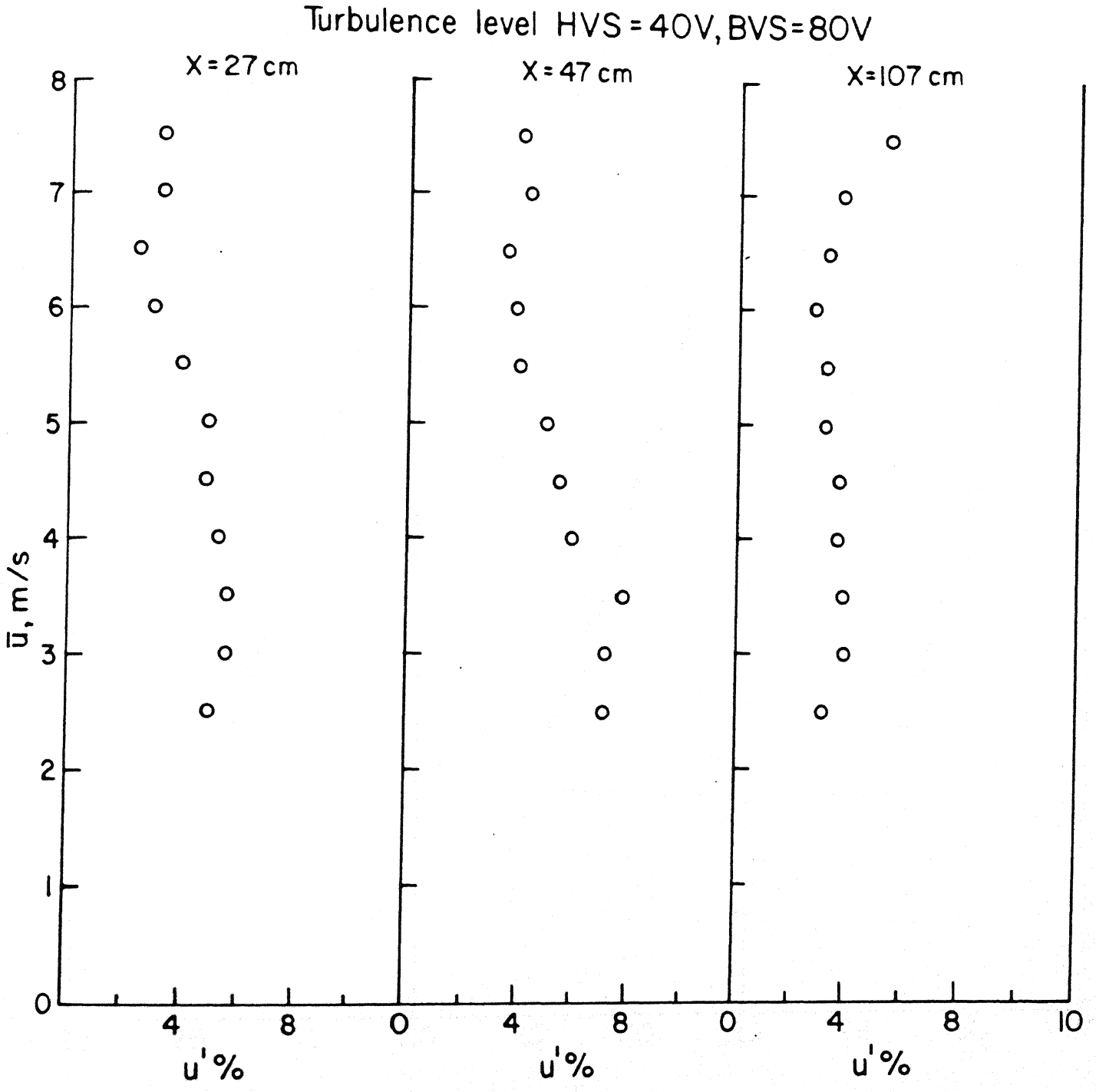

Fig. 4.44. NON_ISOTHERMAL FLOW PAST A CYLINDER

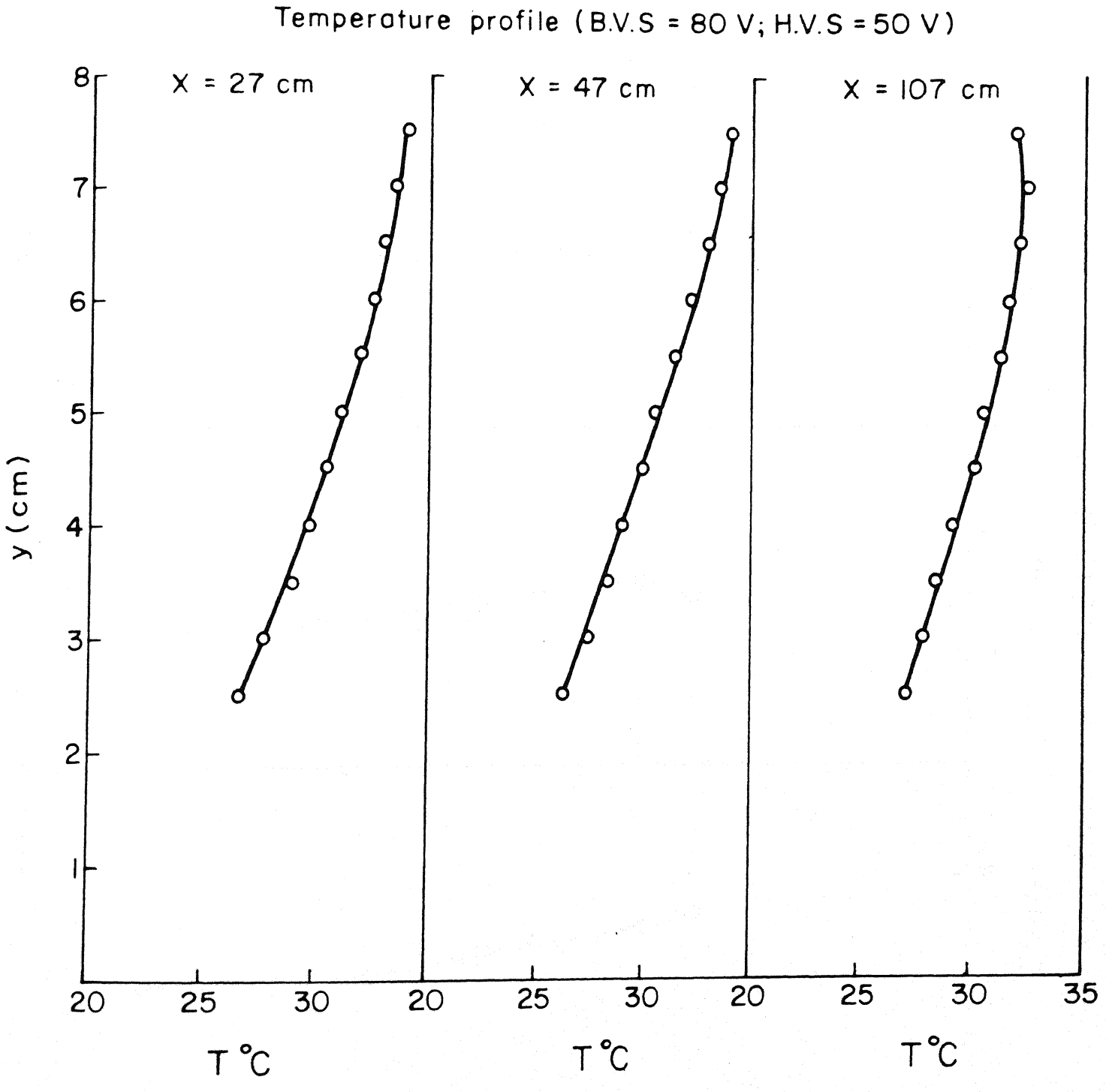

FIG. 4.45 NON-ISOTHERMAL PARALLEL FLOW PAST A CYLINDER

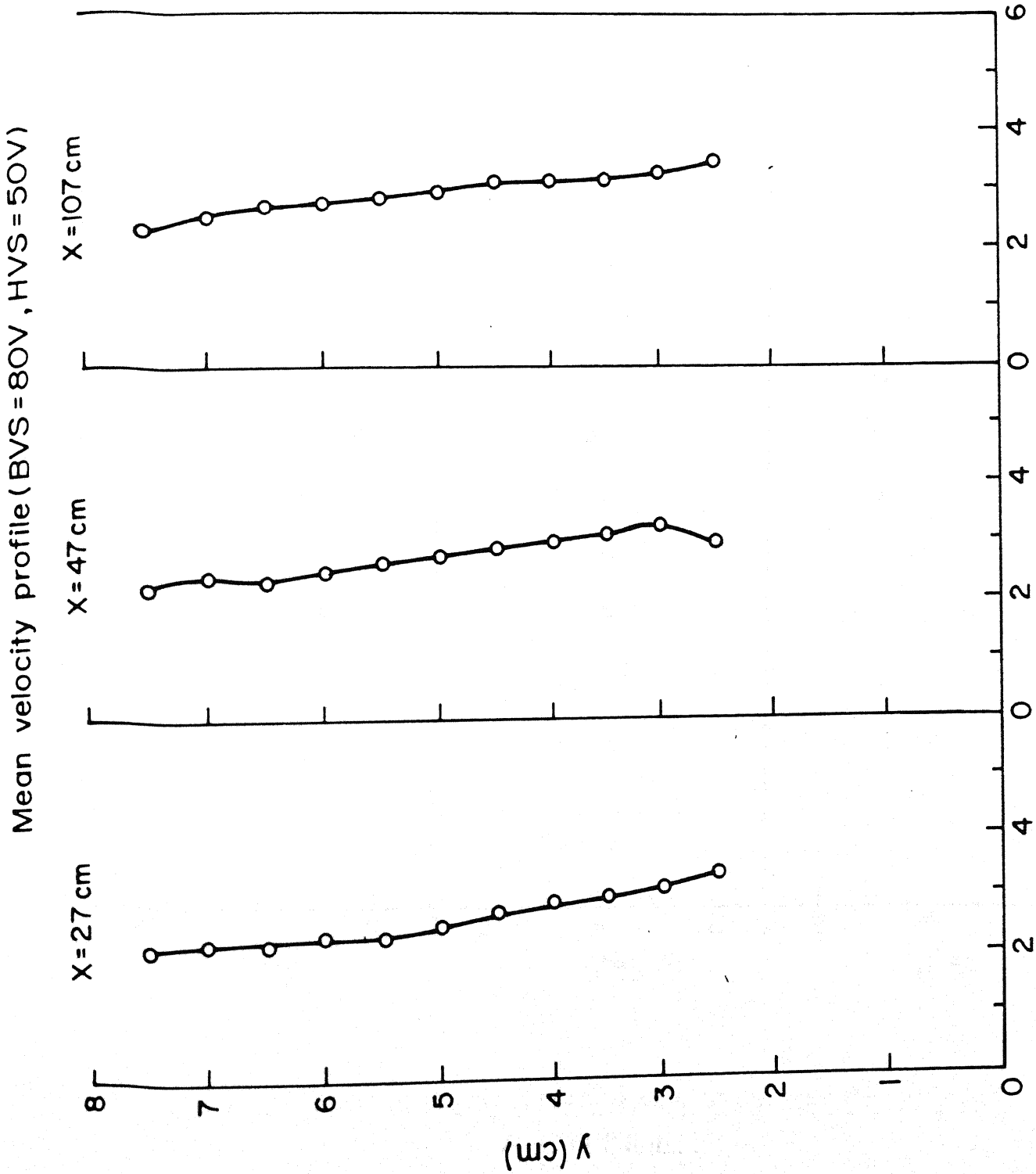

FIG. 4.46 NON-ISOTHERMAL PARALLEL FLOW PAST A CYLINDER

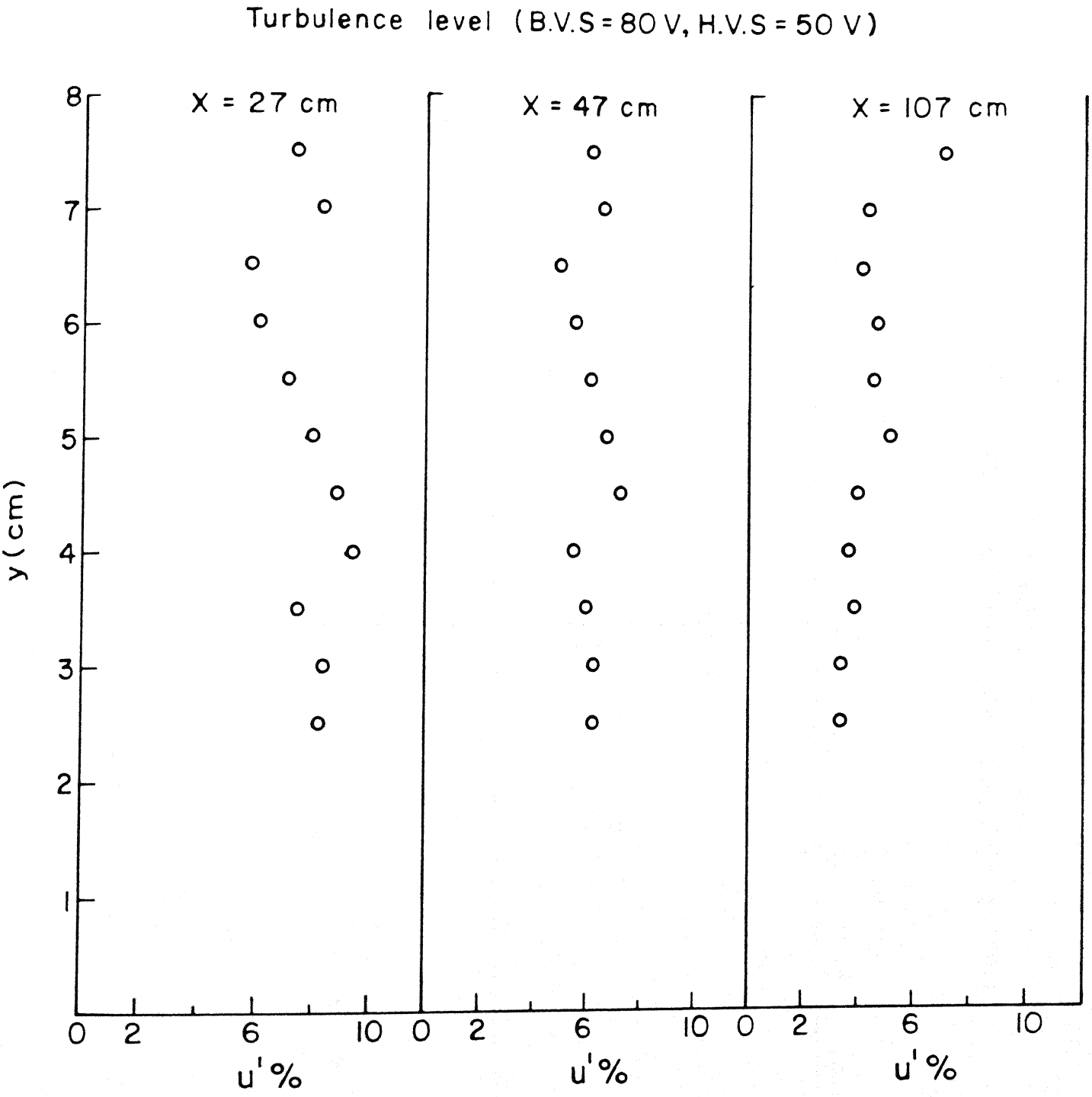

FIG. 4.47 NON-ISOTHERMAL PARALLEL FLOW PAST A CYLINDER

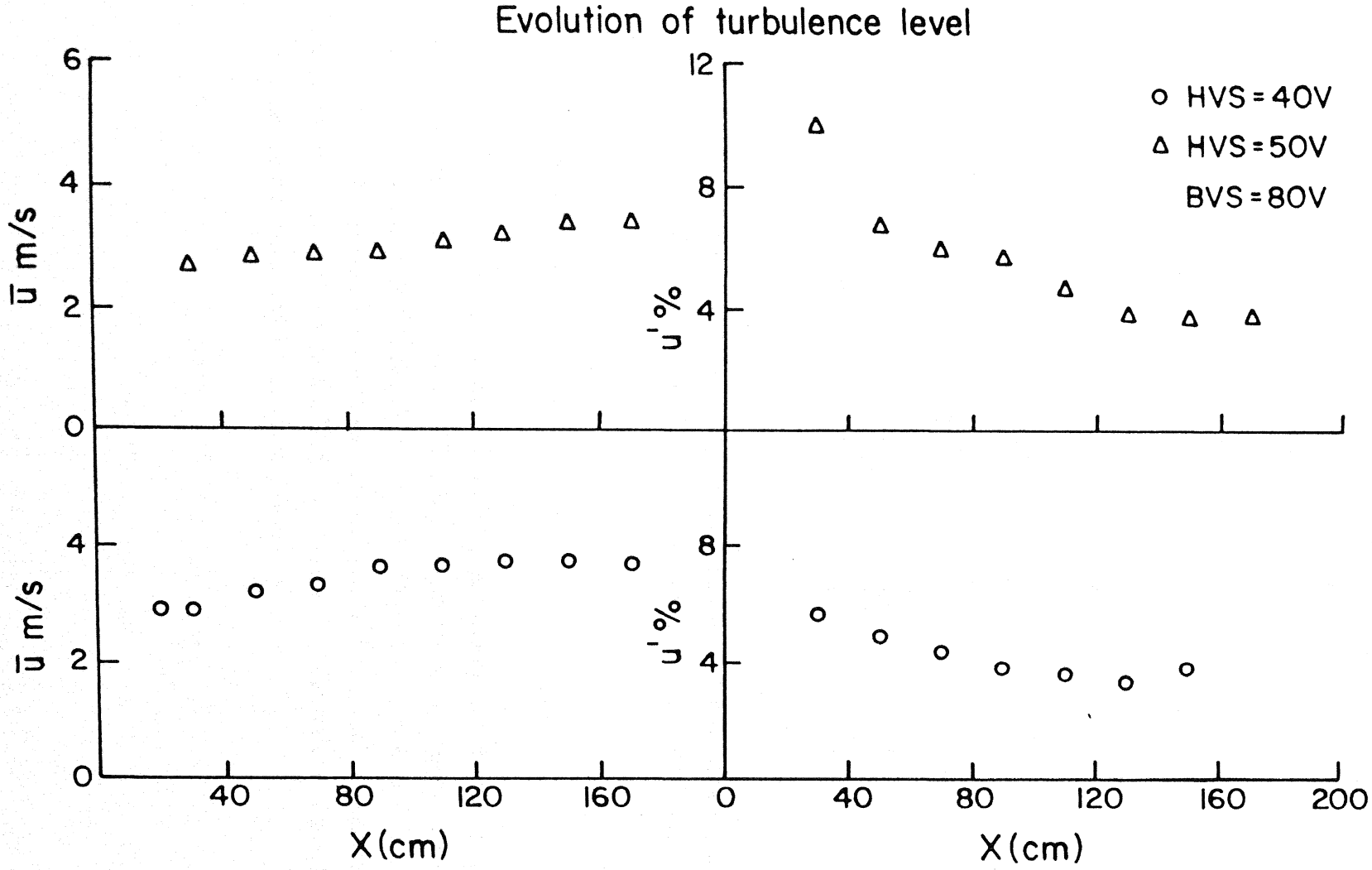

FIG. 4.48 NON-ISOTHERMAL PARALLEL FLOW PAST A CYLINDER

of properties of the flow past the cylinder. Different combinations of BVS and HVS are used to clearly understand the effect of stratification. The average values of velocity and temperature gradients and Ri are listed below.

BVS V	HVS V	X m	Tm °C	dT/dy °C/m	du/dy m/s/m	Ri
70	30	1.1	25.4	80	12	0.215
		1.3	25.5	84	6	0.8976
		1.9	25.7	51	16	0.076
70	40	1.1	29.5	150	20	0.171
		1.3	30.25	150	20	0.1216
		1.9	31.5	105	30	0.038
80	40	1.1	25.6	132	8	0.192
		1.3	27.8	120	8	0.162
		1.9	27.3	51	20	0.047
80	50	1.1	30.37	145	24	0.813
		1.3	30.25	160	14	0.265
		1.9	29.63	95	22	0.065

As stated earlier, the temperature gradient is locally negative near the top wall leading to unstable stratification. These regions experience a local increase in turbulence level.

Non–isothermal Shear Flow :

As an approach towards modeling of atmosphere flows, a parabolic–shaped honeycomb is placed in stably stratified flow. Different combinations of BVS and HVS are used to produce different Richardson numbers. Figures 4.49 to 4.59 show the temperature, velocity and turbulence level profiles. Figures 4.51 and 4.59 show downstream evolution of mean velocity and turbulence for BVS = 70 and 80V. The values of average velocity and temperature gradients and Ri are given below.

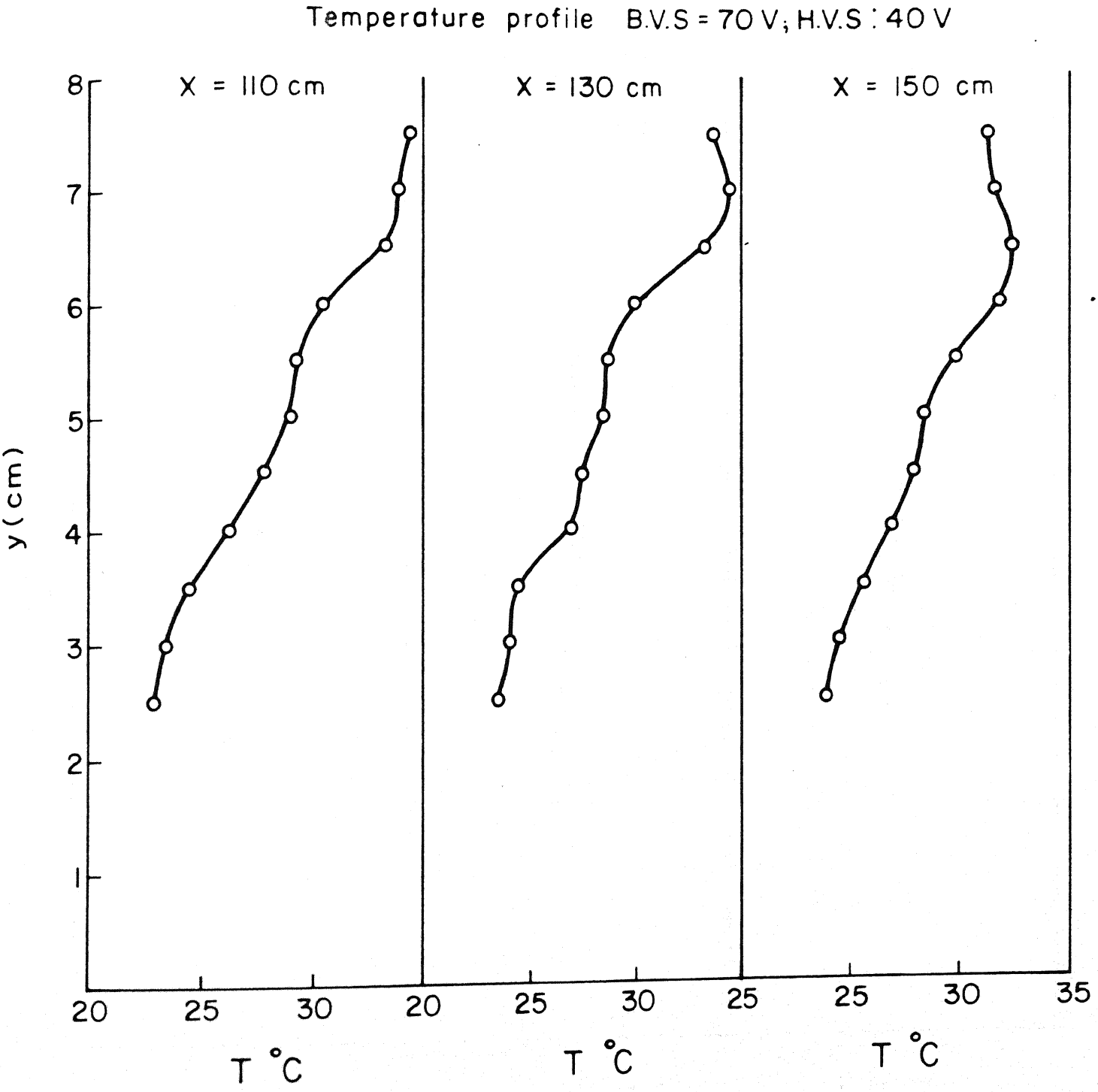

FIG. 4.49 NON-ISOTHERMAL SHEAR FLOW

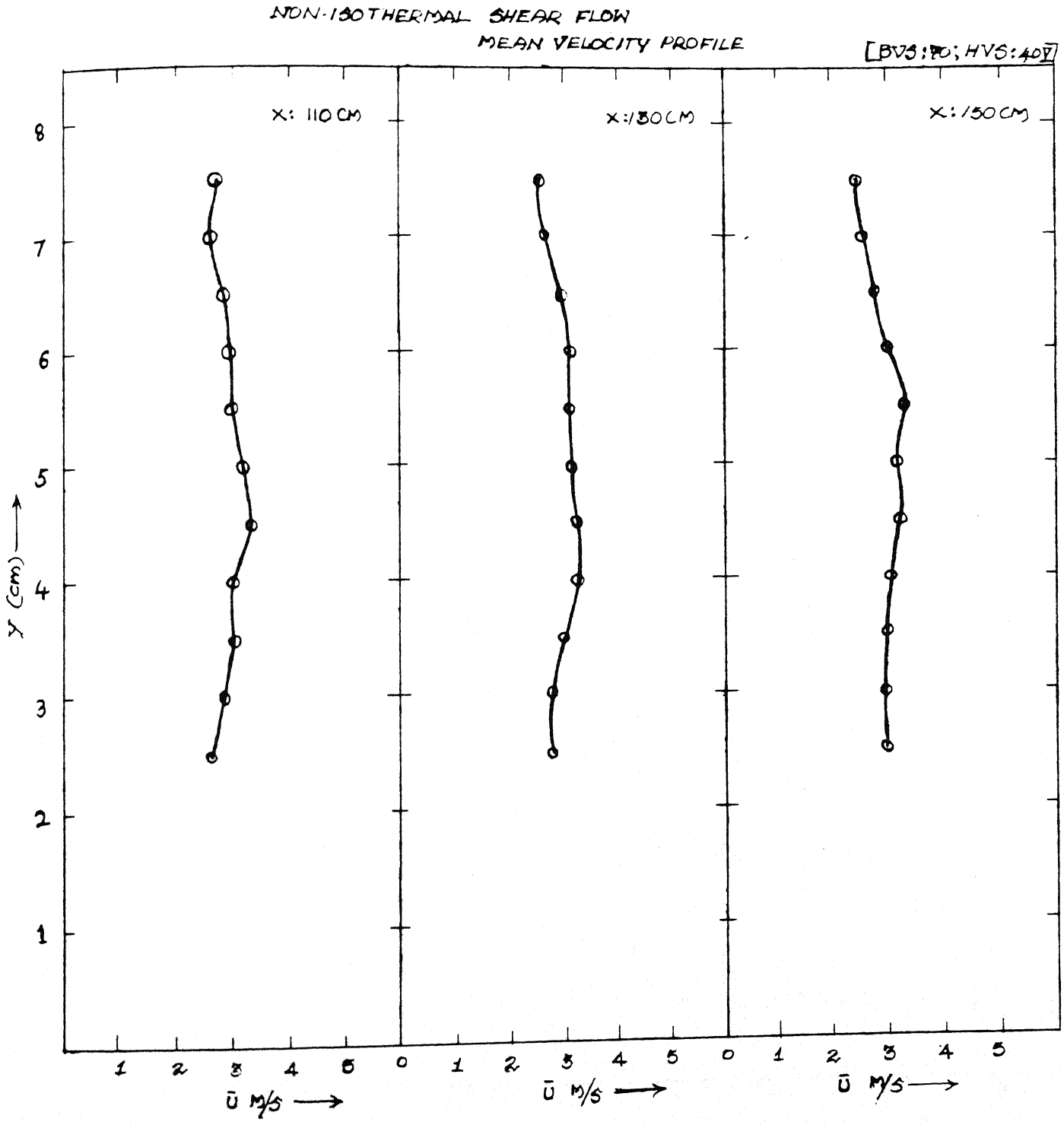

FIG. 4.50 NON-ISOTHERMAL SHEAR FLOW

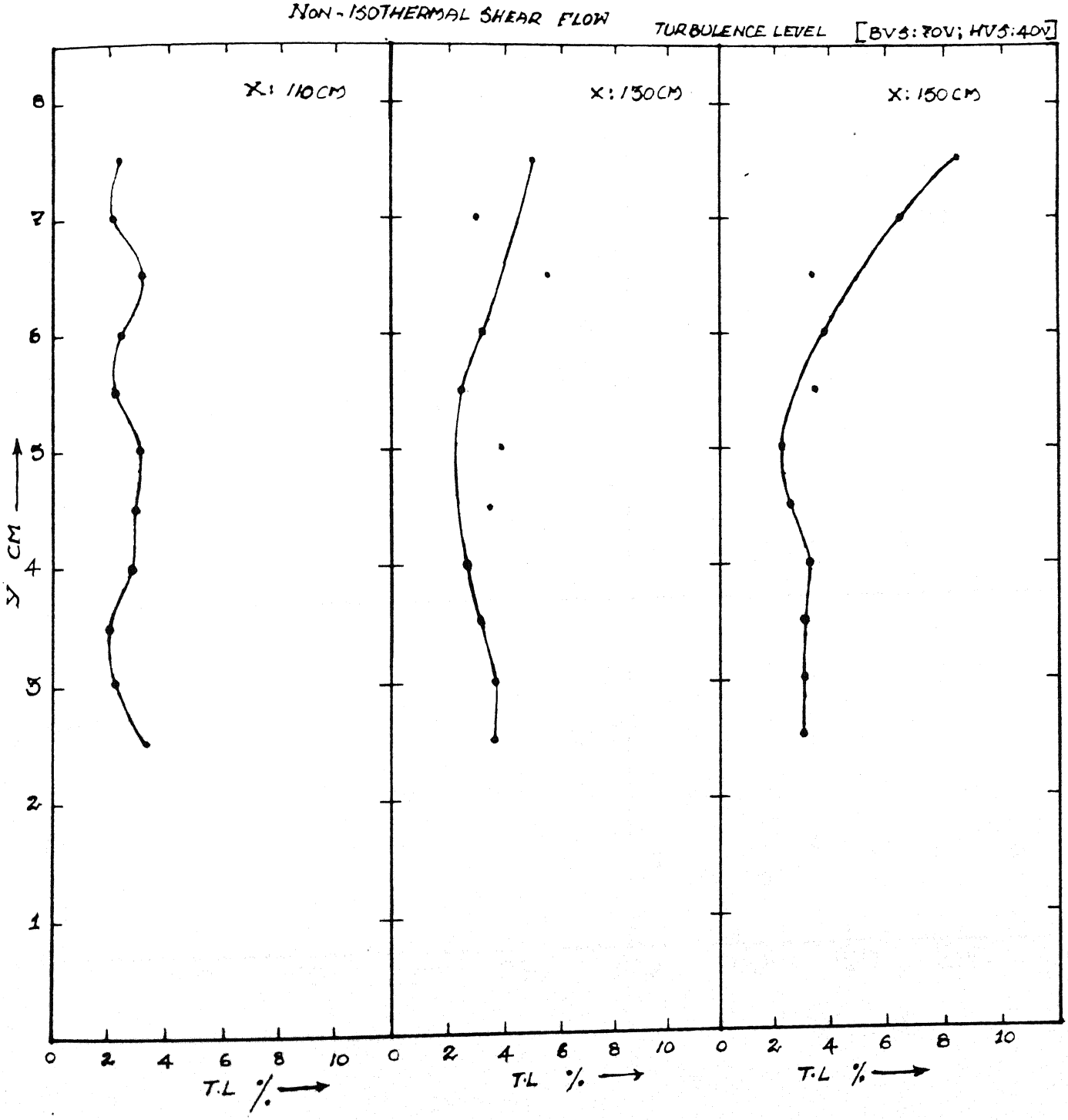

FIG. 4.51 NON-ISOTHERMAL SHEAR FLOW

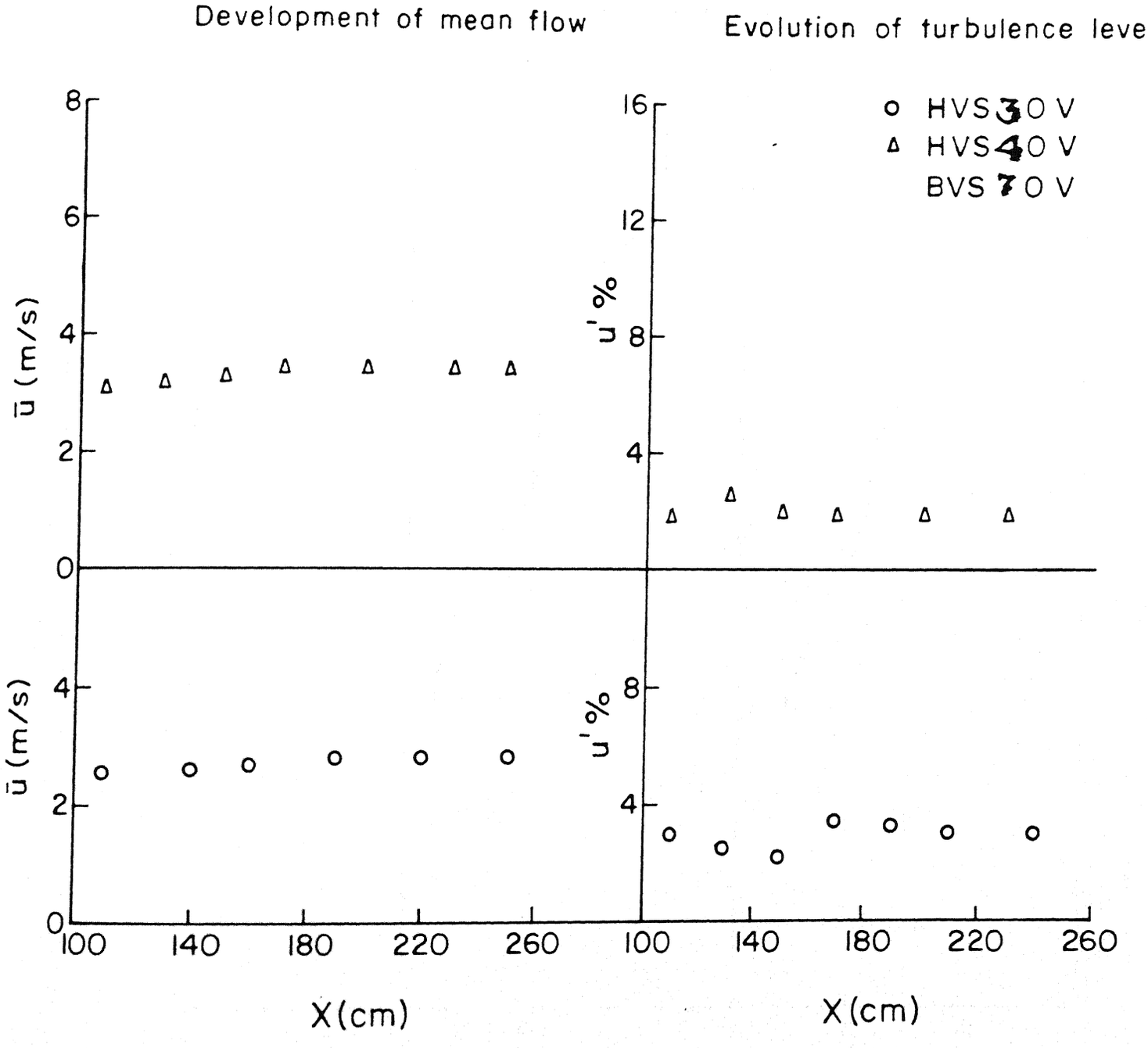

FIG. 4.52 NON-ISOTHERMAL SHEAR FLOW

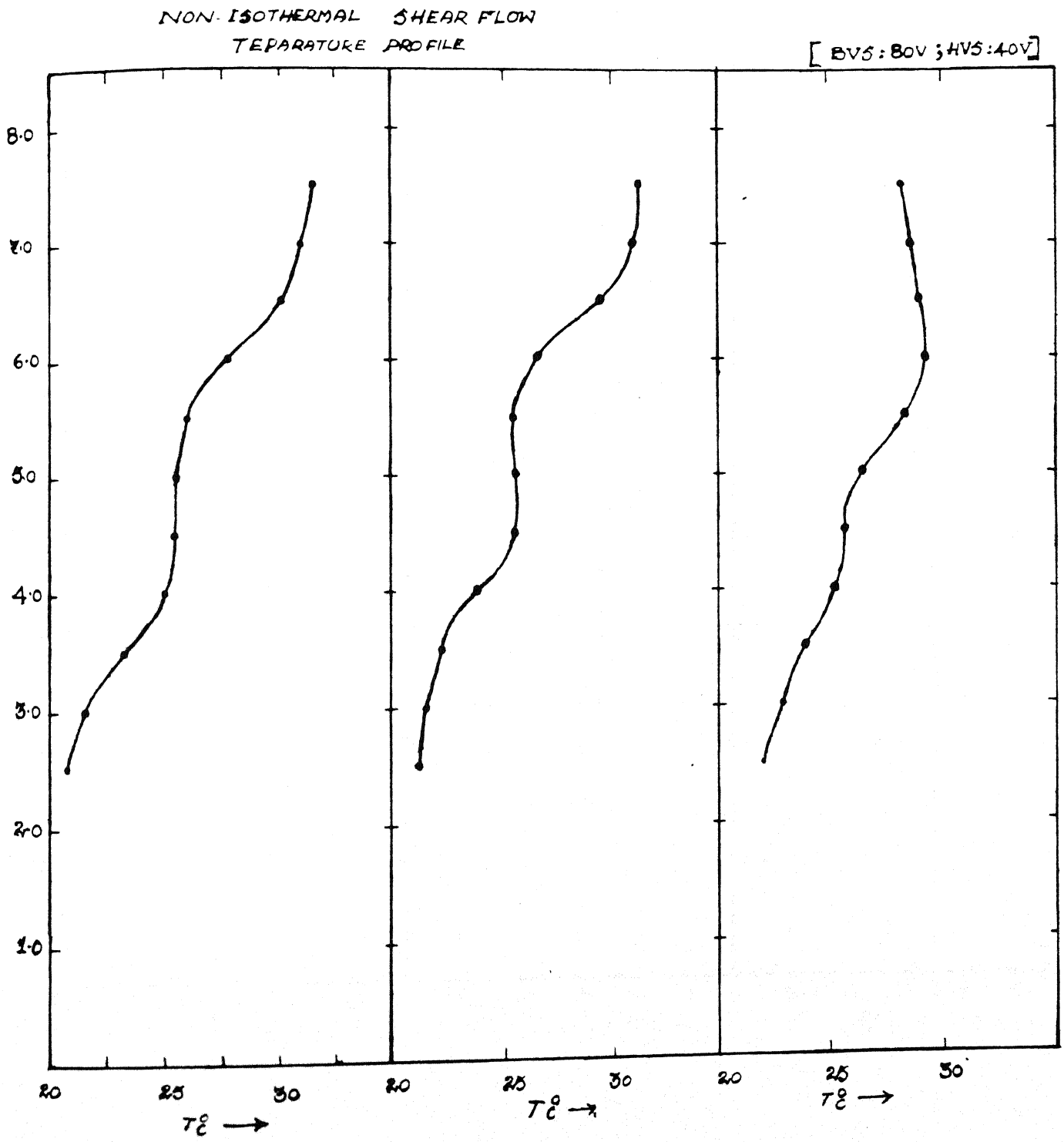

FIG. 4.53 NON-ISOTHERMAL SHEAR FLOW

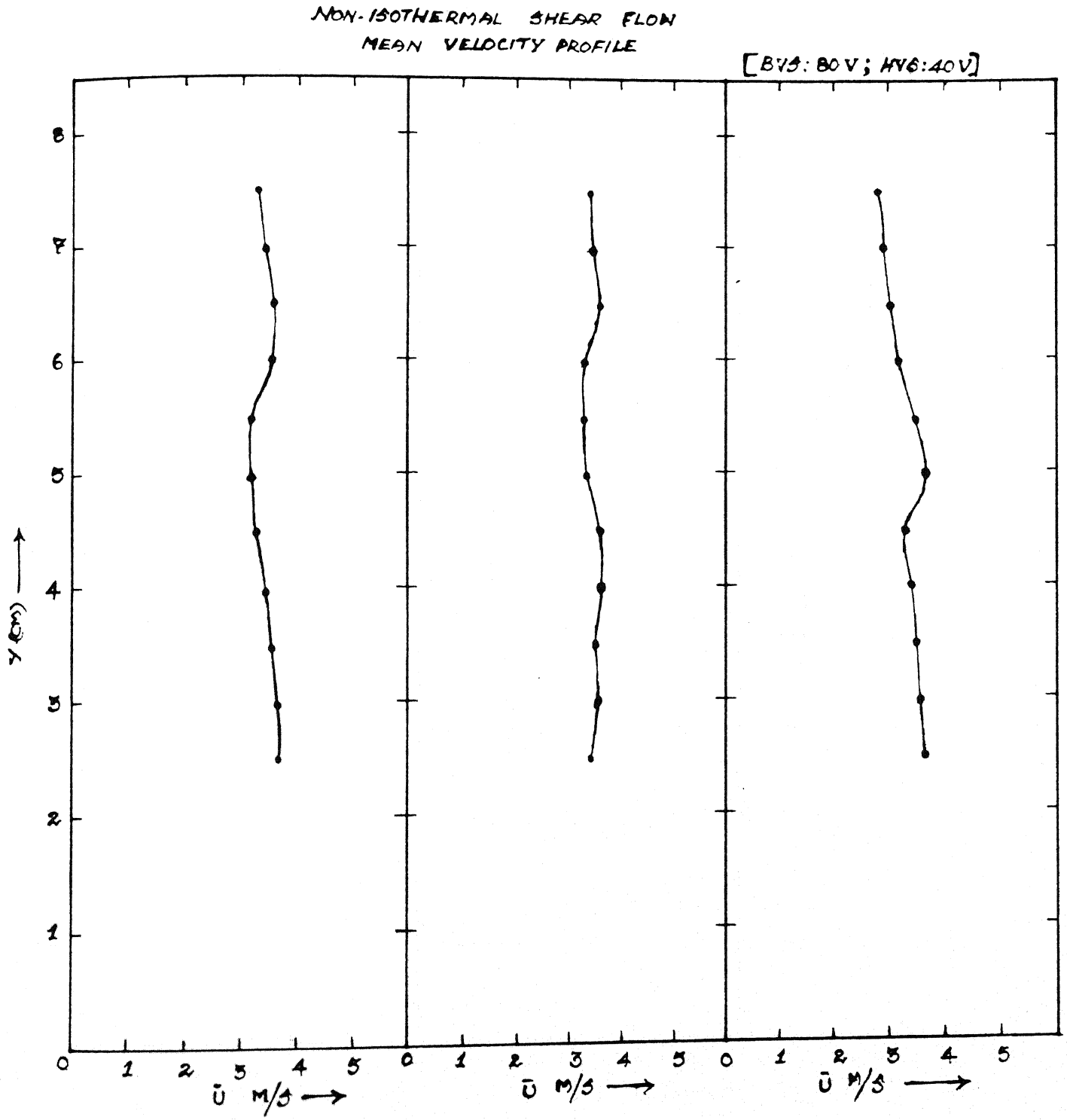

FIG. 4.54 NON-ISOTHERMAL SHEAR FLOW

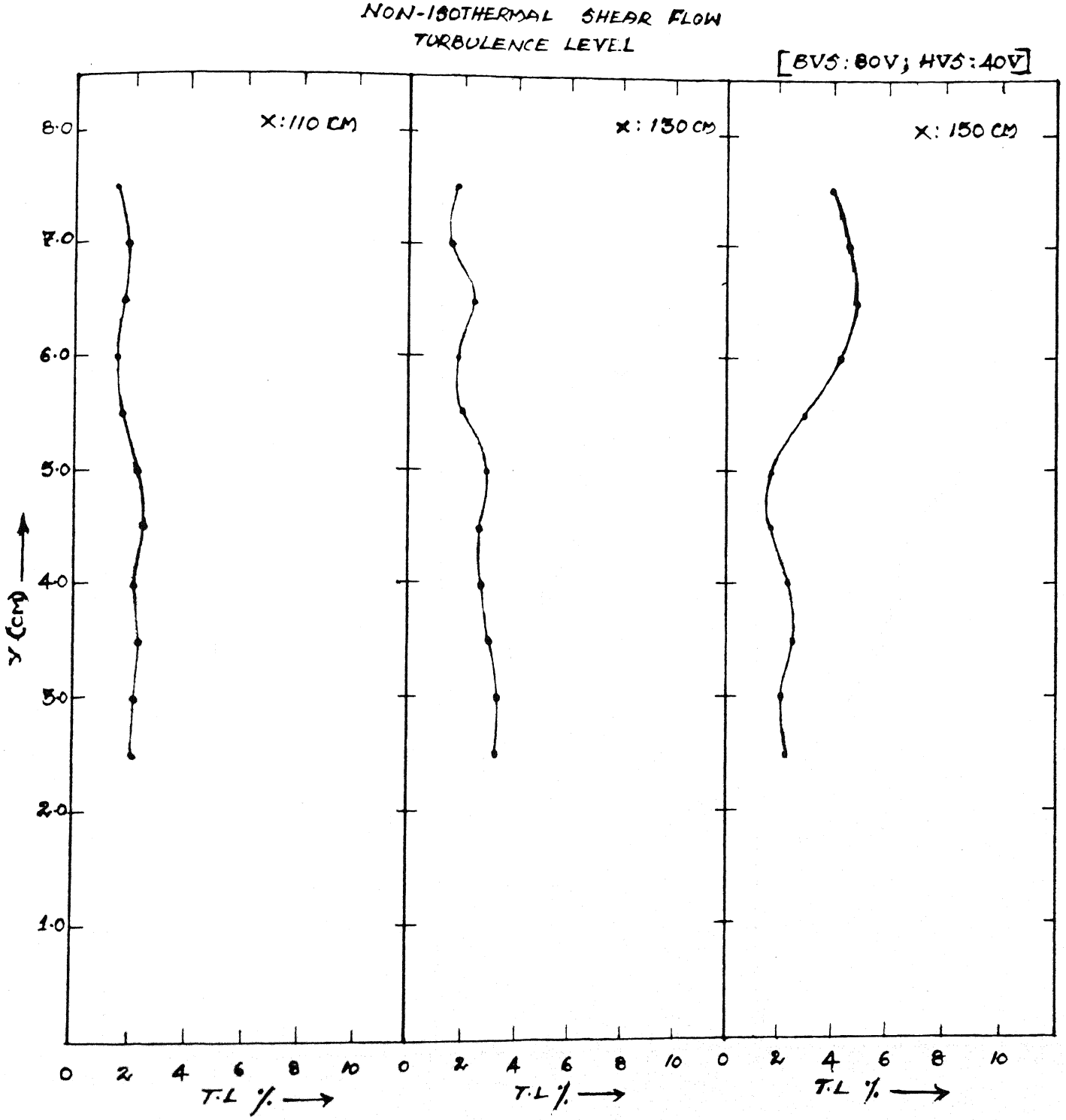

FIG. 4.55 NON-ISOTHERMAL SHEAR FLOW

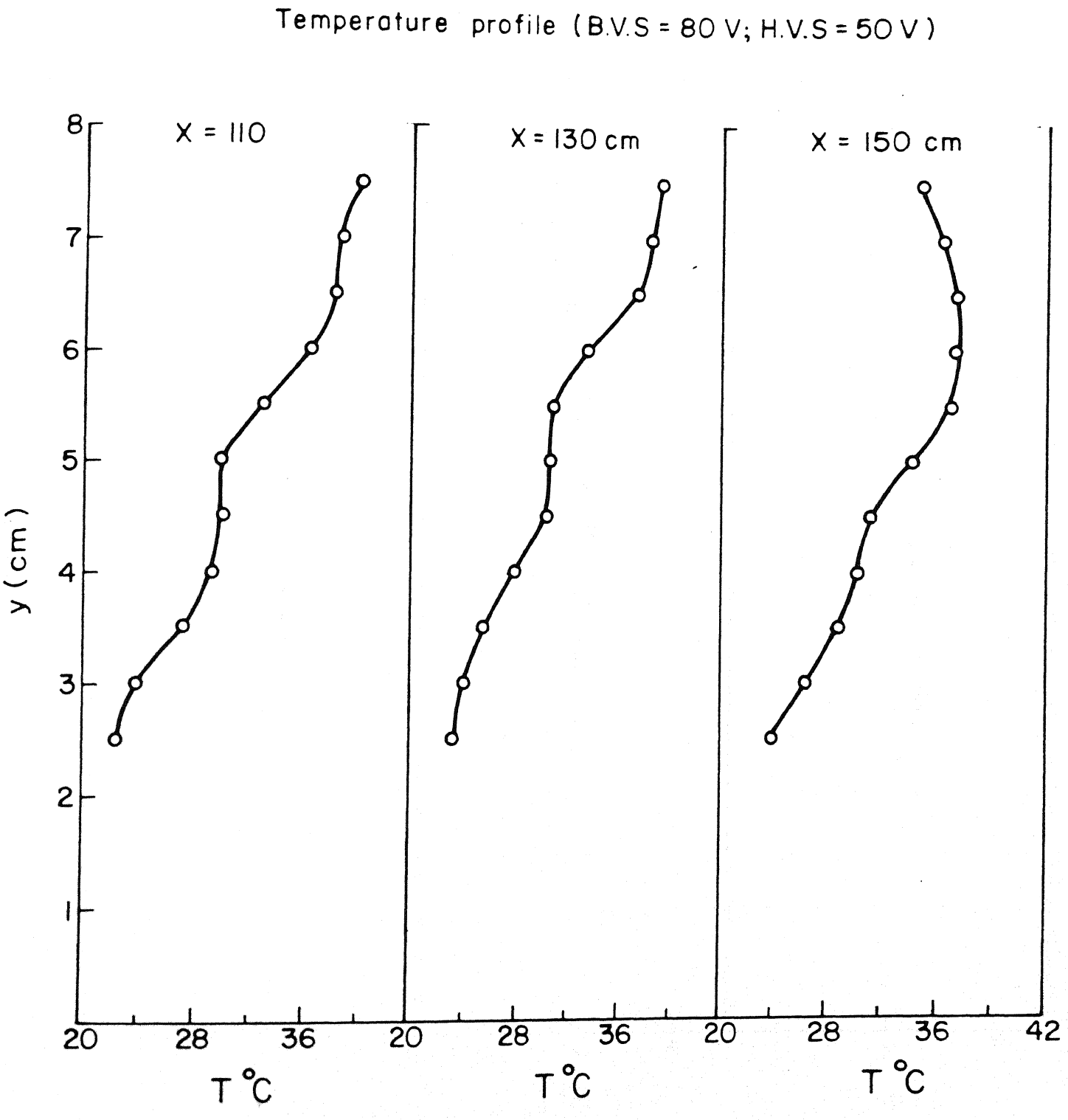

FIG. 4.56 NON-ISOTHERMAL SHEAR FLOW

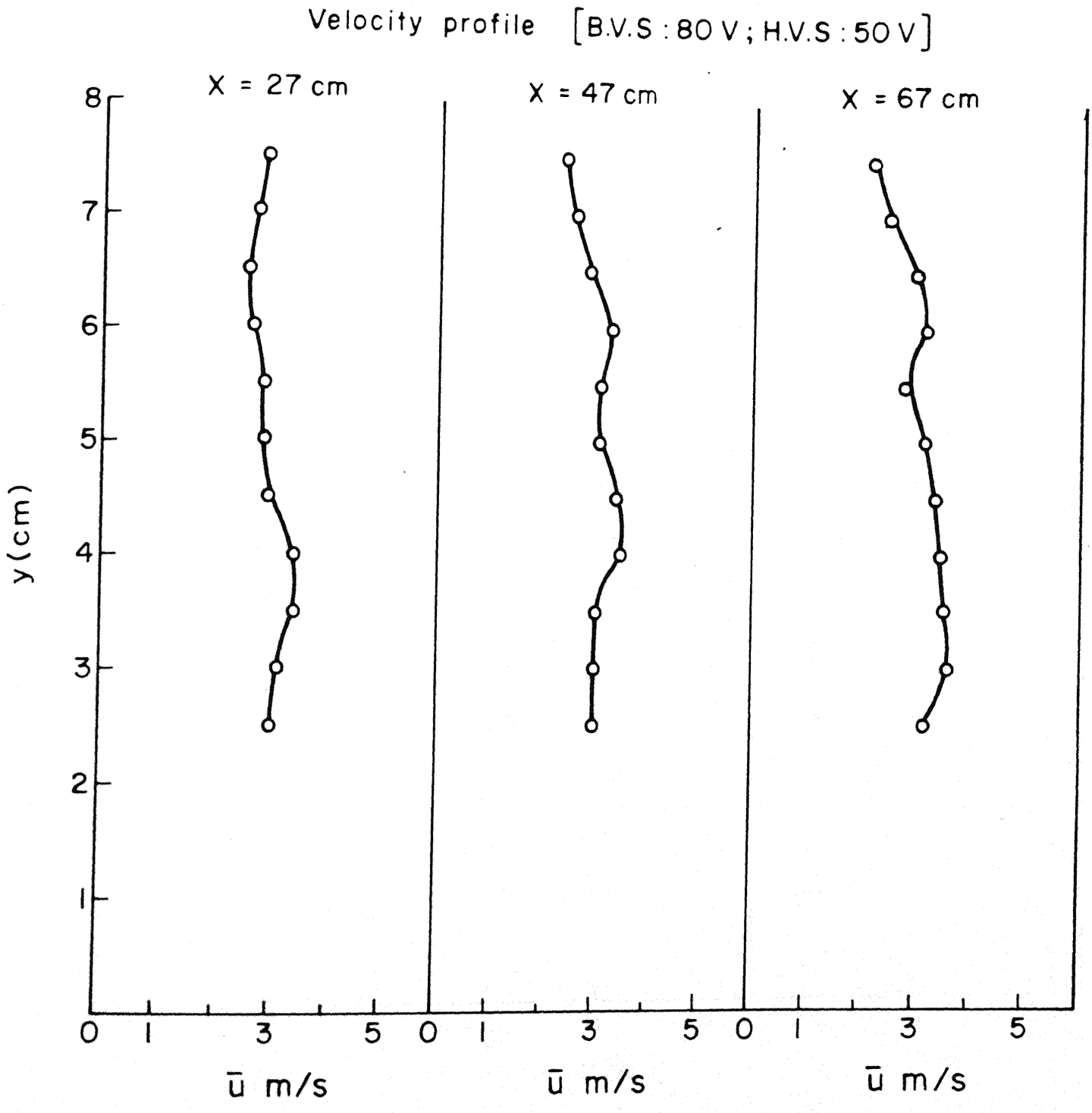

FIG. 4.57 NON-ISOTHERMAL SHEAR FLOW

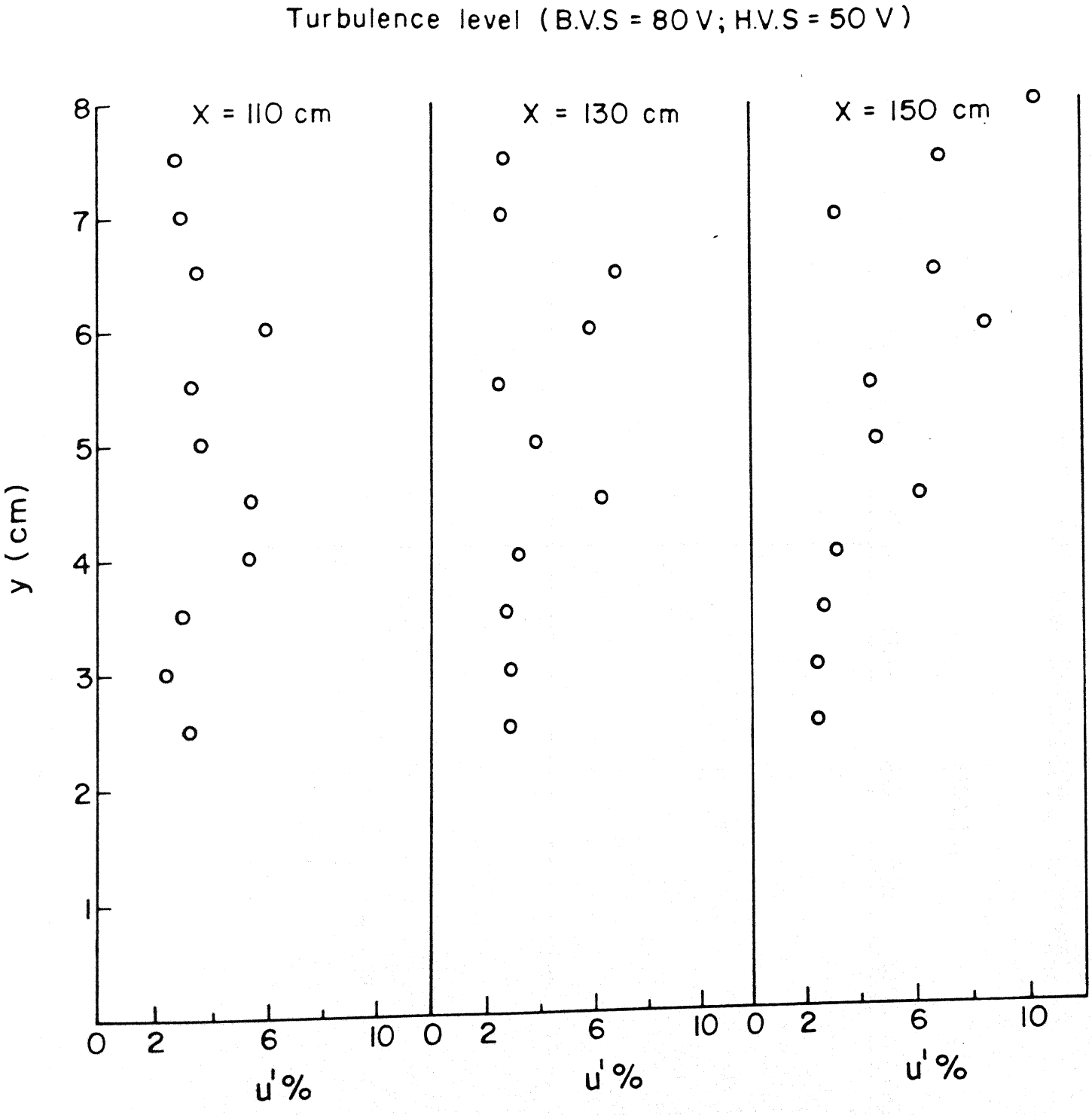

FIG. 4.58 NON-ISOTHERMAL SHEAR FLOW

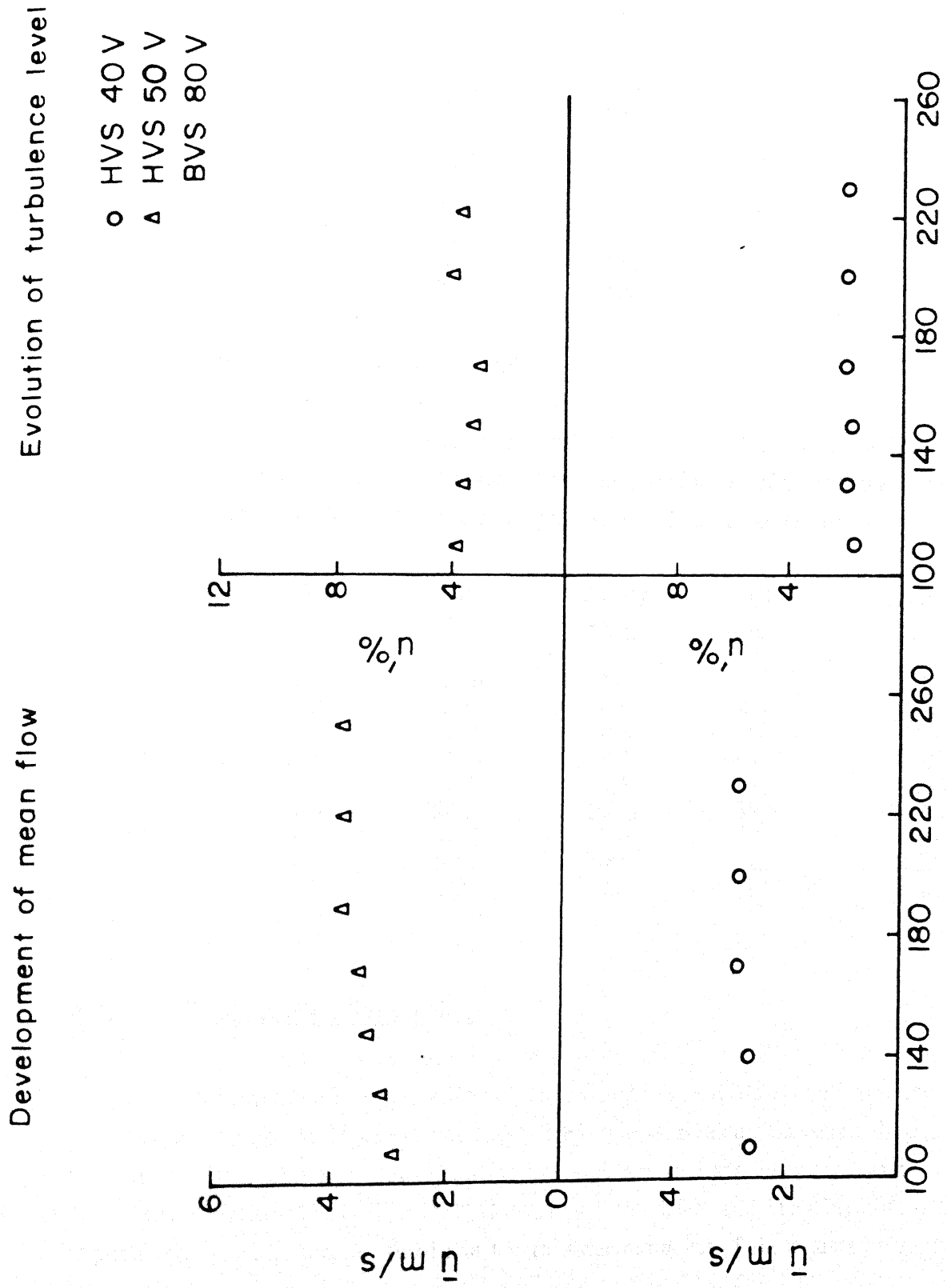

FIG 4.59 NON-ISOTHERMAL SHEAR FLOW

BVS V	HVS V	X m	Tm °C	dT/dy °C/m	du/dy m/s/m	Ri
70	40	1.1	28.75	230	2	19.62
		1.3	28.58	205	4	4.40
		1.9	28.38	175	10	0.605
80	40	1.1	26.13	215	8	1.261
		1.3	26.25	200	4	4.671
		1.9	25.00	120	18	0.145
80	50	1.1	31.20	352	4	6.917
		1.3	33.20	240	12	0.492
		1.9	30.40	427	20	0.344

Non–isothermal Shear Flow Over Cylinder :

Finally we measure temperature, velocity and turbulence profiles for heated shear flow past a cylinder. Figures 4.60–4.72 show the distribution of temperature, velocity and percentage turbulence level. Their average gradients and Ri are given below.

BVS V	HVS V	X m	Tm °C	dT/dy °C/m	du/dy m/s/m	Ri
70	40	1.1	29.25	200	5	2.68
		1.3	27.75	170	6.67	1.35
		1.9	28.50	130	14	0.23
80	40	1.1	27.80	168	4	3.705
		1.3	26.8	136	6	1.586
		1.9	28.1	107.5	12.5	0.255
80	50	1.1	30.40	240	4	4.84
		1.3	29.00	184	4	3.89
		1.9	29.2	187	20	0.157

4.3. Turbulence Statistics

To understand the behavior of stratified turbulent flows we have computed the normalized probability density function (PDF), the equivalent Gaussian distribution and auto–correlation. For each flow condition these parameters are calculated at two different downstream locations. Figures 4.73–4.80 show the PDF and the Gaussian PDF of the required signal. The second, third and fourth order moments of these distributions are given below:

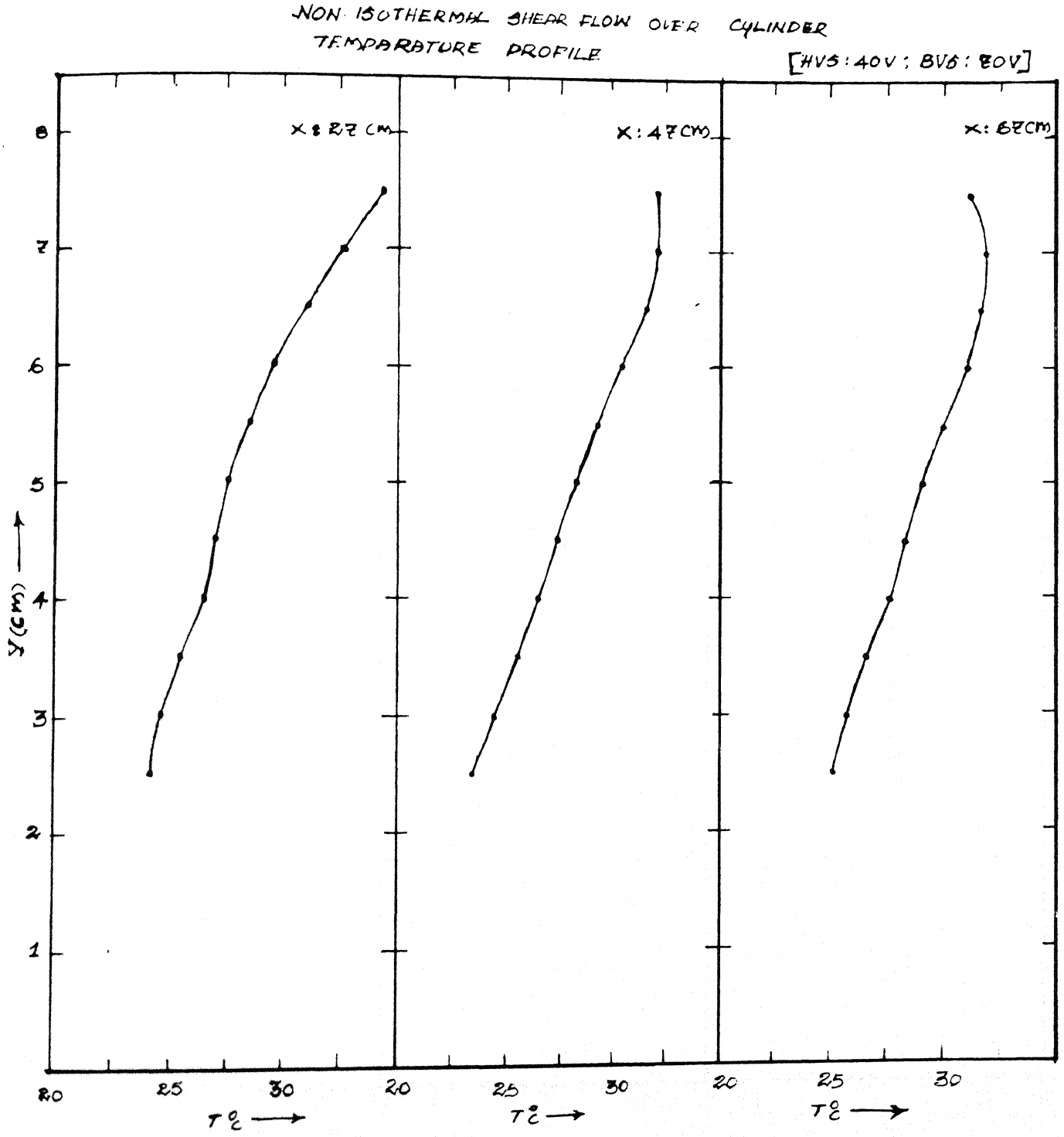

FIG. 4.60 NON-ISOTHERMAL SHEAR FLOW PAST A CYLINDER

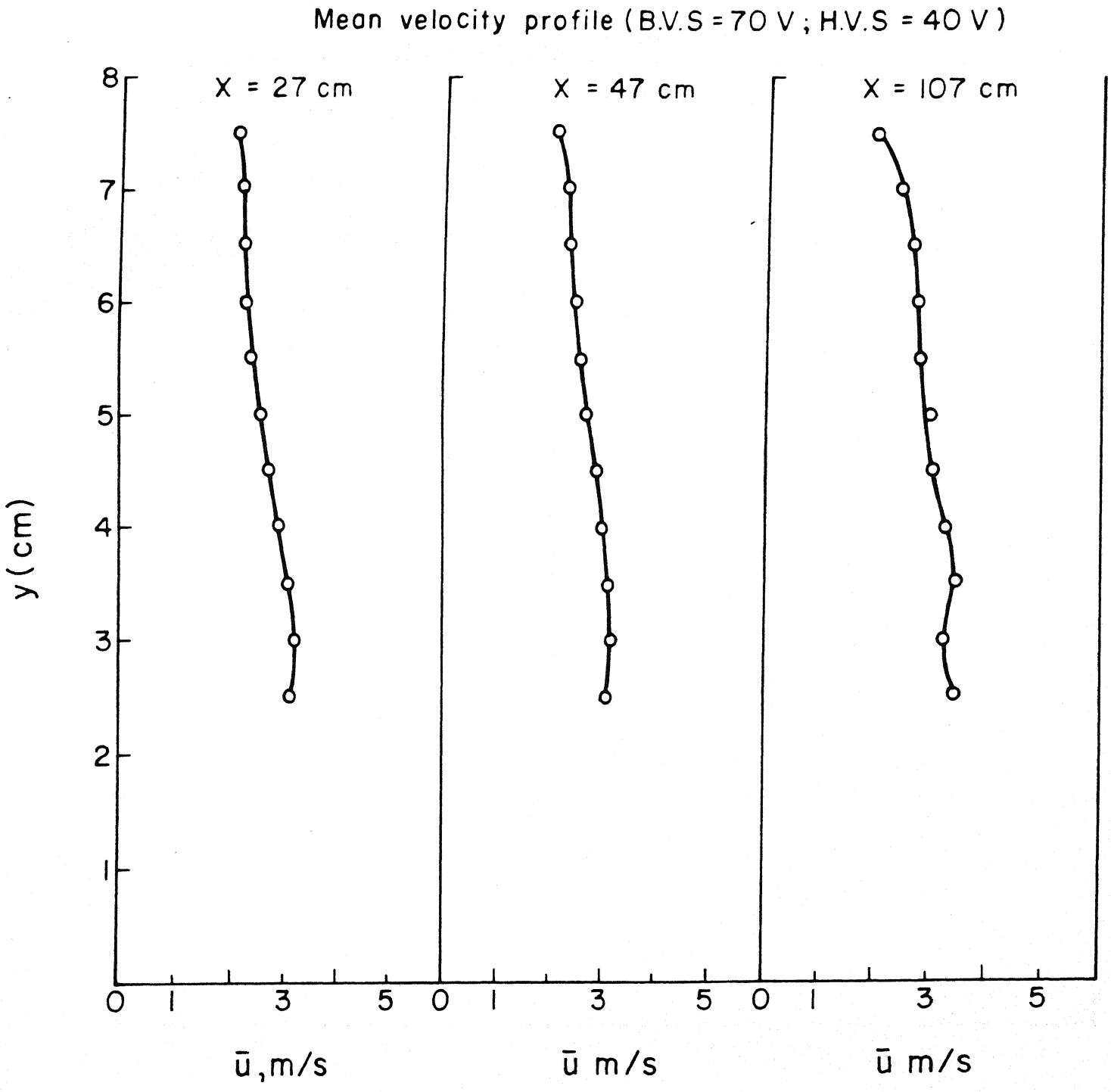

FIG. 4.61 NON-ISOTHERMAL SHEAR FLOW PAST A CYLINDER

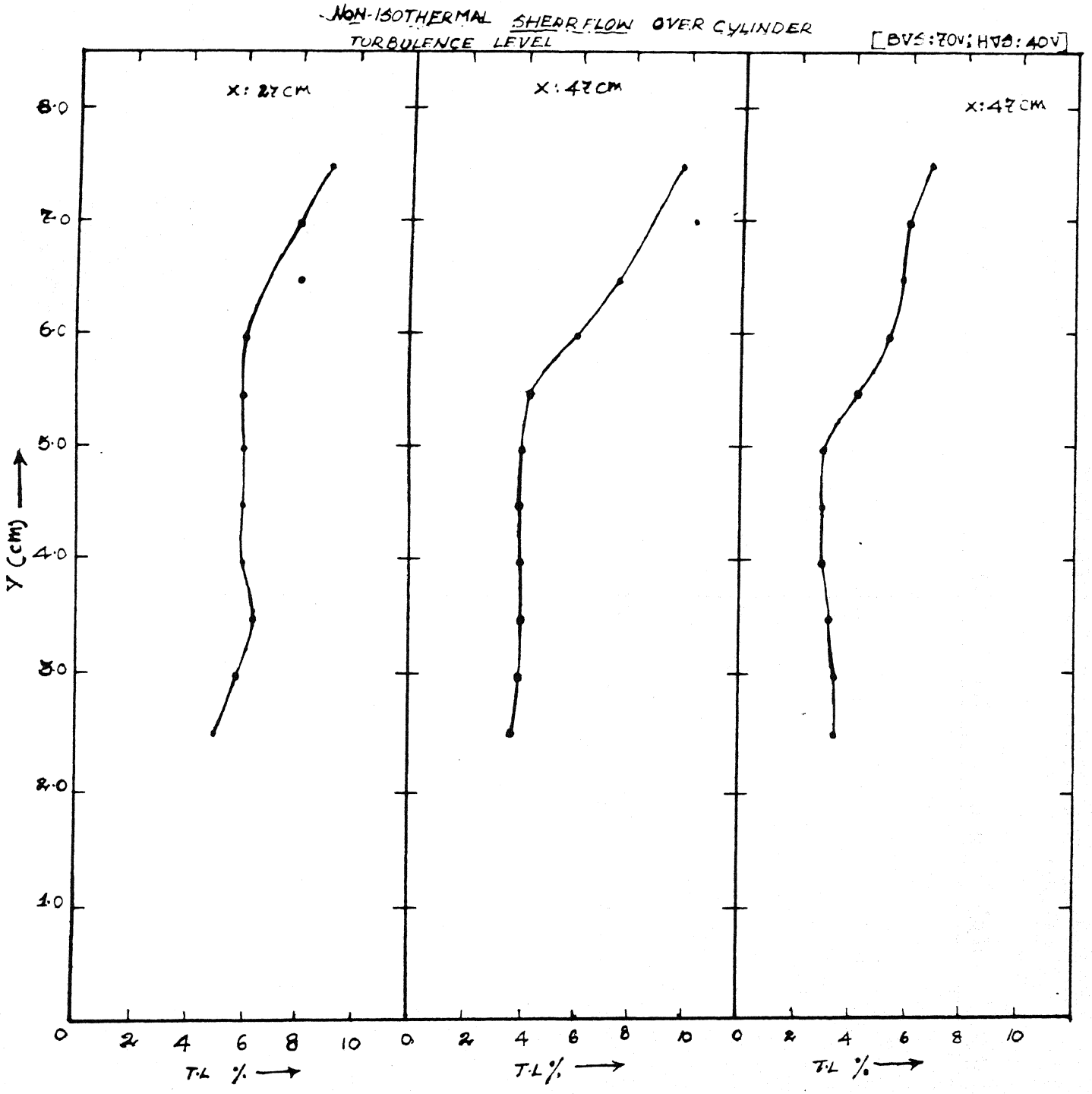

FIG. 4.62 NON-ISOTHERMAL SHEAR FLOW PAST A CYLINDER

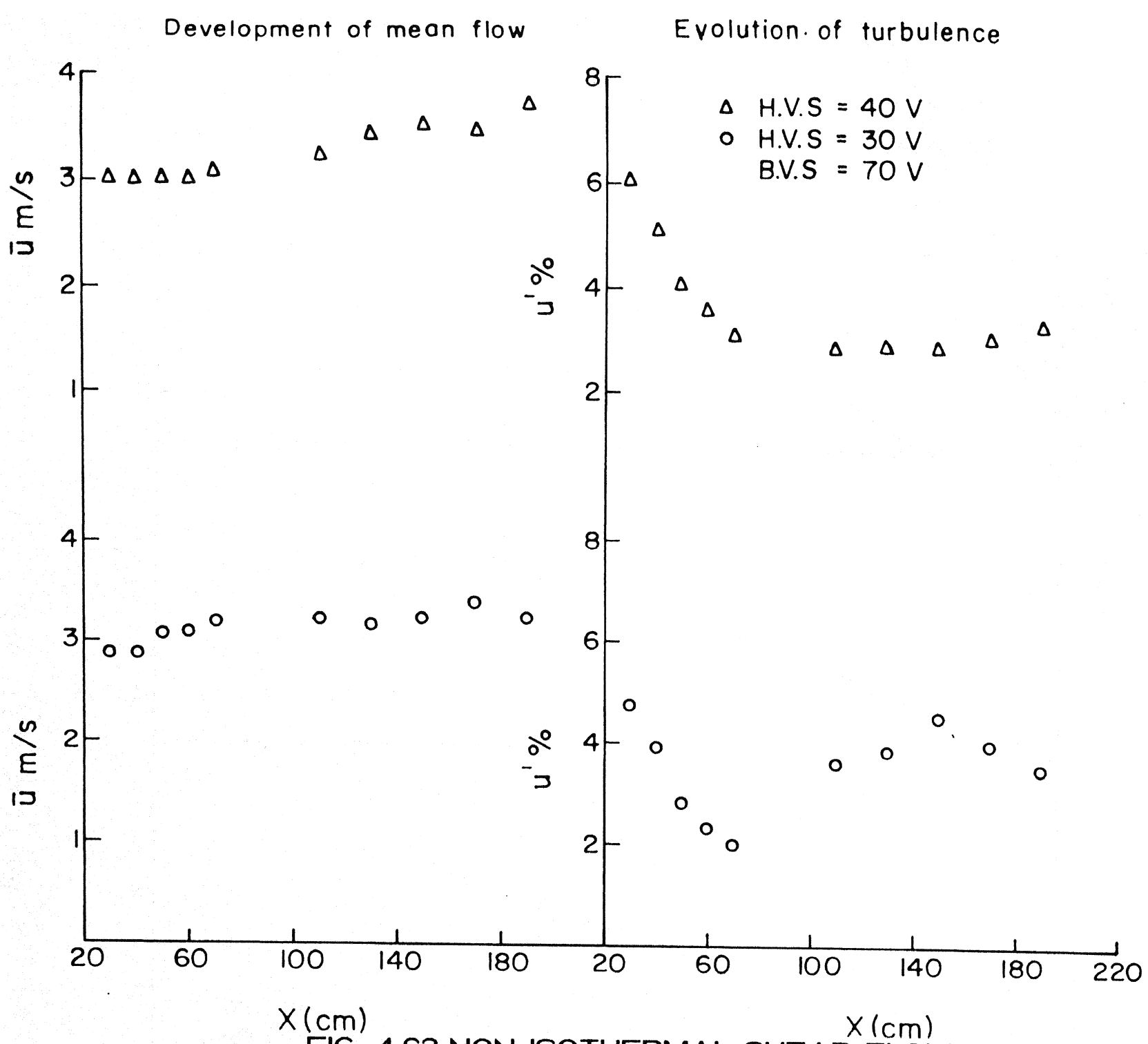

FIG. 4.63 NON-ISOTHERMAL SHEAR FLOW PAST A CYLINDER

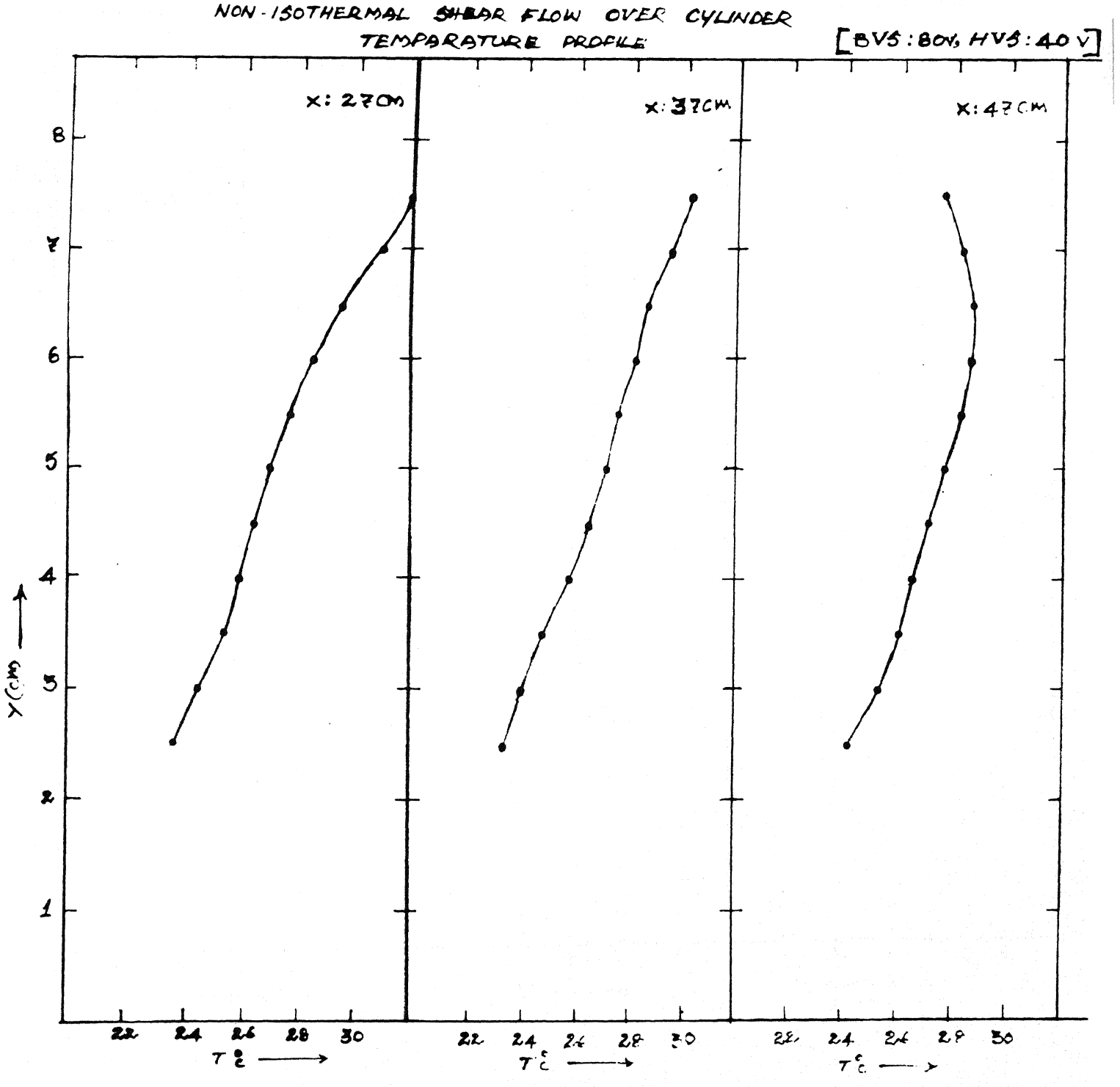

FIG. 4.64 NON-ISOTHERMAL SHEAR FLOW PAST A CYLINDER

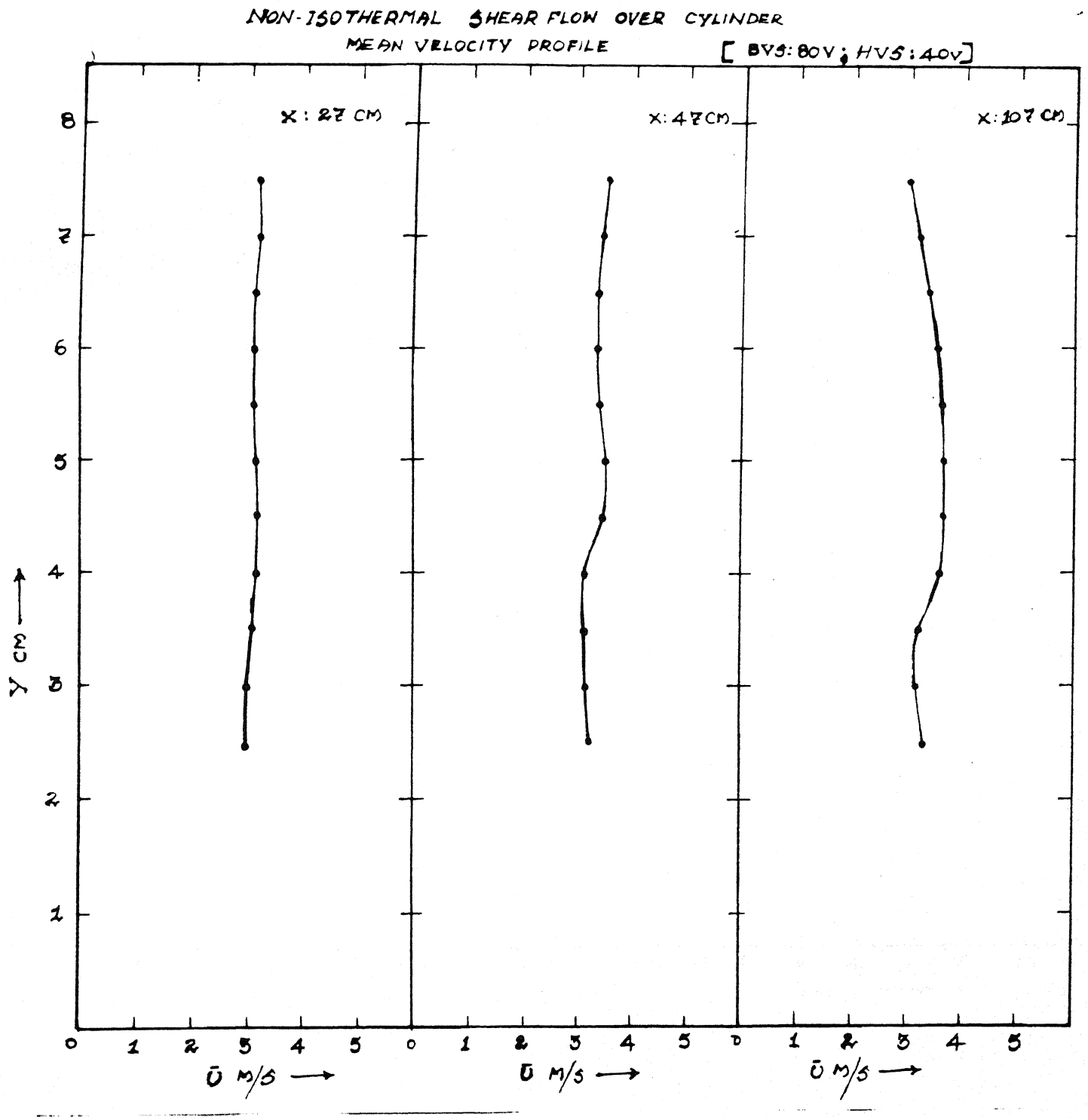

FIG. 4.65 NON-ISOTHERMAL SHEAR FLOW PAST A CYLINDER

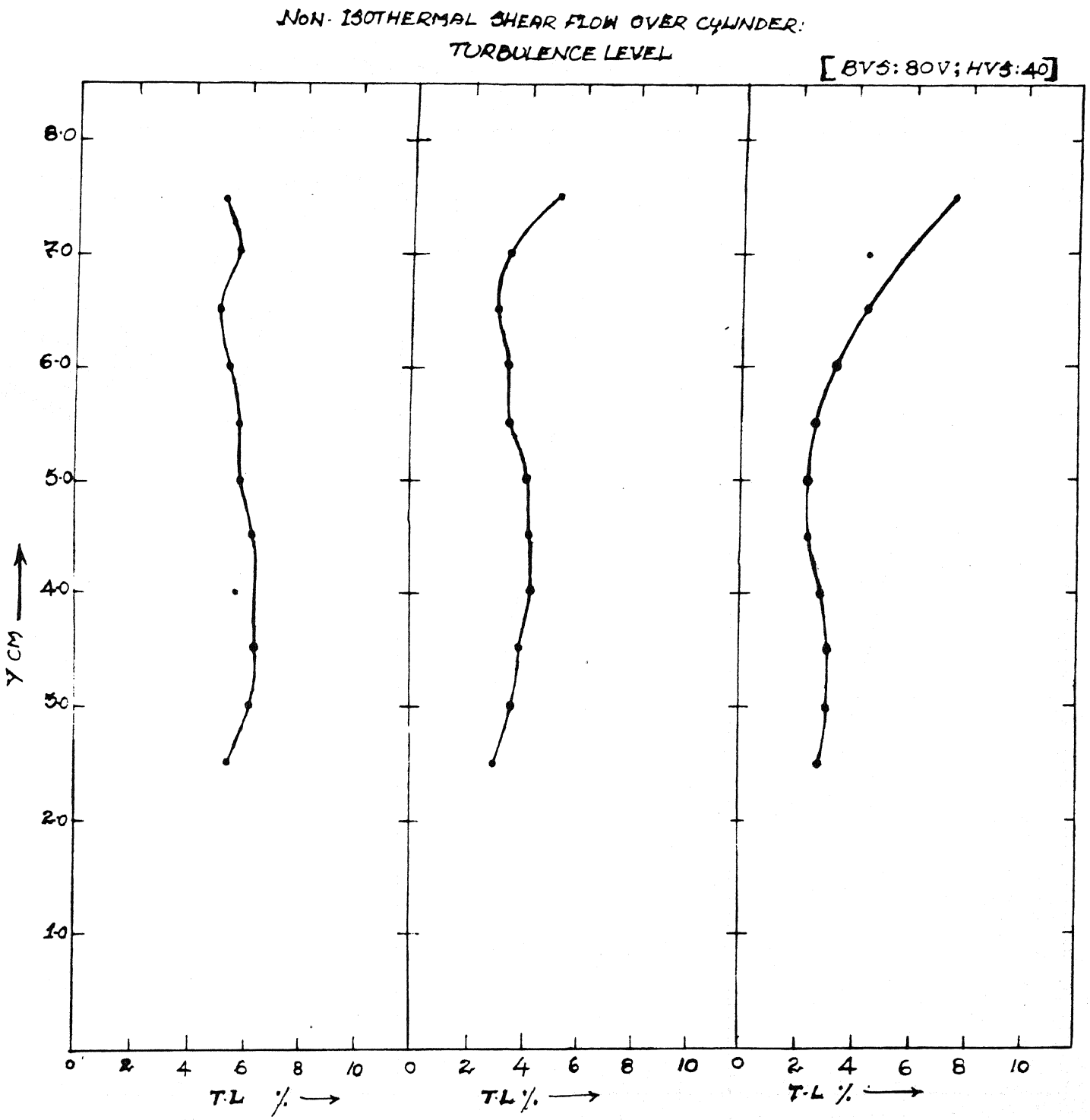

FIG. 4.66 NON-ISOTHERMAL SHEAR FLOW PAST A CYLINDER

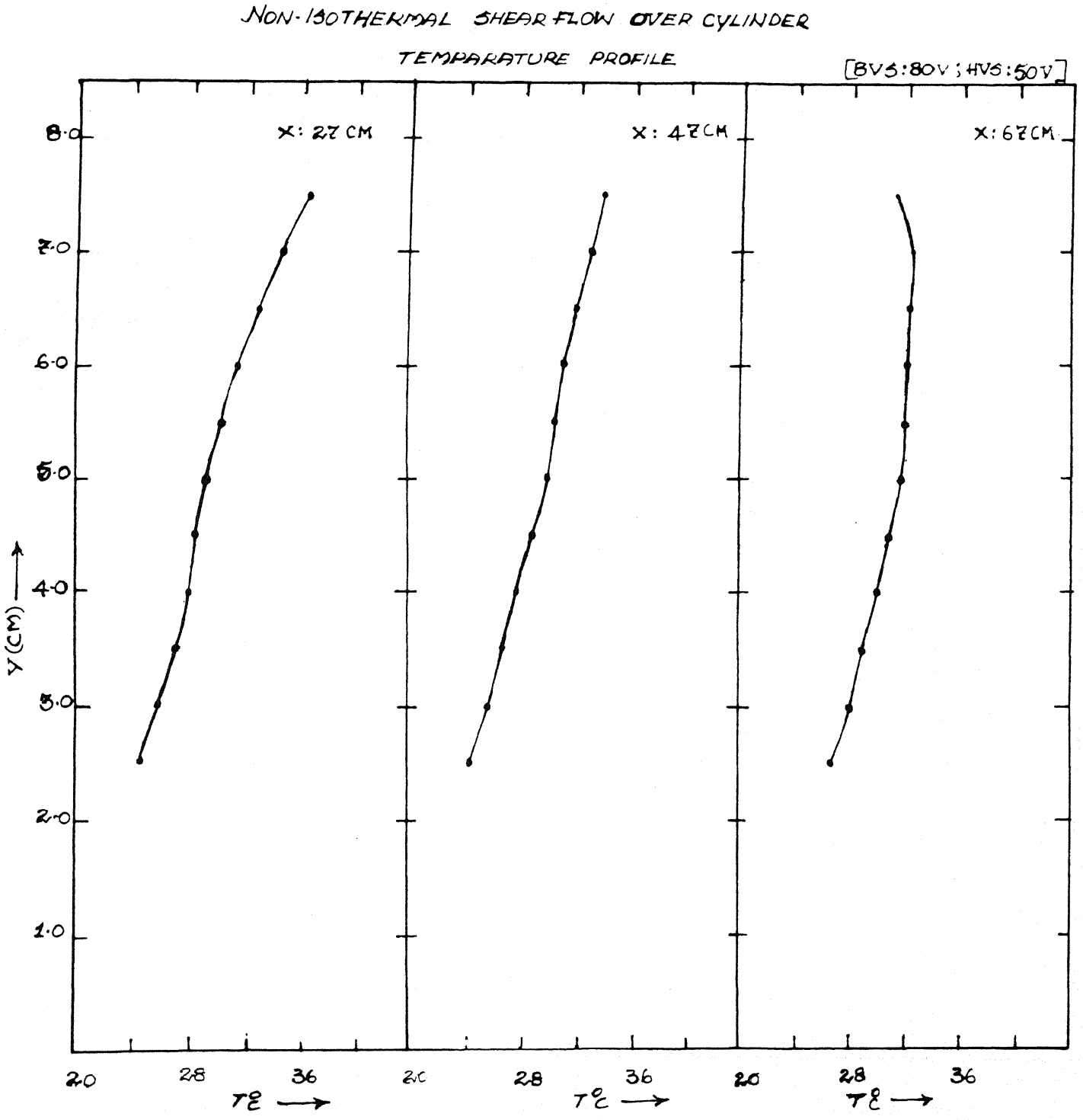

FIG. 4.67 NON-ISOTHERMAL SHEAR FLOW PAST A CYLINDER

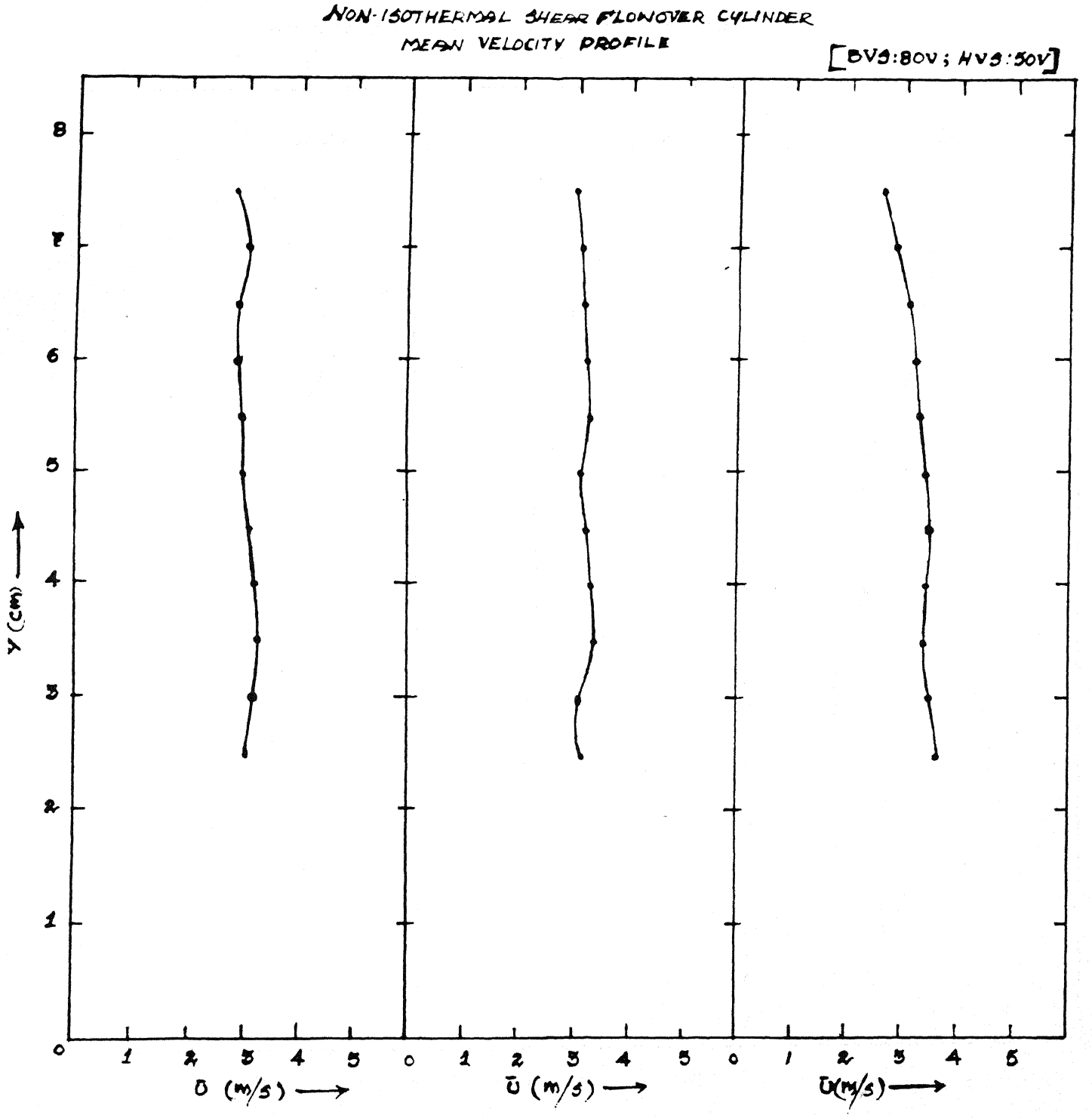

FIG. 4.68 NON-ISOTHERMAL SHEAR FLOW PAST A CYLINDER

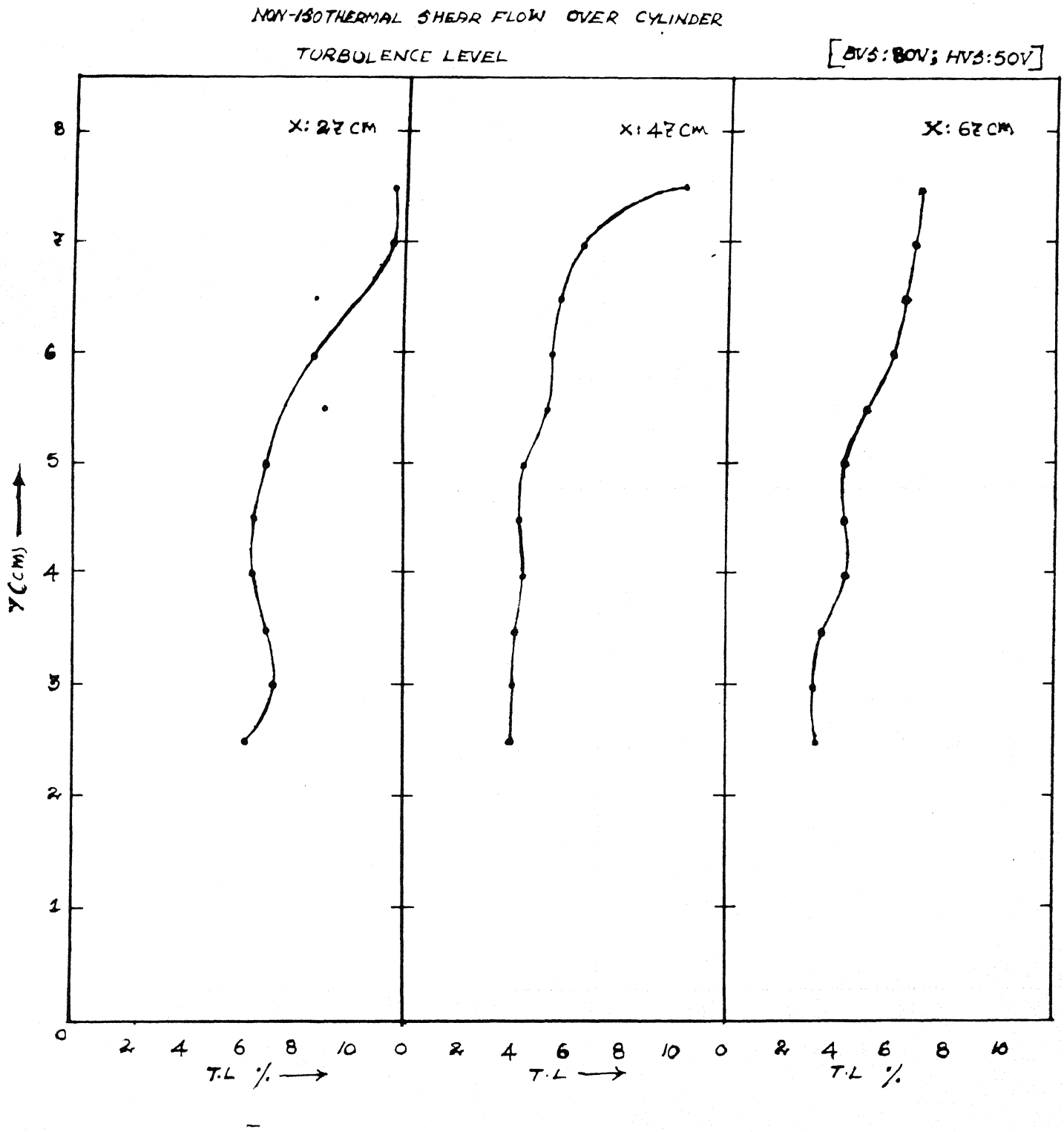

FIG. 4.69 NON-ISOTHERMAL SHEAR FLOW PAST A CYLINDER

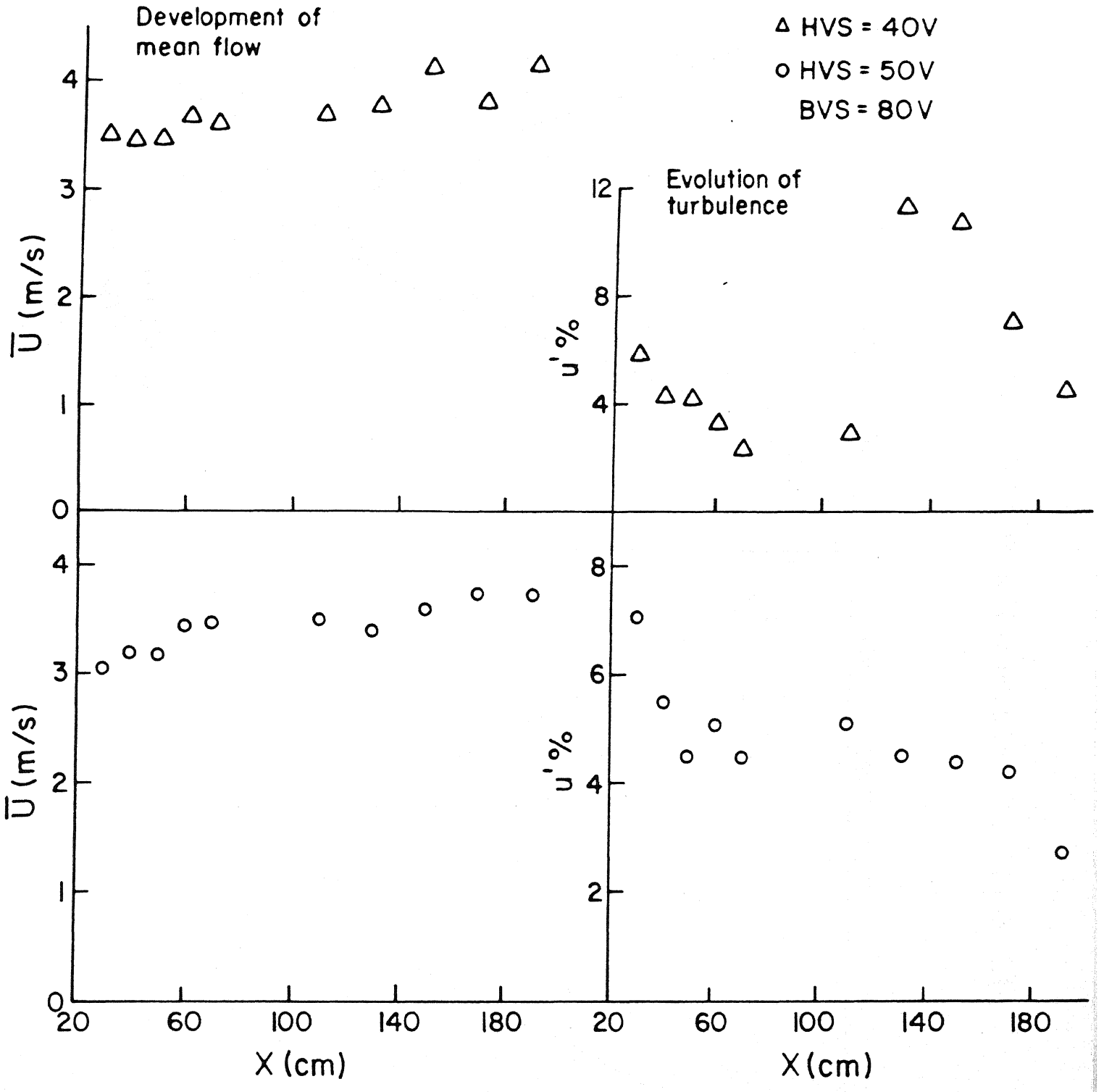

FIG. 4.70 NON-ISOTHERMAL SHEAR FLOW PAST A CYLINDER

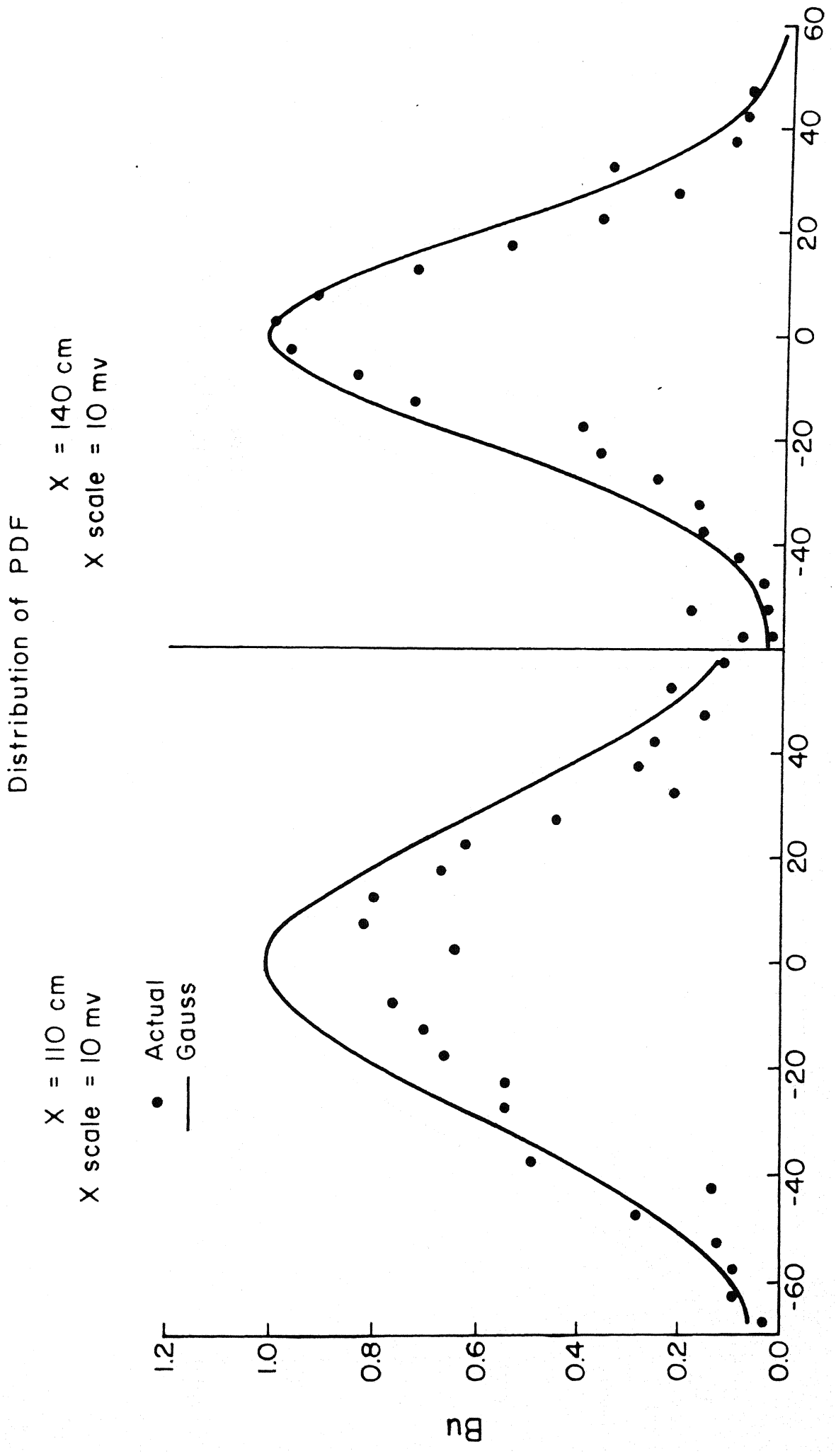

FIG. 4.71 ISOTHERMAL PARALLEL FLOW

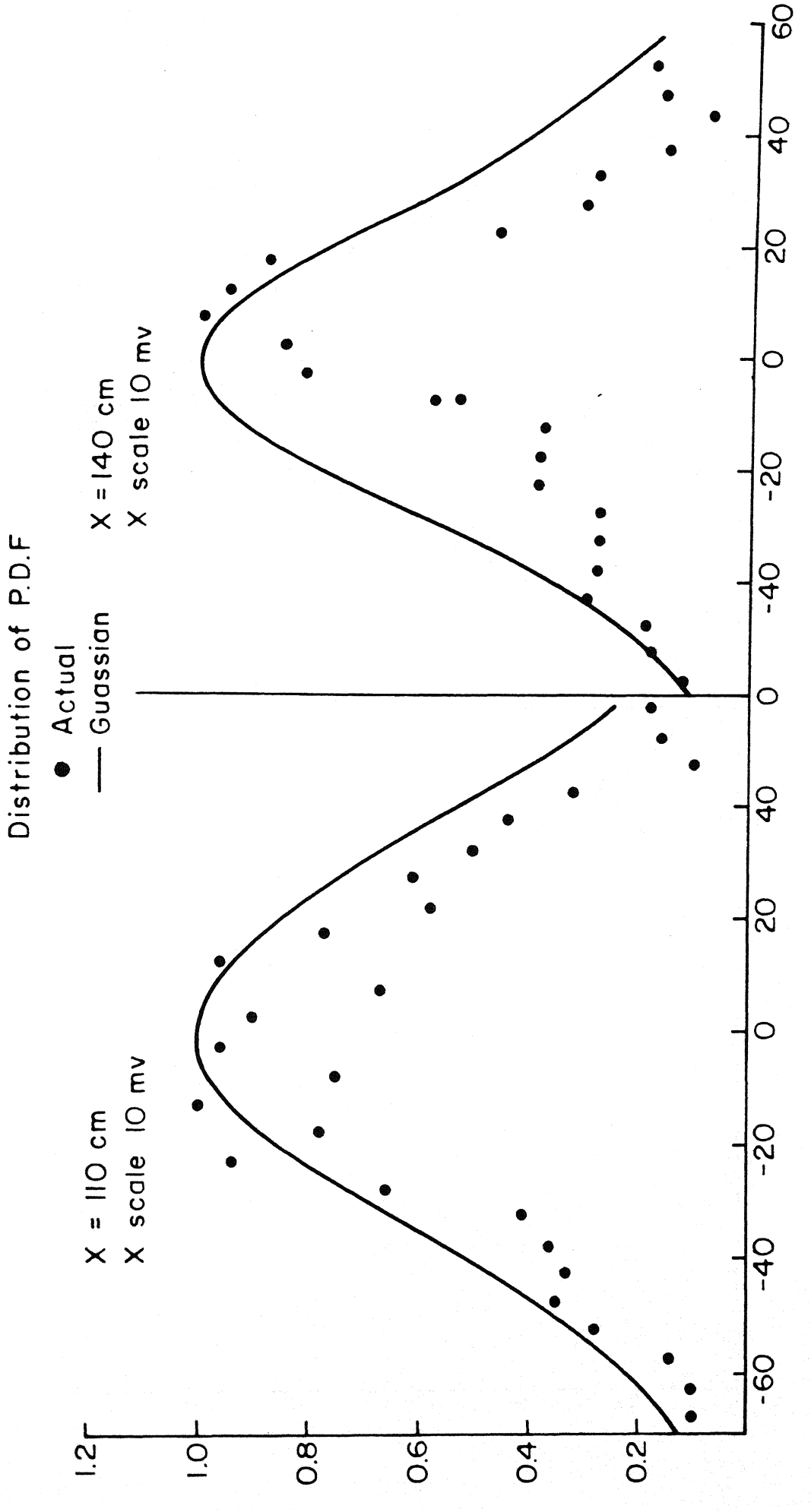

FIG. 4.72 ISOTHERMAL PARALLEL FLOW PAST A CYLINDER

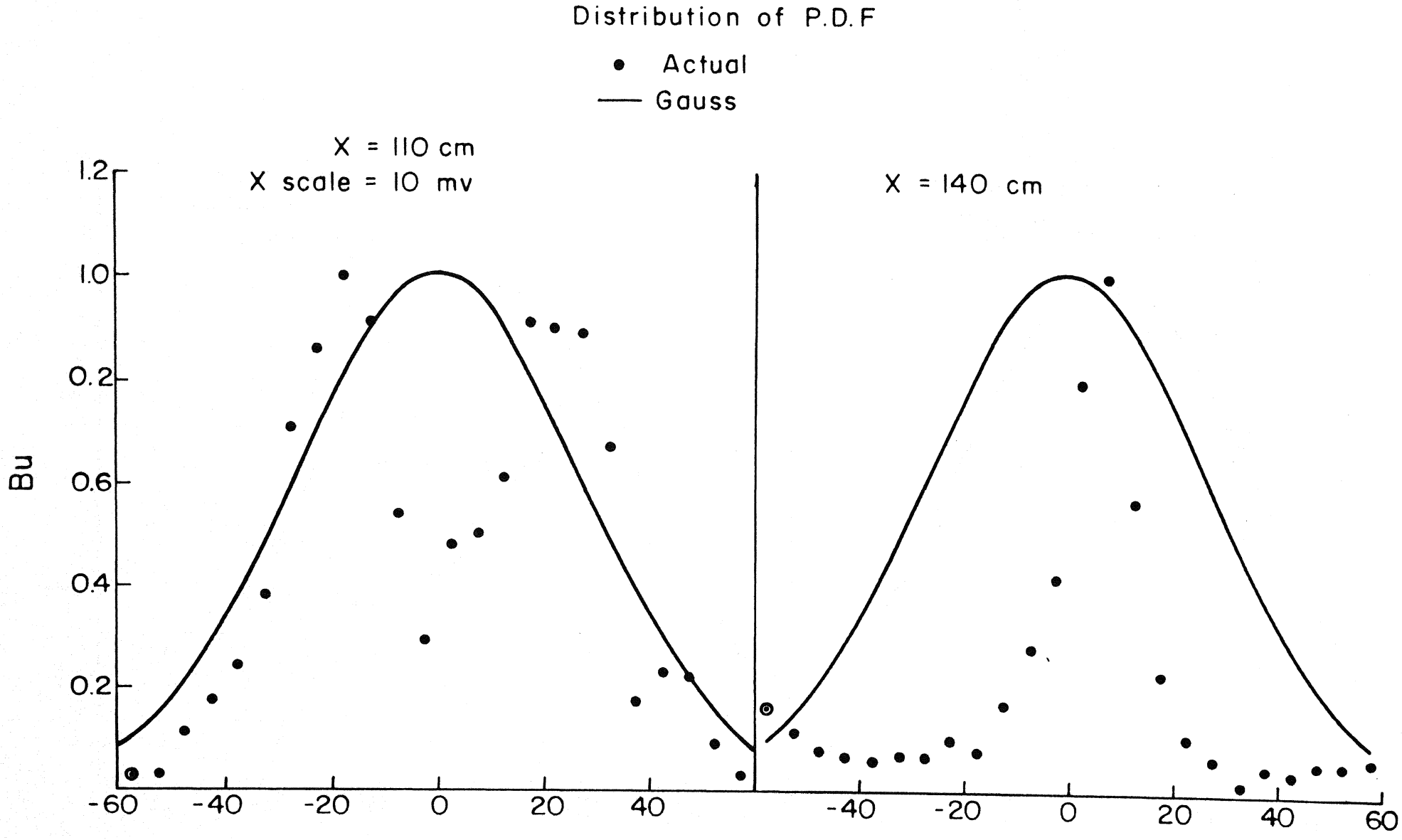

FIG. 4.73 ISOTHERMAL SHEAR FLOW

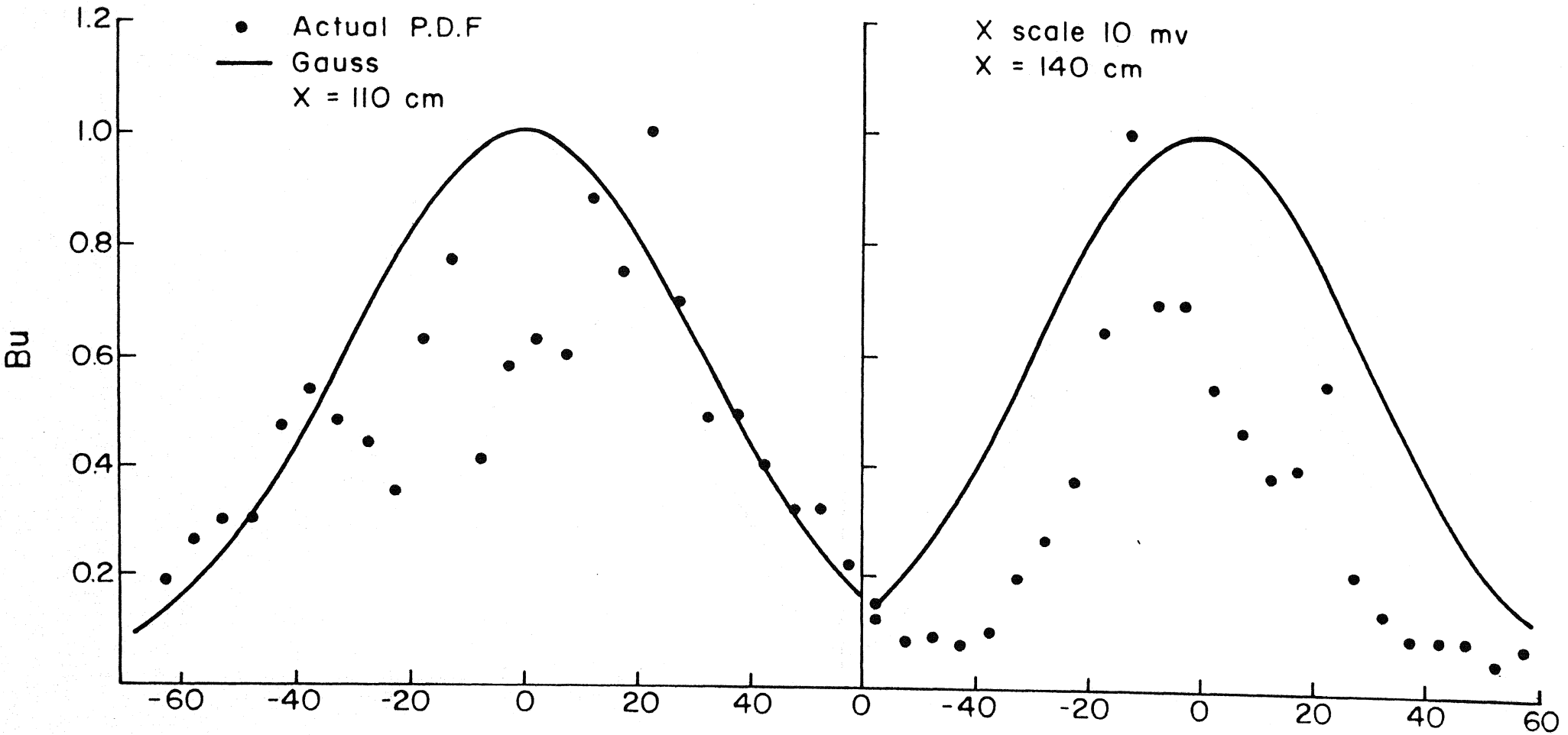

FIG. 4.74 ISOTHERMAL SHEAR FLOW PAST A CYLINDER

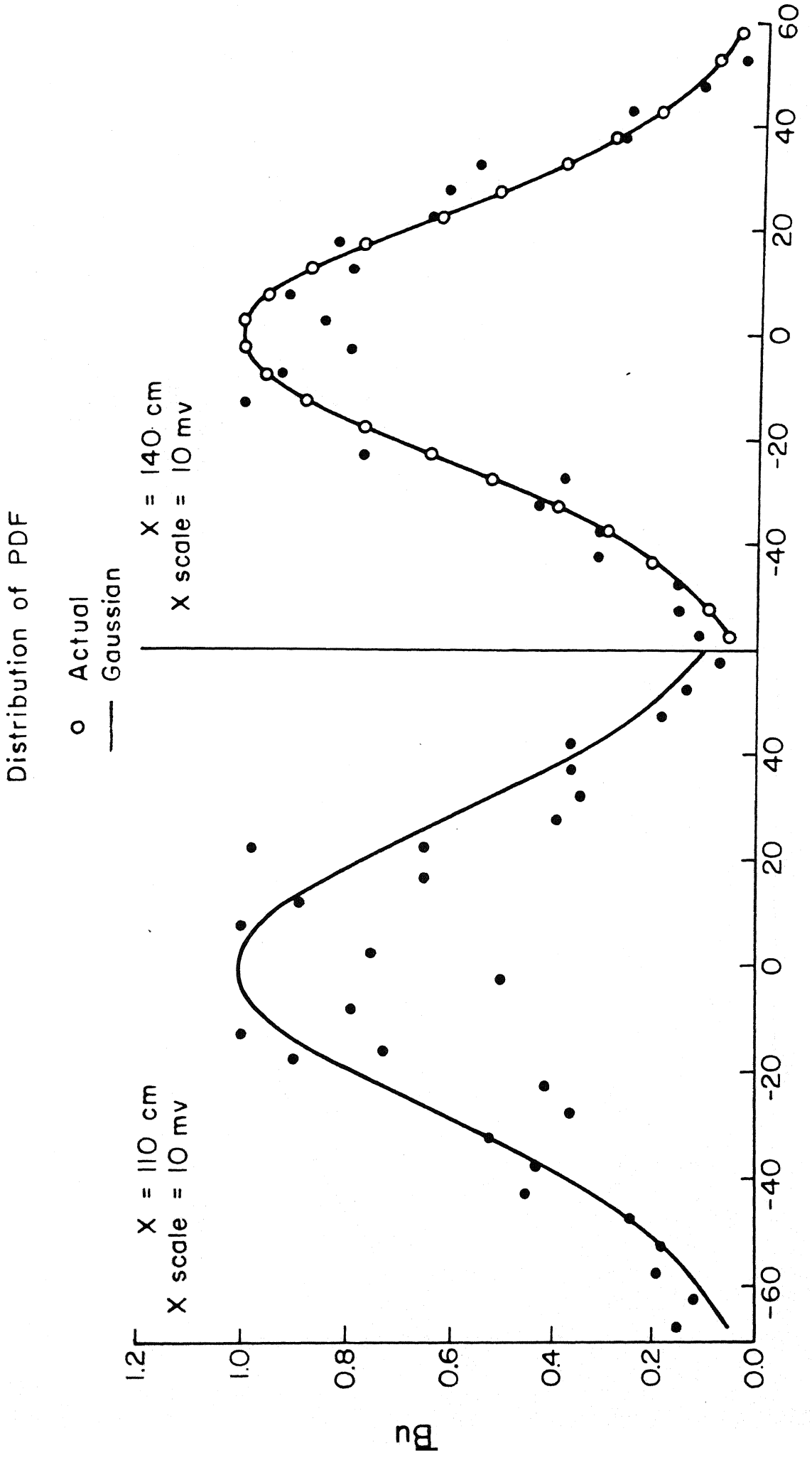

FIG. 4.75 NON-ISOTHERMAL PARALLEL FLOW

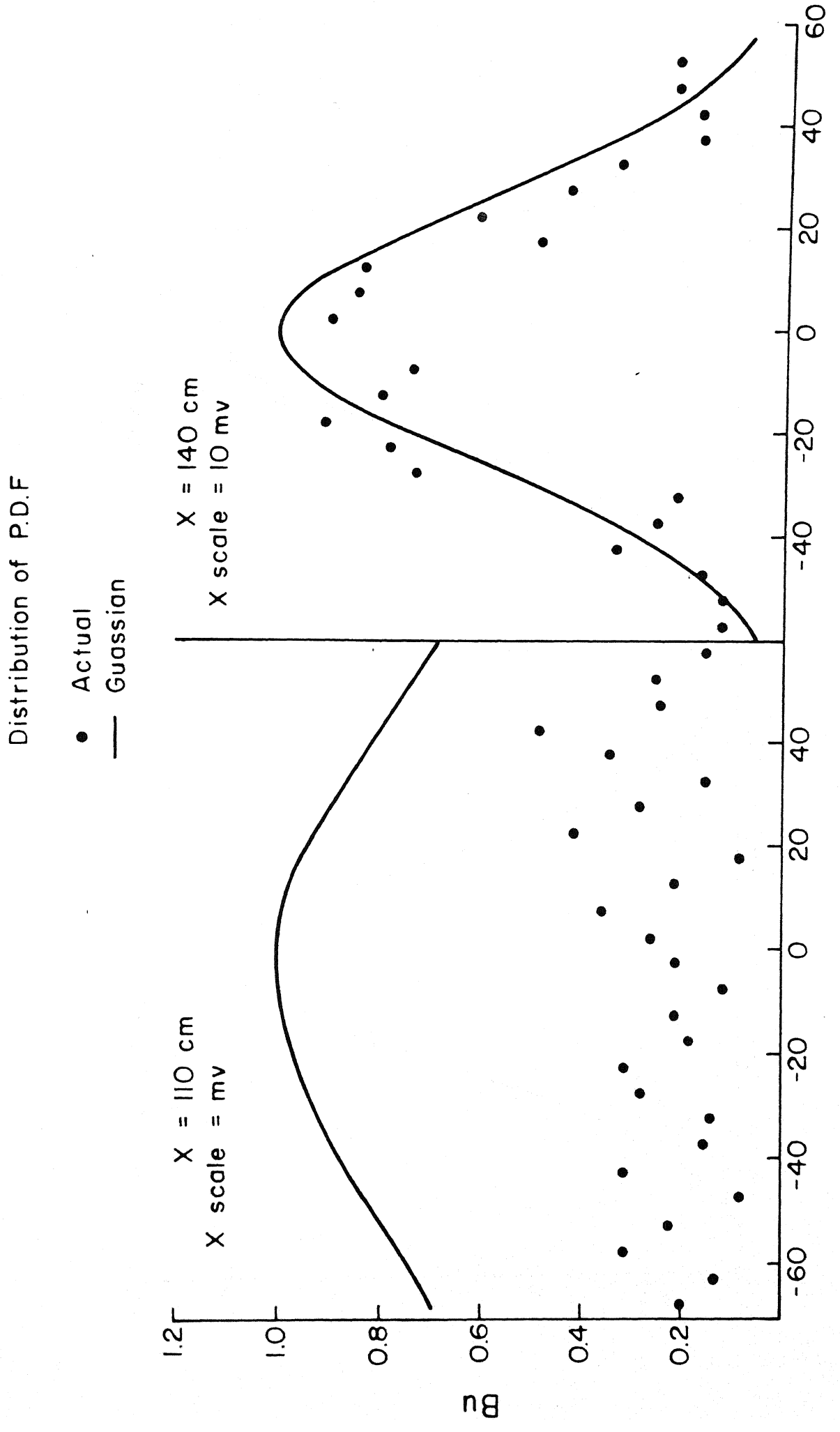

FIG. 4.76 NON-ISOTHERMAL PARALLEL FLOW PAST A CYLINDER

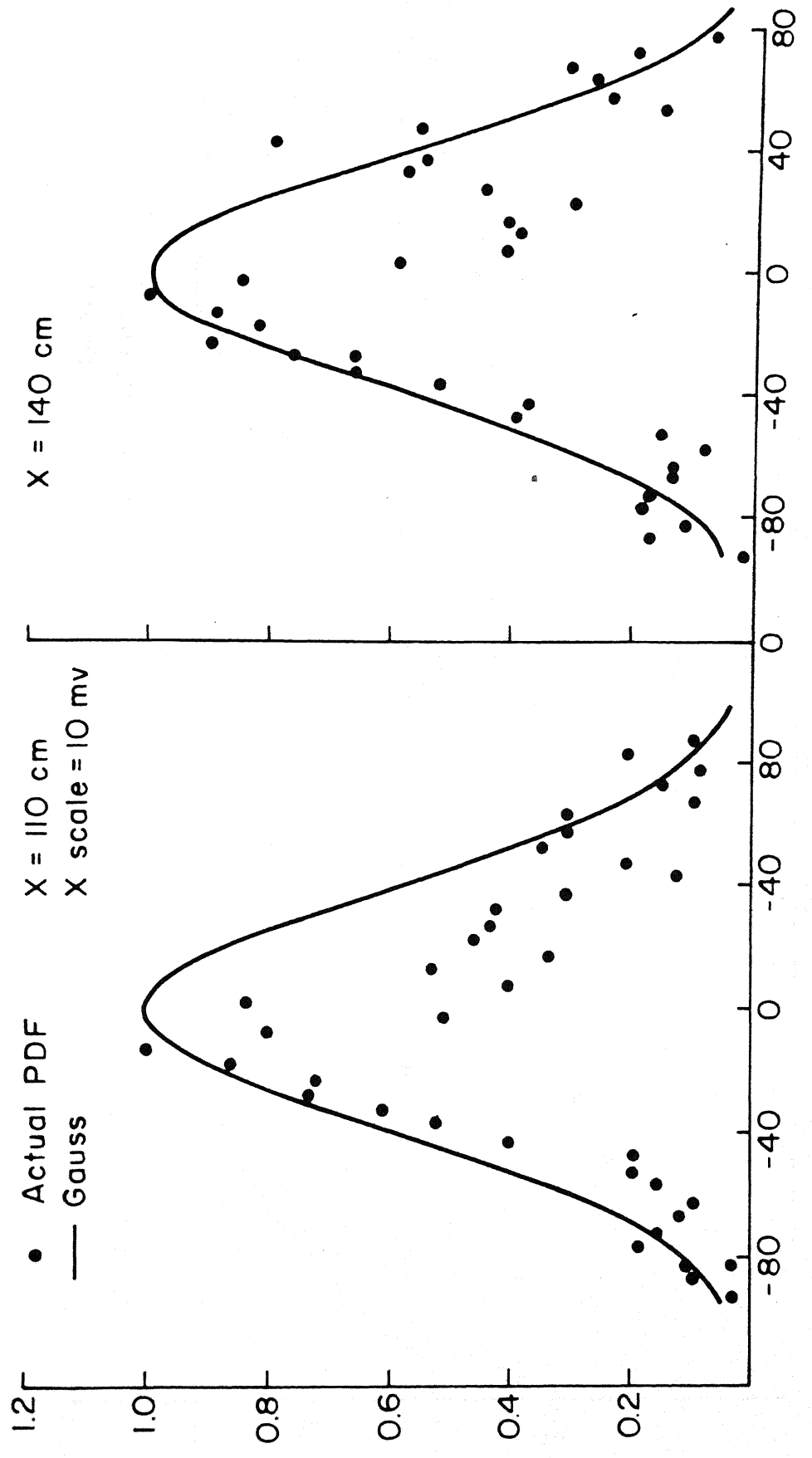

FIG 4.77 NON-ISOTHERMAL SHEAR FLOW

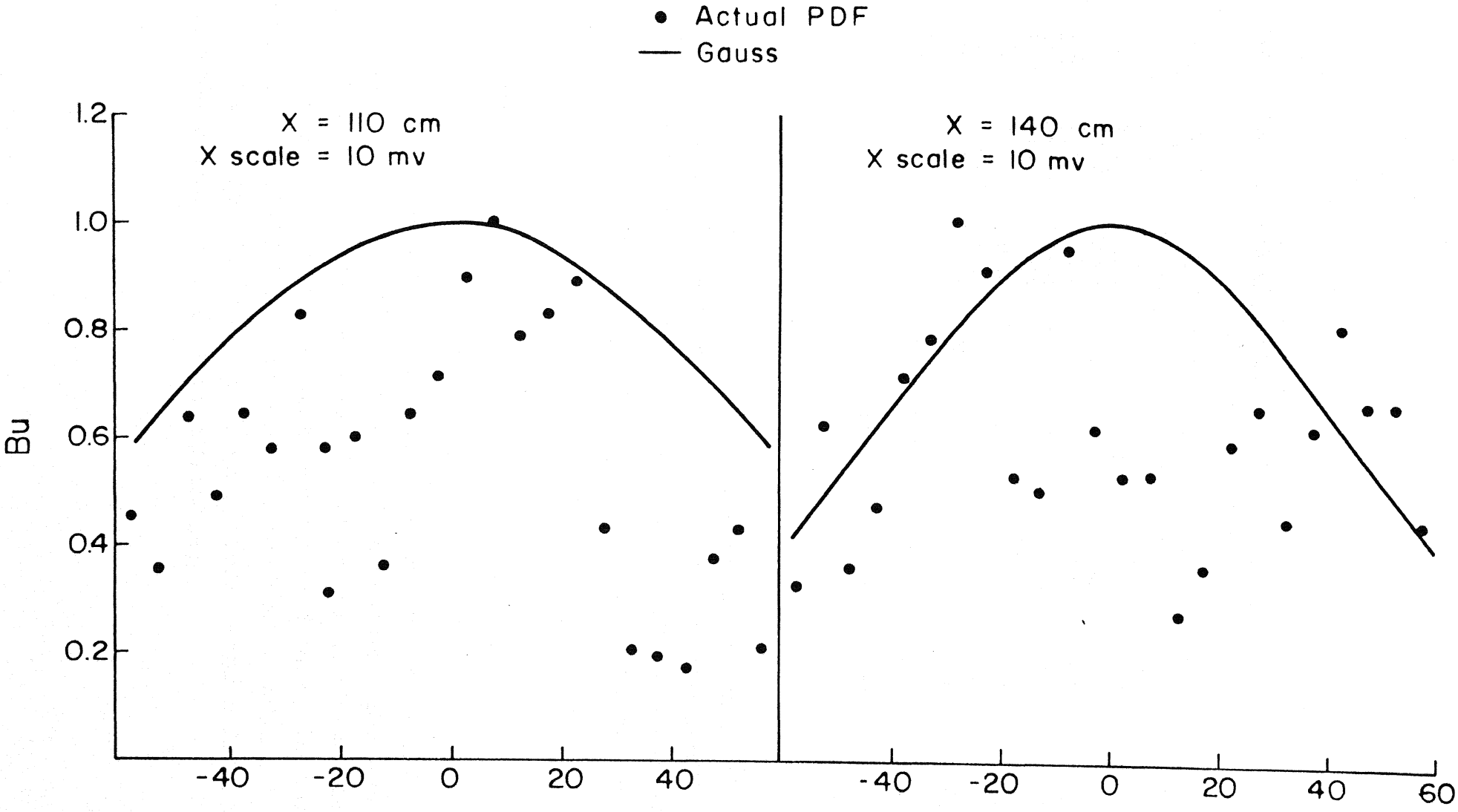

FIG. 4.78 NON-ISOTHERMAL SHEAR FLOW PAST A CYLINDER

Y(cm)	Temp(C)	Vel(m/s)	Fig.No. ($GM_2 = M_2$, $GM_3 = 0$)	M_2	M_3	M_4	GM_4
110	20.60	3.2047	4.73	8.815	4.083	11.27	10.91
140	20.70	3.4483		6.325	–4.715	8.55	7.81
110	20.80	2.8257	4.74	10.76	–3.999	14.69	13.87
140	20.40	3.0385		8.81	–6.52	11.76	10.86
110	30.62	2.5369	4.75	8.68	–6.48	11.04	10.76
140	30.32	2.4603		7.43	–2.39	10.01	9.03
110	29.64	2.3901	4.76	24.52	–15.35	28.34	22.98
140	30.00	2.3459		7.84	–2.39	10.01	9.62
110	20.50	3.0258	4.77	4.23	3.76	5.59	5.56
140	20.80	2.9925		8.40	–6.16	11.83	10.53
110	20.30	2.6924	4.78	9.67	–4.57	11.67	10.56
140	20.30	2.7720	9.20	9.20	7.45	12.00	11.50
110	29.15	2.5444	4.79	11.82	4.27	15.10	14.01
140	30.03	2.6046		11.62	–6.60	14.62	13.50
110	28.20	2.3945	4.80	17.53	–9.10	22.30	20.11
140	29.70	2.5253		13.64	5.96	16.40	15.46

Figures 4.81–4.87 show variation of autocorrelation with increasing time lag. The profiles are calculated for the acquired signals at two different downstream locations to study evolution of turbulence. Typical oscilloscope traces in isothermal and non–isothermal shear flow, with and without a cylinder placed as a turbulence generator are shown in Figures 4.88 – 4.90.

4.4. Discussions

It has not been possible to maintain the constancy of externally imposed parameters such as the mean velocity gradient $\partial u/\partial y$ and the mean temperature gradient $\partial T/\partial y$ over the entire length of the test cell. Beyond a certain point it was observed that the flow became fully developed and hence invariant with distance. The temperature gradients also reduced with distance both due to internal mixing and cooling of the test cell by ambient air. Despite these drawbacks, the general results observed in the literature has been reproduced in our data as well. We note the following.

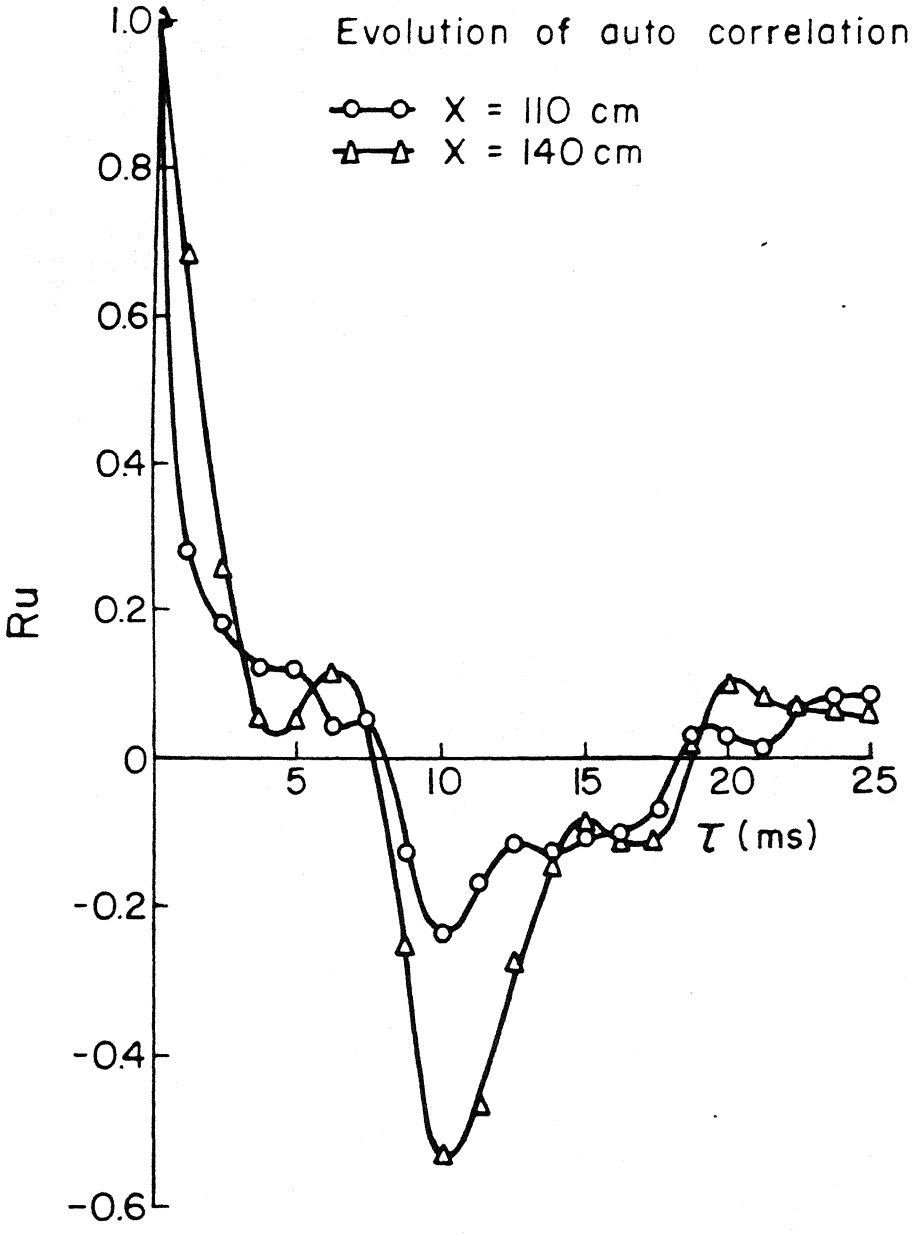

FIG. 4.79 ISOTHERMAL PARALLEL FLOW

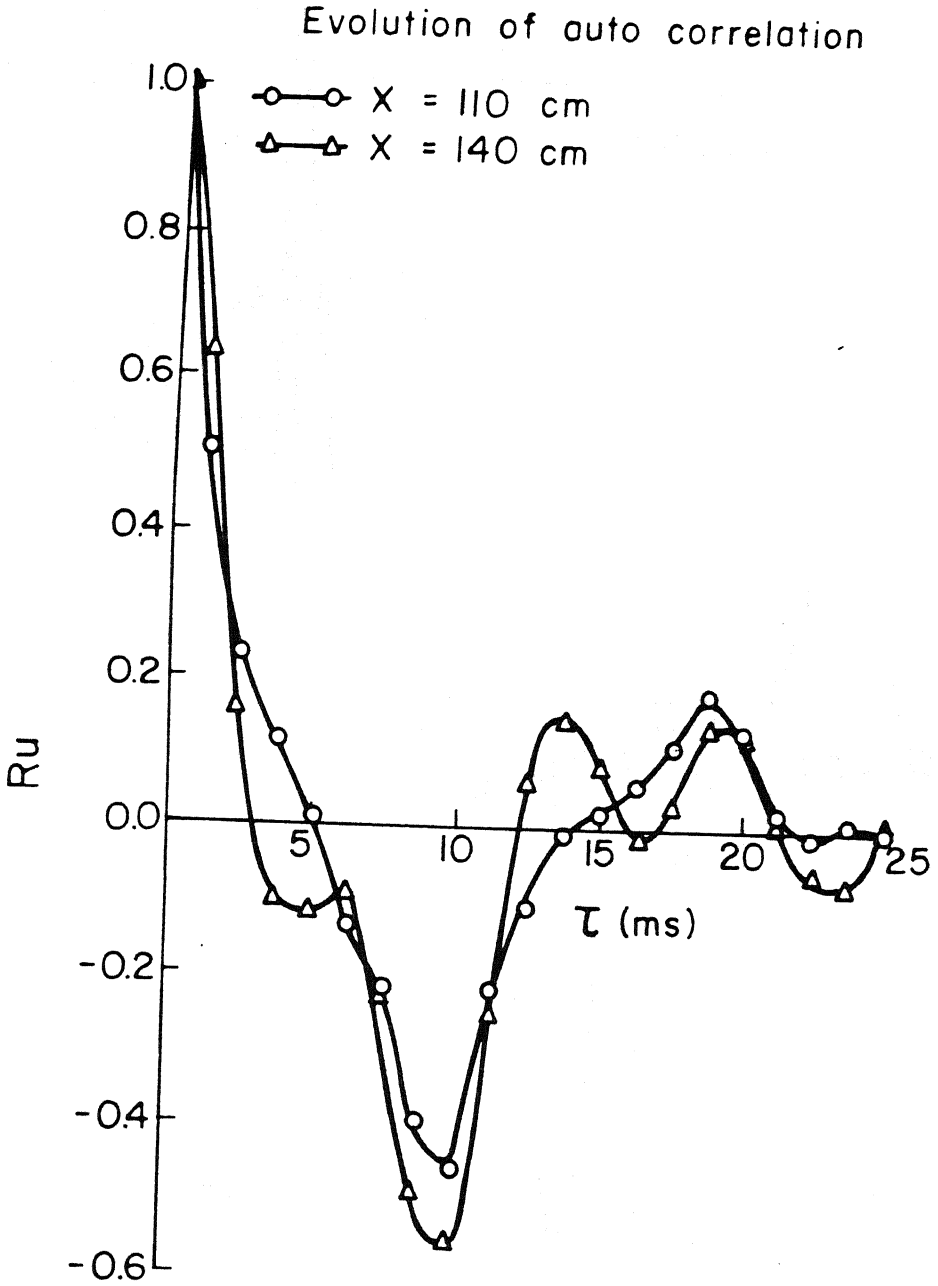

FIG. 4.80 ISOTHERMAL PARALLEL FLOW PAST A CYLINDER

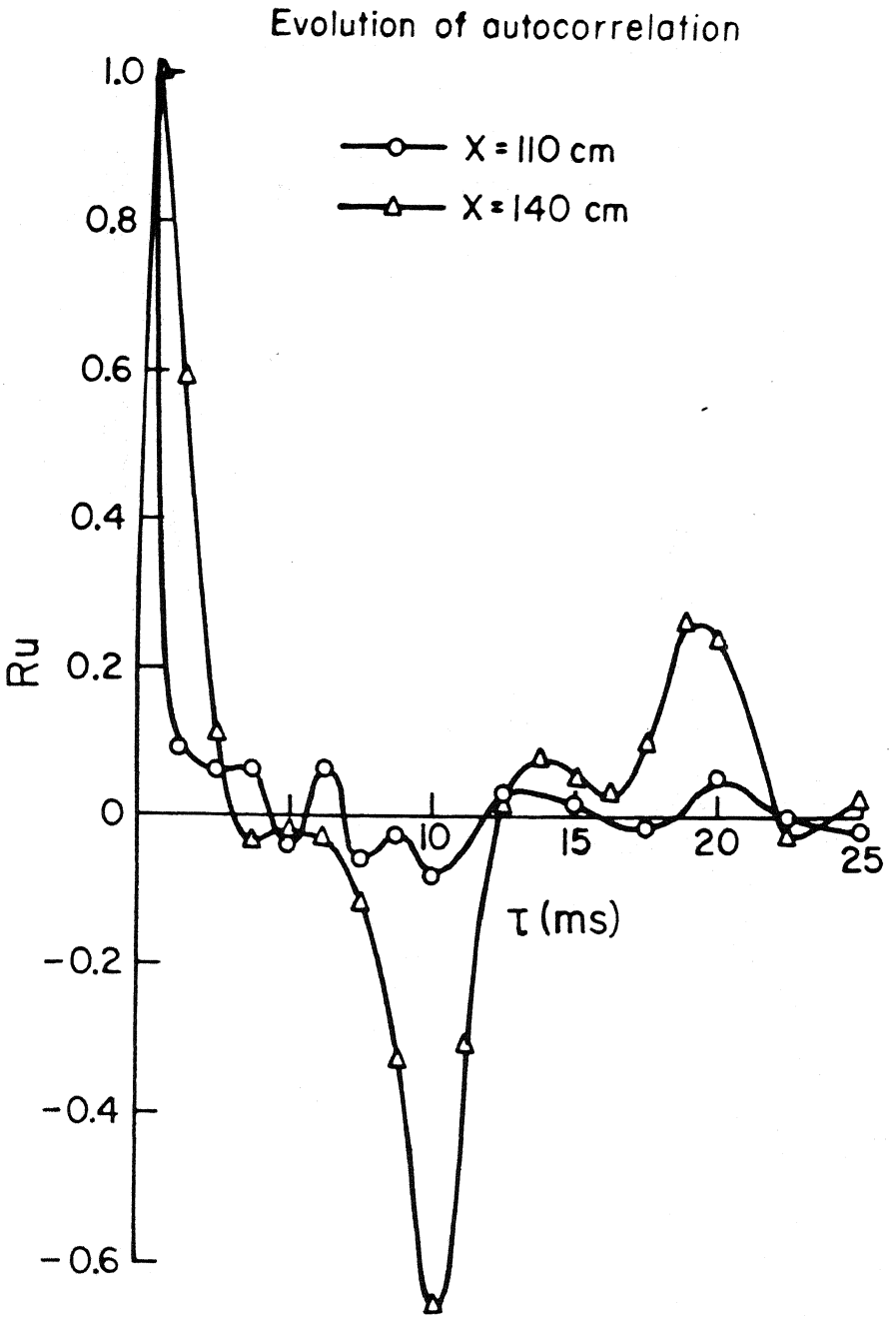

FIG. 4.81 ISOTHERMAL SHEAR FLOW

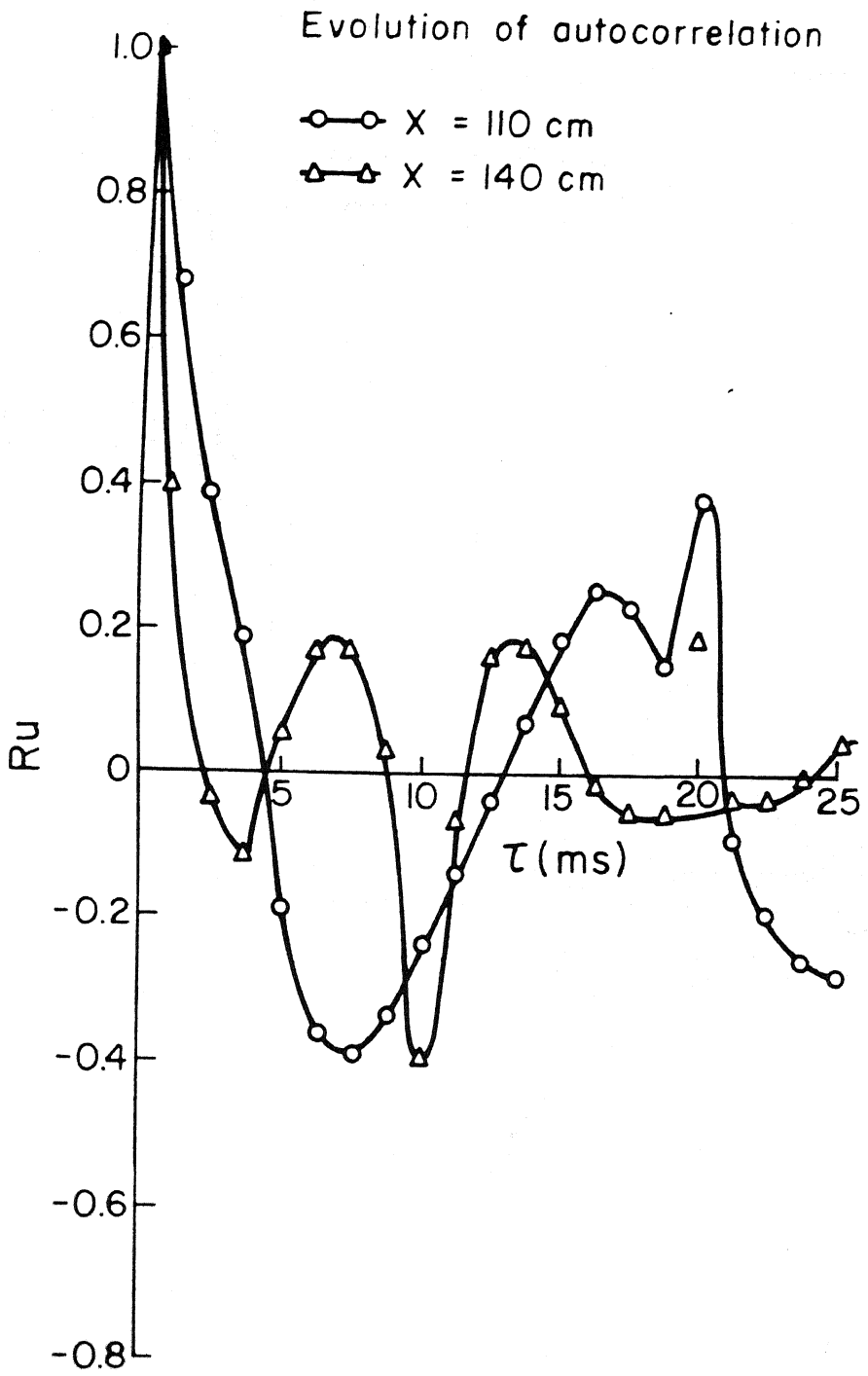

FIG. 4.82 ISOTHERMAL SHEAR FLOW PAST A CYLINDER

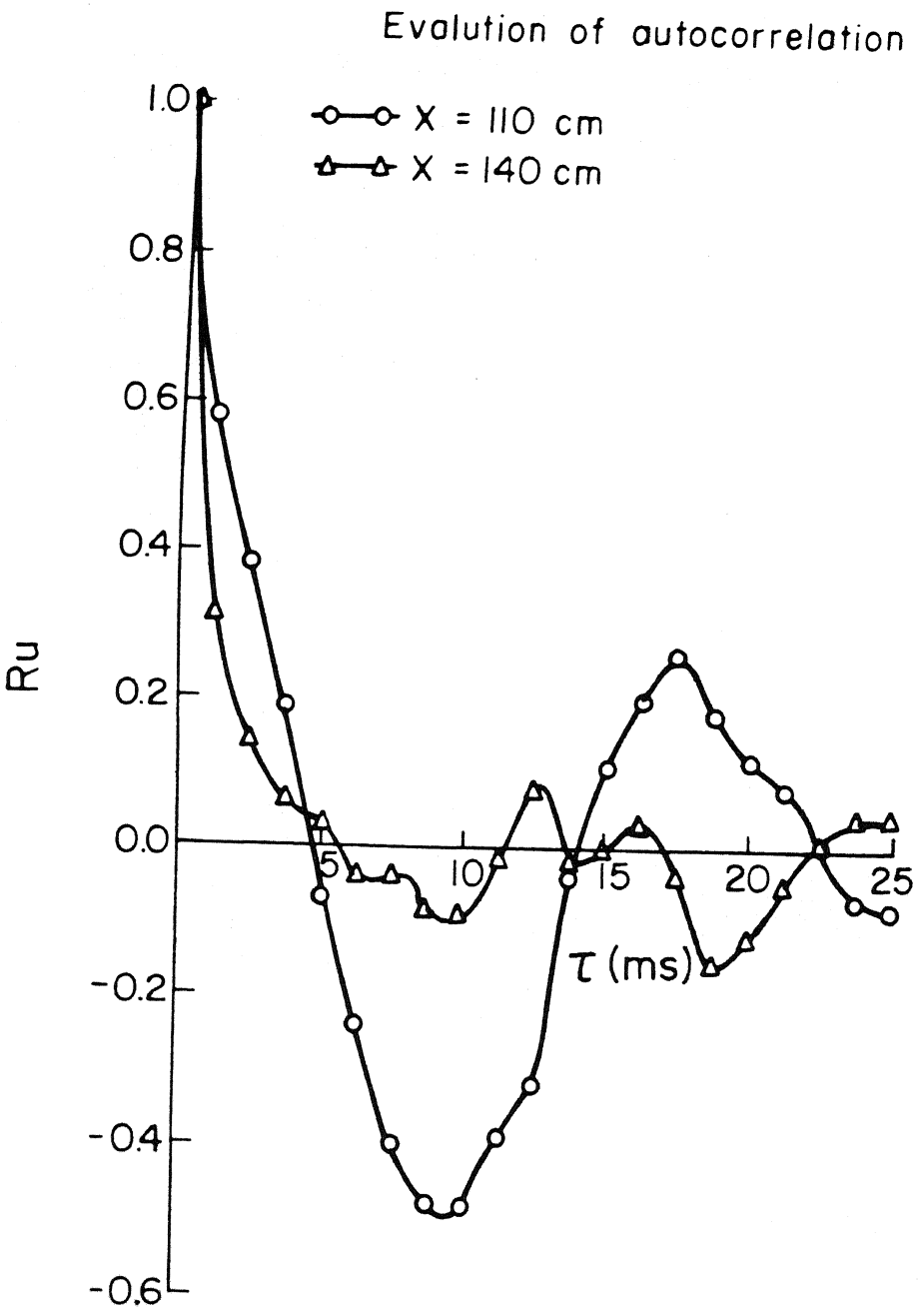

FIG. 4.83 NON-ISOTHERMAL PARALLEL FLOW

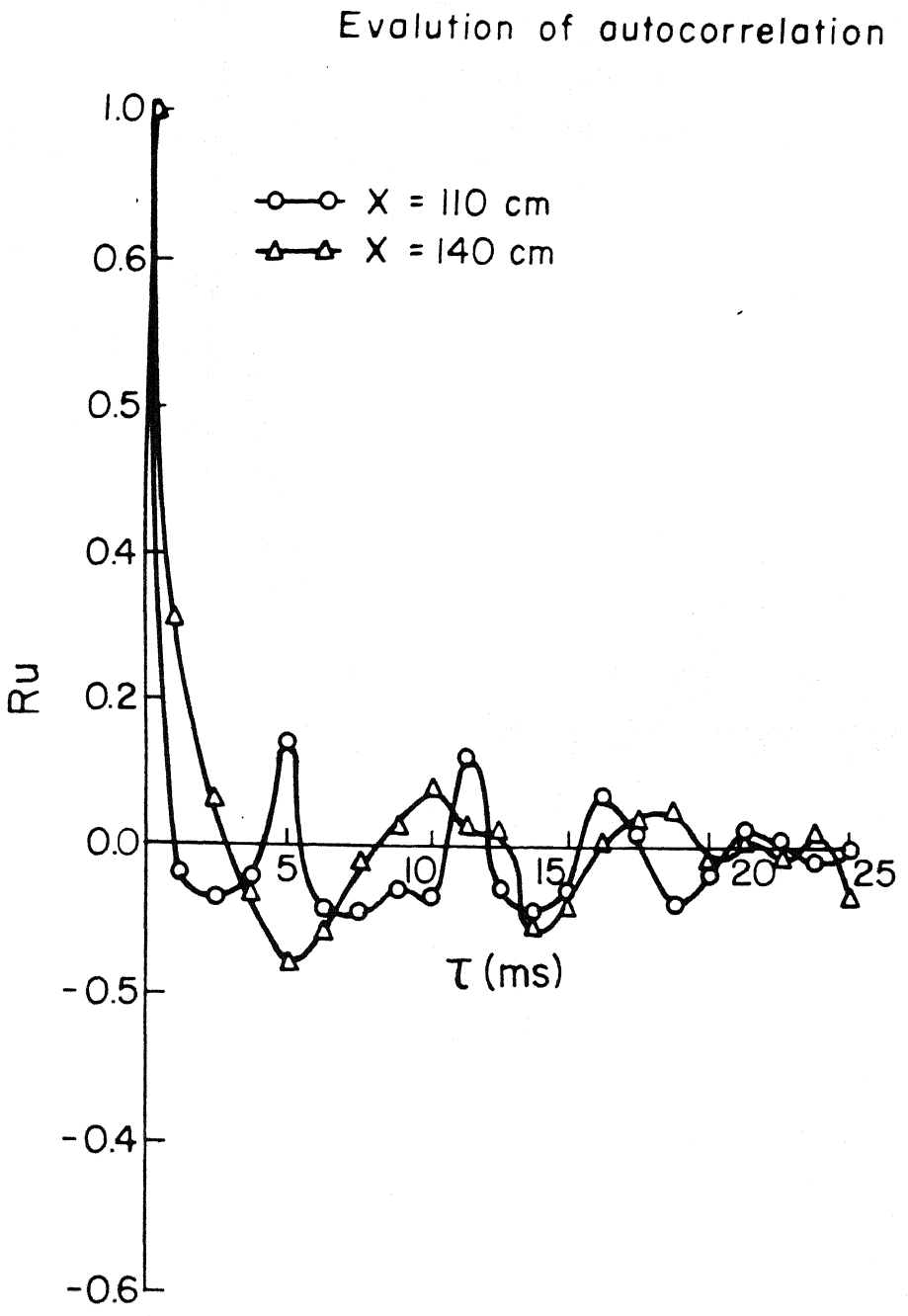

FIG. 4.84 NON-ISOTHERMAL PARALLEL FLOW PAST A CYLINDER

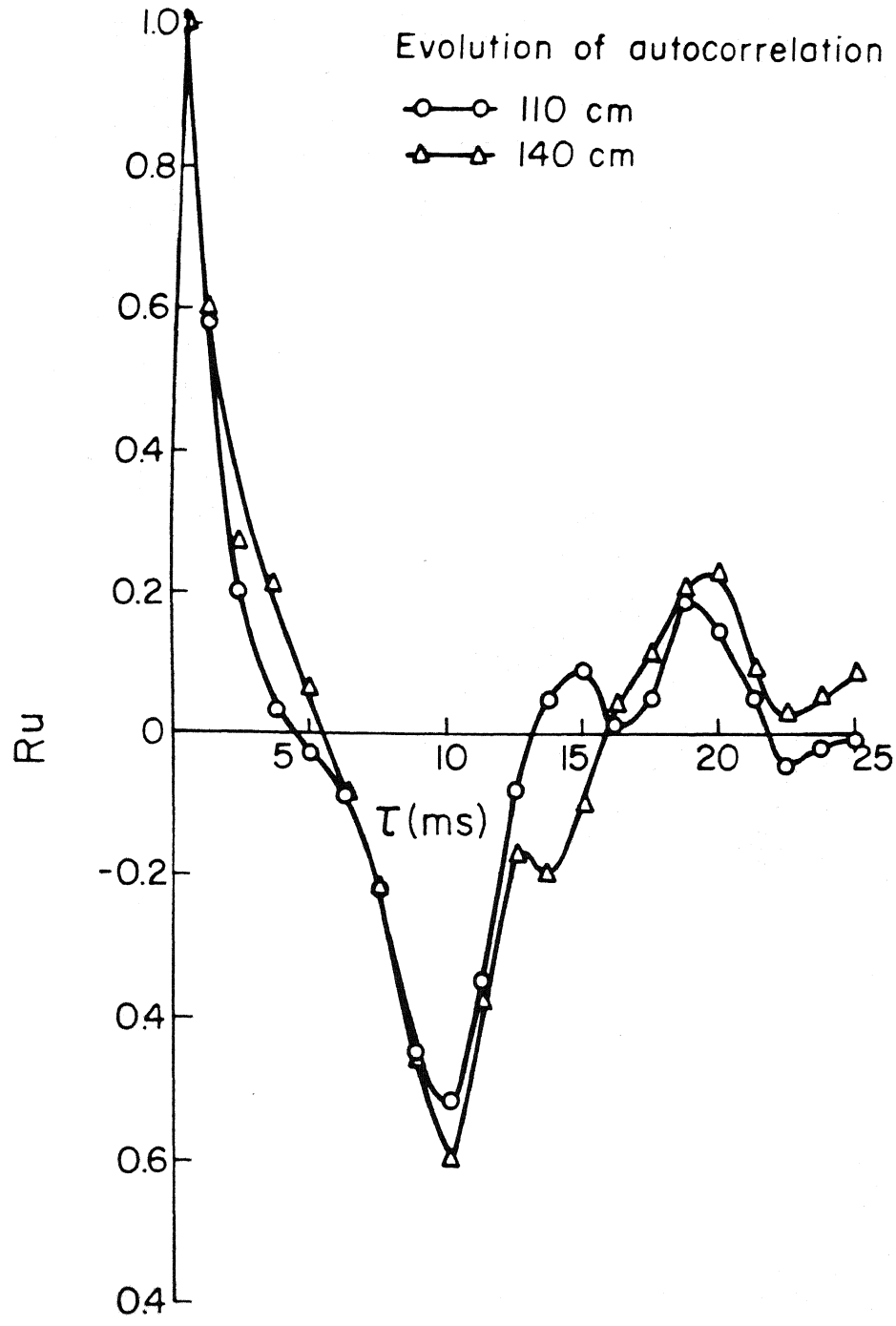

FIG 4.85 NON-ISOTHERMAL SHEAR FLOW

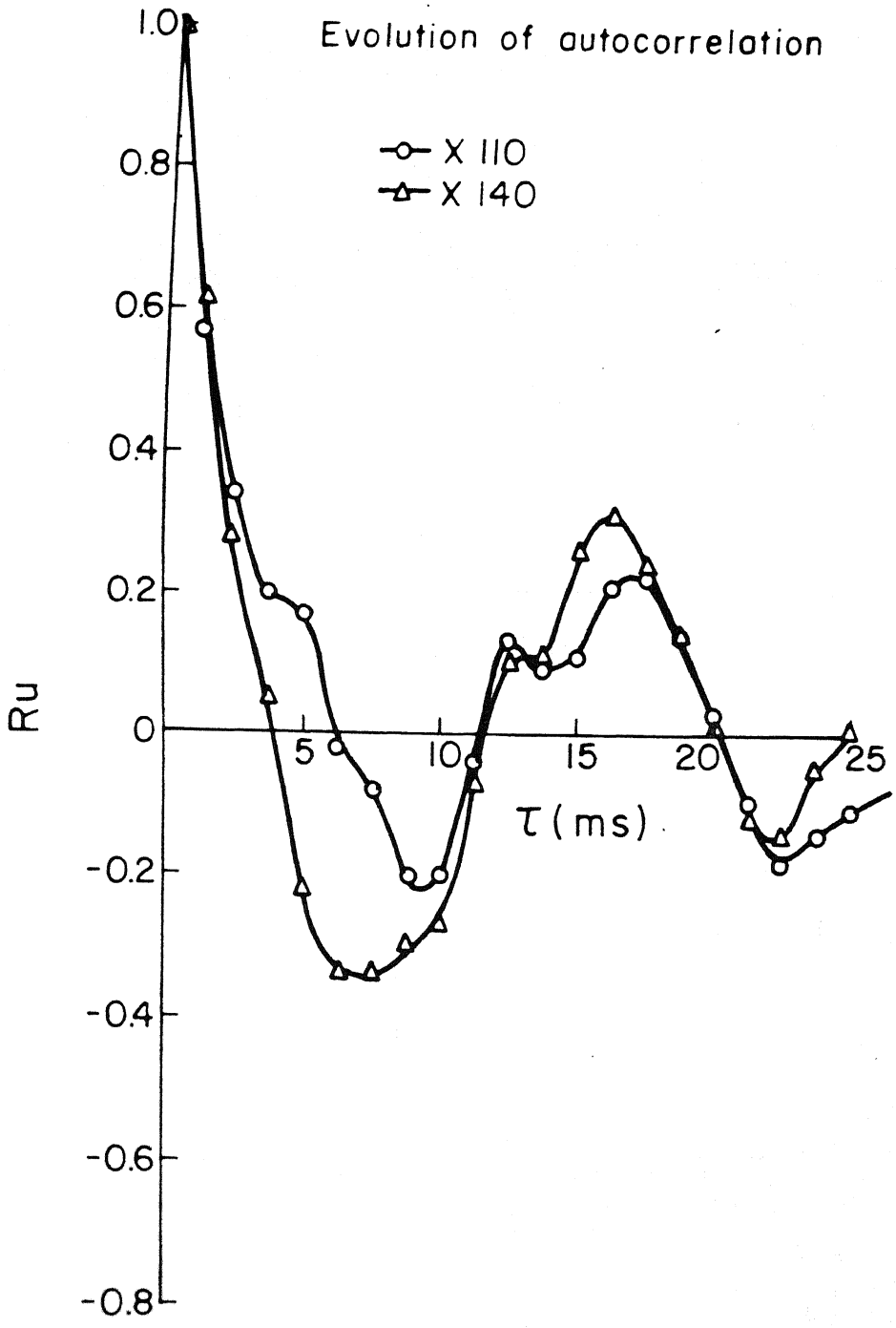

FIG. 4.86 NON-ISOTHERMAL SHEAR FLOW PAST A CYLINDER

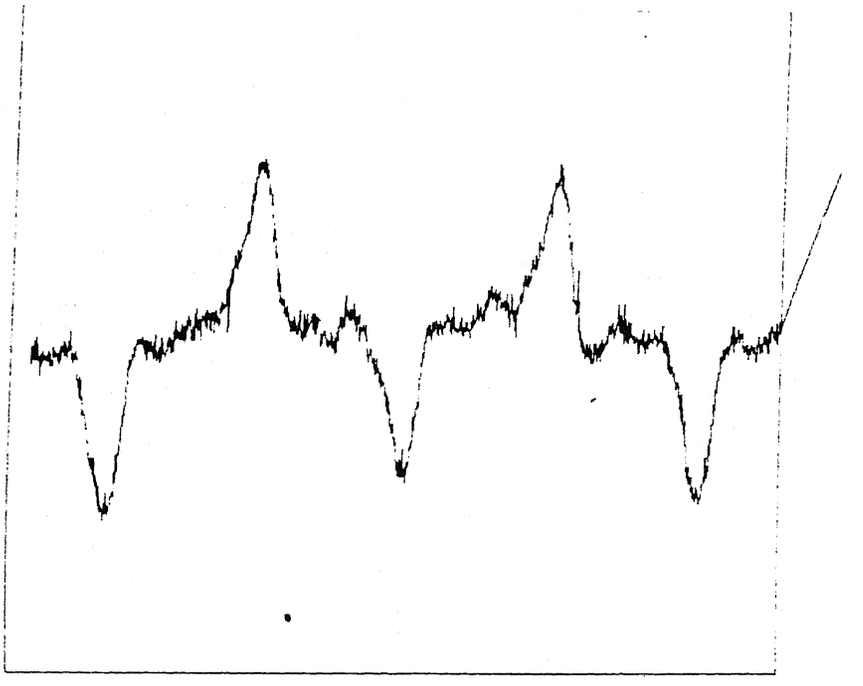

x = 110 cm

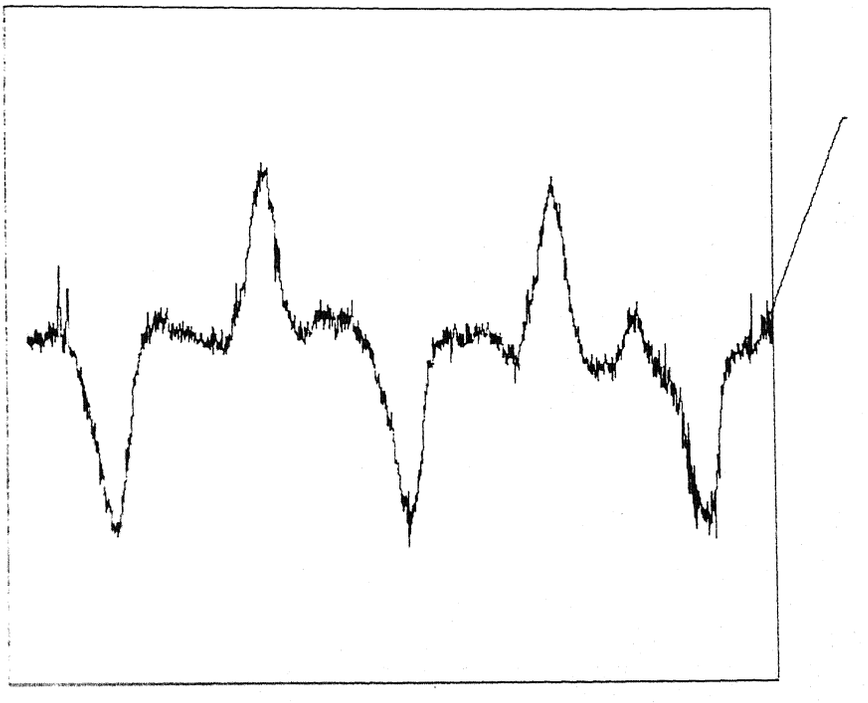

x = 140cm

FIG. 4.87 ISOTHERMAL SHEAR FLOW

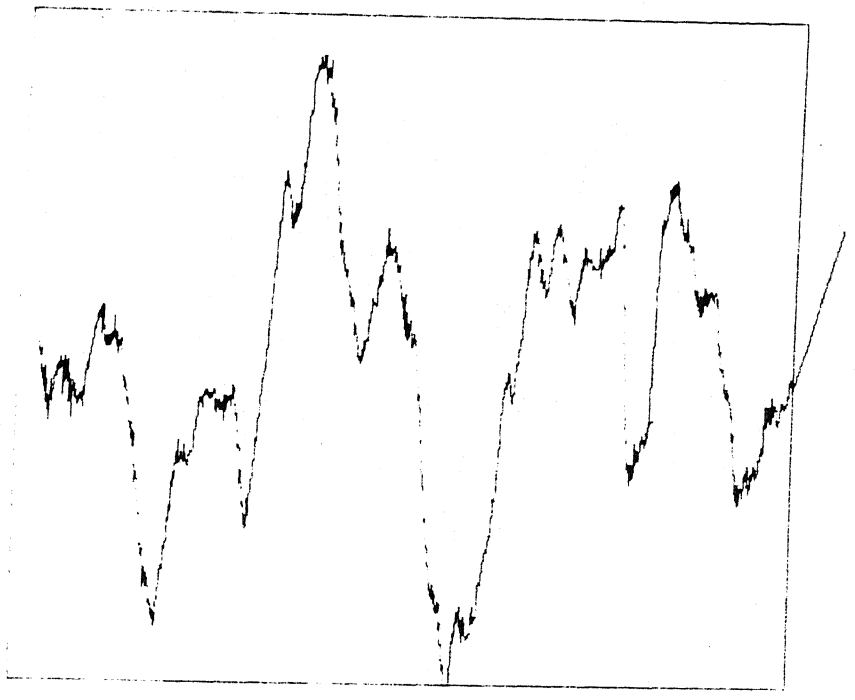

x = 110 cm

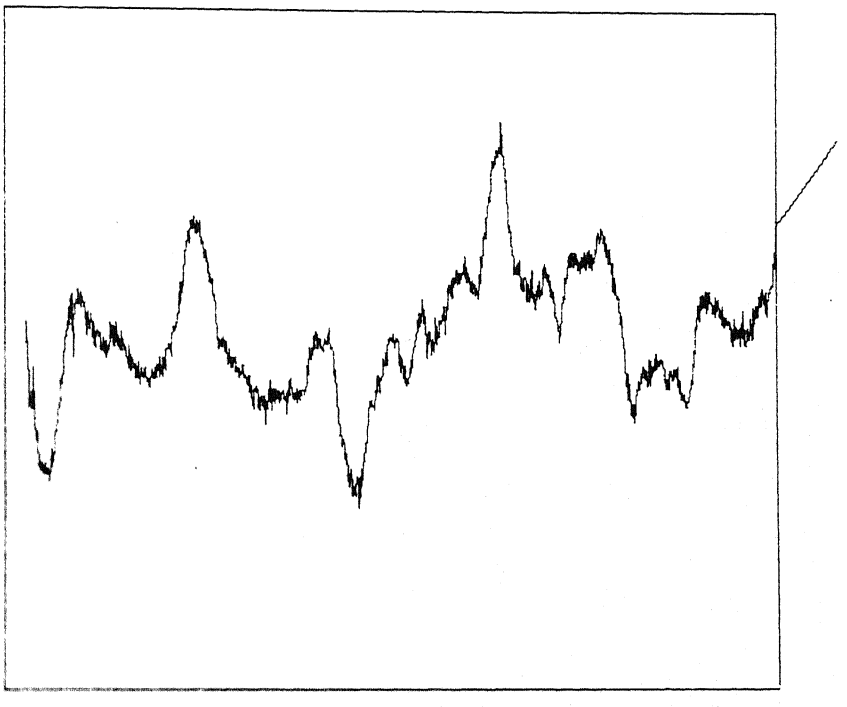

x = 140cm

FIG. 4.88 ISOTHERMAL SHEARL FLOW PAST A CYLINDER

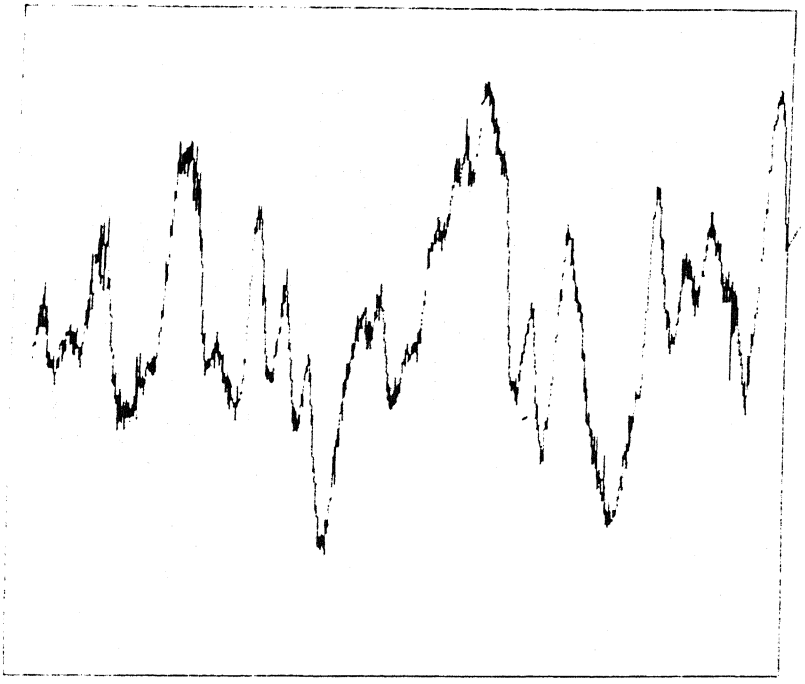

x = 110 cm

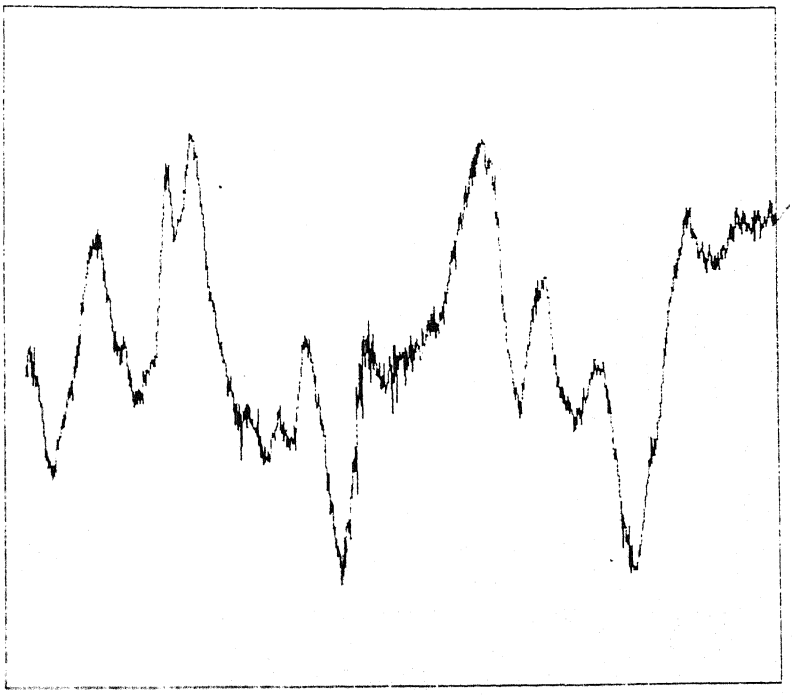

x = 140cm

FIG. 4.89 NON-ISOTHERMAL SHEAR FLOW

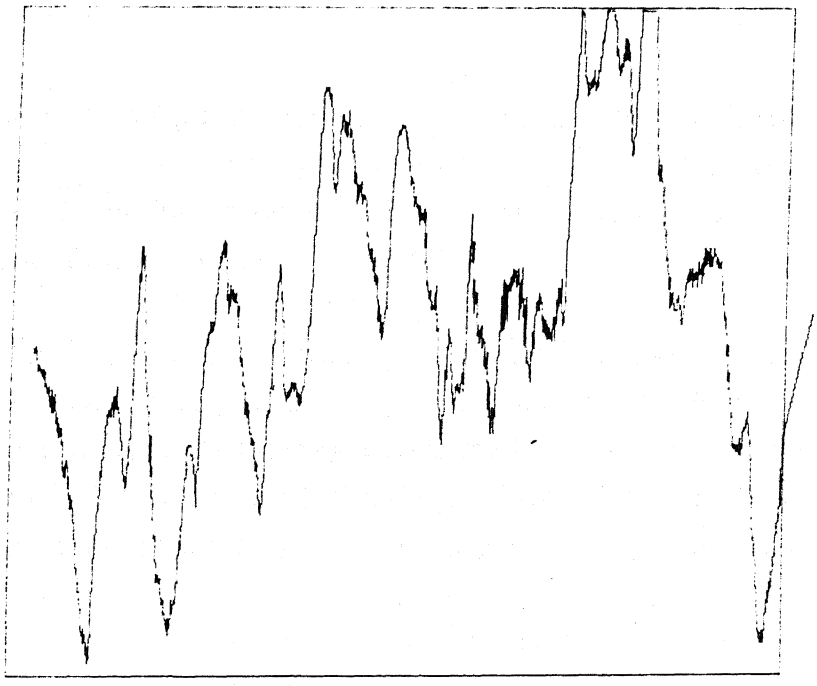

x = 110 cm

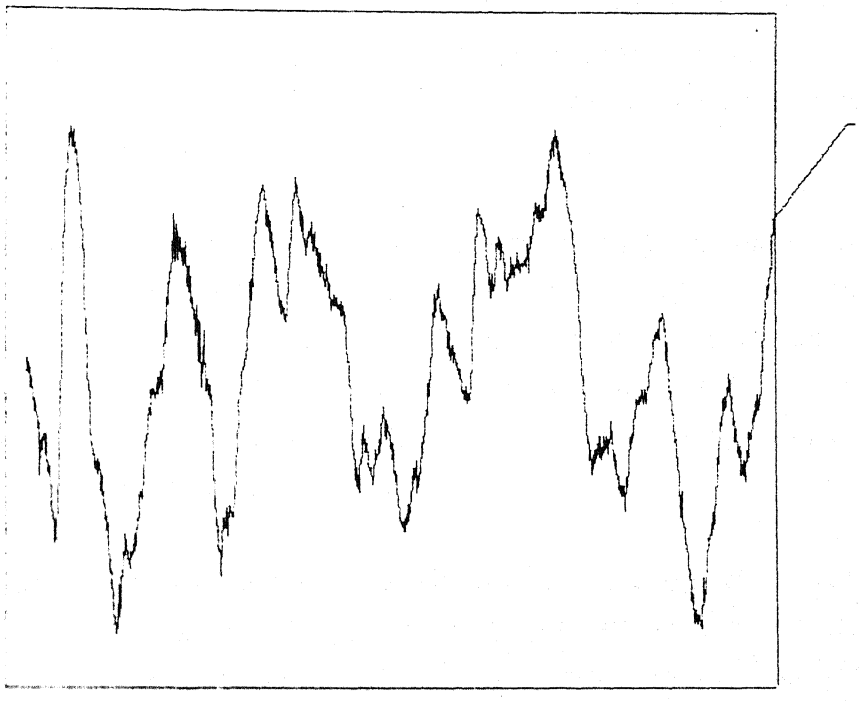

x = 140cm

FIG. 4.90 NON-ISOTHERMAL SHEAR FLOW PAST A CYLINDER

1.In isothermal mesh–related turbulence (generated behind a honeycomb but without a cylinder), a value of the shear parameter Sh > 4 does lead to growth of the percentage turbulence level. In the present work Sh is never less than 4, except in the case of flow behind a cylinder. (Figures 4.1, 4.3, 4.11 and 4.13.)

The velocity gradient is negative in the upper half of the test cell in the absence of the shearing (parabolic shaped) honeycomb, owing to the wall boundary–layers. The velocity gradient changes sign when the shearing honeycomb is placed in the tunnel. (Figures 4.11, 4.13, 4.50, 4.54 and 4.58.) Independent of the sign of the velocity gradient, we see a growth in turbulence level dictated primarily by the shear parameter. (Figure 4.5.)

2. In non–isothermal flow, a stably stratified system does lead to a drop in turbulence level in the mean flow direction. However Miles theorem (Ri < 0.25 for laminarization) has not been verified in this study. This is due to the variation in the Richardson number along the x – direction. The approach to laminarization in parallel flow is reported in the literature to be via the formation of laminar waves characterized by the Brunt – Vaisala frequency. In the present work, the formation of wall boundary–layers and the increase in their thickness downstream continues to keep the shear parameter large. Hence fine–grained turbulence (the high–frequency end of the power spectrum) continues to be active even after the rms turbulence level has fallen in magnitude. See the oscilloscope traces (figures 4.12, 4.14, 4.13 and 4.15) can be seen in this connection.

Besides the presence of mean shear, locally formed unstable regions affect the overall decay rates of the turbulence and its spectrum. In particular, the cooling of the top wall leads to a considerable growth in turbulence for a large value of y, even when fluctuations decay in the core of the cell. Future experiments must provide for special treatment of the top wall to prevent formation such unstable regions. Decay of turbulence in non–isothermal flow is seen in figures 4.27 and 4.34.

The shear parameter due to wall boundary – layers alone is larger than that due to the honeycomb, and the two values are opposite in sign as stated earlier. Though turbulence level increases in isothermal flow in each case, the two problems are considerably different in non–isothermal flow. In the latter problem, the value of Ri which is propotional to $1/(\partial u/\partial y)^2$ is considerably smaller in boundary–layer dominated flow. Hence, in the present study, the honeycomb assists us in producing a high value of Ri. This explains the

continuous drop in percentage turbulence level in non–isothermal flow with a honeycomb. (Figures 4.52 and 4.59.) Without a honeycomb, the larger velocity gradient in flow leads to improved thermal mixing and in a fully mixed flow, turbulence starts to increase in the flow direction (figures 4.27 and 4.34) due to the action of the mean shear.

At very large heater voltage levels, mixed convection effects at the heater rods decrease the local velocity, increase the gradient and consequently reduce the Richardson number. Hence we have not been able to increase Ri by pure heating alone.

3. Flow with a Cylinder as an Obstacle:

(a) Isothermal Flow. The wake of a cylinder is a source of strongly anisotropic turbulence with u' far exceeding v'. It is a well–recorded (but empirical) observation that turbulence tends to return to isotropy unless anisotropy is sustained by external factors such as a wall. This is sometimes referred to as a " return–to–isotropy" hypothesis. The return to isotropy in the turbulent wake occurs by decay of the u' component. For parallel flow, the decay continues in the presence of an overall velocity gradient as well for several cylinder diameters (x = 1.1m, x/d = 110) in the flow direction. Once isotropy is reached, the mean shear raises turbulence levels in the flow. It is expected that the growth of the two velocity fluctuations u' and v' occurs simultaneously. (Figure 4.10.)

(b) Non–isothermal Flow. We study only stably stratified systems in this work. Hence effect of the flow being non–isothermal is to support the natural trend of turbulence decay in the wake of a cylinder. In the absence of the parabolic honeycomb, shear arises primarily from the wall boundary–layers. Simultaneously, the wake promotes thermal mixing in the core of the test cell and the combined result of these two factors is to reduce Richardson number. Despite this, we see no increase in turbulence level over the distance studied in this work. (Figures 4.27, 4.34, 4.52 and 4.59.)

The effect of increasing the heater variac setting are, 1. increase in initial temperature levels, 2. larger thermal losses to the ambient. 3. decrease in local velocity of the high temperature fluid and hence decrease in the Richardson number. Hence an increase in HVS does not automatically stabilize flow. The decay patterns of turbulence in Figures 4.27 and 4.34 are practically, close to each other except in the initial value u'.

With the shearing honeycomb in place, the velocity gradients are mild and mixing among various layers is reduced. Hence the temperature gradients are larger than in the case with no honeycomb. However, the larger temperature levels are also associated with smaller velocities and hence a larger velocity gradient. Hence the Richardson number for this problem doesn't follow a definite trend. As seen in figures 4.27, 4.34, 4.52 and 4.59, the local turbulence level shows an initial period decay followed by momentary growth of sharp drop as dictated by the magnitude of Ri.

4. As a comparison between cases with and without the parabolic honeycomb, the following is to be noted.

i) The presence of a honeycomb, reduces thermal mixing and hence increases temperature gradients. In confined flows, it reduces mean shear as well, through this factor cab be adjusted by suitably designing the honeycomb itself. These factors would suggest a resultant large Richardson number and hence a considerable stabilizing influence on flow.

ii) The increase in local temperature increases pressure drop due to mixed convection effects at the heater rods, the local velocity decreases substantially and as a consequence the increase in shear reduces Ri

iii) Large temperature levels lead to increased thermal losses to the ambient. This again leads to a drop in Ri in the flow direction.

The combined effect of these factors will determine the growth or decay pattern of turbulence in a given problem.

5.Turbulence Statics. The probability density function (PDF) Bu of a stationary signal u(t) with zero mean is defined as the fraction of total time spent by this signal between the amplitude levels u and u+du, where du is called as a window for Bu. Typical values of du range from 2 to 5% of the total signal amplitude (umax–umin). In terms of Bu the nth order moment of the signal is defined as

$$\overline{u^n} = \left[\int_{-\infty}^{\infty} u^n \, Bu \, du \right]^{1/n}$$

This integral can be numerically evaluated say by Trapezoidal rule. The conventional interpretation of the PDF of a signal is obtained in comparison to the Gaussian PDF which is given by the formula

$$B_u = \frac{1}{\overline{u^2}\sqrt{2\pi}} e^{-\frac{u^2}{2\,\overline{u^2}}}$$

The Gaussian PDF represents a state of fully developed turbulence at equilibrium. Hence the extent of deviation from this distribution is a measure of the degree of under development or the presence of spatially correlated structures in the flow. In particular features such as a double peak or a peak away from zero represents the existence of large low frequency eddies produced by vortex shedding for example or due to energy transfer occurring from the mean flow to the velocity fluctuations. A fully noisy signal is characterized by a delta function kind of PDF centered at zero. Hence the flatness of the signal determines the extent to which the signal deviates from being purely noisy. The skewness and flatness of the instantaneous signal are measured by the third and fourth moments $M_3=u^3$ and $M_4=u^4$ respectively.

Two other quantities of interest are the power spectrum Eu(f) and the autocorrelation Ru(τ). The power spectrum is defined as the fraction of kinetic energy present in a frequency band–width f and f+df. The autocorrelation Ru is a measure of the extent of the signal with itself when separated by a finite lag time(τ). It is a measure of the degree of temporal coherence of the signal. For white noise Ru is unity for a zero time lag and Ru is zero for all other finite time lags. This is to say that his signal is entirely uncorrelated with itself when the time lag is greater than zero. In contrast to this a flatter distribution of Ru indicates the presence of low frequency (and hence large) eddies generated by an energetic interaction between mean flow and fluctuations. The integral value $\int_0^\infty$Ru dτ is a measure of a typical time scale in the flow.

In this work we determine Ru as follows.

Frequency Spectrum: U(f) = FT(Filtered u(t)),
Power Spectrum : Eu(f) $\cong$ U2(f)/U2(0),
Autocorrelation: Ru(τ)/Ru(0) = FT(Eu(f)).

A Tunkey–Hanning filter has been used in this work. FT stands for Fourier transform which is obtained from a fast Fourier transform (FFT) algorithm. A broadening of the Ru–τ curve, where t is the time lag represents a mechanism of energy transfer from the mean flow to the fluctuations. This is because the mean flow being associated with a large length scale for example the size of the test cell, correlates better with the low frequency components of turbulence. The occurrence of large negative values of Ru shows that the integral time scale $\int_0^{\infty}$Ru dτ is small. This suggests the formation of smaller eddies by the breakup of larger eddies and an approach towards equilibrium. Since small scale motion is associated with viscous dissipation of turbulence, large negative values of Ru will invariably be associated with turbulence decay or at the most a very gradual increase if the initial state is far removed from equilibrium.

In the present work, the following is observed with respect the probability density function. In isothermal flow, fluctuations are affected by shear due to wall boundary–layers and their PDF approaches a Gaussian distribution (Figure 4.71). In non–isothermal flow, the small eddies get damped in the presence of buoyancy and the remaining low frequency components (large eddies) cause the PDF to have double peaks (Figure 4.75). In isothermal shear flow, the honeycomb along with boundary–layers substantially reduces the average shear and the fluctuations approach a state of pure noise (Figure 4.73). In non–isothermal shear flow, the value of the Richardson number is large, the damping of pronounced double–peak structure. (Figure 4.77). Identical results are observed with the cylinder as well (Figures 4.72,4.74, 4.76 and 4.78) except that the initial distribution Bu itself has twin peaks due to the information of vortex shedding embedded within it.

The autocorrelation profiles (Ru vs τ) are quite consistent with the PDF graphs referred above. For example, in isothermal flow (without a cylinder) Ru develops a large negative values as it evolves downstream showing that the integral time reduces in the direction of flow. (Figure 4.79.) This again indicates a breaking up of eddies and an approach towards a Gaussian equilibrium. This is also seen is isothermal shear flow(Figure 4.81). In non–isothermal flow (Figures 4.83 and 4.85) the damping of the small scales leaves behind nearly periodic fluctuations. These in turn develop into a twin peak structure in the PDF distribution as discussed above. The autocorrelation doesn't develop a broad band profile near origin in any of the cases studied here. This supports the discussion given in this chapter that (1) stable stratification damps the small length scale (high frequency) eddies

making turbulent fluctuations close to sinusoidal and (2) in isothermal flow, shear leads to growth in turbulence at all length scales without in any way affecting the process of equilibration that breakup large eddies to smaller ones. These trends can be seen for flow past a cylinder as well (figures 4.80, 4.82, 4.84 and 4.86).

REFERENCES

Britter, R.E., Hunt, J.C.R, Marsh, G.L. and Snyder, W.H. 1983. "The effect of stable stratification on turbulent diffusion and decay of grid turbulence". J. Fluid Mechanics, 127, 27–44

Collis, D.C. and Williams, J.J. 1959. "Two–dimensional forced convection from cylinder at low Reynolds number". J. Fluid mechanics, 6. 357.

Dickey, T.D. and Mellor, G.L. 1980. " Decaying turbulence in neutral and stratified fluid ". J. Fluid mechanics. 99, 13–31.

Hinze, J.O. 1975. "Turbulence". Mc Graw–Hill Publishing Company, inc.

Hollasch, K. and Gebhart, B. 1972 "Calibration of constant–temperature hot–wire anemometers at low velocities in water with variable fluid temperature.

Koch, F.A. and Gartshor,I.S. 1972. "Temperature effects on hot–wire anemometer calibrations". Journal of physics E: Scientific Instruments, 5. 58–61.

Jones, W.P. and Launder, B.E. 1972. "The Prediction of Laminarization with a Two Equation Model of Turbulence". Int. J. Heat Mass Transfer. 15. 301–314.

Kolmogoroff, A.N. 1941. "Dissipation of energy in locally isotropic turbulence". C.R. Acad. Sci. URSS. 31,538.

Kotansky, D.R. 1966. "The use of honey–combs for shear flow generation". A.I.A.A. Journal 4.

Landahl, M.T. and Mollo–Christensen. 19 "Turbulence and random processes in fluid mechanics". Cambridge university press. Cambridge.

Landeberg et. al. 1969. "World survey of climatology ". 4 Elsevier publishing company. New york.

Lee, B.E. and Ahmed.F. 1988. "The influence of external turbulence field on shear–flow". Aerodynamics/Fluid mechanics/Hydraulics.

Leinhard, J.H. and Van Atta, C.W. 1990. "The decay of turbulence in thermally stratified flows". J. Fluid mechanics. 210, 57–112.

Manca, O. ,Mastrullo.R and Mazzeri, P. 1988. "Calibration of hot–wire probes in air with variable temperature". Dantec Information No. 6.

Montgometry, R.D. 1974. " An experimental study of grid turbulence in a thermally stratified flow". P.hd. dissertation. University of Michigan.

Reynolds, O. 1883. "An experimental investigation of the circumstances which determine whether the motion of water shall be direct or sinuous, and of the law of resistance in parallel channels." Philos. Trans. R. Soc. London 186, 123–161.

Schlichting, H. 1960. "Boundary layer Theory ". Mc Graw–Hill Book Company, inc. New york.

Shih–I Pai, 1957. "Viscous flow theory II –Turbulent flow ". D.Van Nostrand company, inc. Princeton.

Sikdar, S. 1989. " Study of free stream turbulence in an adverse pressure gradient ". M.Tech. thesis. IIT, Kanpur.

Singhal, A.K. and Spalding, D.B. 1981. "Prediction of Two–Dimensional Boundary Layers with the aid of K–ϵ Model of Turbulence". Computer methods in applied mechanics and engineering, 25. 365–383.

Sirivat, A. and Warhoft, Z. 1983. "The effect of a passive cross stream temperature gradient on the evolution of temperature variance and heat flow in grid turbulence". J. Fluid mechanics. 128, 323–346.

Sparrow, et. al. 1964. "Development of mean flow in the entrance of channels and ducts". Physics of Fluids 7, 338.

Stillinger, D.C., Mead, M.J., Helland, K.N. and Van Atta, C.W. 1983a. " A closed –loop gravity–driven water channel for density stratified shear flows. J. Fluid mechanics. 131, 73–89.

Stillinger, D.C., Helland, M.J. and Van Atta, C.W. 1983b. "Experiments of the transition of homogeneous turbulence of internal waves in a stratified fluid". J. Fluid mechanics. 131, 91–122.

Itsweire, E.C., Helland, K.N. and Van Atta, C.W. 1986. " The evolution grid generated turbulence in a stably stratified fluid". J. Fluid mechanics. 162. 299–388.

Taylor, G.I. 1935 "The statistical theory of turbulence ". Part I–IV, Proc. Roy. Soc. London. A151, p421.

Tennekes, H. and Lumely, J.L. 1972. " A first course in turbulence". MIT Press.
Von Karman, Th. 1937. "The fundamentals of statistical theory of turbulence". Jour. Aero. Sci. 4, 134–138.

APPENDIX 1
Program NCAL.F

```
C       INTERPOLATION USING POWER LAW.
        DIMENSION RR(20),EE(50),UU(20,50)
        DIMENSION A1(20,50),B1(20,50),SB1(20,50),
     1   AN1(20,50),C1(20,50)
        DIMENSION R(4),RC(4),E(4),U(4),ERROR(4)
        COMMON / CALIB / E,R,U
        OPEN(UNIT=24,FILE='pmv1.out')
        OPEN(UNIT=25,FILE='pmv2.out')
        OPEN(UNIT=26,FILE='pmv3.out')
        OPEN(UNIT=27,FILE='ncal.out')
        READ(24,*) (EE(I),I=1,40)
        READ(25,*) (RR(I),I=1,12)
        DO 91 I=1,12
        DO 91 J=1,40
        READ(26,*)UU(I,J)
91      CONTINUE
        PRINT *, 'SPECIFY TOTAL NUMBER OF ITERATIONS'
        READ *, ITM
        IT=1
        AN=0.45
        A=1.0
        C=0.5
        B=0.04
        SB=0.0
        ITMAX=100
        DO 71 LL=1,12
        L=12-LL
        DO 72 M=1,40
        E(1)=EE(M)
        E(2)=EE(M+1)
        E(3)=EE(M+1)
        E(4)=EE(M)
        R(3)=RR(L)
        R(4)=RR(L)
        R(1)=RR(L+1)
        R(2)=RR(L+1)
        U(4)=UU(L,M)
        U(3)=UU(L,M+1)
        U(2)=UU(L+1,M+1)
        U(1)=UU(L+1,M)
        IF(U(1).LE.0.0) GO TO 77
        IF(U(2).LE.0.0) GO TO 77
        IF(U(3).LE.0.0) GO TO 77
        IF(U(4).LE.0.0) GO TO 77
        DO 64 K=1,4
        R(K)=R(K)/9.0
64      CONTINUE
500     CONTINUE
        DO 27 I=1,4
        RC(I)=R(I)-C
27      CONTINUE
        T1=0.0
```

```
      T2=0.0
      T3=0.0
      T4=0.0
      T5=0.0
      DO 17 I=1,4
      T1=T1+((E(I)**2)*(U(I)**AN)*(RC(I)**SB))
      T2=T2+((E(I)**2)*(RC(I)**SB))
      T3=T3+(U(I)**AN)
      T4=T4+(U(I)**(2.0*AN))
      T5=T5+(E(I)**2)
17    CONTINUE

      ANUM=T1-((T2*T3)/4.0)
      DENM=T4-((T3*T3)/4.0)
      B=ANUM/DENM
      A=(T5-B*1,4      IF(EC1(I).LE.E(K)) GO TO 2314    CONTINU234
      ERR=100.0*(ABS((SB-DB)/DB))
      IF(ERR.LE.0.01) GO TO 101
      ITER=ITER+1
      IF(ITER.LE.ITMAX) GO TO 100
      PRINT *, 'NO CONVERGENCE IN SMALL B'
101   CONTINUE

      ITER=0
200   CONTINUE
      DC=C
      DELC=0.0001
      ANUM=FUNCTC(A,B,AN,SB,C)
      PRINT *, 'ANUM'
      PRINT *, ANUM
      DENM=(FUNCTC(A,B,AN,SB,C+DELC)-ANUM)/DELC
      C=C-(ANUM/DENM)

      PRINT *, 'VALUE OF C'
      PRINT *, C
      ERR=100.0*(ABS((C-DC)/C))
      IF(ERR.LE.0.01) GO TO 201
      ITER=ITER+1
      IF(ITER.LE.ITMAX) GO TO 200
      PRINT *, 'NO CONVERGENCE IN C'
201   CONTINUE

      PRINT *, A,B,AN,SB,C


      IT=IT+1
      IF(IT.LE.ITM) GO TO 500

      A1(L,M)=A
      AN1(L,M)=AN
      B1(L,M)=B
      SB1(L,M)=SB
      C1(L,M)=C
      GO TO 72
77    A1(L,M)=0.0
```

```
          AN1(L,M)=0.0
          B1(L,M)=0.0
          SB1(L,M)=0.0
          C1(L,M)=0.0


 72       CONTINUE
 71       CONTINUE

          DO 55 I=2,12
 c        IF(A1(I,1).LE.0.0) GO TO 92
 c        GO TO 93
 55       CONTINUE

          DO 95 I=1,12
          DO 96 J=1,40
          WRITE(27,*)A1(I,J),AN1(I,J),B1(I,J),SB1(I,J),C1(I,J)
 96       CONTINUE
 95       CONTINUE

          STOP
          END

          FUNCTION FUNCTB(A,B,AN,SB,C)
          COMMON / CALIB / E(4),R(4),U(4)

          SUM=0.0
          DO 10 I=1,4
          RP=R(I)-C
          SUMI=((E(I)**2)*(RP**SB))-A-(B*(U(I)**AN))
          SUM=SUM+(SUMI*(E(I)**2)*(RP**SB)*(ALOG(RP)))
 10       CONTINUE
          FUNCTB=SUM

          RETURN
          END

          FUNCTION FUNCTC(A,B,AN,SB,C)
          COMMON / CALIB / E(4),R(4),U(4)

          SUM=0.0
          DO 10 I=1,4
          RP=R(I)-C
          SUMI=((E(I)**2)*(RP**SB))-A-(B*(U(I)**AN))
          SUM=SUM+(SUMI*(E(I)**2)*(RP**(SB-1)))
 10       CONTINUE
          PRINT *, 'SUM'
          PRINT *, SUM
          FUNCTC=SUM

          RETURN
          END
```

APPENDIX 2
Program READ.F

```
C       NON-ISOTHERMAL SHEAR FLOWS
C       DETERMINATION OF FLOW PROPERTIES
        DIMENSION E(50),R(20),U(20,50)
        DIMENSION A(20,50),AN(20,50),B(20,50),SB(20,50)
        DIMENSION C(20,50),DER(25)
        DIMENSION Y(25),EC(25),ERMS(25),T(25),RHV(25)
        DIMENSION UU(25),DUE(25),EE(25),EC1(25)
        DIMENSION URMS(25),EDV(25),DUY(25),TUR(25),TUR1(25)
        OPEN(UNIT=24,FILE='pmv1.out')
        OPEN(UNIT=25,FILE='pmv2.out')
        OPEN(UNIT=26,FILE='pmv3.out')
        OPEN(UNIT=96,FILE='ncal1.out')
        OPEN(UNIT=28,FILE='read.dat')
        OPEN(UNIT=29,FILE='read.out')
        DO 11 I=1,12
        READ(25,*)R(I)
11      CONTINUE
        DO 12 J=1,40
        READ(24,*)E(J)
12      CONTINUE
        DO 115 I=1,12
        DO 125 J=1,40
        READ(26,*)U(I,J)
125     CONTINUE
115     CONTINUE
        DO 110 I=1,12
        DO 120 J=1,40
        READ(96,*)A(I,J),AN(I,J),B(I,J),SB(I,J),C(I,J)
120     CONTINUE
110     CONTINUE
        R0=9.4719
        READ(28,*)M,HVS,BVS,X
        DO 15 I=1,M
        READ(28,*)Y(I),EC(I),ERMS(I),T(I)
15      CONTINUE
        DO 16 I=1,M
        IF(EC(I).GE.1.5868) GO TO 16
        BB=R0*(1+23.0*0.0036)
        CC=12.5*(12.5-R0*(1+T(I)*0.0036))
        RHV(I)=BB/2.0+SQRT(BB**2+4.0*CC)/2.0
        DO 18 K=1,40
        IF(EC(I).LE.E(K)) GO TO 163
18      CONTINUE
163     IF(RHV(I).GE.12.500) GO TO 133
        DO 17 J=1,12
        IF(RHV(I).LE.R(J)) GO TO 33
17      CONTINUE
33      PRINT *, J
        PRINT *, R(J)
        J=J-1
        GO TO 134
133     J=12
```

```
134      K=K-1
         DER(I)=-SB(J,K)*(A(J,K)+B(J,K)*U(J,K)**AN(J,K))
         DER(I)=DER(I)/(9.0*(RHV(I)/9.0-C(J,K))**(SB(J,K)+1))
         DD=RHV(I)*(RHV(I)-R0*(1+0.0036*23.0))
         EC1(I)=EC(I)**2-(CC/DD)*DER(I)*0.0036*R0*(T(I)-23)
         EC1(I)=SQRT(EC1(I))
         DO 14 K=1,40
         IF(EC1(I).LE.E(K)) GO TO 234
14       CONTINUE
234      IF(RHV(I).GE.12.5) GO TO 144
         DO 13 J=1,12
         IF(RHV(I).LE.R(J)) GO TO 34
13       CONTINUE
34       J=J-1
         GO TO 334
144      J=12
334      K=K-1
         UU(I)=(EC1(I)**2*(RHV(I)/9.0-C(J,K))**SB(J,K)-A(J,K))
         UU(I)=(UU(I)/B(J,K))**(1.0/AN(J,K))
         DUE(I)=2.0*EC1(I)*(RHV(I)/9.0-C(J,K))**SB(J,K)
         DUE(I)=DUE(I)/(AN(J,K)*B(J,K)*UU(I)**(AN(J,K)-1))
         URMS(I)=ERMS(I)*DUE(I)
         TUR(I)=(URMS(I)/UU(I))
         TUR1(I)=TUR(I)*100
16       CONTINUE
         DO 21 I=2,M-1
         DUY(I)=(UU(I+1)-UU(I-1))/0.01
         EDV(I)=URMS(I)**2/DUY(I)
21       CONTINUE
         DUY(1)=(UU(2)-UU(1))/0.005
         DUY(M)=(UU(M)-UU(M-1))/0.005
         EDV(1)=URMS(1)**2/DUY(1)
         EDV(M)=URMS(M)**2/DUY(M)
         WRITE(29,222)
222      FORMAT(5X,'NON-ISOTHERMAL SHEAR FLOWWITH CYLINDER')
         WRITE(29,2)HVS
2        FORMAT(5X,'HEATER VARIAC SETTING',2X,F4.1,'V')
         WRITE(29,4)BVS
4        FORMAT(/5X,'BLOWER VARIAC SETTING',2X,F4.1,'V')
         WRITE(29,5)X
5        FORMAT(/5X,'DOWNSTREAM DISTANCE',2X,F5.1,'cm')
         WRITE(29,7)
7        FORMAT(//6X,'Y(cm)',4X,'TEMP(C)',3X,'VEL(m/s)',3X,
     1   'TUR(m/s)',5X,'TUR(%)'/)
         DO 66 I=1,M
         WRITE(29,3)Y(I),T(I),UU(I),TUR(I),TUR1(I)
3        FORMAT(5X,5(F7.4,3X))
66       CONTINUE
         STOP
         END
```